UNIVERSITY OF READING
DEPARTMENT OF MATHEMATICS

THE USE OF ROBUST OBSERVERS IN THE SIMULATION OF GAS SUPPLY NETWORKS

by

SIMON M. STRINGER

This thesis is submitted for the degree of
Doctor of Philosophy

NOVEMBER 1993

Abstract

For any gas network, it is desirable to have a reasonable estimate of the demand flows. However, flow meters are much more expensive than pressure sensors to install, and so it would be economical to be able to estimate the flow demands from pressure measurements alone. In this thesis, both model and observer based methods for estimating unmeasured flow demands in linear gas networks with sparse pressure telemetry are investigated.

Firstly, we introduce the basic gas network model in the form of a linear time invariant descriptor system, which requires the upstream pressure and all flow demands as inputs. Thus the basic model is useless for estimating the flow demands since these are needed to drive the model. Hence, we proceed to derive rearranged and augmented gas network models that contain the flow demands in their state vectors, and that are capable of flow demand estimation.

The first two flow estimation models investigated are simply pressure driven models that have their system eigenvalues within the unit circle. These models are capable of asymptotically estimating the flow demands. We next explore a *completely observable* model constructed by incorporating trivial difference equations of the form

$$flow\ demand\ _{k+1} = flow\ demand\ _{k}.$$

Two techniques for constructing *robust* observers are employed: robust eigenstructure assignment and singular value assignment. These are shown to help reduce the effects of the modelling error introduced by the above trivial difference equations. Such modelling error is then further reduced by making use of the known time profiles for the flow demands.

Unfortunately, the pressure measurements available are subject to constant bias and white noise. The measurement biases very badly degrade the flow demand estimates, and so must be estimated. This is achieved by constructing a further model variation that incorporates the biases into an augmented state vector, but now includes information about the flow demand profiles in a new form, which allows the estimation of the measurement biases, as well as the flow demands themselves. Finally, less sensitive flow estimation models are presented with smoothing techniques to reduce the effects of measurement noise.

Acknowledgements

I would like to thank my academic supervisor, Dr Nancy Nichols, for my introduction to the mathematics of the real world; and thank British Gas for giving me the opportunity to work on such an interesting practical problem. I would also like to thank my industrial supervisors, Dr John Piggott, Dr Alan Lowdon, Dr Jim Mallinson and Mr Michael Gardiner, for their encouragement during my three years at Reading.

Finally, I would like to acknowledge both the Science and Engineering Research Council and British Gas for their financial support for the period of my studies.

Contents

Chapter 1

Introduction

For any gas network, it is desirable to have a reasonable estimate of the demand flows. However, flow meters are much more expensive than pressure sensors to install, and so it would be economical to be able to estimate the flow demands from pressure measurements alone. In this thesis, both model and observer based methods for estimating unmeasured flow demands in linear gas networks with sparse pressure telemetry are investigated. Two techniques for constructing *robust* observers are employed: robust eigenstructure assignment [24], [25], and singular value assignment [34], [4].

The gas networks considered are linear and consist of a number of pipe sections with a gas source at the upstream end and flow demands at pipe junctions and at the downstream end. For example, for a three pipe network we would have

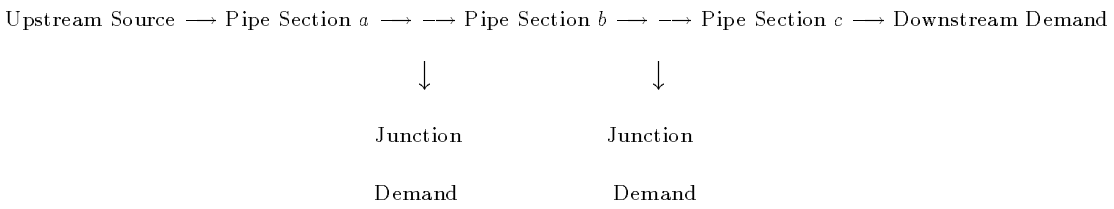

We assume the only measurements of the real gas network available are discrete pressure measurements at all sites of gas inflow (the upstream end) and outflow (the pipe junctions and downstream end). These measurement sites are the natural 'boundaries' of the network, where some data (pressure or flow demand) need to be specified to drive a network model.

In chapter 2 we introduce the basic gas network model from [34], based on two partial differential equations for modelling natural gas flow in high pressure pipelines, derived by mass and momentum balance arguments [19], [30]. Such a model, which we denote by $\mathcal{M}0$, is in the form of a linear time invariant descriptor system

$$E_0 \underline{x}_0(k+1) = A_0 \underline{x}_0(k) + B_0^1 \underline{u}_0(k+1) + B_0^2 \underline{u}_0(k)$$

which results from linearising the original differential equations about a steady state and discretising the linearised equations using the θ-method [37]. All pressure and flow variables are thus perturbations away from that steady state. An $\mathcal{M}0$ model requires the upstream pressure and all flow demands as inputs; thus an $\mathcal{M}0$ model is useless for estimating the flow demands since these are needed to drive the model. Hence, we proceed to derive rearranged and augmented gas network models that are capable of flow demand estimation. The major advantage of this linear time-invariant model over other time-varying or non-linear models [18], [21], is that we may use the large amount of control theory that already exists for linear time-invariant systems.

In chapter 3, we investigate a new gas network model variation, denoted by $\mathcal{M}1$, which requires only pressure measurements as inputs. Such a model can be shown to be asymptotically stable and allows asymptotic estimation of the pressure profiles. From these pressure profiles the flow demands may be estimated. In chapter 4 we investigate a further rearrangement of the basic $\mathcal{M}0$ model to give a new model variation, denoted by $\mathcal{M}2$, with the flow demands now moved into the state vector. Such a model can also be shown to be asymptotically stable (under slightly more restrictive conditions) and allows asymptotic estimation of the flow demands. However, due to a different difference approximation, $\mathcal{M}2$ models are shown to allow more accurate flow demand estimation than $\mathcal{M}1$ models.

In chapter 5, we discuss techniques, known collectively as *observers*, capable of estimating the entire system state of discrete dynamical systems that have the property of *complete observability* [29], [2]. In particular, two techniques for constructing *robust* observers are described: robust eigenstructure assignment and singular value assignment. In chapter 6 we introduce a further gas network model variation, denoted by $\mathcal{M}3$, that contains the flow demands in its state vector, but which is also completely observable, and for which we may construct observers. An $\mathcal{M}3$ model is constructed by incorporating

trivial difference equations of the form

$$flow\ demand\ _{k+1} = flow\ demand\ _{k}.$$

Obviously, if such a model were run, the estimates of the flow demands would not change. However, if the flow demands change slowly with time, then observers constructed upon such models can track the flow demands fairly well; although the above difference equation for the flows will contain some modelling error. Such trivial difference equations have been used previously for both leak detection [3] and state estimation [32]. Experimental and theoretical evidence is given to show how the two techniques, robust eigenstructure assignment and singular value assignment, reduce the effects of the above modelling error upon the observer state estimate. The $\mathcal{M}3$ model is further developed by making use of the known time profiles for the flow demands to remove the modelling error introduced by the above trivial difference equations. The new trivial difference equations for the flow demands become

$$flow\ demand_{k+1}^{demand\ site} = flow\ demand_{k}^{demand\ site} + f_{k}^{demand\ site}$$

where the $f_{k}^{demand\ site}$ may be estimated from the telemetry from other *measured* demand flows.

In chapter 7, we introduce a new observer technique, which we term 'cycling'. Cycling involves a series of dynamic observers, travelling along the time axis, one after another. Each dynamic observer uses information about the flow demand profiles given by the previous observer. The convergence properties of this type of cycling technique are investigated theoretically.

In chapter 8 we investigate the effects of measurement bias on the various state estimation techniques. It may be the case that the pressure measurements at the sites of flow demand are subject to a constant bias, i.e. instead of using a true value for $\underline{p}_2(k)$, the vector of pressures at the sites of gas inflow and gas outflow, we drive the models and observers with

$$\underline{p}_{2_{measured}}(k) = \underline{p}_2(k) + \underline{b}$$

where $\underline{b}$ represents a vector of constant biases. These constant biases will introduce error into the state estimates of the different estimation techniques. This is a serious problem for flow demand estimation due to the sensitivity of the flow demand variables

to perturbations in the pressures. In chapter 9 a standard approach from [34] is explored but shown to be inadequate without a new approach to encoding information about the flow demand time profiles. We investigate a further model variation, denoted by $\mathcal{M}4$, capable of estimating both flow demands and pressure measurement bias, but which uses trivial difference equations for the flow demands of the form

$$flow\ demand\ _{k+1} \ = \ w_k^{demand\ site} \times flow\ demand\ _k$$

where the $w_k^{demand\ site}$ are estimated from other measured flow demands. This new way of incorporating information about the flow profiles allows the estimation of the measurement biases, as well as the flow demands themselves. However, the $\mathcal{M}4$ models have time-varying system matrices and basic control theory for time-invariant systems does not always extend to time-varying systems [41], [26], [6], [7]. Our observer designs must also be modified [15].

In chapter 10 we examine the problem of measurement white noise. We avoid Kalman filters due to their unexceptional performance in [17], [40], [35], and instead examine two simple smoothing techniques, and derive two final model variations, $\mathcal{M}5$ and $\mathcal{M}6$, to deal with the problem of the sensitivity of the flow demand estimates. $\mathcal{M}5$ and $\mathcal{M}6$ models have only a single total flow demand perturbation state variable that is the sum of all the individual demand flow perturbation variables. Such models are less sensitive to pressure measurement noise.

Finally, in chapter 11 we make some final conclusions and suggest some proposals for future work.

Chapter 2

The Standard System Model ($\mathcal{M}0$)

In this chapter, the standard underlying model, based directly on [34], is constructed for a simple linear network with demand flows. This initial model, which we denote as an $\mathcal{M}0$ model, actually assumes that all flow demands are measured and used as inputs to drive the model. Hence, obviously an $\mathcal{M}0$ model, itself, cannot be used for flow demand estimation.

2.1 The Linearised Differential Equations Governing Gas Pipe Dynamics

Firstly, we derive the linearised equations governing gas dynamics in a single section of pipe. For each section, from [34], we have the following two equations

$$D_x(P^2) + \epsilon_1(1 - \tau P)Q|Q|^{\alpha-1} = 0, \tag{2.1}$$

the momentum balance equation ignoring time variations in Q, and

$$D_t(P) + \epsilon_2(1 - \tau P)^2 D_x(Q) = 0, \tag{2.2}$$

the mass balance equation, where:

$P(x,t)$ is the gas pressure in bar

$Q(x,t)$ is the mass flow rate in m.s.c.m.h. (millions of standard cubic metres per hour)

x is distance along pipe in metres

t is time in hours

$\epsilon_1, \epsilon_2, \tau, \alpha$ are constants, and D_x, D_t are partial derivatives with respect to x and t respectively. τ is used in the linear expression for compressibility, $Z = 1 - \tau P$, which is always positive.

We begin by modelling a straight section of pipe of length L, with constant cross-sectional area.

For computational ease, we normalise the pipe section length, pressure and mass flow rate:

$$x \rightarrow x/L \ , \ P \rightarrow P/N_p \ , \ Q \rightarrow Q/N_q \tag{2.3}$$

where N_p and N_q are positive constants which are chosen such that $|P|, |Q| \leq 1$. The normalisation results in

$$D_x \rightarrow (1/L)D_x \ , \ \tau \rightarrow \tau N_p \ , \ \epsilon_1 \rightarrow (\epsilon_1 L N_q^{\alpha})/(N_p^2) \ , \ \epsilon_2 \rightarrow (\epsilon_2 N_q)/(L N_p). \tag{2.4}$$

The normalised equations (2.1) and (2.2) are, therefore, to be solved for $0 < x < 1$ and $t > 0$. The boundary and initial conditions are yet to be specified.

Our approach is to linearise about a mass flow rate and pressure profile in order to obtain two linear equations which approximate equations (2.1) and (2.2). Our mass flow rate and pressure profile are

$$Q(x,t) = \mathcal{Q}, \tag{2.5}$$

$$P(x,t) = \mathcal{P}(x), \tag{2.6}$$

where $\mathcal{Q}$ is a positive constant mass flow rate from $x = 0$ to $x = 1$, and $\mathcal{P}(x)$ is the constant pressure profile.

Substituting (2.5) and (2.6) into equation (2.1) gives

$$D_x(\mathcal{P}^2) + \epsilon_1(1 - \tau\mathcal{P})\mathcal{Q}^{\alpha} = 0,$$

which is equivalent to

$$(2\mathcal{P}D_x(\mathcal{P}))/(1 - \tau\mathcal{P}) + \epsilon_1\mathcal{Q}^{\alpha} = 0, \tag{2.7}$$

which is permissible because the compressibility, $Z = 1 - \tau P$, is always positive. But

$$(2\mathcal{P}D_x(\mathcal{P}))/(1 - \tau\mathcal{P}) \equiv -(2/\tau)D_x(\mathcal{P} + \tau^{-1}ln(1 - \tau\mathcal{P})),$$

which can be substituted into (2.7) to give

$$-(2/\tau)D_x(\mathcal{P} + \tau^{-1}ln(1-\tau\mathcal{P})) + \epsilon_1\mathcal{Q}^\alpha = 0.$$

This is easily integrated from 0 to x and then rearranged to give

$$\tau\mathcal{P}(x) + ln(1-\tau\mathcal{P}(x)) = \tau\mathcal{P}(0) + ln(1-\tau\mathcal{P}(0)) + \beta\mathcal{Q}^\alpha x, \tag{2.8}$$

where $\beta = \tau^2\epsilon_1/2$. For each pipe section in the network, equation (2.8) is used to find a consistent steady state pressure profile, $\mathcal{P}(x)$, about which to linearise. An assumed steady value for the inline flow, $\mathcal{Q}$ and a value for $\mathcal{P}(0)$ are substituted into equation (2.8), and then a steady pressure profile is generated using an iterative technique such as Newton's [23], [5].

Now let

$$P(x,t) = \mathcal{P}(x) + p(x,t), \tag{2.9}$$

$$Q(x,t) = \mathcal{Q} + q(x,t), \tag{2.10}$$

where q and p are perturbations about the mass flow rate and pressure profile and are smaller in magnitude than $\mathcal{Q}$ and $\mathcal{P}$ respectively. We can thus assume that P and Q are positive and substitute equations (2.9) and (2.10) into equation (2.1) to get

$$D_x(\mathcal{P}+p)^2 + \epsilon_1(1-\tau\mathcal{P}-\tau p)(\mathcal{Q}+q)^\alpha = 0,$$

which can be linearised by expanding the $(\mathcal{Q}+q)^\alpha$ term using the binomial theorem, neglecting all the second order terms and cancelling out the terms corresponding to equation (2.7). Thus we derive

$$2D_x(\mathcal{P}p) + \alpha\epsilon_1(1-\tau\mathcal{P})\mathcal{Q}^{\alpha-1}q = \epsilon_1\tau\mathcal{Q}^\alpha p,$$

which can be rearranged into

$$\begin{aligned} q &= \frac{-2\mathcal{P}D_x(p) - 2D_x(\mathcal{P})p + \epsilon_1\tau\mathcal{Q}^\alpha p}{\alpha\epsilon_1\mathcal{Q}^{\alpha-1}(1-\tau\mathcal{P})} \\ &= \frac{-2\Gamma D_x(p) - 2(1-\tau\mathcal{P})D_x(\Gamma)p + \epsilon_1\tau\mathcal{Q}^\alpha p/(1-\tau\mathcal{P})}{\alpha\epsilon_1\mathcal{Q}^{\alpha-1}}, \end{aligned}$$

where

$$\Gamma(\mathcal{P}) = \mathcal{P}/(1-\tau\mathcal{P}), \tag{2.11}$$

and hence

$$D_x(\Gamma) = D_x(\mathcal{P})/(1-\tau\mathcal{P})^2. \tag{2.12}$$

Using equation (2.7) to substitute for $\epsilon_1\mathcal{Q}^\alpha$, and then using equation (2.12), gives

$$q = \frac{-2(\Gamma D_x(p) + D_x(\Gamma)p)}{\alpha\epsilon_1\mathcal{Q}^{\alpha-1}},$$

which gives

$$q = -\epsilon_3 D_x(\Gamma p), \tag{2.13}$$

where $\epsilon_3 = 2/(\alpha\epsilon_1\mathcal{Q}^{\alpha-1})$.

Turning our attention now to equation (2.2) and substituting for P and Q using equations (2.9) and (2.10) we have

$$D_t(\mathcal{P}+p) + \epsilon_2(1-\tau\mathcal{P}-\tau p)^2 D_x(\mathcal{Q}+q) = 0,$$

and, because $\mathcal{P}$ is a function of x only and $\mathcal{Q}$ is a constant, this immediately simplifies to

$$D_t(p) + \epsilon_2(1-\tau\mathcal{P}-\tau p)^2 D_x(q) = 0.$$

This equation can be linearised by a similar process to that used for the momentum balance equation by neglecting second order terms in p and q. This gives

$$D_t(p) + \epsilon_2(1-\tau\mathcal{P})^2 D_x(q) = 0. \tag{2.14}$$

If we now differentiate both sides of equation (2.13) partially with respect to x, we can then substitute for $D_x(q)$ in equation (2.14) to obtain

$$D_t(p) = \Omega D_{xx}(\Gamma p), \tag{2.15}$$

where

$$\Omega(\mathcal{P}) = \epsilon_2\epsilon_3(1-\tau\mathcal{P})^2.$$

Thus we replace the non-linear equations (2.1) and (2.2) with the equations (2.13) and (2.15), which are linearised about a mass flow rate and pressure profile. Equation (2.15) is used to approximate the perturbations in pressure and is solved for $0 < x < 1$ and $t > 0$.

The initial conditions for a pipe section are taken to be

$$p(x,0) = 0 \quad for \;\; 0 \leq x \leq 1.$$

The following boundary data are required at the ends of the pipe section:
at $x = 0$ we require

$$p(0,t) = P(0,t) - \mathcal{P}(0),$$

or

$$q(0,t) = -\epsilon_3 D_x(\Gamma p) \mid_{x=0} = Q(0,t) - \mathcal{Q},$$

and at $x = 1$, we require

$$p(1,t) = P(1,t) - \mathcal{P}(1),$$

or

$$q(1,t) = -\epsilon_3 D_x(\Gamma p) \mid_{x=1} = Q(1,t) - \mathcal{Q}.$$

2.2 The Finite Difference Approximation

Each of the pipe sections have nodes at either end and a number of regularly spaced internal nodes. For an arbitrary pipe section with $s+1$ nodes, we have

Nodes: 0——1——2——3.....s

←————Pipe section————→

Firstly, we introduce some notation. For any pipe section with $s+1$ nodes, we let our numerical approximations be

$$p_{i,k} \approx p(i\delta x, k\delta t),\ q_{i,k} \approx q(i\delta x, k\delta t),\ \Gamma_i \approx \Gamma(\mathcal{P}(i\delta x)),\ \Omega_i \approx \Omega(\mathcal{P}(i\delta x)),$$

where i = 0,1,2,3,....,s, δx is the spatial discretisation interval of the pipe and δt is the sample period with k=0,1,2,...

In our numerical model, we use a finite difference scheme based on the nodal *pressure perturbations only*; the perturbations in inline flows can then be calculated separately

from the computed pressure perturbation profile using a difference approximation based on equation (2.13).

For any pipe section, at any of its nodes, the governing differential equation

$$D_t(p) = \Omega D_{xx}(\Gamma p) \tag{2.16}$$

can be approximated by the weighted average finite difference scheme

$$p_{i,k+1} - p_{i,k} = \theta\Omega_i r(\Gamma_{i-1}p_{i-1,k+1} - 2\Gamma_i p_{i,k+1} + \Gamma_{i+1}p_{i+1,k+1})$$

$$+(1-\theta)\Omega_i r(\Gamma_{i-1}p_{i-1,k} - 2\Gamma_i p_{i,k} + \Gamma_{i+1}p_{i+1,k})$$

for $0 \leq \theta \leq 1$, where $r = \delta t/(\delta x)^2$. This finite difference equation can be rewritten as

$$-\theta\Omega_i r\Gamma_{i-1}p_{i-1,k+1} + (1 + 2\theta\Omega_i r\Gamma_i)p_{i,k+1} - \theta\Omega_i r\Gamma_{i+1}p_{i+1,k+1} =$$

$$(1-\theta)\Omega_i r\Gamma_{i-1}p_{i-1,k} + (1 - 2(1-\theta)\Omega_i r\Gamma_i)p_{i,k} + (1-\theta)\Omega_i r\Gamma_{i+1}p_{i+1,k}. \tag{2.17}$$

In [34], the truncation error [37], [28], of difference equation (2.17) is shown to be $O(\delta x)^2 + O(\delta t)^2$ for $\theta = 1/2$, and $O(\delta x)^2 + O(\delta t)$ for $0 \leq \theta < 1/2$ and $1/2 < \theta \leq 1$. Hence, difference equation (2.17) is consistent with differential equation (2.16) for $0 \leq \theta \leq 1$. However, for $\theta = 1/2$, difference equation (2.17) is a Crank-Nicolson scheme with the highest order of accuracy.

For a simple numerical model, the initial conditions for any pipe section with $s+1$ nodes may be taken to be

$$p_{i,0} = 0$$

for all pressure perturbation variables.

At end nodes 0 and s, we require boundary data. For example if pressure is given, then at node 0 we have

$$p_{0,k} = P(0, k\delta t) - \mathcal{P}(0), \qquad for \quad k = 0, 1, 2, ...,$$

while at node s we have

$$p_{s,k} = P(1, k\delta t) - \mathcal{P}(1), \qquad for \quad k = 0, 1, 2, ...$$

For *flow* boundary conditions given at node s in a general pipe section, we use the following theory.

Using equation (2.13) we derive the finite difference equation

$$-\epsilon_3(\Gamma_{s+1}p_{s+1,k} - \Gamma_{s-1}p_{s-1,k}) = 2\delta x q_{s,k} \tag{2.18}$$

for the boundary flow condition at the node $i = s$ for any pipe section. From [37], approximating the derivative $D_x(\Gamma p)$ by

$$D_x(\Gamma p) \approx (\Gamma_{s+1}p_{s+1,k} - \Gamma_{s-1}p_{s-1,k})/2\delta x$$

involves a leading error on the right hand side of order $(\delta x)^2$. Eliminating $\Gamma_{s+1}p_{s+1,k}$ and $\Gamma_{s+1}p_{s+1,k+1}$ between equation (2.17), with $i = s$, and equation (2.18), gives as the general finite difference equation for any pipe section with a flow boundary condition at $i = s$

$$-2\theta\Omega_s r\Gamma_{s-1}p_{s-1,k+1} + (1 + 2\theta\Omega_s r\Gamma_s)p_{s,k+1} + (2\theta\Omega_s r\delta x/\epsilon_3)q_{s,k+1} =$$

$$2(1-\theta)\Omega_s r\Gamma_{s-1}p_{s-1,k} + (1 - 2(1-\theta)\Omega_s r\Gamma_s)p_{s,k} - (2(1-\theta)\Omega_s r\delta x/\epsilon_3)q_{s,k}. \tag{2.19}$$

For a flow boundary condition at node 0 of a general pipe section, equation (2.13) gives

$$-\epsilon_3(\Gamma_1 p_{1,k} - \Gamma_{-1}p_{-1,k}) = 2\delta x q_{0,k}. \tag{2.20}$$

Similarly, approximating the derivative $D_x(\Gamma p)$ by

$$D_x(\Gamma p) \approx (\Gamma_1 p_{1,k} - \Gamma_{-1}p_{-1,k})/2\delta x$$

involves a leading error on the right hand side of order $(\delta x)^2$. Eliminating $\Gamma_{-1}p_{-1,k}$ and $\Gamma_{-1}p_{-1,k+1}$ between equation (2.17), with i=0, and equation (2.20), gives the general finite difference equation for any pipe section with a flow boundary condition at i=0

$$(1 + 2\theta\Omega_0 r\Gamma_0)p_{0,k+1} - 2\theta\Omega_0 r\Gamma_1 p_{1,k+1} - (2\theta\Omega_0 r\delta x/\epsilon_3)q_{0,k+1} =$$

$$(1 - 2(1-\theta)\Omega_0 r\Gamma_0)p_{0,k} + 2(1-\theta)\Omega_0 r\Gamma_1 p_{1,k} + (2(1-\theta)\Omega_0 r\delta x/\epsilon_3)q_{0,k}. \tag{2.21}$$

2.3 The Network Model

Now we consider how to link up the separate finite difference models for the single pipe sections into a network model. For the network model, we use superscripts to denote

particular pipe sections.

Regarding the initial linearisation procedure, we linearise about different inline flows for all pipe sections. Hence, for our linear network, we linearise about a steady state where the flow demands at the junctions are not zero. In practice, a value for the steady flow, $\mathcal{Q}^z$, in each pipe section z may be suggested by, say, substituting the values of the pressure measurements at the opposite ends of the pipe section into equation (2.8) and solving for $\mathcal{Q}^z$. It may be the case that we have to make a best guess for a value for $\mathcal{Q}^z$.

Firstly, we use equation (2.8) to linearise for the upstream section (i.e. section a for the example network) by substituting in an assumed steady value for the inline flow, $\mathcal{Q}^{upstream\ section}$, and a value for $\mathcal{P}^{upstream\ section}(0)$, and generating a steady pressure profile using an iterative technique such as Newton's. In practice, a value for $\mathcal{P}^{upstream\ section}(0)$ is suggested by the upstream pressure measurement of that section.

Next, the same procedure is carried out for neighbouring sections downstream in turn, using different steady inline flows, $\mathcal{Q}^z$, for linearising each general pipe z, and using the calculated value for $\mathcal{P}^{z-1}(1)$ from the adjacent upstream section as the value for $\mathcal{P}^z(0)$ each time.

This means that at each pipe section junction we are linearising about a steady demand flow

$$\mathcal{Q}^{z/z+1} = \mathcal{Q}^z - \mathcal{Q}^{z+1}$$

where $\mathcal{Q}^z$ is the steady flow we linearised about in the upstream section z, and $\mathcal{Q}^{z+1}$ is the steady flow we linearised about in the downstream section $z+1$.

Now we examine how to link up the separate finite difference schemes for two general adjacent pipe sections, z and $z+1$, in a linear network. Pipe sections z and $z+1$ have, say, s^z+1 and $s^{z+1}+1$ nodes respectively (although one of these nodes is shared by both pipe sections).

Nodes: 0^z——1^z——2^z——3^z.....$(s^z)^z/0^{z+1}$——1^{z+1}——2^{z+1}——3^{z+1}.....$(s^{z+1})^{z+1}$

←————Section z————→ ←————Section $z+1$————→

For our 'internal boundary node' $(s^z)^z/0^{z+1}$, we derive a finite difference equation that links up the finite difference equations for the two pipe sections on either side, z and $z+1$.

We assume that at time level k, we have a normalised flow demand, $D_k^{z/z+1}$, out of the pipe junction, $z/z+1$, where

$$D_k^{z/z+1} = \mathcal{Q}^{z/z+1} + d_k^{z/z+1},$$

$\mathcal{Q}^{z/z+1}$ is the demand flow out of the pipe junction $z/z+1$ chosen for the linearisation, and $d_k^{z/z+1}$ is a perturbation away from that steady demand flow. Then to enforce continuity of mass flow at node $(s^z)^z/0^{z+1}$, we require

$$-[\theta q^z_{s^z,k+1} + (1-\theta)q^z_{s^z,k}] + [\theta q^{z+1}_{0,k+1} + (1-\theta)q^{z+1}_{0,k}] + [\theta d^{z/z+1}_{k+1} + (1-\theta)d^{z/z+1}_k] = 0. \quad (2.22)$$

Rearranging both equation (2.19) for pipe z and equation (2.21) for pipe $z+1$, for $q^z_{i,k}$ etc., and substituting into equation (2.22) gives us the following finite difference equation for our internal boundary node $(s^z)^z/0^{z+1}$.

$$\begin{aligned}
&-(\Phi^{z/z+1}\epsilon_3^z\Gamma^z_{s^z-1}\theta/\delta x^z)p^z_{s^z-1,k+1} + (1+\Phi^{z/z+1}\epsilon_3^z\Gamma^{z/z+1}\theta/\delta x^z + \Phi^{z/z+1}\epsilon_3^{z+1}\Gamma^{z/z+1}\theta/\delta x^{z+1})p^{z/z+1}_{k+1} \\
&\qquad -(\Phi^{z/z+1}\epsilon_3^{z+1}\Gamma_1^{z+1}\theta/\delta x^{z+1})p^{z+1}_{1,k+1} + \Phi^{z/z+1}\theta d^{z/z+1}_{k+1} = \\
&(\Phi^{z/z+1}\epsilon_3^z\Gamma^z_{s^z-1}(1-\theta)/\delta x^z)p^z_{s^z-1,k} + (1-\Phi^{z/z+1}\epsilon_3^z\Gamma^{z/z+1}(1-\theta)/\delta x^z - \Phi^{z/z+1}\epsilon_3^{z+1}\Gamma^{z/z+1}(1-\theta)/\delta x^{z+1})p^{z/z+1}_k \\
&\qquad + (\Phi^{z/z+1}\epsilon_3^{z+1}\Gamma_1^{z+1}(1-\theta)/\delta x^{z+1})p^{z+1}_{1,k} - \Phi^{z/z+1}(1-\theta)d^{z/z+1}_k \qquad (2.23)
\end{aligned}$$

where we have defined

$$\Phi^{z/z+1} = \left(\frac{\epsilon_3^z}{2r^z\delta x^z\Omega^z_{s^z}} + \frac{\epsilon_3^{z+1}}{2r^{z+1}\delta x^{z+1}\Omega_0^{z+1}}\right)^{-1}$$

and where, because $p^z_{s^z,k} \equiv p^{z+1}_{0,k}$ and $\Gamma^z_{s^z} \equiv \Gamma_0^{z+1}$, at the junction we have denoted the pressure perturbation by $p_k^{z/z+1} \equiv p^z_{s^z,k} \equiv p^{z+1}_{0,k}$, and denoted Γ by $\Gamma^{z/z+1} \equiv \Gamma^z_{s^z} \equiv \Gamma_0^{z+1}$. This equation is our 'connectivity equation', which is the actual finite difference equation we use at the node between two pipe sections z and $z+1$. Equivalent connectivity equations are also derived for other pipe junctions. The junction demand flows, $d_k^{junction}$, must be known and used as an input to the model rather like an internal boundary condition.

For consistency of notation, the numerically computed flow demand at the downstream end of the last pipe of the linear network, $Q^{end-pipe}(1, k\delta t)$, is denoted by $D_k^{end-pipe}$. Also, we denote the demand flow perturbation at the downstream end, $q_{end-node,k}^{end-pipe}$, by $d_k^{end-pipe}$. Then we have

$$D_k^{end-pipe} = \mathcal{Q}^{end-pipe} + d_k^{end-pipe},$$

where $\mathcal{Q}^{end-pipe}$ is the steady flow through the end-pipe section about which we linearised.

For any linear gas network with g pipes, with pressure input data available at the upstream end and flow demand input data available at the g sites of outflow, the corresponding n dimensional $\mathcal{M}0$ model takes the form

$$E_0 \underline{x}_0(k+1) = A_0 \underline{x}_0(k) + B_0^1 \underline{u}_0(k+1) + B_0^2 \underline{u}_0(k), \tag{2.24}$$

where $\underline{x}_0(k)$ is the n dimensional state vector containing the nodal pressure variables, $\underline{u}_0(k)$ is the $g+1$ dimensional input vector containing the upstream pressure input and the g flow boundary inputs to drive the model, and E_0, A_0 and B_0^1, B_0^2 are system matrices derived from the underlying finite difference equations, with dimensions $n \times n$ and $n \times (g+1)$ respectively.

If we have pressure measurements available at the sites of flow demand, this corresponds to having g measurements of the $\mathcal{M}0$ state variables

$$\underline{y}_0(k) = C_0 \underline{x}_0(k) \quad for \ k = 0, 1, 2, ..., \tag{2.25}$$

where the matrix C_0 is the 'measurement matrix'.

If we arrange the pressure variables in the state vector in their order along the pipe network, i.e. in the following way

$$\underline{x}_0(k) = [p_{1,k}^1, p_{2,k}^1, ..., p_{s^1-1,k}^1, p_k^{1/2}, p_{1,k}^2, p_{2,k}^2, ..., p_{s^2-1,k}^2, p_k^{2/3}, ..., p_k^{g-1/g}, p_{1,k}^g, p_{2,k}^g ...., p_{s^g-1,k}^g, p_{s^g,k}^g]^T,$$

where each pipe has $s^{pipe}+1$ nodes, then E_0 and A_0 are tridiagonal.

E_0 and A_0 take the form

$$E_0 = \begin{bmatrix} [\mathrm{E}^1]_{\mathrm{x}\,\mathrm{x}\,\mathrm{x}} & & & \\ {}^{\mathrm{x}}[\mathrm{E}^2]_{\mathrm{x}\,\mathrm{x}\,\mathrm{x}} & & & \\ & \ddots & & \\ & & {}^{\mathrm{x}\,\mathrm{x}\,\mathrm{x}}[\mathrm{E}^{g-1}]_{\mathrm{x}\,\mathrm{x}\,\mathrm{x}} & \\ & & {}^{\mathrm{x}}[\mathrm{E}^{g}]_{\mathrm{x}\,\mathrm{x}} \end{bmatrix}$$

$$A_0 = \begin{bmatrix} [\mathrm{A}^1]_{\mathrm{x}\,\mathrm{x}\,\mathrm{x}} & & & \\ {}^{\mathrm{x}}[\mathrm{A}^2]_{\mathrm{x}\,\mathrm{x}\,\mathrm{x}} & & & \\ & \ddots & & \\ & & {}^{\mathrm{x}\,\mathrm{x}\,\mathrm{x}}[\mathrm{A}^{g-1}]_{\mathrm{x}\,\mathrm{x}\,\mathrm{x}} & \\ & & {}^{\mathrm{x}}[\mathrm{A}^{g}]_{\mathrm{x}\,\mathrm{x}} \end{bmatrix}$$

where $[\mathrm{E}^z]$ and $[\mathrm{A}^z]$ are general tridiagonal square blocks containing the coefficients of the inner pressures along pipe z from difference equations (2.17). The blocks, $[\mathrm{E}^z]$ and $[\mathrm{A}^z]$, are sandwiched between single rows corresponding to the $g-1$ connectivity equations (2.23) and downstream flow boundary equation (2.19) for pipe g, and single columns containing the coefficients of the pressures at the pipe junctions and the downstream end. These rows and columns maintain the tridiagonal structure of E_0 and A_0; the non-zero elements of these rows and columns being represented by x^s.

The general i^{th} row of the general rectangular block $[{}^{\mathrm{x}}[\mathrm{E}^z]_{\mathrm{x}}]$ takes the form

$$[0, ..., 0, \quad -r^z\theta\Omega_i^z\Gamma_{i-1}^z \quad , \quad 1 + 2r^z\theta\Omega_i^z\Gamma_i^z \quad , \quad -r^z\theta\Omega_i^z\Gamma_{i+1}^z \quad , 0, ...0],$$

and of the general rectangular block $[{}^{\mathrm{x}}[\mathrm{A}^z]_{\mathrm{x}}]$ takes the form

$$[0, ..., 0, \quad r^z(1-\theta)\Omega_i^z\Gamma_{i-1}^z \quad , \quad 1 - 2r^z(1-\theta)\Omega_i^z\Gamma_i^z \quad , \quad r^z(1-\theta)\Omega_i^z\Gamma_{i+1}^z \quad , 0, ...0],$$

where, for $z = 1$ and $i = 1$ the first nonzero elements of the above general rows are absent.

The row corresponding to a 'connectivity equation' (2.23) at the junction of pipes z and $z+1$, in the E_0 matrix has the form

$$[0, ..., 0, \quad -(\Phi^{z/z+1}\epsilon_3^z\Gamma^z_{s^z-1}\theta/\delta x^z) \quad , \quad (1+\Phi^{z/z+1}\epsilon_3^z\Gamma^{z/z+1}\theta/\delta x^z + \Phi^{z/z+1}\epsilon_3^{z+1}\Gamma^{z/z+1}\theta/\delta x^{z+1}) \quad ,$$

$$-(\Phi^{z/z+1}\epsilon_3^{z+1}\Gamma_1^{z+1}\theta/\delta x^{z+1}) \quad , 0, ...0],$$

and in the A_0 matrix has the form

$$[0, ..., 0, \quad \Phi^{z/z+1}\epsilon_3^z\Gamma^z_{s^z-1}(1-\theta)/\delta x^z \quad , \quad (1-\Phi^{z/z+1}\epsilon_3^z\Gamma^{z/z+1}(1-\theta)/\delta x^z - \Phi^{z/z+1}\epsilon_3^{z+1}\Gamma^{z/z+1}(1-\theta)/\delta x^{z+1}) \quad ,$$

$$\Phi^{z/z+1}\epsilon_3^{z+1}\Gamma_1^{z+1}(1-\theta)/\delta x^{z+1} \quad , 0, ...0].$$

The row corresponding to the flow boundary equation (2.19) at the downstream end, in the E_0 matrix has the form

$$[0, ..., 0, \quad -2r^g\theta\Omega^g_{s^g}\Gamma^g_{s^g-1} \quad , \quad 1+2r^g\theta\Omega^g_{s^g}\Gamma^g_{s^g}],$$

and in the A_0 matrix has the form

$$[0, ..., 0, \quad 2r^g(1-\theta)\Omega^g_{s^g}\Gamma^g_{s^g-1} \quad , \quad 1-2r^g(1-\theta)\Omega^g_{s^g}\Gamma^g_{s^g}].$$

2.4 Theorems

In this section, we firstly prove that the matrix E_0 of an $\mathcal{M}0$ model is full rank if $\theta > 0$. We next prove that the $\mathcal{M}0$ system eigenvalues are real if $\theta > 0$. Lastly, we prove that the $\mathcal{M}0$ system eigenvalues are within the unit circle for $1/2 \leq \theta \leq 1$.

All theorems rely on the following inequalities. $\Gamma^{pipe}_{node} > 0$, $\Gamma^{junction} > 0$, $\delta x^{pipe} > 0$, $r^{pipe} > 0$, $\theta > 0$, $\Omega^{pipe}_{node} > 0$, $\epsilon_3^{pipe} > 0$ and $\Phi^{junction} > 0$ for all pipes, nodes and junctions.

We firstly define three new matrices.

We define the diagonal matrix, D_0, where the i^{th} diagonal element of D_0 is equal to the value of Γ^{pipe}_{node} at the i^{th} node along the linear gas network (starting at node 1 of the upstream pipe section). Since $\Gamma^{pipe}_{node} > 0$ and $\Gamma^{junction} > 0$ by definition, the matrix D_0 is full rank with all diagonal elements positive.

Next, for $\theta \neq 0$, let the matrix $M_0 = -(1/\theta)(I - E_0)$. Then it can be easily verified that

$$E_0 = I + \theta M_0 \tag{2.26}$$

and

$$A_0 = I - (1 - \theta)M_0. \tag{2.27}$$

By inspection, M_0 is real and tridiagonal, with all off-diagonal elements, $m_{i,j}$ with $|i - j| = 1$, non-zero and negative. Hence, from Theorem 12.3 in the appendix, all the eigenvalues of M_0 are real.

Lastly, let $G_0 = M_0 D_0^{-1}$. By inspection, G_0 has the following properties:

- tridiagonal
- diagonally dominant with strict inequality at $i = 1$
- $g_{i,i} > 0$, $g_{i,j} < 0$ for all i and j with $|i - j| = 1$.

From Theorem 12.1 in the appendix, we have that G_0 is full rank.

Theorem 2.1 *If $\theta > 0$, the matrix E_0 of an $\mathcal{M}0$ model is full rank.*

Proof

Let $F_0 = E_0 D_0^{-1}$. Assuming $\theta > 0$, we can derive $F_0 = D_0^{-1} + \theta G_0$, which, due to the properties of D_0 and G_0, must be strictly diagonally dominant. Hence, from Theorem 12.2 in the appendix, F_0 is full rank, and hence $E_0 = F_0 D_0$ must be full rank also. □

Theorem 2.2 *If $\theta > 0$, the eigenvalues of an $\mathcal{M}0$ model are real.*

Proof

Since, if $\theta > 0$, the matrix E_0 is invertible, from equations (2.26), (2.27), we have

$$det(A_0 - \mu E_0) = 0 \iff det((I + \theta M_0)^{-1}(I - (1 - \theta)M_0) - \mu I) = 0.$$

Thus, for $\mu_i \in \lambda(A_0, E_0)$ and $\tau_i \in \lambda(M_0)$, for $i = 1, ..., n$,

$$\mu_i = \frac{1 - (1 - \theta)\tau_i}{1 + \theta\tau_i}$$

where $\lambda(A_0, E_0)$ denotes the spectrum of the matrix $E_0^{-1}A_0$ and $\lambda(M_0)$ denotes the spectrum of the matrix M_0. Hence, since the eigenvalues, τ_i, of M_0 are real then so are the eigenvalues, μ_i, of $(E_0^{-1}A_0)$ real. □

Theorem 2.3 *An $\mathcal{M}0$ model has system eigenvalues within the unit circle, and hence is asymptotically stable, if* $(1/2)\leq\theta\leq 1$.

Proof

From equations (2.26), (2.27), we have

$$det(A_0 - \mu E_0) = det((1-\mu)I + ((1-\mu)\theta - 1)M_0). \tag{2.28}$$

Since the determinant of the product of two matrices is equal to the product of the determinants of the individual matrices, from equation (2.28) we can derive

$$det(A_0 - \mu E_0) = det((1-\mu)D_0^{-1} + ((1-\mu)\theta - 1)G_0)det(D_0).$$

We show $det(A_0 - \mu E_0)\neq 0$ for $|\mu|\geq 1$ and $(1/2)\leq\theta\leq 1$.

The matrix D_0 is full rank, and hence $det(D_0)\neq 0$.

By inspection, if $\mu\geq 1$, then $(1-\mu)\leq 0$ and $((1-\mu)\theta - 1)\leq -1$. Also, if $\mu\leq -1$, then $(1-\mu)\geq 2$ and $((1-\mu)\theta - 1)\geq 0$.

So, for $|\mu|\geq 1$, we have the following two cases.

Case 1) If $((1-\mu)\theta - 1) = 0$ then $(1-\mu)\geq 2$ and $((1-\mu)D_0^{-1} + ((1-\mu)\theta - 1)G_0) = (1-\mu)D_0^{-1}$ which is full rank. Then $det((1-\mu)D_0^{-1} + ((1-\mu)\theta - 1)G_0)\neq 0$.

Case 2) If $((1-\mu)\theta - 1)\neq 0$ then, due to the properties of D_0 and G_0, the matrix $((1-\mu)D_0^{-1} + ((1-\mu)\theta - 1)G_0)$ has the following properties

- tridiagonal
- diagonally dominant with strict inequality for $i = 1$
- off-diagonal elements with $|i-j| = 1$ are non-zero and of opposite sign to diagonal elements.

and, from Theorem 12.1 in the appendix, is full rank.

Then $det((1-\mu)D_0^{-1} + ((1-\mu)\theta - 1)G_0) \neq 0$.

Hence, for $|\mu| \geq 1$, $det(A_0 - \mu E_0) = det((1-\mu)D_0^{-1} + ((1-\mu)\theta - 1)G_0)det(D_0) \neq 0$.

Thus, if $(1/2) \leq \theta \leq 1$, the eigenvalues of the $\mathcal{M}0$ system matrices have modulus less than 1, and the $\mathcal{M}0$ model is asymptotically stable. □

The *Lax stability* [37] of the $\mathcal{M}0$ model is defined in terms of the boundedness of the solution to the finite difference equations at a fixed timestep, T, as δt and δx tend to zero with $r = \delta t/(\delta x)^2$ kept fixed. It is related via Lax's Equivalence Theorem [37] to the convergence of the solution of the $\mathcal{M}0$ system to the solution of the governing differential equations (2.16), as the computational mesh is refined. However, unlike the asymptotic, or Liapunov, stability already investigated above, Lax stability is not directly dependent on the eigenvalues of the system. Some attempt was made to provide proofs of both the Lax stability of the $\mathcal{M}0$ system and the convergence of the solution of the $\mathcal{M}0$ system to the solution of the governing differential equations (2.16), as the computational mesh was refined. Unfortunately, this was not achieved, the difficulty being the space-varying nature of the system coefficients. Two good references that deal with this specific problem are [36] and [16]. Providing such stability and convergence proofs for $\mathcal{M}0$ systems and all other systems explored in this thesis would be a worthwhile area of future research. However, experimentally, the solution of the $\mathcal{M}0$ model was found to be convergent, for both $\theta = 1/2$ and $\theta = 1$, as the computational mesh was refined with $r = 0.6666$ for all pipes.

This base $\mathcal{M}0$ model has also been tested thoroughly in [34] with real gas network data, and was found to model the behaviour of real gas networks quite accurately.

Chapter 3

Formulation of a New $\mathcal{M}1$ Variant Model

The gas networks we wish to estimate are linear with pressure measurement only; and these measurements are only available at the upstream source and at sites of flow demand. We now show how a new model variation, denoted by $\mathcal{M}1$, which is capable of estimating flow demands, may be constructed from a base $\mathcal{M}0$ model. The $\mathcal{M}1$ model is simply a pressure driven model, and is derived from an $\mathcal{M}0$ model by first removing the $g-1$ connectivity equations and the downstream flow boundary equation from the system, and then removing the g flow demand variables. The $\mathcal{M}1$ model is still in the form of a discrete descriptor system, but where the state vector now contains the nodal pressures *except* those pressures at sites of gas outflow. The $\mathcal{M}1$ model is essentially a disconnected set of equations for each pipe.

The base $\mathcal{M}0$ model can be rearranged and partitioned as

$$\begin{bmatrix} \mathcal{E}_{1,1} & \mathcal{E}_{1,2} \\ \mathcal{E}_{2,1} & \mathcal{E}_{2,2} \end{bmatrix} \begin{bmatrix} \underline{p}_1(k+1) \\ \underline{p}_2(k+1) \end{bmatrix} = \begin{bmatrix} \mathcal{A}_{1,1} & \mathcal{A}_{1,2} \\ \mathcal{A}_{2,1} & \mathcal{A}_{2,2} \end{bmatrix} \begin{bmatrix} \underline{p}_1(k) \\ \underline{p}_2(k) \end{bmatrix} + \begin{bmatrix} \mathcal{B}^1_{1,1} & 0 \\ 0 & \mathcal{B}^1_{2,2} \end{bmatrix} \begin{bmatrix} \underline{p}_3(k+1) \\ \underline{d}(k+1) \end{bmatrix} + \begin{bmatrix} \mathcal{B}^2_{1,1} & 0 \\ 0 & \mathcal{B}^2_{2,2} \end{bmatrix} \begin{bmatrix} \underline{p}_3(k) \\ \underline{d}(k) \end{bmatrix}, \tag{3.1}$$

where $\underline{p}_2(k)$ is a g dimensional vector containing measured pressure perturbation state variables at the sites of flow demand, $\underline{p}_1(k)$ is a $n-g$ dimensional vector containing the remaining pressure perturbation state variables along the pipes, $\underline{p}_3(k)$ is the upstream

pressure input (assumed known), and $\underline{d}(k)$ is a g dimensional vector containing the flow demand perturbation input variables that we wish to estimate. The top $n-g$ rows correspond to general difference equations (2.17), and the lower g rows correspond to the $g-1$ connectivity equations and the single downstream flow boundary equation.

The new $\mathcal{M}1$ system has the form

$$\mathcal{E}_{1,1}\underline{p}_1(k+1) = \mathcal{A}_{1,1}\underline{p}_1(k) - \mathcal{E}_{1,2}\underline{p}_2(k+1) + \mathcal{B}^1_{1,1}\underline{p}_3(k+1) + \mathcal{A}_{1,2}\underline{p}_2(k) + \mathcal{B}^2_{1,1}\underline{p}_3(k) \quad (3.2)$$

which can be expressed in the general descriptor system form

$$E_1\underline{x}_1(k+1) = A_1\underline{x}_1(k) + B^1_1\underline{u}_1(k+1) + B^2_1\underline{u}_1(k) \quad (3.3)$$

where

$$\underline{u}_1(k) = [\underline{p}_3(k)^T, \underline{p}_2(k)^T]^T.$$

If we arrange the pressure variables in the state vector in their order along the pipe network, i.e. in the following way

$$\underline{x}_1(k) = [p^1_{1,k}, p^1_{2,k}, ..., p^1_{s^1-1,k}, p^2_{1,k}, p^2_{2,k}, ..., p^2_{s^2-1,k}, ..., p^g_{1,k}, p^g_{2,k}...., p^g_{s^g-1,k}]^T,$$

where each pipe has $s^{pipe}+1$ nodes, then the $\mathcal{M}1$ system matrices, E_1 and A_1, are tridiagonal. E_1 and A_1 take the form

$$E_1 = \begin{bmatrix} [\mathrm{E}^1] & & & & \\ & [\mathrm{E}^2] & & & \\ & & \ddots & & \\ & & & [\mathrm{E}^{g-1}] & \\ & & & & [\mathrm{E}^g] \end{bmatrix}$$

$$A_1 = \begin{bmatrix} [\mathrm{A}^1] & & & & \\ & [\mathrm{A}^2] & & & \\ & & \ddots & & \\ & & & [\mathrm{A}^{g-1}] & \\ & & & & [\mathrm{A}^g] \end{bmatrix}$$

where $[\mathrm{E}^z]$ and $[\mathrm{A}^z]$ are general tridiagonal square blocks containing the coefficients of the inner pressures along pipe z from difference equations (2.17). The general square blocks $[\mathrm{E}^z]$ and $[\mathrm{A}^z]$ are as previously described for the $\mathcal{M}0$ model.

As an $\mathcal{M}1$ model is run, the normalised inline flow perturbations at the ends of each pipe section are estimated by applying a forwards or backwards difference discretisation of equation (2.13). In other words, at the upstream end of a general pipe z, we would have

$$q^z_{0,k} = -\epsilon^z_3(\Gamma^z_1 p^z_{1,k} - \Gamma^z_0 p^z_{0,k})/\delta x^z. \tag{3.4}$$

From [37], approximating the derivative $D_x(\Gamma p)$ by

$$D_x(\Gamma p) \approx (\Gamma^z_1 p^z_{1,k} - \Gamma^z_0 p^z_{0,k})/\delta x^z$$

involves a leading error on the right hand side of order δx^z. At the downstream end, we would have

$$q^z_{s^z,k} = -\epsilon^z_3(\Gamma^z_{s^z} p^z_{s^z,k} - \Gamma^z_{s^z-1} p^z_{s^z-1,k})/\delta x^z. \tag{3.5}$$

Similarly, approximating the derivative $D_x(\Gamma p)$ by

$$D_x(\Gamma p) \approx (\Gamma^z_{s^z} p^z_{s^z,k} - \Gamma^z_{s^z-1} p^z_{s^z-1,k})/\delta x^z$$

involves a leading error on the right hand side of order δx^z. To estimate the demand flow, $d^{z/z+1}_k$ at a general pipe junction $z/z+1$, we use

$$d^{z/z+1}_k = q^z_{s^z,k} - q^{z+1}_{0,k}. \tag{3.6}$$

3.1 Theorems

We are able to derive identical theorems for $\mathcal{M}1$ models as we have done for $\mathcal{M}0$ models. Firstly it is proved that the matrix E_1 of an $\mathcal{M}1$ model is full rank if $\theta > 0$. Then it is proved that the $\mathcal{M}1$ system eigenvalues are real if $\theta > 0$. Finally, it is proved that the $\mathcal{M}1$ system eigenvalues are within the unit circle for $1/2 \leq \theta \leq 1$.

As with $\mathcal{M}0$ models, all theorems rely on the following inequalities. $\Gamma^{pipe}_{node} > 0$, $\Gamma^{junction} > 0$, $\delta x^{pipe} > 0$, $r^{pipe} > 0$, $\theta > 0$, $\Omega^{pipe}_{node} > 0$, $\epsilon^{pipe}_3 > 0$ and $\Phi^{junction} > 0$ for all

pipes, nodes and junctions.

We firstly define three new types of matrix.

We define the general diagonal matrix, D^z, corresponding to pipe z for $z = 1, ..., g$, where the i^{th} diagonal element of D^z is equal to the value of Γ_i^z for $i = 1, ..., s^z - 1$. Since $\Gamma_{node}^{pipe} > 0$, the matrices D^z are full rank with all diagonal elements positive.

Next, for $\theta \neq 0$, we define the general matrix M^z, corresponding to pipe z for $z = 1, ..., g$, where $\mathrm{M}^z = -(1/\theta)(I - \mathrm{E}^z)$. Then it can be easily verified that

$$\mathrm{E}^z = I + \theta \mathrm{M}^z \tag{3.7}$$

and

$$\mathrm{A}^z = I - (1 - \theta)\mathrm{M}^z. \tag{3.8}$$

By inspection, the matrices M^z are real and tridiagonal, with all the off-diagonal elements, $m_{i,j}^z$ with $|i - j| = 1$, non-zero and negative. Hence, from Theorem 12.3 in the appendix, all the eigenvalues of the matrices M^z are real.

Lastly, we define the general matrix G^z, corresponding to pipe z for $z = 1, ..., g$, where $\mathrm{G}^z = \mathrm{M}^z \mathrm{D}^{z^{-1}}$. By inspection, the matrices G^z have the following properties:

- tridiagonal
- diagonally dominant with strict inequality at $i = 1$ and $i = s^z - 1$
- $g_{i,i} > 0$, $g_{i,j} < 0$ for all i and j with $|i - j| = 1$.

From Theorem 12.1 in the appendix, we have that the matrices G^z are full rank.

Theorem 3.1 *If $\theta > 0$, The matrix E_1 of an $\mathcal{M}1$ model is full rank.*

Proof

To show the matrix E_1 is full rank, we show the matrix blocks, E^z, are full rank.

For a general pipe section z, let $\mathrm{F}^z = \mathrm{E}^z\mathrm{D}^{z^{-1}}$. Assuming $\theta > 0$, we can derive $\mathrm{F}^z = \mathrm{D}^{z^{-1}} + \theta\mathrm{G}^z$, which, due to the properties of D^z and G^z, must be strictly diagonally dominant. Hence, from Theorem 12.2 in the appendix, F^z is full rank, and hence $\mathrm{E}^z = \mathrm{F}^z\mathrm{D}^z$ must be full rank also. □

Theorem 3.2 *If $\theta > 0$, the eigenvalues of an $\mathcal{M}1$ model are real.*

Proof

To show the eigenvalues of an $\mathcal{M}1$ model are real, we show the eigenvalues of the blocks $\mathrm{E}^{z^{-1}}\mathrm{A}^z$ are real.

For a general pipe section z, since the matrix E^z is invertible if $\theta > 0$, from equations (3.7), (3.8), we have

$$det(\mathrm{A}^z - \mu\mathrm{E}^z) = 0 \Longleftrightarrow det((I + \theta\mathrm{M}^z)^{-1}(I - (1-\theta)\mathrm{M}^z) - \mu I) = 0.$$

Thus, for $\mu_i \in \lambda(\mathrm{A}^z, \mathrm{E}^z)$ and $\tau_i \in \lambda(\mathrm{M}^z)$, for $i = 1, ..., s^z - 1$,

$$\mu_i = \frac{1 - (1-\theta)\tau_i}{1 + \theta\tau_i}.$$

Hence, since the eigenvalues, τ_i, of M^z are real then so are the eigenvalues, μ_i, of $(\mathrm{E}^{z^{-1}}\mathrm{A}^z)$ real. □

Theorem 3.3 *An $\mathcal{M}1$ model has system eigenvalues within the unit circle, and hence is asymptotically stable, if $(1/2) \leq \theta \leq 1$.*

Proof

To show the eigenvalues of an $\mathcal{M}1$ model are within the unit circle, we show the eigenvalues of the blocks $\mathrm{E}^{z^{-1}}\mathrm{A}^z$ are within the unit circle.

For a general pipe section z, from equations (3.7), (3.8), we have

$$det(\mathrm{A}^z - \mu\mathrm{E}^z) = det((1-\mu)I + ((1-\mu)\theta - 1)\mathrm{M}^z). \tag{3.9}$$

Since the determinant of the product of two matrices is equal to the product of the determinants of the individual matrices, from equation (3.9) we can derive

$$det(\mathrm{A}^z - \mu \mathrm{E}^z) = det((1-\mu)\mathrm{D}^{z^{-1}} + ((1-\mu)\theta - 1)\mathrm{G}^z) det(\mathrm{D}^z).$$

We show $det(\mathrm{A}^z - \mu \mathrm{E}^z) \neq 0$ for $|\mu| \geq 1$ and $(1/2) \leq \theta \leq 1$.

The matrix D^z is full rank, and hence $det(\mathrm{D}^z) \neq 0$.

By inspection, if $\mu \geq 1$, then $(1-\mu) \leq 0$ and $((1-\mu)\theta - 1) \leq -1$. Also, if $\mu \leq -1$, then $(1-\mu) \geq 2$ and $((1-\mu)\theta - 1) \geq 0$.

So, for $|\mu| \geq 1$, we have the following two cases.

Case 1) If $((1-\mu)\theta - 1) = 0$ then $(1-\mu) \geq 2$ and $((1-\mu)\mathrm{D}^{z^{-1}} + ((1-\mu)\theta - 1)\mathrm{G}^z) = (1-\mu)\mathrm{D}^{z^{-1}}$ which is full rank. Then $det((1-\mu)\mathrm{D}^{z^{-1}} + ((1-\mu)\theta - 1)\mathrm{G}^z) \neq 0$.

Case 2) If $((1-\mu)\theta - 1) \neq 0$ then, due to the properties of D^z and G^z, the matrix $((1-\mu)\mathrm{D}^{z^{-1}} + ((1-\mu)\theta - 1)\mathrm{G}^z)$ has the following properties

- tridiagonal
- diagonally dominant with strict inequality for $i = 1$ and $i = s^z - 1$
- off-diagonal elements with $|i - j| = 1$ are non-zero and of opposite sign to diagonal elements.

and, from Theorem 12.1 in the appendix, is full rank.

Then $det((1-\mu)\mathrm{D}^{z^{-1}} + ((1-\mu)\theta - 1)\mathrm{G}^z) \neq 0$.

Hence, for $|\mu| \geq 1$, $det(\mathrm{A}^z - \mu \mathrm{E}^z) = det((1-\mu)\mathrm{D}^{z^{-1}} + ((1-\mu)\theta - 1)\mathrm{G}^z) det(\mathrm{D}^z) \neq 0$.

Thus, if $(1/2) \leq \theta \leq 1$, the eigenvalues of the matrix blocks $\mathrm{E}^{z^{-1}}\mathrm{A}^z$ have modulus less than 1. □

3.2 Experiments

For all experiments in this thesis, a standard $\mathcal{M}0$ model of the linear three pipe network from chapter 1, was run to simulate a real gas network with the upstream pressure, junction demand flows, and downstream flow demand specified as boundary inputs to the system. The parameters for this base $\mathcal{M}0$ model, and all other models investigated in this thesis, are given in the appendix. Except for a few experiments in chapter 10, the flows at demand sites A/B, B/C and C were in the ratio 2:5:13.

When the $\mathcal{M}0$ model had been running for a while, the pressures at the upstream end and the sites of flow demand were recorded at each timestep and fed into an $\mathcal{M}1$ model. The flow demands predicted by the $\mathcal{M}1$ model were then compared with the true flows used as inputs to the $\mathcal{M}0$ model. For experiments 3.1 to 3.3, the $\mathcal{M}0$ model simulating a gas network was identical to the $\mathcal{M}0$ model upon which the $\mathcal{M}1$ model was constructed. For experiments 3.4 and 3.5, the $\mathcal{M}0$ model simulating a gas network had a much finer discretisation (in both space and time) than the $\mathcal{M}1$ model to give some idea of the effects of the modelling error due to the finite difference approximation of the original differential equations.

For each experiment, the true flow demand profiles for the demands, $D_k^{A/B}$, $D_k^{B/C}$ and D_k^C are shown as thick lines in Figs. A, B and C respectively, and the state estimates for $D_k^{A/B}$, $D_k^{B/C}$ and D_k^C are shown as thin lines. The percentage errors between the state estimates of $D_k^{A/B}$, $D_k^{B/C}$ and D_k^C and their true values are shown in Figs. D, E and F respectively.

Since, throughout this thesis, the different state estimation techniques tended to produce large errors during the first few timesteps, the results graphs may begin only after a few timesteps have already passed.

Data taken from $\mathcal{M}0$ model with identical mesh - both $\mathcal{M}0$ and $\mathcal{M}1$ models have 5 spatial nodes along each pipe.

Experiment 3.1) $\mathcal{M}1$ Model with $\theta = 1$

Experiment 3.2) $\mathcal{M}1$ Model with $\theta = 0.75$

Experiment 3.3) $\mathcal{M}1$ Model with $\theta = 0.5$

Data taken from $\mathcal{M}0$ model with much finer mesh - $\mathcal{M}1$ model has 5 spatial nodes along each pipe.

Experiment 3.4) $\mathcal{M}1$ Model with $\theta = 1$

Data taken from $\mathcal{M}0$ model with much finer mesh - $\mathcal{M}1$ model has 10 spatial nodes along each pipe.

Experiment 3.5) $\mathcal{M}1$ Model with $\theta = 1$

Experiment 3.1

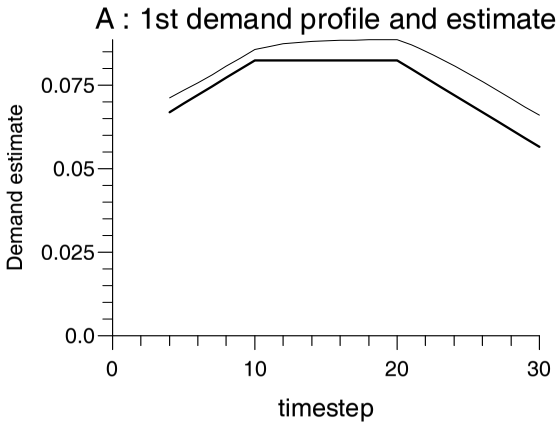

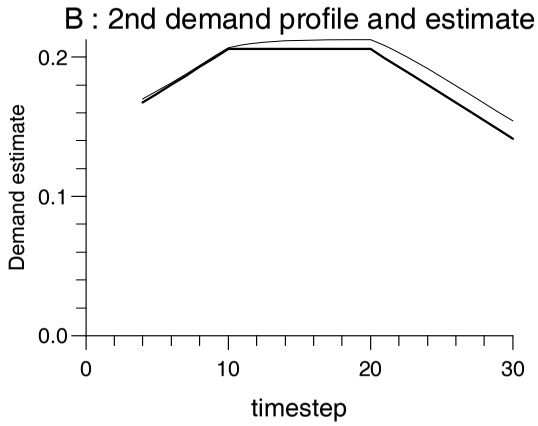

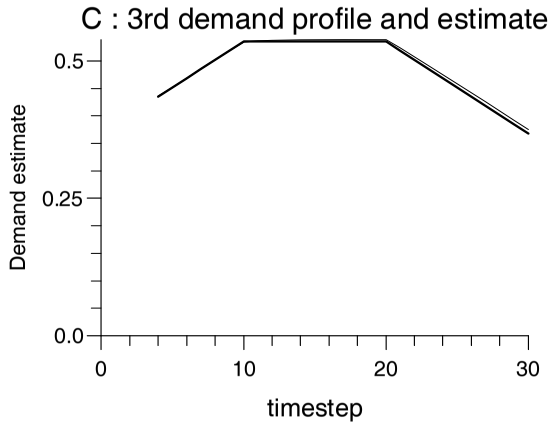

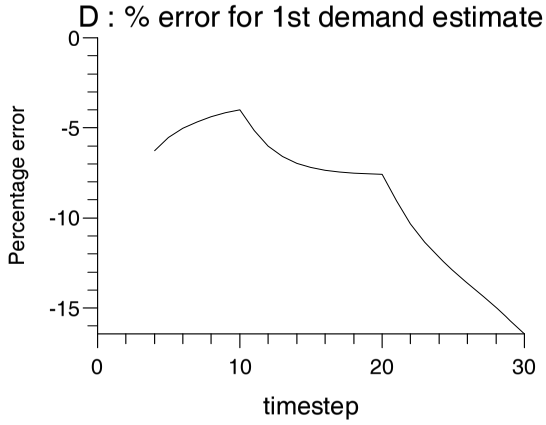

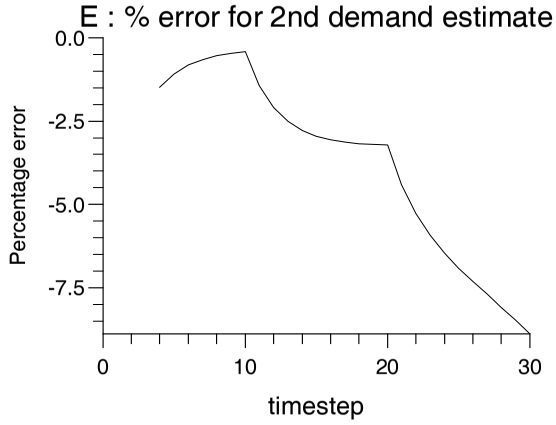

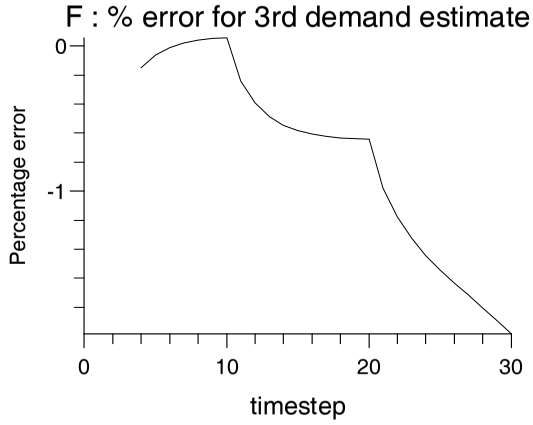

Experiment 3.2

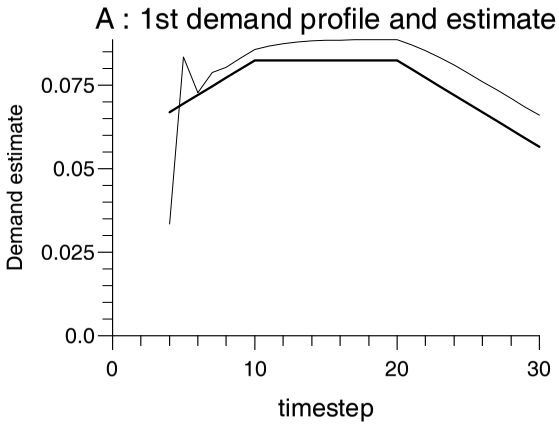

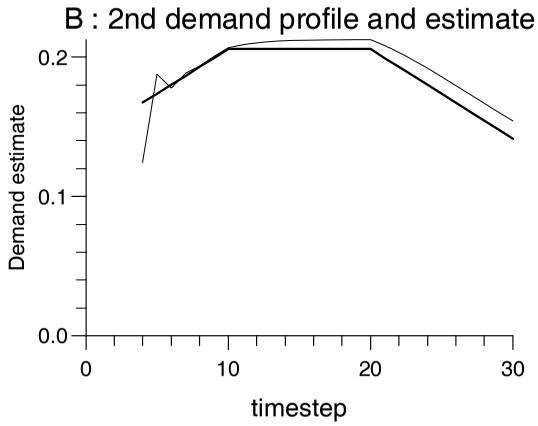

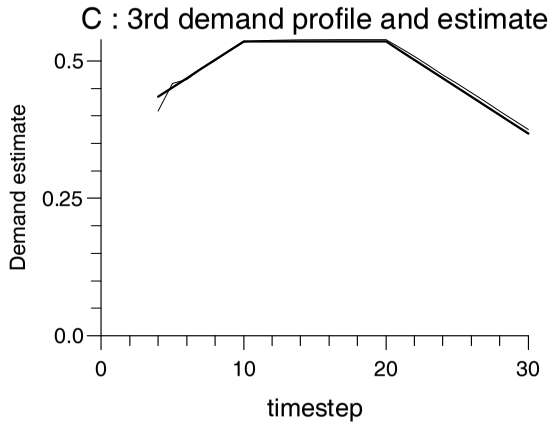

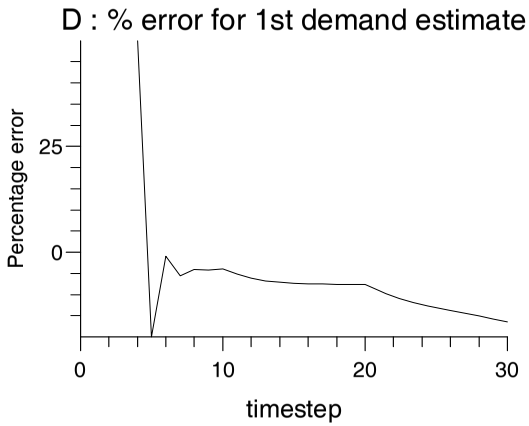

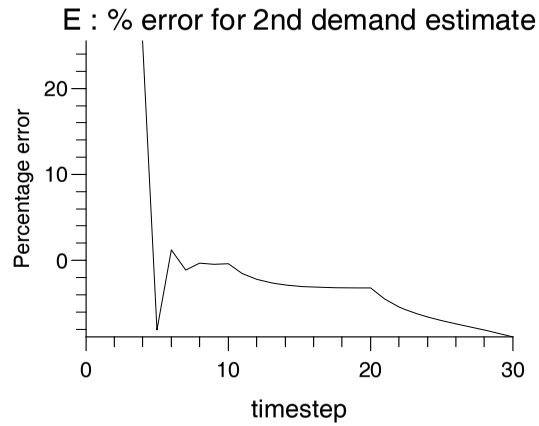

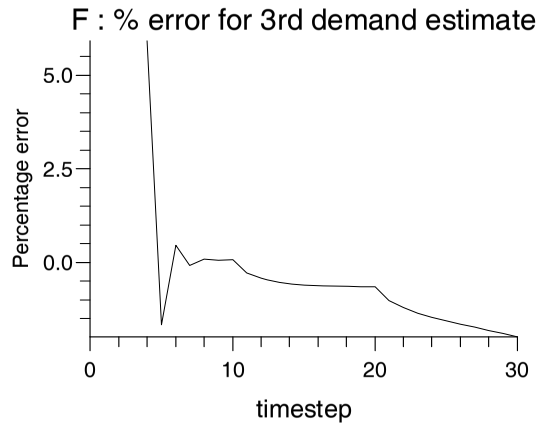

Experiment 3.3

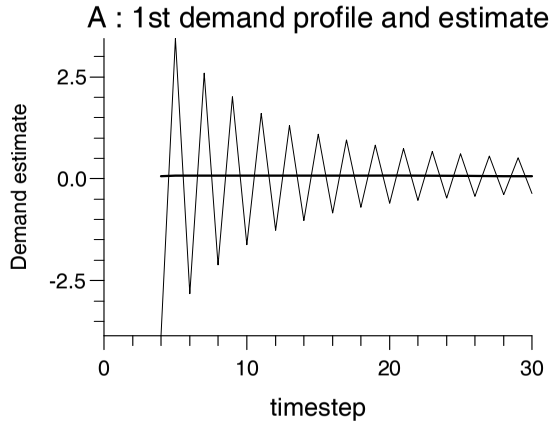

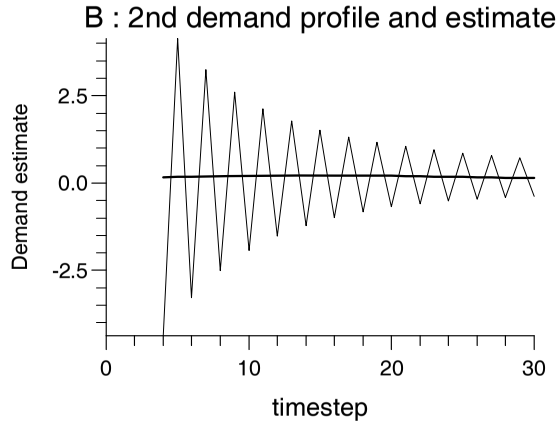

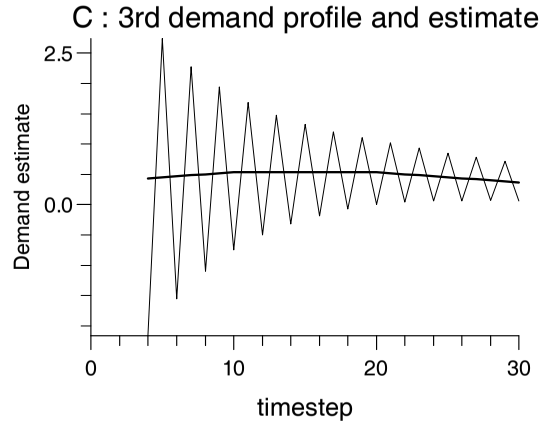

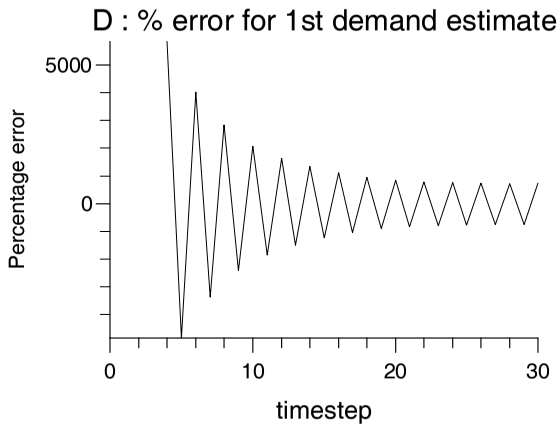

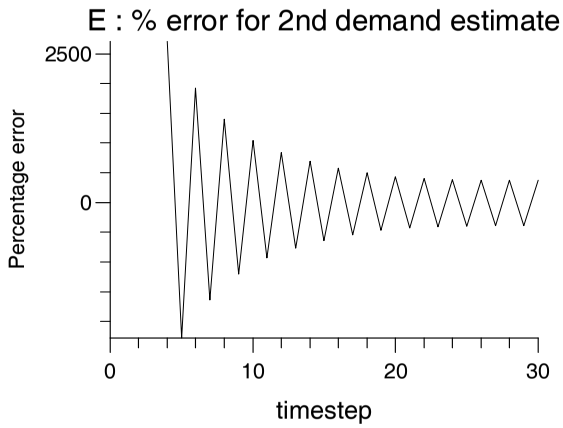

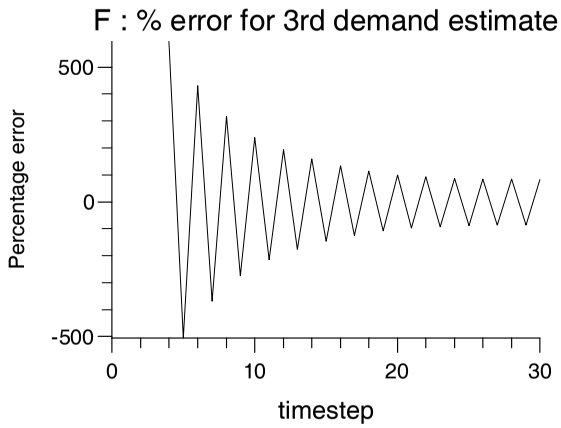

Experiment 3.4

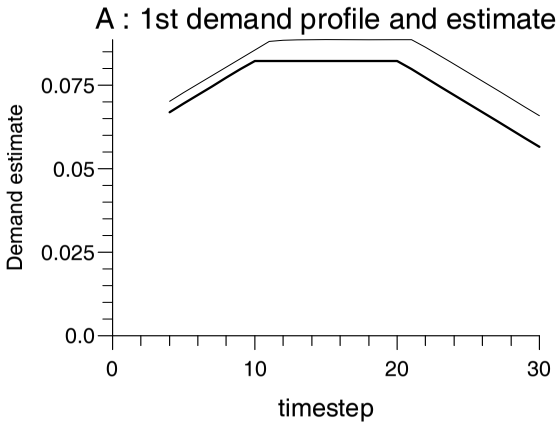

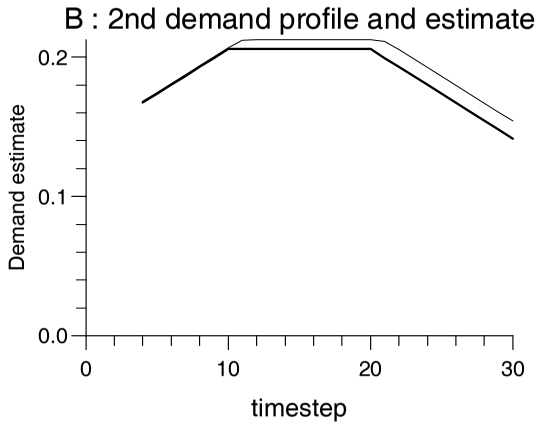

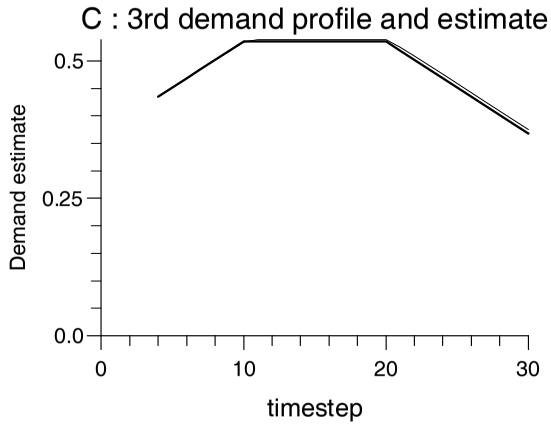

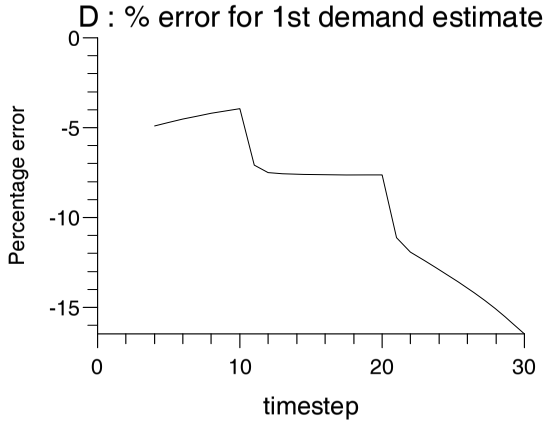

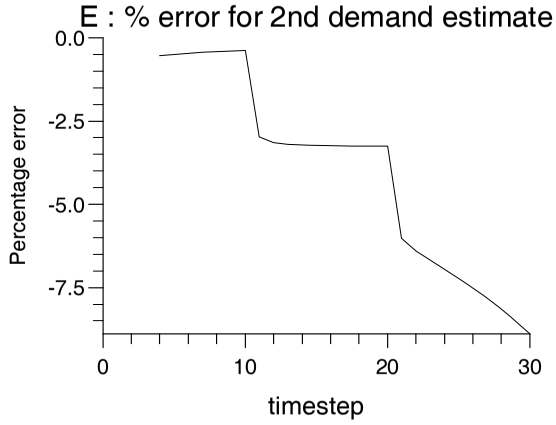

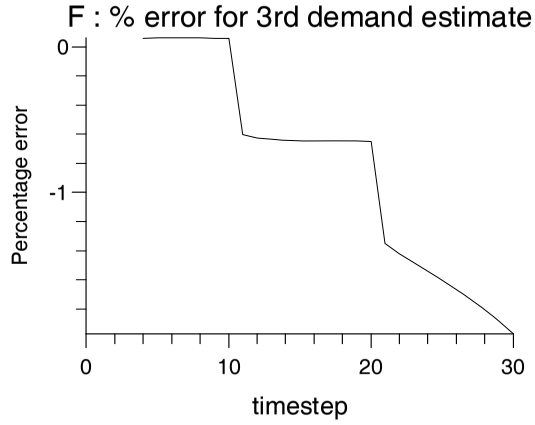

Experiment 3.5

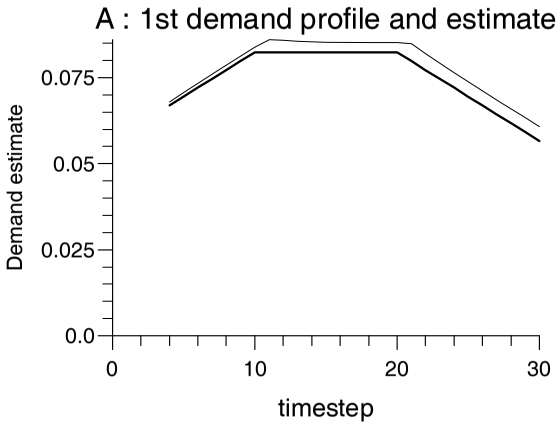

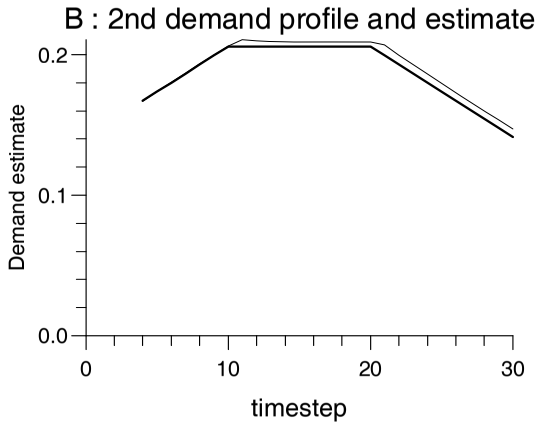

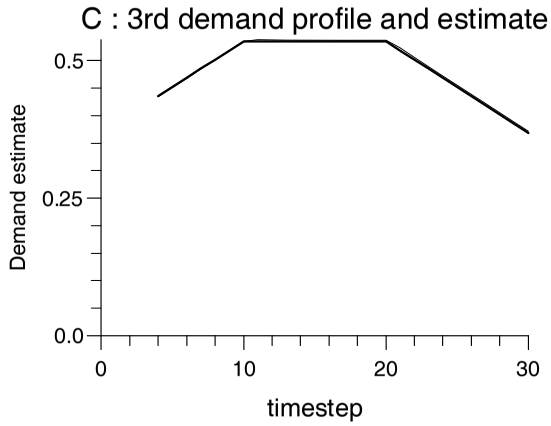

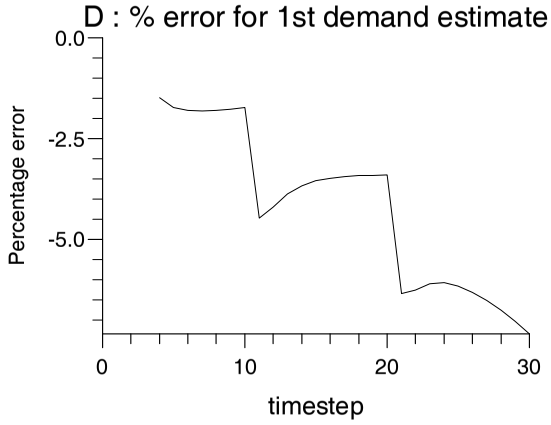

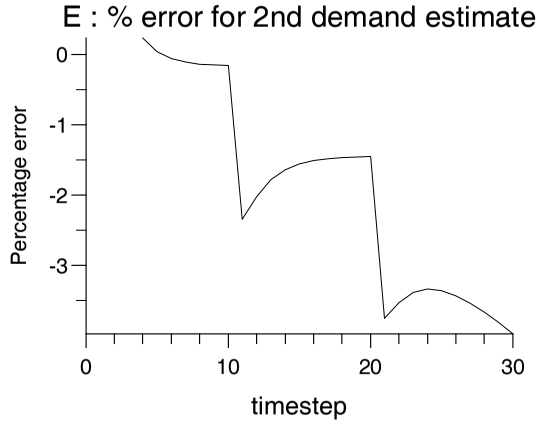

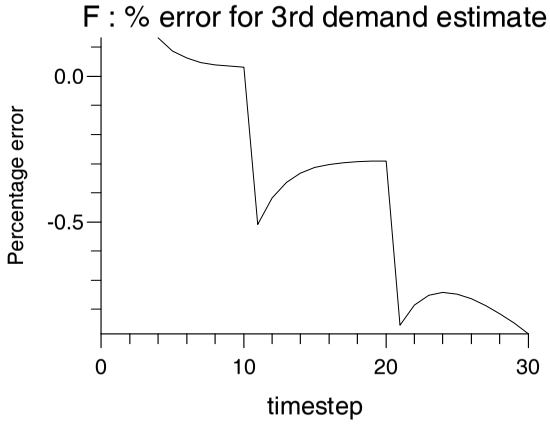

3.3 Discussion

In all experiments, there was some error due to the crude forwards and backwards difference approximations used to discretise equation (2.13). However, as the computational mesh of the $\mathcal{M}1$ model was refined, this error decreased. No theoretical analysis is presented here to prove that such error should decay as the computational mesh is refined, and the possibility of such analysis would be worth exploring. As mentioned in the previous chapter, two good references for this problem are [36] and [16]. From the experiments with pressure data taken from an $\mathcal{M}0$ model constructed upon a much finer mesh, it could be seen that the modelling error introduced by discretising the original differential equations would not affect the flow estimates too adversely if a sufficiently fine computational mesh was used.

For $\theta = 1/2$, the $\mathcal{M}1$ model converged very slowly to a reasonable estimate of the flow demands. However, as θ moved closer to 1, it was found experimentally that the eigenvalues of the $\mathcal{M}1$ system tended to move closer to the origin, and there was faster convergence. For experiments 3.1, 3.2 and 3.3, the $\mathcal{M}1$ system eigenvalues for various values of θ are given in the following table.

$\theta = 1$	$\theta = 0.75$	$\theta = 0.5$
0.04677	−0.25145	−0.82126
0.01417	−0.30826	−0.94411
0.00834	−0.31854	−0.96689
0.04568	−0.25333	−0.82524
0.01383	−0.30886	−0.94543
0.00814	−0.31889	−0.96769
0.03679	−0.26871	−0.85804
0.01106	−0.31373	−0.95622
0.00651	−0.32178	−0.97412

Hence, the choice of θ is to some extent a balance between the order of accuracy of the finite difference scheme, and the speed of convergence of the system.

The main disadvantage of an $\mathcal{M}1$ model is the error introduced into the state estimate by the crude forwards and backwards difference approximations used to discretise

equation (2.13). In the next chapter we investigate a new model, which we term an $\mathcal{M}2$ model, which uses a central difference approximation of equation (2.13). It is shown that the flow estimates of such a model contain significantly less error.

Chapter 4

Formulation of a New $\mathcal{M}2$ Variant Model

We now show how a new pressure driven model variation, denoted by $\mathcal{M}2$, which is capable of estimating flow demands from the available pressure telemetry, may be constructed from a base $\mathcal{M}0$ model using the same central difference discretisation of equation (2.13) that the base $\mathcal{M}0$ model uses. The $\mathcal{M}2$ model is derived from an $\mathcal{M}0$ model by swapping over the flow variables from the input vector with the local pressure variables from the state vector. It is still in the form of a discrete descriptor system, but where the state vector now contains the demand flows and all nodal pressures *except* those pressures at sites of gas outflow. The new input vector now contains those pressures at sites of gas outflow.

The base $\mathcal{M}0$ model can be rearranged and partitioned as

$$\begin{bmatrix} E' & E'' \end{bmatrix} \begin{bmatrix} \underline{p}_1(k+1) \\ \underline{p}_2(k+1) \end{bmatrix} = \begin{bmatrix} A' & A'' \end{bmatrix} \begin{bmatrix} \underline{p}_1(k) \\ \underline{p}_2(k) \end{bmatrix} + \begin{bmatrix} B^{1'} & B^{1''} \end{bmatrix} \begin{bmatrix} \underline{p}_3(k+1) \\ \underline{d}(k+1) \end{bmatrix} + \begin{bmatrix} B^{2'} & B^{2''} \end{bmatrix} \begin{bmatrix} \underline{p}_3(k) \\ \underline{d}(k) \end{bmatrix}, \tag{4.1}$$

where $\underline{p}_1$, $\underline{p}_2$, $\underline{p}_3$ and $\underline{d}$ are as described earlier.

The new $\mathcal{M}2$ system has the form

$$\begin{bmatrix} E' & -B^{1''} \end{bmatrix} \begin{bmatrix} \underline{p}_1(k+1) \\ \underline{d}(k+1) \end{bmatrix} = \begin{bmatrix} A' & B^{2''} \end{bmatrix} \begin{bmatrix} \underline{p}_1(k) \\ \underline{d}(k) \end{bmatrix} + \begin{bmatrix} B^{1'} & -E'' \end{bmatrix} \begin{bmatrix} \underline{p}_3(k+1) \\ \underline{p}_2(k+1) \end{bmatrix}$$

$$+ \begin{bmatrix} B^{2'} & A'' \end{bmatrix} \begin{bmatrix} \underline{p}_3(k) \\ \underline{p}_2(k) \end{bmatrix} \tag{4.2}$$

which can be expressed in the general descriptor system form

$$E_2 \underline{x}_2(k+1) = A_2 \underline{x}_2(k) + B_2^1 \underline{u}_2(k+1) + B_2^2 \underline{u}_2(k). \tag{4.3}$$

4.1 Theorems

We are able to derive similar theoretical results as for $\mathcal{M}0$ and $\mathcal{M}1$ models; however, sufficient conditions for asymptotic stability are slightly more restrictive. Firstly, we prove that the matrix E_2 of an $\mathcal{M}2$ model is full rank if $\theta > 0$. It is then proved that the $\mathcal{M}2$ system eigenvalues are real if $\theta > 0$. Next, it is proved that the $\mathcal{M}2$ system eigenvalues are within the unit circle for $1/2 < \theta \leq 1$, and are within or on the unit circle for $\theta = 1/2$. Lastly, we prove the following. When pressure data is fed from a base $\mathcal{M}0$ model into its corresponding $\mathcal{M}2$ model, then, if the $\mathcal{M}2$ model is asymptotically stable, the system state of the $\mathcal{M}2$ model tends with time to the state of the base $\mathcal{M}0$ model and its flow inputs.

As with $\mathcal{M}0$ models, all theorems rely on the following inequalities. $\Gamma_{node}^{pipe} > 0$, $\Gamma^{junction} > 0$, $\delta x^{pipe} > 0$, $r^{pipe} > 0$, $\theta > 0$, $\Omega_{node}^{pipe} > 0$, $\epsilon_3^{pipe} > 0$ and $\Phi^{junction} > 0$ for all pipes, nodes and junctions.

If the base $\mathcal{M}0$ model is rearranged and partitioned as equation (3.1), then the corresponding $\mathcal{M}2$ model has the form

$$\begin{bmatrix} \mathcal{E}_{1,1} & 0 \\ \mathcal{E}_{2,1} & -\mathcal{B}_{2,2}^1 \end{bmatrix} \begin{bmatrix} \underline{p}_1(k+1) \\ \underline{d}(k+1) \end{bmatrix} = \begin{bmatrix} \mathcal{A}_{1,1} & 0 \\ \mathcal{A}_{2,1} & \mathcal{B}_{2,2}^2 \end{bmatrix} \begin{bmatrix} \underline{p}_1(k) \\ \underline{d}(k) \end{bmatrix} + \begin{bmatrix} \mathcal{B}_{1,1}^1 & -\mathcal{E}_{1,2} \\ 0 & -\mathcal{E}_{2,2} \end{bmatrix} \begin{bmatrix} \underline{p}_3(k+1) \\ \underline{p}_2(k+1) \end{bmatrix}$$

$$+ \begin{bmatrix} \mathcal{B}_{1,1}^2 & \mathcal{A}_{1,2} \\ 0 & \mathcal{A}_{2,2} \end{bmatrix} \begin{bmatrix} \underline{p}_3(k) \\ \underline{p}_2(k) \end{bmatrix}. \tag{4.4}$$

We can immediately see that the spectrum of an $\mathcal{M}2$ system contains all the eigenvalues of the corresponding $\mathcal{M}1$ system.

If the flow demand perturbation variables are arranged in the $\mathcal{M}2$ state vector in their order along the pipe network, i.e.

$$\underline{d}(k) = [d_k^{1/2}, d_k^{2/3}, ..., d_k^{g-1/g}, d_k^g]^T,$$

then the $g \times g$ matrix blocks $\mathcal{B}_{2,2}^1$ and $\mathcal{B}_{2,2}^2$ are diagonal. For $i = 1, ..., g-1$, the i^{th} diagonal elements of $-\mathcal{B}_{2,2}^1$ and $\mathcal{B}_{2,2}^2$ are $\Phi^{i/i+1}\theta$ and $-\Phi^{i/i+1}(1-\theta)$ respectively. The g^{th} diagonal elements of $-\mathcal{B}_{2,2}^1$ and $\mathcal{B}_{2,2}^2$ are $2\theta\Omega_{sg}^g r^g \delta x^g/\epsilon_3^g$ and $-2(1-\theta)\Omega_{sg}^g r^g \delta x^g/\epsilon_3^g$ respectively.

Theorem 4.1 *If $\theta > 0$, the matrix E_2 of an $\mathcal{M}2$ model is full rank.*

Proof

For $\theta \neq 0$, it may be seen that the matrix block $-\mathcal{B}_{2,2}^1$ is a diagonal matrix with all diagonal elements non-zero. Hence, $-\mathcal{B}_{2,2}^1$ is full rank. Also, by Theorem 3.1, the matrix block $\mathcal{E}_{1,1}$ is full rank for $\theta > 0$. Hence, by inspection of the structure of E_2, we see that E_2 is full rank. □

Theorem 4.2 *If $\theta > 0$, the eigenvalues of an $\mathcal{M}2$ model are real.*

Proof

From equation (4.4), it can be seen that the eigenvalues, μ_i, of an $\mathcal{M}2$ system are given by the values of μ for which

$$det(A_2 - \mu E_2) = det(\begin{bmatrix} \mathcal{A}_{1,1} & 0 \\ \mathcal{A}_{2,1} & \mathcal{B}_{2,2}^2 \end{bmatrix} - \mu \begin{bmatrix} \mathcal{E}_{1,1} & 0 \\ \mathcal{E}_{2,1} & -\mathcal{B}_{2,2}^1 \end{bmatrix}) = 0.$$

Hence the eigenvalues, μ_i, of an $\mathcal{M}2$ system are given by the eigenvalues of the matrix blocks $\mathcal{E}_{1,1}^{-1}\mathcal{A}_{1,1}$ and $(-\mathcal{B}_{2,2}^1)^{-1}\mathcal{B}_{2,2}^2$. By Theorem 3.2, if $\theta > 0$, the eigenvalues of $\mathcal{E}_{1,1}^{-1}\mathcal{A}_{1,1}$ are real. By inspection, $(-\mathcal{B}_{2,2}^1)^{-1}\mathcal{B}_{2,2}^2$ is a diagonal matrix with real diagonal elements $-(1-\theta)/\theta$, and hence real eigenvalues. Hence, the eigenvalues of an $\mathcal{M}2$ model are real. □

Theorem 4.3 *The eigenvalues of an $\mathcal{M}2$ model have modulus less than 1 if $(1/2) < \theta \leq 1$, and have modulus less than or equal to 1 if $\theta = (1/2)$ (in which case there are g eigenvalues equal to -1).*

Proof

Above it was shown that the eigenvalues, μ_i, of an $\mathcal{M}2$ system are given by the eigenvalues of the matrix blocks $\mathcal{E}_{1,1}^{-1}\mathcal{A}_{1,1}$ and $(-\mathcal{B}_{2,2}^{1})^{-1}\mathcal{B}_{2,2}^{2}$. By Theorem 3.3, the eigenvalues of $\mathcal{E}_{1,1}^{-1}\mathcal{A}_{1,1}$ are within the unit circle for $1/2 \leq \theta \leq 1/2$. The eigenvalues of $(-\mathcal{B}_{2,2}^{1})^{-1}\mathcal{B}_{2,2}^{2}$ are its diagonal elements $-(1-\theta)/\theta$. For $\theta = 1/2$ these diagonal elements are equal to -1, and hence the $\mathcal{M}2$ system will have g eigenvalues equal to -1. For $(1/2) < \theta \leq 1$, we have $|(1-\theta)| < 1/2$, and hence we have $|(1-\theta)|/|\theta| < 1$. Thus, for $(1/2) < \theta \leq 1$, we have $|-(1-\theta)/\theta| < 1$ and the g eigenvalues of $(-\mathcal{B}_{2,2}^{1})^{-1}\mathcal{B}_{2,2}^{2}$ are within the unit circle. □

The advantage of an $\mathcal{M}2$ model over an $\mathcal{M}1$ model is that an $\mathcal{M}2$ model uses the original $g-1$ 'connectivity equations' (2.23) and the single downstream flow boundary equation (2.19) in the estimation of the flow demands. These flow equations are based on *central* difference approximations of equation (2.13); whereas to estimate the flow demands with an $\mathcal{M}1$ model requires the use of less accurate forward or backward differences of equation (2.13). For $\mathcal{M}2$ models we have the following theorem.

Theorem 4.4 *When pressure data is fed from a base $\mathcal{M}0$ model into its corresponding $\mathcal{M}2$ model, then for $1/2 < \theta \leq 1$, the system state of the $\mathcal{M}2$ model tends with time to the state of the base $\mathcal{M}0$ model and its flow inputs.*

Proof

We can rewrite the $\mathcal{M}0$ model as

$$E'\underline{p}_1(k+1) + E''\underline{p}_2(k+1) - B^{1'}\underline{p}_3(k+1) - B^{1''}\underline{d}(k+1) =$$

$$A'\underline{p}_1(k) + A''\underline{p}_2(k) + B^{2'}\underline{p}_3(k) + B^{2''}\underline{d}(k) \tag{4.5}$$

and we can rewrite the $\mathcal{M}2$ model as

$$E'\underline{\tilde{p}}_1(k+1) + E''\underline{p}_2(k+1) - B^{1'}\underline{p}_3(k+1) - B^{1''}\underline{\tilde{d}}(k+1) =$$

$$A'\underline{\tilde{p}}_1(k) + A''\underline{p}_2(k) + B^{2'}\underline{p}_3(k) + B^{2''}\underline{\tilde{d}}(k) \tag{4.6}$$

where the $\mathcal{M}2$ state vector is

$$\underline{x}_2(k) = [\tilde{\underline{p}}_1^T(k)\ ,\ \tilde{\underline{d}}^T(k)]^T.$$

Subtracting equation (4.6) from equation (4.5) gives

$$E'(\underline{p}_1(k+1) - \tilde{\underline{p}}_1(k+1)) - B^{1''}(\underline{d}(k+1) - \tilde{\underline{d}}(k+1)) = A'(\underline{p}_1(k) - \tilde{\underline{p}}_1(k)) + B^{2''}(\underline{d}(k) - \tilde{\underline{d}}(k)). \tag{4.7}$$

If we define the errors

$$\underline{e}_1(k) = \underline{p}_1(k) - \tilde{\underline{p}}_1(k)$$

$$\underline{e}_2(k) = \underline{d}(k) - \tilde{\underline{d}}(k)$$

then equation (4.7) becomes

$$E'\underline{e}_1(k+1) - B^{1''}\underline{e}_2(k+1) = A'\underline{e}_1(k) + B^{2''}\underline{e}_2(k). \tag{4.8}$$

Equation (4.8) can be arranged as the system

$$E_2\underline{e}(k+1) = A_2\underline{e}(k)$$

where $\underline{e}(k)$ is n dimensional and has the form

$$\underline{e}(k) = \begin{bmatrix} \underline{e}_1(k) \\ \underline{e}_2(k) \end{bmatrix}$$

and E_2 and A_2 are identical to the system matrices of the $\mathcal{M}2$ model.

From Theorem 4.3, if $1/2 < \theta \leq 1$ then $\mathcal{M}2$ system is asymptotically stable, and we can see that the error, $\underline{e}(k)$, decays away. Then the system state of the $\mathcal{M}2$ model tends with time to the state of the base $\mathcal{M}0$ model and its flow inputs. □

If a real gas network, from which pressure data was taken to drive the $\mathcal{M}2$ model, was accurately modelled by the base $\mathcal{M}0$ model, then for $\theta \in (1/2, 1]$ the $\mathcal{M}2$ model state should tend to the true state of the gas network.

4.2 Experiments

When the $\mathcal{M}0$ model had been running for a while, the pressures at the upstream end and the sites of flow demand were recorded at each timestep and fed into an $\mathcal{M}2$ model. The

flow demands predicted by the $\mathcal{M}2$ model were then compared with the true flows used as inputs to the $\mathcal{M}0$ model. For experiments 4.1 to 4.3, the $\mathcal{M}0$ model simulating a gas network was identical to the $\mathcal{M}0$ model upon which the $\mathcal{M}2$ model was constructed. For experiment 4.4, the $\mathcal{M}0$ model simulating a gas network had a much finer discretisation (in both space and time) than the $\mathcal{M}2$ model.

For each experiment, the true flow demand profiles for the demands, $D_k^{A/B}$, $D_k^{B/C}$ and D_k^C are shown as thick lines in Figs. A, B and C respectively and the state estimates for $D_k^{A/B}$, $D_k^{B/C}$ and D_k^C are shown as thin lines. The percentage errors between the state estimates of $D_k^{A/B}$, $D_k^{B/C}$ and D_k^C and their true values are shown in Figs. D, E and F respectively.

Data taken from $\mathcal{M}0$ model with identical mesh - both $\mathcal{M}0$ and $\mathcal{M}2$ models have 10 spatial nodes along each pipe.

Experiment 4.1) $\mathcal{M}2$ Model with $\theta = 1$

Experiment 4.2) $\mathcal{M}2$ Model with $\theta = 0.75$

Experiment 4.3) $\mathcal{M}2$ Model with $\theta = 0.5$

Data taken from $\mathcal{M}0$ model with much finer mesh - $\mathcal{M}2$ model has 10 spatial nodes along each pipe.

Experiment 4.4) $\mathcal{M}2$ Model with $\theta = 1$

Experiment 4.1

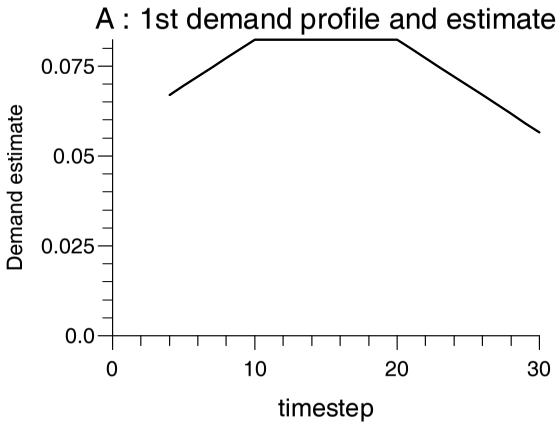

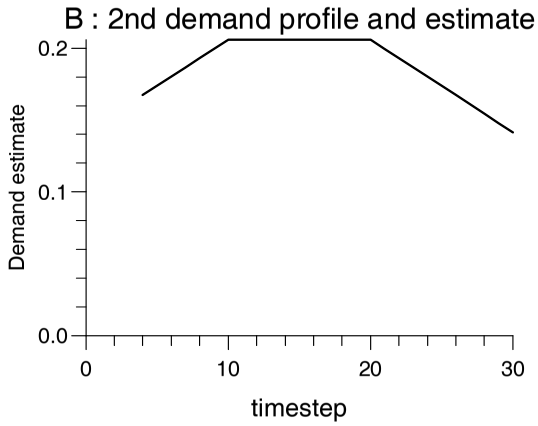

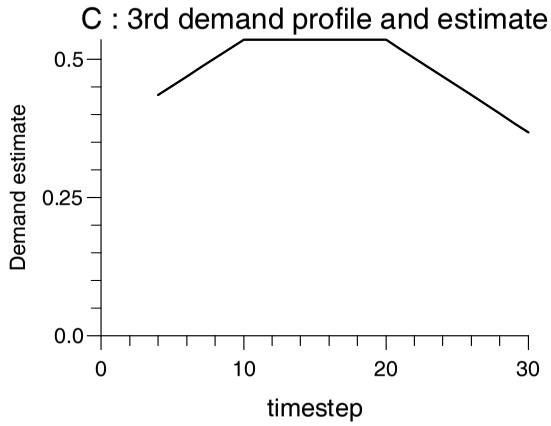

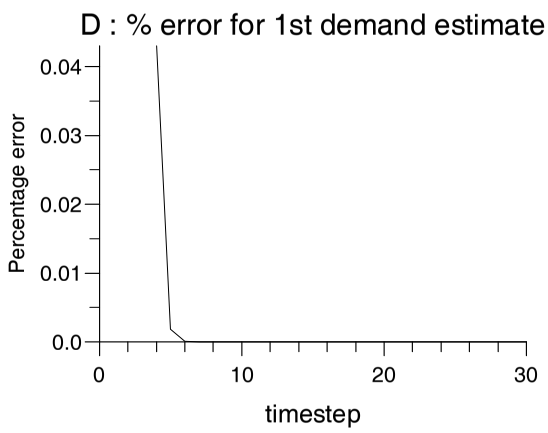

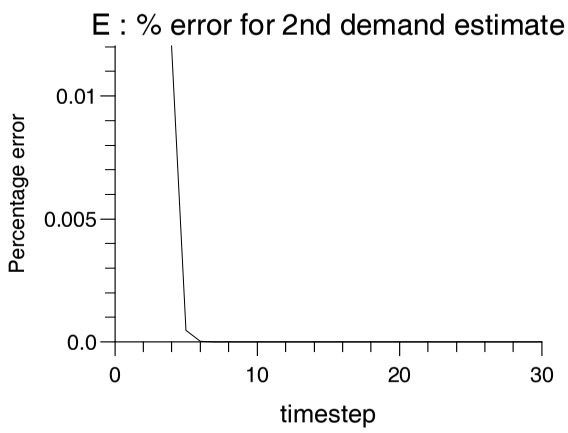

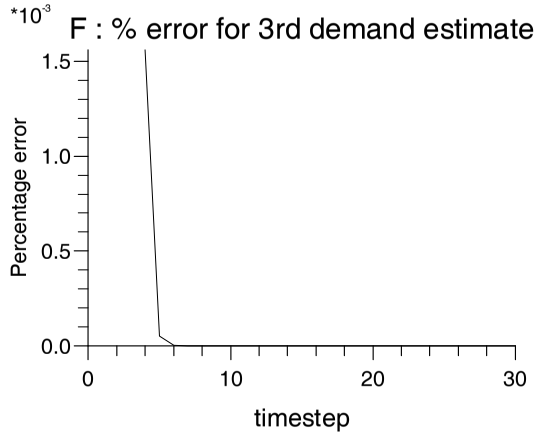

Experiment 4.2

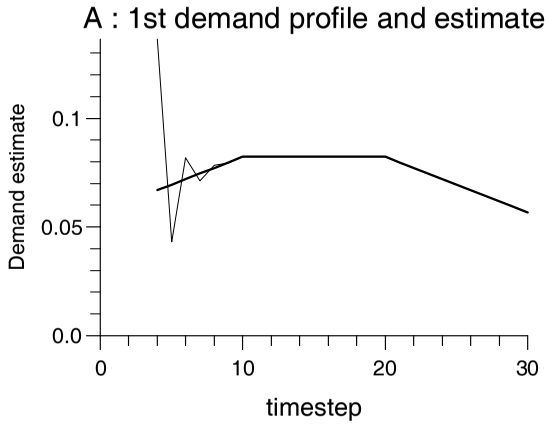

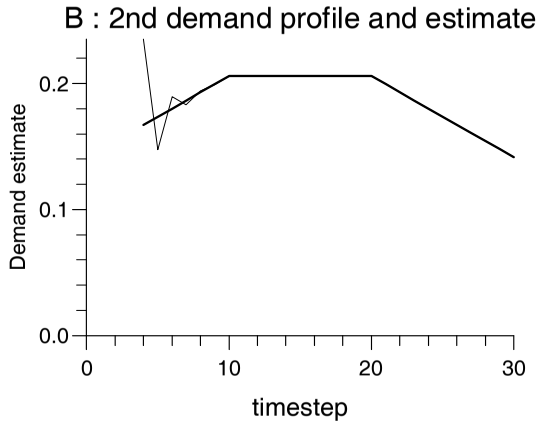

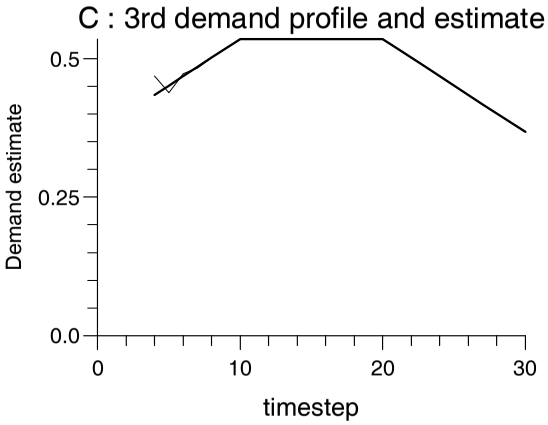

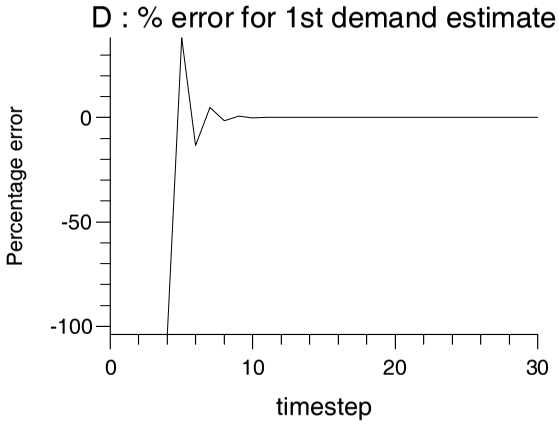

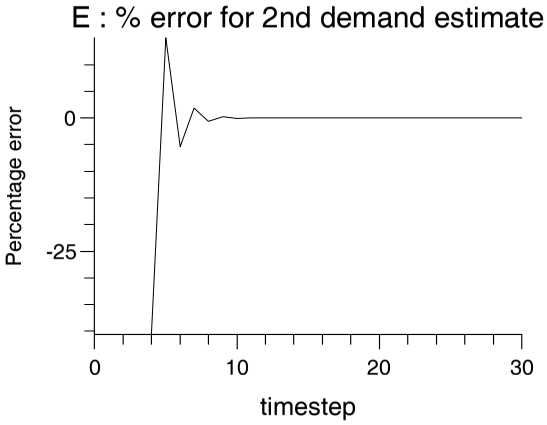

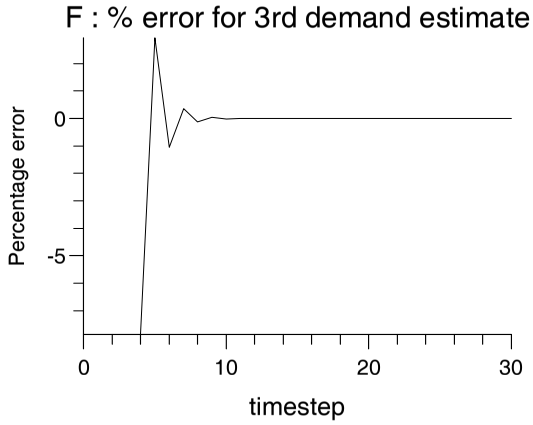

Experiment 4.3

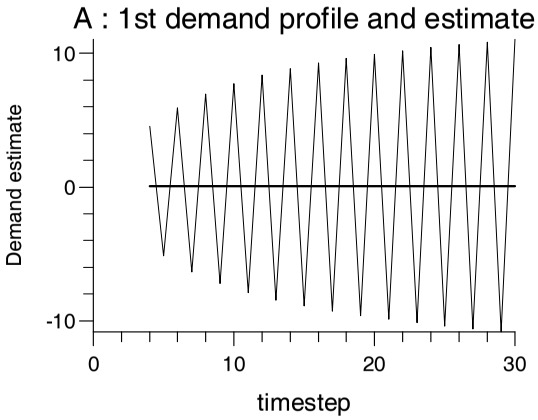

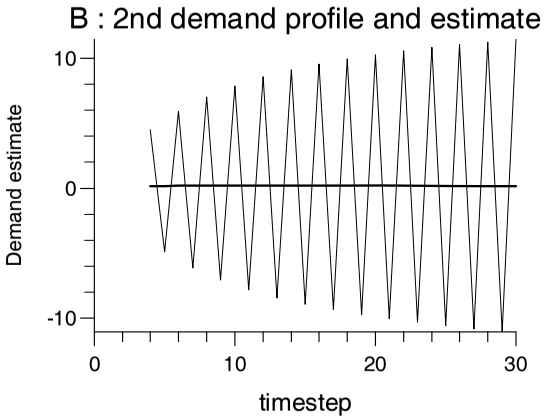

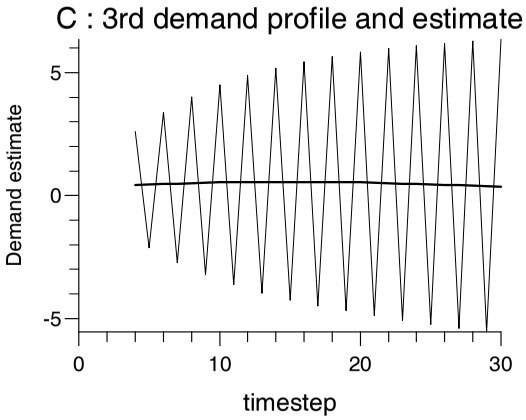

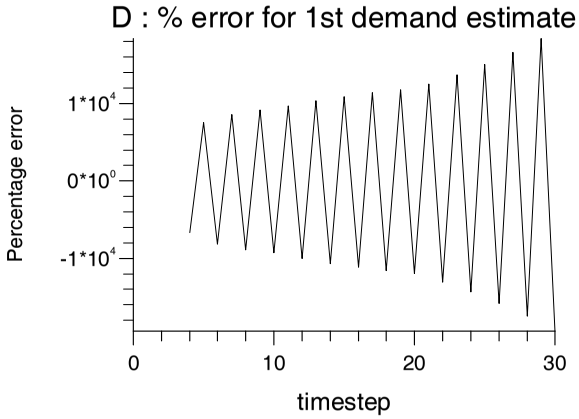

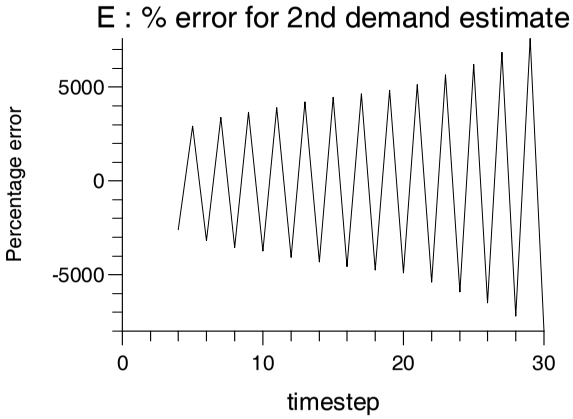

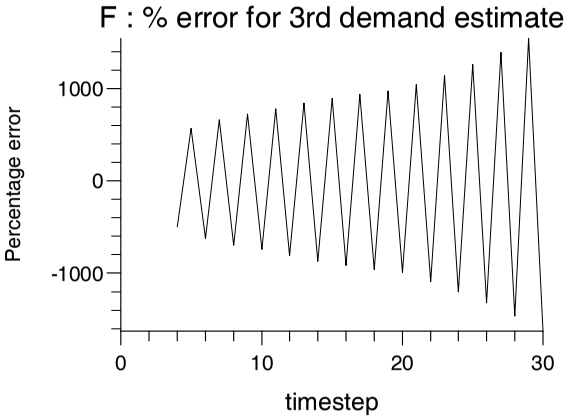

Experiment 4.4

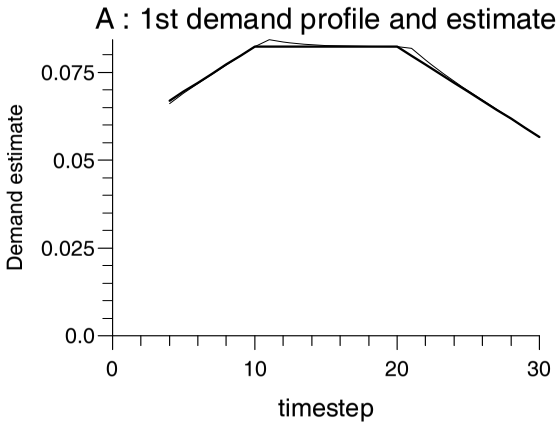

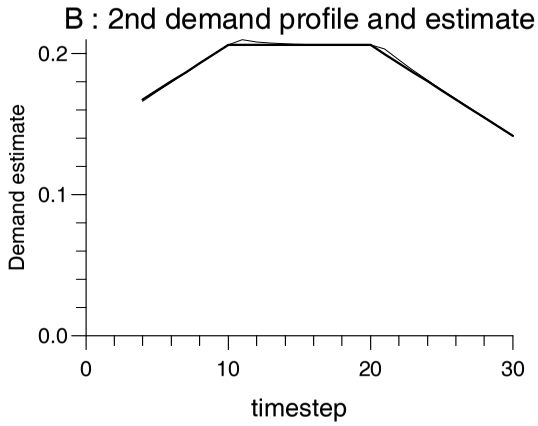

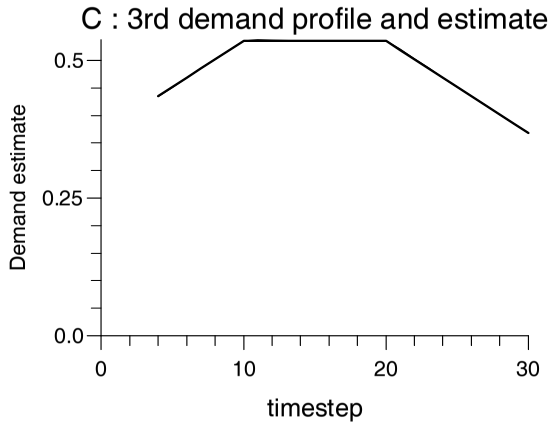

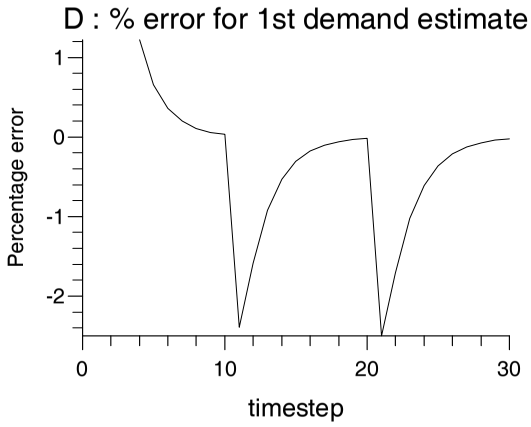

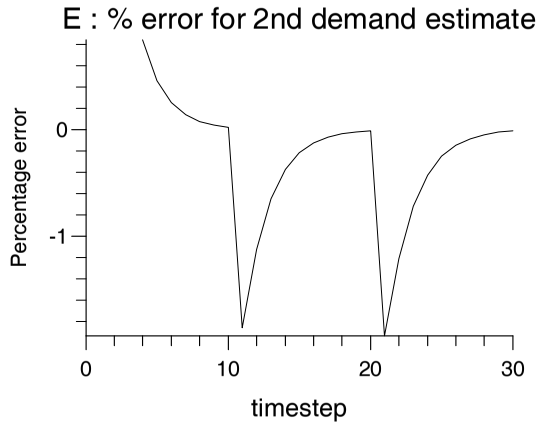

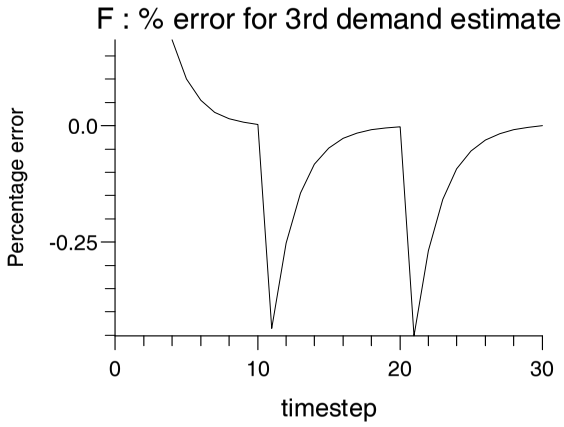

4.3 Discussion

It is immediately apparant that the central difference approximation of equation (2.13) has very greatly reduced the error in the estimates of the flow demands. Indeed, it can be seen that, for $1/2 < \theta \leq 1$, with identical meshes the state of the $\mathcal{M}2$ model tends with time to the *exact* state of the base $\mathcal{M}0$ model and its flow inputs. However, like the $\mathcal{M}1$ models, we have not presented a theoretical guarantee of the convergence of the solution to the $\mathcal{M}2$ model to the solution of the governing differential equations (2.16), (2.13), as the computational mesh is refined. The possibility of such a proof would be worth exploring, and as mentioned previously, two good references for this problem are [36] and [16]. From the experiments with pressure data taken from an $\mathcal{M}0$ model constructed upon a much finer mesh, it can be seen that the modelling error introduced by discretising the original differential equations would not affect the flow estimates too adversely.

When $\theta = 1/2$, the $\mathcal{M}2$ model was found to have multiple eigenvalues equal to -1 and the $\mathcal{M}2$ model flow estimates failed to converge. As θ moved from $1/2$ to 1, the modulus of the eigenvalues of the $\mathcal{M}2$ system appeared generally to decrease in a similar manner to an $\mathcal{M}1$ system. Indeed, we have already shown that the spectrum of an $\mathcal{M}2$ system contains all the eigenvalues of the corresponding $\mathcal{M}1$ system (a table of $\mathcal{M}1$ system eigenvalues for various values of θ was given in the previous chapter). The remaining g eigenvalues of the $\mathcal{M}2$ system have been shown to be equal to $-(1-\theta)/\theta$. For $\theta = 1/2$ these eigenvalues are -1, but as θ moves to 1 we see that these eigenvalues tend to zero. As the modulus of the eigenvalues decreased, the $\mathcal{M}2$ model state converged more rapidly with time to the base $\mathcal{M}0$ model state. The most rapid convergence occurred when $\theta = 1$.

However, $\theta = 1/2$ represented a Crank-Nicolson finite difference scheme with the highest order of accuracy, and unfortunately this value of θ could not be used in practice. For this reason, we now turn to alternative techniques for state estimation, *observers*, which are introduced in the next chapter. These lead to working state estimation techniques constructed upon gas network models with both $\theta = 1/2$ and a central difference discretisation of equation (2.13).

Chapter 5

Observers

For a dynamical system, only a few measurements may be available; and the challenge of state estimation is to determine the state of the whole system from these measurements over time. If a dynamical system has measurements available corresponding to linear combinations of state variables of its system model, then the system may be *completely observable*, and an observer employed for state estimation [29], [2].
We consider the time-invariant linear descriptor system

$$E\underline{x}(k+1) = A\underline{x}(k) + B^1\underline{u}(k+1) + B^2\underline{u}(k) \tag{5.1}$$

where $E, A \in \mathbf{R}^{n\times n}$, $B^1, B^2 \in \mathbf{R}^{n\times m}$, with discrete measurements of the real system given by

$$\underline{y}(k) = C\underline{x}(k) \quad for\ k = 0, 1, 2, ..., \tag{5.2}$$

where $C \in \mathbf{R}^{g\times n}$. We assume E is full rank, and C is full row rank.

We firstly define *complete observability* and then discuss techniques, known collectively as *observers*, capable of estimating the entire system state of discrete dynamical systems (5.1), (5.2) that have the property of *complete observability*.

5.1 Observability

The system (5.1), (5.2) is *completely observable* if and only if knowledge of the inputs and measurements over some timesteps is enough to determine uniquely an initial state

$x(0)$.

The following theorem gives a necessary and sufficient condition for complete observability, known as the *Hautus condition* [42], [13], [25].

Theorem 5.1 *A system of the form (5.1), where the matrix E is non-singular, with measurements available of the form (5.2), is completely observable if and only if we have the following condition.*

For all $\mu \in \mathbf{C}$

$$(A - \mu E)\underline{v} = \underline{0} \quad , \quad C\underline{v} = \underline{0} \iff \underline{v} = \underline{0} \tag{5.3}$$

where $\underline{v} \in \mathbf{R}^n$.

5.2 Design A : The *Direct* Observer

Assume the behaviour of a system is described by (5.1), (5.2). The method solves the matrix equation

$$\Theta \underline{\mathcal{X}} = \underline{\Delta}, \tag{5.4}$$

where Θ is the matrix

$$\begin{bmatrix}
A & -E & 0 & 0 & . & . & . & . & . \\
0 & A & -E & 0 & 0 & . & . & . & . \\
0 & 0 & A & -E & 0 & 0 & . & . & . \\
: & : & : & : & : & : & : & : & : \\
: & : & : & : & : & : & : & : & : \\
C & 0 & 0 & 0 & . & . & . & . & . \\
0 & C & 0 & 0 & . & . & . & . & . \\
0 & 0 & C & 0 & . & . & . & . & . \\
0 & 0 & 0 & C & . & . & . & . & . \\
: & : & : & : & : & : & : & : & : \\
: & : & : & : & : & : & : & : & :
\end{bmatrix},$$

and

$$\underline{\mathcal{X}}^T = [\underline{\hat{x}}(k)^T, \underline{\hat{x}}(k+1)^T, \underline{\hat{x}}(k+2)^T, ...\underline{\hat{x}}(k+n-1)^T]$$

where $\underline{\hat{x}}(k)$ is the observer estimate for $\underline{x}(k)$, and

$$\underline{\Delta}^T = [-(B^1\underline{u}(k+1) + B^2\underline{u}(k))^T, -(B^1\underline{u}(k+2) + B^2\underline{u}(k+1))^T, ...$$

$$...., -(B^1\underline{u}(k+n-1) + B^2\underline{u}(k+n-2))^T, \underline{y}^T(k), \underline{y}^T(k+1), ...\underline{y}^T(k+n-1)]$$

where n is the dimension of system (5.1), and is the number of timesteps over which equation (5.4) is solved.

The number of timesteps over which equation (5.4) needs to be solved might not be quite as large as n. However, if the system is completely observable, then from [2] it can be shown that n is the maximum number of timesteps needed. If the matrix Θ does not attain a large enough rank to determine $\underline{\mathcal{X}}$ uniquely after n timesteps, then the system is not observable. The situation is somewhat more complicated when we consider numerical error, and for a good discussion of this problem, see [31].

For a current state estimate, at each timestep we would collect measurements from the current and previous $n-1$ timesteps, and then solve equation (5.4) over this time window.

5.3 Design B : The *Dynamic* Observer

Assume the behaviour of a system is described by (5.1), (5.2). We form a new descriptor system

$$E\underline{\hat{x}}(k+1) = (A - GC)\underline{\hat{x}}(k) + B^1\underline{u}(k+1) + B^2\underline{u}(k) + G\underline{y}(k). \tag{5.5}$$

This is our dynamic observer system. Our aim is to construct the matrix G so that $\underline{\hat{x}}(k) \longrightarrow \underline{x}(k)$ as $k \longrightarrow \infty$ regardless of the true value of $\underline{x}(0)$, which we assume to be unknown. Subtracting system (5.5) from system (5.1), gives

$$E(\underline{x}(k+1) - \underline{\hat{x}}(k+1)) = A(\underline{x}(k) - \underline{\hat{x}}(k)) - G(\underline{y}(k) - C\underline{\hat{x}}(k)) \tag{5.6}$$

where the last term is equivalent to $-G(C\underline{x}(k) - C\underline{\hat{x}}(k))$. If we define the error between the two systems (5.1) and (5.5) at time level k to be

$$\underline{e}(k) = \underline{x}(k) - \underline{\hat{x}}(k) \tag{5.7}$$

then substituting equation (5.7) into equation (5.6) gives

$$E\underline{e}(k+1) = A\underline{e}(k) - GC\underline{e}(k)$$

or

$$E\underline{e}(k+1) = (A - GC)\underline{e}(k). \tag{5.8}$$

We require $\underline{e}(k) \longrightarrow \underline{0}$ as $k \longrightarrow \infty$; and for this we require the eigenvalues of the matrix pencil $(A - GC, E)$ to have modulus less than unity. Hence, designing our observer system is equivalent to finding a matrix G such that all the eigenvalues of the matrix pencil $(A - GC, E)$ lie strictly within the unit circle. If the system, (5.1), (5.2), has an invertible matrix E and is observable, then we can find such a matrix G [4], [13], [25].

5.3.1 Eigenvalue Assignment Technique: Eigenstructure Assignment

We use a technique described in [24], [25]. Let us assume that we have a set Λ of n distinct real eigenvalues that we wish to assign to the observer system; where

$$\Lambda = \{\lambda_1, ...\lambda_n\}$$

with $|\lambda_i| < 1, \ for \ i = 1, ..., n$. Let $D = diag[\lambda_i]$.

Let $X = [\underline{x}_1, ..., \underline{x}_n]$ be the modal matrix of the pencil $(A - GC, E)$, and let $Y = [\underline{y}_1, ..., \underline{y}_n]$ be the modal matrix of the pencil $(A^T - C^T G^T, E^T)$. Then

$$(A - GC)X = EXD \tag{5.9}$$

and

$$(A^T - C^T G^T)Y = E^T Y D. \tag{5.10}$$

Now compute the QR decomposition of C^T

$$C^T = QR, \tag{5.11}$$

where

$$Q^T = \begin{bmatrix} \tilde{Q}_c^T \\ Q_c^T \end{bmatrix},$$

and

$$R = \begin{bmatrix} C_0 \\ 0 \end{bmatrix},$$

and C_0 is $g \times g$, upper triangular and non-singular. If equation (5.10) is rearranged and factorisation (5.11) substituted in, then

$$RG^T Y = Q^T(A^T Y - E^T Y D),$$

from which

$$G^T = C_0^{-1} \tilde{Q}_c^T (A^T Y - E^T Y D) Y^{-1} \tag{5.12}$$

and

$$0 = Q_c^T (A^T Y - E^T Y D). \tag{5.13}$$

Equation (5.13) implies

$$(A^T - \lambda_i E^T) \underline{y}_i \in Im(C^T), \ for \ i = 1, ..., n, \tag{5.14}$$

or

$$\underline{y}_i \in \mathcal{N}\{Q_c^T (A^T - \lambda_i E^T)\},$$

where $\mathcal{N}$ represents the right null space. If the dimension, g, of the measurement vector is greater than one, then there is a certain amount of freedom in the choice of the $\underline{y}_i$. This freedom may be utilised in selecting a set of $\underline{y}_i$ such that the observer eigenvalues are as insensitive as possible to perturbations in the matrices A, E, C and G.

A generalised eigenvalue of the matrix pencil $(A - GC, E)$ can be described by the pair $(\mu_i, \delta_i) \in \mathbf{C}\text{x}\mathbf{R}$ (where $\mathbf{C}\text{x}\mathbf{R}$ is the cartesian product of the spaces of complex and real numbers respectively) where the associated eigenvalue is $\lambda_i = \mu_i / \delta_i$, for $i = 1, ..., n$. Then from equations (5.9) and (5.10), we assume that for left and right eigenvectors $\underline{y}_i$ and $\underline{x}_i$ respectively we have

$$\begin{aligned} \delta_i (A - GC) \underline{x}_i &= \mu_i E \underline{x}_i, \\ \delta_i \underline{y}_i^T (A - GC) &= \mu_i \underline{y}_i^T E \end{aligned} \tag{5.15}$$

and

$$\underline{y}_i^T E \underline{x}_j = 0, \quad for \ i \neq j \ . \tag{5.16}$$

In a non-defective pencil, perturbations of $O(\epsilon)$ in A, E, C and G cause perturbations of $O(\epsilon)\kappa(\mu_i, \delta_i)$ in a simple eigenvalue where $\kappa(\mu_i, \delta_i)$ is the condition number:

$$\kappa(\mu_i, \delta_i) = \|\underline{y}_i\|_2 \|\underline{x}_i\|_2 \ / \ (|\mu_i|^2 \ + \ \delta_i^2)^{1/2}, \tag{5.17}$$

and $\underline{x}_i$ and $\underline{y}_i$ are assumed to be normalised such that

$$\underline{y}_i^T E \underline{x}_i = \delta_i, \tag{5.18}$$

$$\underline{y}_i^T (A - GC)\underline{x}_i = \mu_i, \tag{5.19}$$

[39].

Now, since we are assuming E is full rank, we may assume we have a set of eigenvector/eigenvalue pairs, $(\underline{x}_i, \underline{y}_i), (\mu_i, \delta_i)$, for $i = 1, ..., n$, where the eigenvectors are scaled such that $\|\underline{y}_i\|_2 = 1$ and $\delta_i = 1$ for $i = 1, ..., n$. Then to minimise the condition numbers (5.17), we need to minimise the $\|\underline{x}_i\|_2$. From equation (5.18) with all $\delta_i = 1$, we have

$$Y^T E X = I, \tag{5.20}$$

from which we have

$$X = (Y^T E)^{-1}. \tag{5.21}$$

So to minimise the $\|\underline{x}_i\|_2$, we can select the $\underline{y}_i$ such that

$$\|(Y^T E)^{-1}\|_F = \|X\|_F = (\Sigma_i \|\underline{x}_i\|_2^2)^{1/2}$$

is minimised.

To select a set of left eigenvectors, $\underline{y}_i$, such that $\|(Y^T E)^{-1}\|_F$ is minimised, we use a simple method that, although it cannot be guaranteed to converge to the minimum value of $\|(Y^T E)^{-1}\|_F$ attainable, has been found to significantly reduce the value of $\|(Y^T E)^{-1}\|_F$ over a number of iterations.

The method begins by selecting a set of vectors which satisfy equation (5.13). For each eigenvalue in the set Λ, we calculate the QR decomposition

$$Q_1^T (A - \lambda_i E) Q_c = R_1 \tag{5.22}$$

where

$$Q_1^T = \begin{bmatrix} \tilde{S}_i^T \\ S_i^T \end{bmatrix}$$

and

$$R_1 = \begin{bmatrix} \tilde{R} \\ 0 \end{bmatrix},$$

and S_i is $n \times g$. If $\underline{y}_i = S_i \underline{v}_i$ for some $\underline{v}_i \in \mathbf{R}^g$, then equation (5.14) is satisfied. Now assume we have a set of independent vectors, $\{\underline{y}_i\}$, chosen for each i from span$\{S_i\}$, as the columns of Y, the initial choice being somewhat arbitrary. Let

$$Y_k = [\underline{y}_1, ..., \underline{y}_{k-1}, \underline{y}_{k+1}, ..., \underline{y}_n]$$

and calculate the QR decomposition

$$Q_2^T Y_k = R_2 \tag{5.23}$$

where

$$Q_2^T = \begin{bmatrix} \tilde{Z}_k^T \\ \underline{z}_k^T \end{bmatrix}$$

and

$$R_2 = \begin{bmatrix} \tilde{Y}_k \\ 0 \end{bmatrix}.$$

The vector $\underline{z}_k$ is orthogonal to the columns of Y_k, and so, from equation (5.16) we have that $\underline{z}_k$ is parallel to $E\underline{x}_k$. Thus, if we choose the new $\underline{y}_k$ with $\|\underline{y}_k\|_2$=1 from span$\{S_i\}$, to be as 'parallel to' $\underline{z}_k$ as possible, and hence as parallel to $E\underline{x}_k$ as possible, and assume $\underline{x}_k$ is normalised such that

$$\underline{y}_k^T E \underline{x}_k = 1 \ ,$$

then we are minimising $\|\underline{x}_k\|_2$ and hence $\kappa(\mu_i, \delta_i)$. So the updated $\underline{y}_k$ is obtained by projecting $\underline{z}_k$ orthogonally onto the subspace S_k and normalising to give

$$\underline{y}_k = S_k S_k^T \underline{z}_k / \| S_k^T \underline{z}_k \|_2. \tag{5.24}$$

The method then continues with Y_{k+1} from equation (5.23) and one sweep of the method is completed when k has run from 1 to n.

Over a few sweeps of the method, $\|(Y^T E)^{-1}\|_F$ should reduce since we are minimising the condition numbers $\kappa(\mu_i, \delta_i)$. So, for each sweep, $\|(Y^T E)^{-1}\|_F$ is monitored, and when it reaches a local minimum value, the method is terminated. G is then calculated from equation (5.12).

General Eigenvalue Assignment Algorithm

1) Compute the QR decomposition of C^T

$$C^T = QR,$$

where

$$Q^T = \begin{bmatrix} \tilde{Q}_c^T \\ Q_c^T \end{bmatrix},$$

and

$$R = \begin{bmatrix} C_0 \\ 0 \end{bmatrix}.$$

2) For each eigenvalue λ_i for $i = 1, ..., n$ in the set Λ, calculate the QR decomposition

$$Q_1^T(A - \lambda_i E)Q_c = R_1,$$

where

$$Q_1^T = \begin{bmatrix} \tilde{S}_i^T \\ S_i^T \end{bmatrix}$$

and

$$R_1 = \begin{bmatrix} \tilde{R} \\ 0 \end{bmatrix}$$

and S_i is $n \times p$.

3) For each $i = 1, ..., n$, choose any vector, $\underline{y}_i$ from span$\{S_i\}$ as one of the columns of the matrix Y.

4) For $k = 1, ..., n$, let

$$Y_k = [\underline{y}_1, ..., \underline{y}_{k-1}, \underline{y}_{k+1}, ..., \underline{y}_n],$$

and calculate the QR decomposition

$$Q_2^T Y_k = R_2,$$

where

$$Q_2^T = \begin{bmatrix} \tilde{Z}_k^T \\ \underline{z}_k^T \end{bmatrix}$$

and

$$R_2 = \begin{bmatrix} \tilde{Y}_k \\ 0 \end{bmatrix}.$$

Let

$$y_k = S_k S_k^T \underline{z}_k / \| S_k^T \underline{z}_k \|_2.$$

5) Calculate $\|(Y^T E)^{-1}\|_F$.

6) Repeat steps (4) and (5) until $\|(Y^T E)^{-1}\|_F$ reaches a local minimum.

7) Let

$$G^T = C_0^{-1} \tilde{Q}_c^T (A^T Y - E^T Y D) Y^{-1}.$$

5.4 Design C : The Dynamic Observer with Feedback at the Current Time level

Here we present an observer design from [34], which has been found to give significantly reduced errors at the measurement points. This method uses feedback at the current time level.

Assume the behaviour of a system is described by (5.1), (5.2). We form a new descriptor system

$$(E - HC)\underline{\hat{x}}(k+1) = (A - GC)\underline{\hat{x}}(k) + B^1 \underline{u}(k+1) + B^2 \underline{u}(k) - H\underline{y}(k+1) + G\underline{y}(k), \quad (5.25)$$

where the H and G matrices are to be chosen. This is our dynamic observer system. The term in H represents feedback at the current time level, and the term in G represents the familiar feedback at the previous time level.

If we define the error between the two systems (5.1) and (5.25) at time level k to be

$$\underline{e}(k) = \underline{x}(k) - \underline{\hat{x}}(k), \quad (5.26)$$

then subtracting equation (5.25) from equation (5.1) gives

$$(E - HC)\underline{\epsilon}(k+1) = (A - GC)\underline{\epsilon}(k). \tag{5.27}$$

If H can be chosen such that $(E-HC)$ is nonsingular, then its inverse can be calculated to give an explicit expression for $\underline{\epsilon}(k+1)$ from equation (5.27). We notice that $(E-HC)^{-1}$ would multiply all the terms on the right hand side of equation (5.27). Therefore, if $\|(E-HC)^{-1}\|$ could be made small for a suitable norm, then the effects of certain forms of modelling error, that will be described later, should be reduced. It would also be advisable to ensure the condition number of $(E-HC)$ is not too large since this matrix has to be inverted implicitly in equation (5.25) to calculate $\underline{\hat{x}}(k+1)$.

We know that if

$$E - HC = U\Sigma V^T \tag{5.28}$$

is the singular value decomposition of $(E-HC)$, where $\Sigma = diag[\sigma_i]$ and the σ_i are arranged in nonincreasing order, then

$$\|E - HC\|_2 = \sigma_1$$

$$\|(E - HC)^{-1}\|_2 = \sigma_n^{-1}$$

and we define the 2-norm condition number

$$cond_2(E - HC) = \sigma_1/\sigma_n.$$

Hence, if we choose the 2-norm, then the problem reduces to calculating the matrix H to make σ_n as large as possible whilst keeping σ_1 as small as possible. This would satisfy all three conditions: $(E-HC)$ nonsingular, $\|(E-HC)^{-1}\|_2$ small, and $cond_2(E-HC)$ small.

Once the matrix H has been calculated, the observer design is completed by using a method, such as eigenstructure assignment presented in the previous section, to calculate a matrix G to assign a set of eigenvalues, all less than unity in modulus, to the matrix $(E-HC)^{-1}(A-GC)$. Then from equation (5.27), we can readily see that the error, $\underline{\epsilon}(k)$, between the observer state estimate, $\underline{\hat{x}}(k)$, and the true system state, $\underline{x}(k)$, must tend to zero.

5.4.1 Singular Value Assignment

We use a method from [34], [4] for determining the matrix H with g of the singular values of $(E - HC)$ assigned arbitrarily.

Let the QR-decomposition of matrix C^T be

$$C^T = QR, \tag{5.29}$$

where

$$Q^T = \begin{bmatrix} \tilde{Q}_c^T \\ Q_c^T \end{bmatrix}$$

and

$$R = \begin{bmatrix} C_0 \\ 0 \end{bmatrix}.$$

If equation (5.28) is transposed and the factorisation (5.29) applied to C^T then we have

$$RH^T = Q^T(E^T - V\Sigma U^T). \tag{5.30}$$

Let $U = [\underline{u}_1, ..., \underline{u}_n]$ and $V = [\underline{v}_1, ..., \underline{v}_n]$. Then from equation (5.30) we see that the $\underline{u}_i$, $\underline{v}_i$ and σ_i must satisfy

$$Q_c^T(E^T\underline{u}_i - \sigma_i\underline{v}_i) = \underline{0} \quad for\ i = 1, ..., n,$$

which implies that

$$E^T\underline{u}_i - \sigma_i\underline{v}_i \in Im(C^T) \quad for\ i = 1, ..., n. \tag{5.31}$$

Therefore, to assign any singular values to the matrix $E - HC$, we must find $2n$ vectors $\{\underline{u}_i, \underline{v}_i\}$ and n scalars $\{\sigma_i\}$ which satisfy condition (5.31) and the orthogonality constraints on the matrices U and V. This method calculates the U and V matrices with $n-g$ of the singular values of $E - HC$ fixed to $n-g$ of the singular values of E, and the remaining g singular values assigned arbitrarily. Unfortunately, a certain set of $n-g$ singular values of E cannot be affected by the addition of the term HC, and will always be singular values of the matrix $E - HC$ for any feedback matrix H [4].

First of all, form $Q_c^T E^T$ and calculate the SVD

$$Q_c^T E^T[\tilde{U}_1\ ,\ \tilde{U}_2] = \tilde{V}[\Sigma_1\ ,\ 0] \tag{5.32}$$

and since rank$(E) = n$ and rank$(C) = g$ we have

$$\Sigma_1 = diag\{\sigma_1, \sigma_2, ..., \sigma_{n-g}\}.$$

Refering now to the matrices U and V in equations (5.28) and (5.30), let

$$U = [\tilde{U}_1 \ , \ \tilde{U}_2] \tag{5.33}$$

where $\tilde{U}_1$ and $\tilde{U}_2$ are from equation (5.32) and let

$$V = [Q_c\tilde{V} \ , \ \tilde{Q}_c] \tag{5.34}$$

where $\tilde{V}$ is also from equation (5.32), and $\tilde{Q}_c$ and Q_c are from equation (5.29). It can be verified that the $\{\underline{u}_i, \underline{v}_i\}$ and $\{\sigma_i\}$ satisfy the condition (5.31) for $i = 1, ..., n-g$, where the σ_i are the singular values of $Q_c^T E^T$. The matrices U and V as defined in (5.33) and (5.34) also satisfy the orthogonality condition.

Now assume that we wish to assign the set $\{\sigma_j\}$ for $j = n-g+1, ..., n$ as the remaining g singular values of $E - HC$. Let $\Sigma_2 = diag\{\sigma_j\}$ for $j = n-g+1, ..., n$ and calculate

$$H = (E\tilde{Q}_c - \tilde{U}_2\Sigma_2)C_0^{-T}, \tag{5.35}$$

where $C_0^{-T} = (C_0^T)^{-1} = (C_0^{-1})^T$.

Then, by using equation (5.35) to substitute for H in equation (5.28), and substituting in (5.33) and (5.34), the QR decomposition (5.29) and the SVD (5.32) may be used to verify that

$$[\tilde{U}_1 \ , \ \tilde{U}_2]^T(E - HC)[Q_c\tilde{V} \ , \ \tilde{Q}_c] = \Sigma \tag{5.36}$$

where

$$\Sigma = \begin{bmatrix} \Sigma_1 & 0 \\ 0 & \Sigma_2 \end{bmatrix}.$$

Since the n-g singular values contained in Σ_1 remain fixed, if the g singular values of Σ_2 are chosen such that

$$\sigma_{n-g}(\Sigma_1) \leq \sigma_j(\Sigma_2) \leq \sigma_1(\Sigma_1) \quad for \ j = 1, ..., g, \tag{5.37}$$

then we know that

$$\sigma_1(E - HC) = \sigma_1(Q_c^T E^T)$$

and

$$\sigma_n(E - HC) = \sigma_{n-g}(Q_c^T E^T).$$

For a more robust observer design, we ideally want

$$\sigma_n(E) < \sigma_{n-g}(\Sigma_1) \leq \sigma_1(\Sigma_1) \leq \sigma_1(E).$$

General Singular Value Assignment Algorithm

1) Compute the QR decomposition of C^T

$$C^T = QR,$$

where

$$Q^T = \begin{bmatrix} \tilde{Q}_c^T \\ Q_c^T \end{bmatrix}$$

and

$$R = \begin{bmatrix} C_0 \\ 0 \end{bmatrix}.$$

2) Form $Q_c^T E^T$ and calculate the SVD

$$Q_c^T E^T [\tilde{U}_1 \ , \ \tilde{U}_2] = \tilde{V} [\Sigma_1 \ , \ 0],$$

where

$$\Sigma_1 = diag\{\sigma_1, \sigma_2, ..., \sigma_{n-g}\}$$

is a diagonal matrix with the $n - g$ *fixed* singular values which cannot be modified.

3) Assume that we wish to assign the set $\{\sigma_j\}$ for $j = n-g+1, ..., n$ as the remaining g singular values of $E - HC$. Let $\Sigma_2 = diag\{\sigma_j\}$ for $j = n - g + 1, ..., n$ and calculate

$$H = (E\tilde{Q}_c - \tilde{U}_2\Sigma_2)C_0^{-T},$$

where $C_0^{-T} = (C_0^T)^{-1} = (C_0^{-1})^T$.

Chapter 6

Formulation of a New $\mathcal{M}3$ Variant Model for Use in Direct and Dynamic Observers

We now show how a new model variation, denoted by $\mathcal{M}3$, which is capable of estimating flow demands, may be constructed from a base $\mathcal{M}0$ model using information about the flow demands, such that these new $\mathcal{M}3$ models are observable.

Since, in practice the flow demands change very slowly with time, the $\mathcal{M}3$ models assume

$$flow\ demand_{k+1}^{demand\ site} = flow\ demand_{k}^{demand\ site},$$

i.e.

$$d_{k+1}^{demand\ site} = d_{k}^{demand\ site} \quad for\ all\ k. \tag{6.1}$$

The key feature of $\mathcal{M}3$ models is that they contain difference equations of the form (6.1).

Then to form an $\mathcal{M}3$ model, we start from a base $\mathcal{M}0$ model and move the g dimensional vector, $\underline{d}(k)$, from the input vector to the state vector. We then introduce g new trivial difference equations of the form

$$\underline{d}(k+1) = \underline{d}(k) \tag{6.2}$$

into the new system. Assuming the base $\mathcal{M}0$ model is arranged and partitioned as in

equation (4.1), then the new $n+g$ dimensional $\mathcal{M}3$ system has the form

$$\begin{bmatrix} E_0 & -B^{1''} \\ 0 & I \end{bmatrix} \begin{bmatrix} \underline{x}_0(k+1) \\ \underline{d}(k+1) \end{bmatrix} = \begin{bmatrix} A_0 & B^{2''} \\ 0 & I \end{bmatrix} \begin{bmatrix} \underline{x}_0(k) \\ \underline{d}(k) \end{bmatrix} + \begin{bmatrix} B^{1'} \\ 0 \end{bmatrix} \underline{p}_3(k+1) + \begin{bmatrix} B^{2'} \\ 0 \end{bmatrix} \underline{p}_3(k) \tag{6.3}$$

which can be expressed in the general descriptor system form

$$E_3 \underline{x}_3(k+1) = A_3 \underline{x}_3(k) + B_3^1 \underline{u}_3(k+1) + B_3^2 \underline{u}_3(k). \tag{6.4}$$

For such an $\mathcal{M}3$ model, the only input required is the upstream pressure (assumed known). The g pressure measurements of the real gas network at the sites of flow demand are not needed as inputs to the $\mathcal{M}3$ model, and are in fact measurements of its state variables

$$\underline{y}_3(k) = C_3 \underline{x}_3(k) \tag{6.5}$$

available for use in a direct or dynamic observer.

6.1 Theorems

In this section, we firstly prove that the matrix E_3 of an $\mathcal{M}3$ model is full rank if $\theta > 0$. We next prove that if $\theta > 0$, then an $\mathcal{M}0$ model with pressure measurements available at the sites of flow demand is completely observable. This result is then used to prove that for $1/2 \leq \theta \leq 1$, $\mathcal{M}3$ models are completely observable if there are pressure measurements available at all the sites of flow demand. Lastly, it is proved that $\mathcal{M}3$ models are not completely observable if there are fewer measured pressures than flow demands.

Theorem 6.1 *If $\theta > 0$, the matrix E_3 of an $\mathcal{M}3$ model is full rank.*

Proof

E_3 is $(n+g)\times(n+g)$ and takes the form

$$E_3 = \begin{bmatrix} E_0 & -B^{1''} \\ 0 & I \end{bmatrix}$$

where I is $g \times g$.

By construction, since we have already shown E_0 is invertible for $\theta > 0$, E_3^{-1} is $(n+g)\times(n+g)$ and takes the form

$$E_3^{-1} = \begin{bmatrix} E_0^{-1} & E_0^{-1}B^{1''} \\ 0 & I \end{bmatrix}$$

where I is $g\times g$.

Hence, the matrix E_3 of an $\mathcal{M}3$ model is full rank. □

Theorem 6.2 *If $\theta > 0$, an $\mathcal{M}0$ model with pressure measurements available at the sites of flow demand is completely observable.*

Proof

The $\mathcal{M}0$ system (2.24) has g pressure measurements available at the sites of flow demand, corresponding to the following g dimensional vector of state variables

$$\underline{y}_0(k) = C_0\underline{x}_0(k) \tag{6.6}$$

where C_0 is $g\times n$ and is the measurement matrix.

Since we have shown that the eigenvalues of an $\mathcal{M}0$ system are real for $\theta > 0$, the $\mathcal{M}0$ system with measurements (6.6), is observable if and only if for $\mu\in\mathbf{R}$

$$(A_0 - \mu E_0)\underline{v} = \underline{0} \tag{6.7}$$

$$C_0\underline{v} = \underline{0} \tag{6.8}$$

$$\Longleftrightarrow$$

$$\underline{v} = \underline{0} \tag{6.9}$$

where $\underline{v}\in\mathbf{R}^n$.

Equation (6.9) $\Longrightarrow$ equations (6.7), (6.8) trivially.

We assume the pressure variables are arranged in the state vector in their order along the pipe network, i.e. in the following way

$$\underline{x}_0(k) = [p^1_{1,k}, p^1_{2,k}, ..., p^1_{s^1-1,k}, p^{1/2}_k, p^2_{1,k}, p^2_{2,k}, ..., p^2_{s^2-1,k}, p^{2/3}_k, ..., p^{g-1/g}_k, p^g_{1,k}, p^g_{2,k}...., p^g_{s^g-1,k}, p^g_{s^g,k}]^T,$$

where each pipe has $s^{pipe}+1$ nodes. E_0 and A_0 are then tridiagonal.

For $\theta \neq 0$, from equations (2.26) and (2.27), we have

$$A_0 - \mu E_0 = (1-\mu)I + ((1-\mu)\theta - 1)M_0.$$

If $((1-\mu)\theta - 1) = 0$, we can readily see that

$$A_0 - \mu E_0 = (1-\mu)I,$$

and so all the off-diagonal elements of $(A_0 - \mu E_0)$ are all zero and all the diagonal elements of $(A_0 - \mu E_0)$ are all $1-\mu$.

However, if $((1-\mu)\theta - 1) = 0$, then $\mu \neq 1$, and so, all the diagonal elements of $(A_0 - \mu E_0)$ are non-zero. Then $(A_0 - \mu E_0)$ will be full rank.

Hence, equation (6.7) implies equation (6.9).

If $((1-\mu)\theta - 1) \neq 0$, then due to the properties of M_0, we can readily see that $A_0 - \mu E_0 = (1-\mu)I + ((1-\mu)\theta - 1)M_0$ is tridiagonal with non-zero off-diagonal elements for $|i-j| = 1$.

Equation (6.8) zeros the last element of $\underline{v}$ corresponding to the downstream end pressure variable. Then, by induction, either going up or down the scalar equations in system (6.7), we find all the elements of $\underline{v}$ are zero.

Hence, equations (6.7), (6.8) $\Longrightarrow$ equation (6.9).

Hence, if $\theta > 0$, an $\mathcal{M}0$ model with pressure measurements available at the sites of flow demand is completely observable. □

Theorem 6.3 *If $1/2 \leq \theta \leq 1$, an $\mathcal{M}3$ model is completely observable.*

Proof

By inspection, the eigenvalues of an $\mathcal{M}3$ system consist of the n eigenvalues of the base $\mathcal{M}0$ system, and g eigenvalues equal to 1. Hence, for $\theta > 0$, the eigenvalues of the $\mathcal{M}3$ system are real.

The $\mathcal{M}3$ system is observable if and only if for all $\mu \in \mathbf{R}$

$$(A_3 - \mu E_3)\underline{v} = \underline{0} \tag{6.10}$$

$$C_3\underline{v} = \underline{0} \tag{6.11}$$

$$\Longleftrightarrow$$

$$\underline{v} = \underline{0} \tag{6.12}$$

where $\underline{v} \in \mathbf{R}^{n+g}$.

Equation (6.12) $\Longrightarrow$ equations (6.10), (6.11) trivially.

Equations (6.10), (6.11) and (6.12) can be expressed in the following way. The $\mathcal{M}3$ system is observable if and only if for all $\mu \in \mathbf{R}$

$$(A_0 - \mu E_0)\underline{v}_n + (B^{2''} - \mu(-B^{1''}))\underline{v}_g = \underline{0} \tag{6.13}$$

$$(1 - \mu)\underline{v}_g = \underline{0} \tag{6.14}$$

$$C_0\underline{v}_n = \underline{0} \tag{6.15}$$

$$\Longleftrightarrow$$

$$\underline{v}_n = \underline{0}\ ,\ \underline{v}_g = \underline{0} \tag{6.16}$$

where $\underline{v} = [\underline{v}_n^T, \underline{v}_g^T]^T$, and $\underline{v}_n \in \mathbf{R}^n$, $\underline{v}_g \in \mathbf{R}^g$.

We firstly consider the case $\mu \neq 1$.

From equation (6.14) we have $\underline{v}_g = \underline{0}$.

Substituting $\underline{v}_g = \underline{0}$ into equation (6.13) gives

$$(A_0 - \mu E_0)\underline{v}_n = \underline{0}. \tag{6.17}$$

Since we have shown the original $\mathcal{M}0$ system is observable for $\theta > 0$, we have for all $\mu \in \mathbf{R}$

$$(A_0 - \mu E_0)\underline{v}_n = \underline{0}\ \ ,\ \ C_0\underline{v}_n = \underline{0}\ ,\ \Longleftrightarrow \underline{v}_n = \underline{0}. \tag{6.18}$$

Hence, we have $\underline{v}_n = \underline{0}$, $\underline{v}_g = \underline{0}$; and so equations (6.10), (6.11) $\Longrightarrow$ (6.12).

We secondly consider the case $\mu = 1$.

Let the base $\mathcal{M}0$ system be partitioned according to equation (4.1). Then equation (6.13) can be written as the following system of n equations for the $n+g$ dimensional vector $\underline{v}$

$$[(A' - \mu E') \quad (A'' - \mu E'') \quad (B^{2''} - \mu(-B^{1''}))] \begin{bmatrix} \underline{v}'_n \\ \underline{v}''_n \\ \underline{v}_g \end{bmatrix} = \underline{0} \tag{6.19}$$

where

$$\underline{v}_n = \begin{bmatrix} \underline{v}'_n \\ \underline{v}''_n \end{bmatrix}$$

and $\underline{v}'_n \in \mathbf{R}^{n-g}$ and $\underline{v}''_n \in \mathbf{R}^g$.

Equation (6.15) zeros the elements of $\underline{v}''_n$. Removing $\underline{v}''_n$ from system (6.19) gives the system

$$[(A' - \mu E') \quad (B^{2''} - \mu(-B^{1''}))] \begin{bmatrix} \underline{v}'_n \\ \underline{v}_g \end{bmatrix} = \underline{0}. \tag{6.20}$$

However, the system matrices of an $\mathcal{M}2$ model corresponding to the base $\mathcal{M}0$ model have the form

$$E_2 = [E' \quad -B^{1''}]$$

$$A_2 = [A' \quad B^{2''}].$$

So system (6.20) has the form

$$(A_2 - \mu E_2) \begin{bmatrix} \underline{v}'_n \\ \underline{v}_g \end{bmatrix} = \underline{0}. \tag{6.21}$$

Since the $\mathcal{M}2$ system stability theorem shows that for $1/2 \leq \theta \leq 1$, $\mu = 1$ is not an eigenvalue of an $\mathcal{M}2$ system, $(A_2 - \mu E_2)$ is full rank, and hence system (6.21) implies

$$\begin{bmatrix} \underline{v}'_n \\ \underline{v}_g \end{bmatrix} = \underline{0}.$$

Hence, we have $\underline{v}'_n = \underline{0}$, $\underline{v}''_n = \underline{0}$, $\underline{v}_g = \underline{0}$; and so equations (6.10), (6.11) $\Longrightarrow$ (6.12).

Hence, if $1/2 \leq \theta \leq 1$, an $\mathcal{M}3$ model is completely observable. $\square$

Theorem 6.4 *An $\mathcal{M}3$ model will* not *be completely observable if there are fewer measured pressures than flow demand state variables.*

Proof

We assume we have g flow demand state variables, and less than g pressure measurements.

Necessary and sufficient conditions for the complete observability of an $\mathcal{M}3$ system are given by equations (6.10), (6.11) and (6.12).

If $\mu = 1$, then, since there are g flow demand state variables, the bottom g rows of the matrix $(A_3 - \mu E_3)$ are zero vectors. Hence the maximum rank of $(A_3 - \mu E_3)$ is n. Also, since there are less than g pressure measurements, the maximum rank of C_3 is less than g.

Hence, for $\mu = 1$, if we combine systems (6.10) and (6.11) into a single system to solve for $\underline{v}$, such a system would have rank less than $n + g$. Hence, equations (6.10) and (6.11) would have non-zero solutions for $\underline{v}$.

Thus, equations (6.10) and (6.11) do not imply equation (6.12), and hence the $\mathcal{M}3$ system is not observable. □

For $\mathcal{M}3$ models constructed with trivial difference equations of the form (6.1), it was found direct observers did not work well. Thus to estimate the flow demands in the gas network, a *dynamic* observer constructed upon an $\mathcal{M}3$ model is run assuming all the pressure and flow perturbations are initially zero. The pressure perturbation measurements are fed in at each time level, and the observer state tends to the state of the gas network with time. Perfect asymptotic convergence is not obtained unless the flow demands do not vary with time, since equations (6.2) contain modelling error. If the flow demands are changing, although not too rapidly, the observer still tracks the state of the gas network fairly well. Indeed, typically, the flow demands in gas networks change only slowly throughout the day.

6.2 Weighted $\mathcal{M}3$ Models

In fact, the profiles of the flow demands are fairly well known from other measured demands that change thoughout the day with similar patterns of gas consumption. More accurate $\mathcal{M}3$ models may be constructed using such information available about the *shapes* of the flow demand profiles with time. This corresponds to knowing the constants $f_k^{demand\ site}$ in

$$flow\ demand_{k+1}^{demand\ site} = flow\ demand_k^{demand\ site} + f_k^{demand\ site}$$

where the $f_k^{demand\ site}$ may be estimated from the telemetry from other *measured* demand flows. After normalisation, we would have

$$normalised\ flow\ demand_{k+1}^{demand\ site} = normalised\ flow\ demand_k^{demand\ site} + \tilde{f}_k^{demand\ site}$$

where $\tilde{f}_k^{demand\ site} = f_k^{demand\ site}/Nq$, i.e., we would have

$$\mathcal{Q}^{demand\ site} + d_{k+1}^{demand\ site} = \mathcal{Q}^{demand\ site} + d_k^{demand\ site} + \tilde{f}_k^{demand\ site}$$

and cancelling $\mathcal{Q}^{demand\ site}$ from both sides gives the new trivial difference equations for the flow demand perturbations

$$d_{k+1}^{demand\ site} = d_k^{demand\ site} + \tilde{f}_k^{demand\ site} \quad for\ all\ k. \tag{6.22}$$

The $\mathcal{M}3$ models now contain difference equations of the form (6.22) where the weightings, $\tilde{f}_k^{demand\ site}$, are contained in a new vector added to the right hand side of the $\mathcal{M}3$ system. The new weighted $\mathcal{M}3$ models have the form

$$E_3\underline{x}_3(k+1) = A_3\underline{x}_3(k) + B_3^1\underline{u}_3(k+1) + B_3^2\underline{u}_3(k) + \underline{l}_3(k) \tag{6.23}$$

where the vector $\underline{l}_3(k)$ contains the weightings, $\tilde{f}_k^{demand\ site}$. The addition of the vector $\underline{l}_3(k)$ to the $\mathcal{M}3$ model does not alter its observability. Note that only the *shape* of the flow demand profile is needed and not its placement relative to the flow magnitude axis. Thus, estimating the demand flows means placing the profiles up or down the flow demand magnitude axis.

To estimate the flow demands in the gas network, a dynamic observer may be constructed upon a weighted $\mathcal{M}3$ model and run as before. Now there is perfect asymptotic

convergence because we have lost the modelling error in the extra trivial difference equations (6.22) for the flow demand perturbations. However, now *direct* observers work well enough to be used as well. Obviously, in practice, the estimates of the $\tilde{f}_k^{demand\ site}$ would not be exact, and there would still be some error in the observer estimate.

6.3 Experiments

When the $\mathcal{M}0$ model had been running for a while, the pressures at the upstream end and the sites of flow demand were recorded at each timestep and fed into the various $\mathcal{M}3$ model-based observers. The flow demands predicted by these techniques were compared with the true flows used as inputs to the $\mathcal{M}0$ model. For experiments 6.1 to 6.7 and 6.11 to 6.13, the $\mathcal{M}0$ model simulating a gas network was identical to the $\mathcal{M}0$ model upon which the $\mathcal{M}3$ model was constructed. For the remaining experiments, the $\mathcal{M}0$ model simulating a gas network had a much finer discretisation (in both space and time) than the $\mathcal{M}3$ model.

In experiments 6.1 to 6.10, no weightings, $\tilde{f}_k^{demand\ site}$, were incorporated into the $\mathcal{M}3$ models. However, for experiments 6.11 to 6.18, the $\mathcal{M}3$ models incorporated the exact values of the weightings, calculated from the flow demand inputs to the $\mathcal{M}0$ model.

The two types of dynamic observer were run with either 'large' eigenvalues spread evenly in the interval $(0, 0.5)$, or 'smaller' eigenvalues spread evenly in the interval $(0, 0.025)$. For each dynamic observer design, the eigenvalues were assigned robustly except for experiment 6.5, where step 6 of the robust eigenstructure assignment algorithm was omitted. When the design C observer was run, the arbitrarily assignable singular values were spread in the interval described by equation (5.37).

For each experiment, the true flow demand profiles for the demands, $D_k^{A/B}$, $D_k^{B/C}$ and D_k^C are shown as thick lines in Figs. A, B and C respectively and the state estimates for $D_k^{A/B}$, $D_k^{B/C}$ and D_k^C are shown as thin lines. The percentage errors between the state estimates of $D_k^{A/B}$, $D_k^{B/C}$ and D_k^C and their true values are shown in Figs. D, E and F respectively.

6.3.1 Experiments with *no* weightings, $\tilde{f}_k^{demand\ site}$, included in the trivial flow demand difference equations

Data taken from $\mathcal{M}0$ model with identical mesh - both $\mathcal{M}0$ and $\mathcal{M}3$ models have 10 spatial nodes along each pipe.

Experiment 6.1) Observer Design B (large eigenvalues) with $\theta = 1$

Experiment 6.2) Observer Design B (small eigenvalues) with $\theta = 1$

Experiment 6.3) Observer Design B (large eigenvalues) with $\theta = 0.5$

Experiment 6.4) Observer Design B (small eigenvalues) with $\theta = 0.5$

Experiment 6.5) Observer Design B (small eigenvalues) with $\theta = 0.5$ (*Eigenvalues not assigned robustly*)

Experiment 6.6) Observer Design C (small eigenvalues) with $\theta = 1$

Experiment 6.7) Observer Design C (small eigenvalues) with $\theta = 0.5$

Data taken from $\mathcal{M}0$ model with much finer mesh - $\mathcal{M}3$ model has 10 spatial nodes along each pipe.

Experiment 6.8) Observer Design B (small eigenvalues) with $\theta = 1$

Experiment 6.9) Observer Design B (small eigenvalues) with $\theta = 0.5$

Experiment 6.10) Observer Design C (small eigenvalues) with $\theta = 1$

6.3.2 Experiments with weightings, $\tilde{f}_k^{demand\ site}$, included in the trivial flow demand difference equations

Data taken from $\mathcal{M}0$ model with identical mesh - both $\mathcal{M}0$ and $\mathcal{M}3$ models have 10 spatial nodes along each pipe.

Experiment 6.11) Observer Design B (small eigenvalues) with $\theta = 1$

Experiment 6.12) Observer Design B (small eigenvalues) with $\theta = 0.5$

Experiment 6.13) Observer Design C (small eigenvalues) with $\theta = 1$

Data taken from $\mathcal{M}0$ model with much finer mesh - $\mathcal{M}3$ model has 10 spatial nodes along each pipe.

Experiment 6.14) Observer Design B (small eigenvalues) with $\theta = 1$

Experiment 6.15) Observer Design B (small eigenvalues) with $\theta = 0.5$

Experiment 6.16) Observer Design C (small eigenvalues) with $\theta = 1$

Data taken from $\mathcal{M}0$ model with much finer mesh - $\mathcal{M}3$ model has 5 spatial nodes along each pipe.

Experiment 6.17) Observer Design A with $\theta = 1$

Experiment 6.18) Observer Design A with $\theta = 0.5$

Experiment 6.1

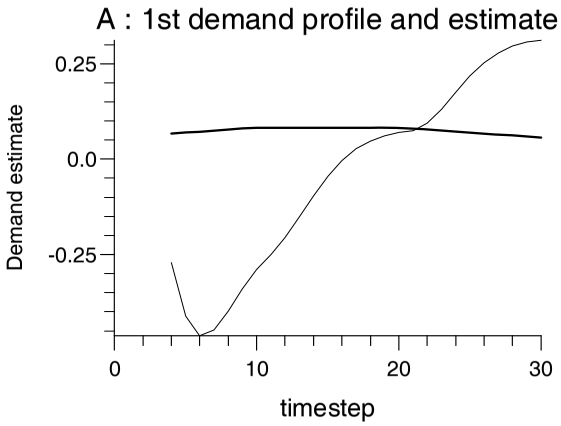

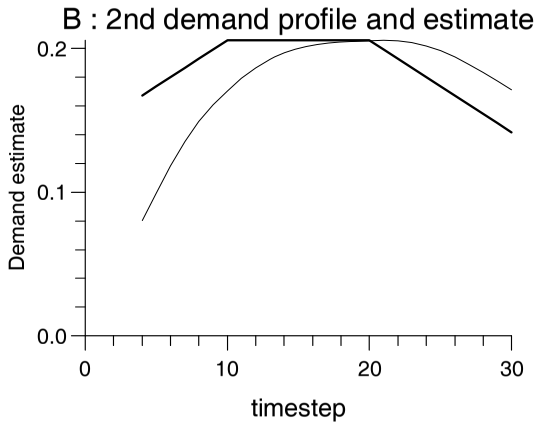

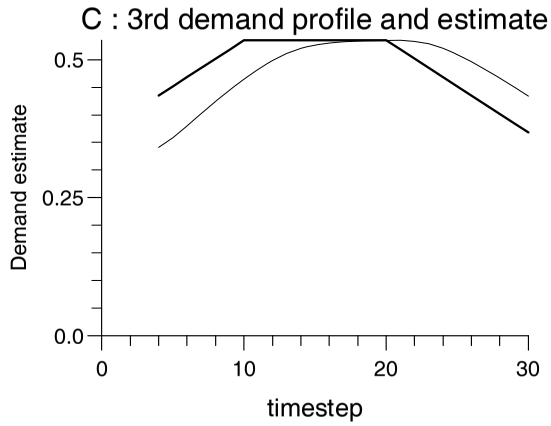

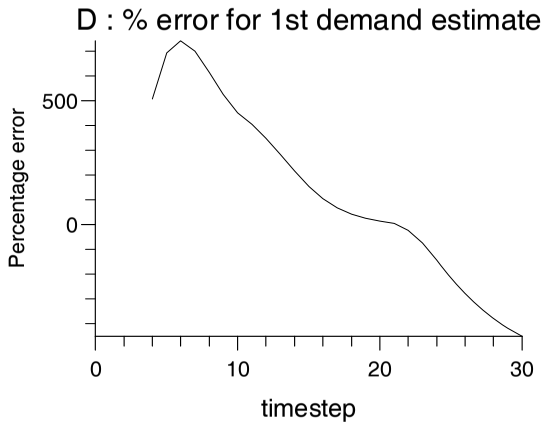

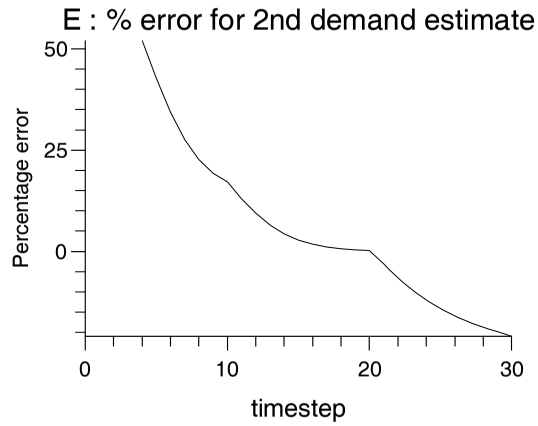

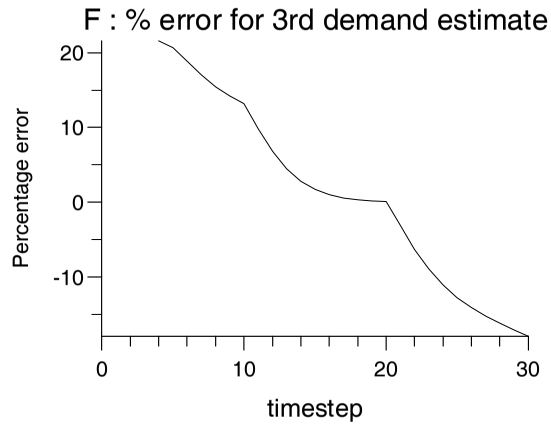

Experiment 6.2

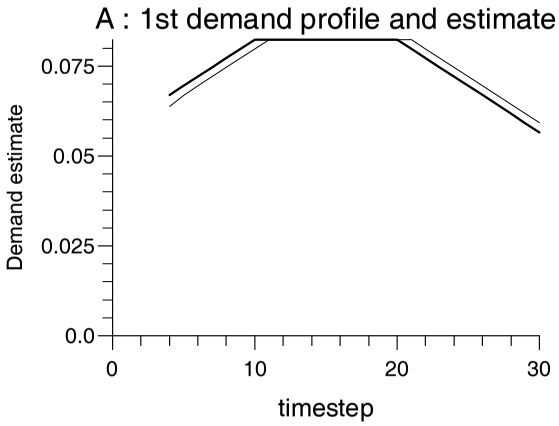

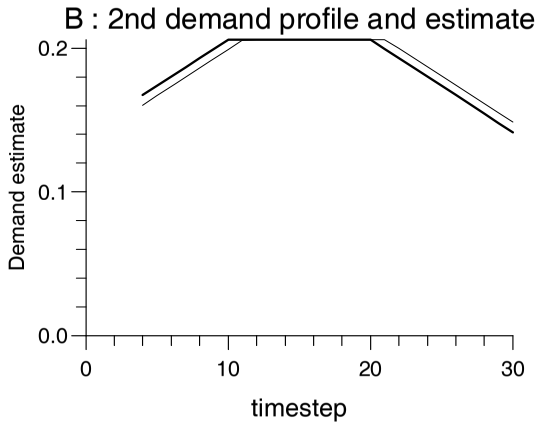

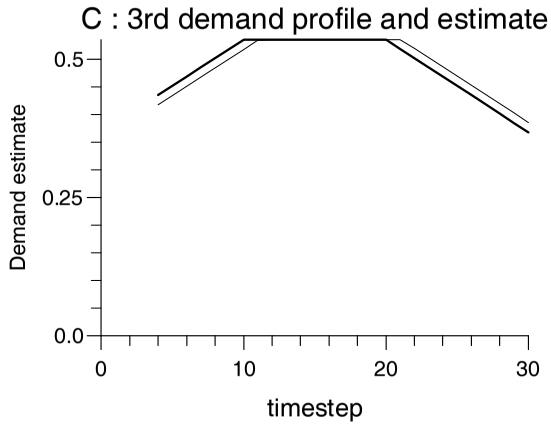

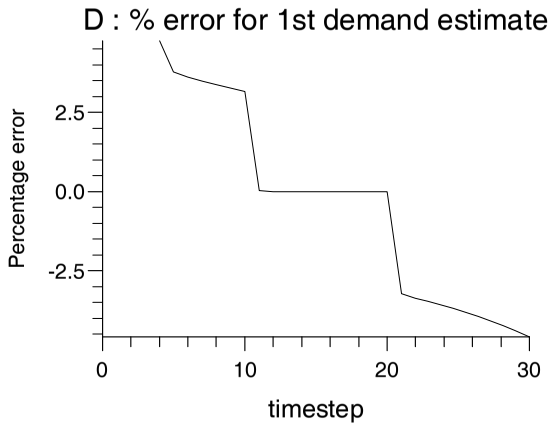

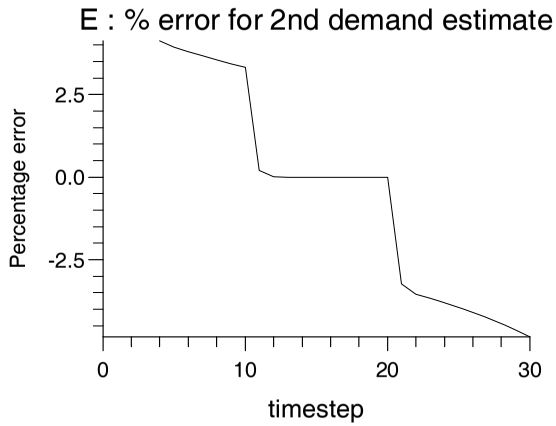

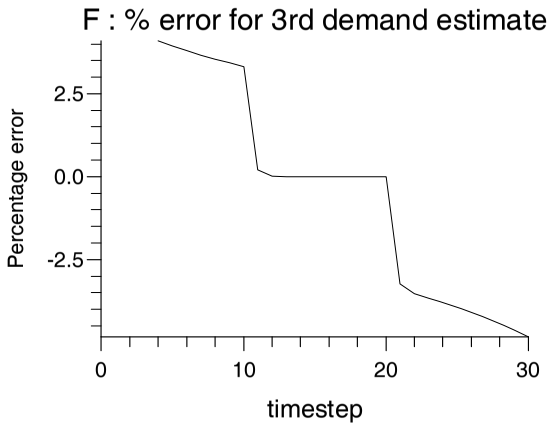

Experiment 6.3

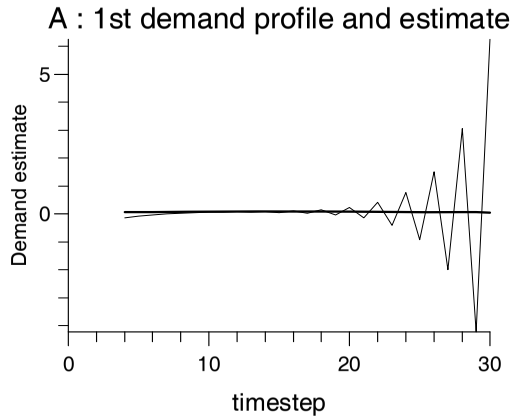

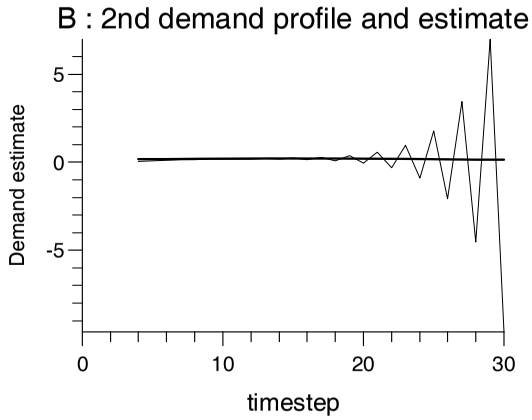

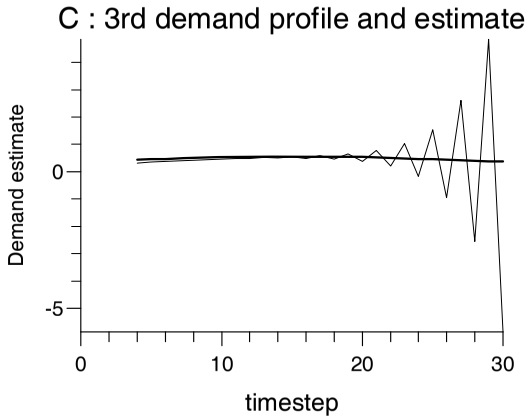

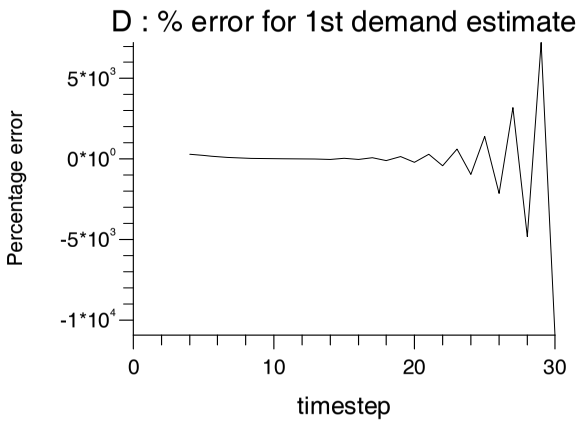

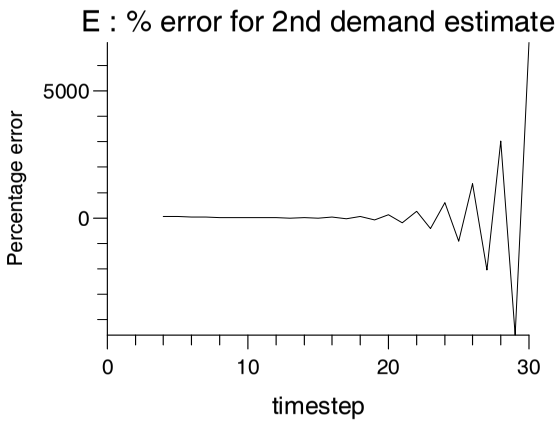

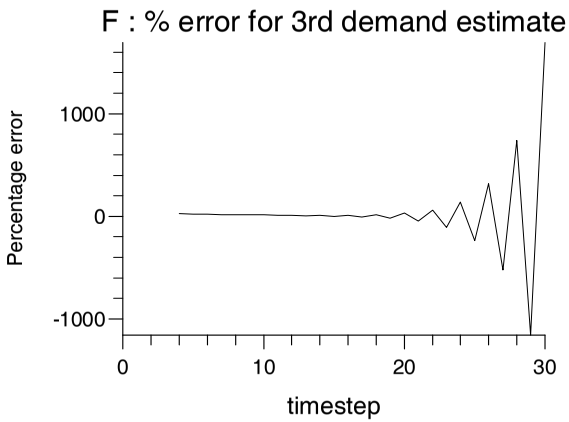

Experiment 6.4

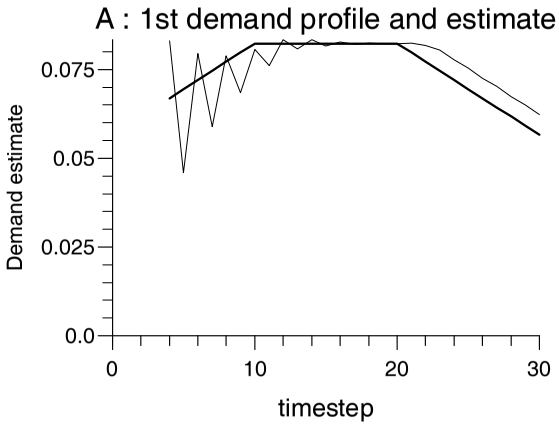

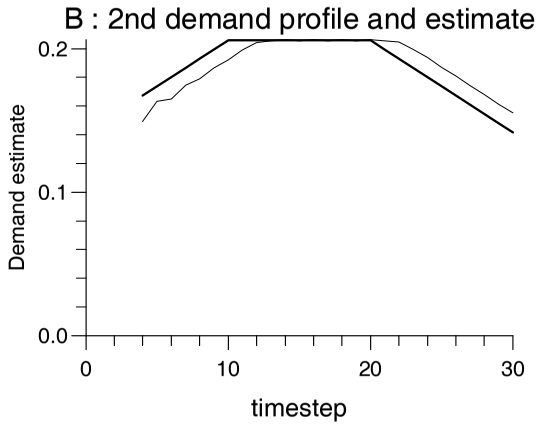

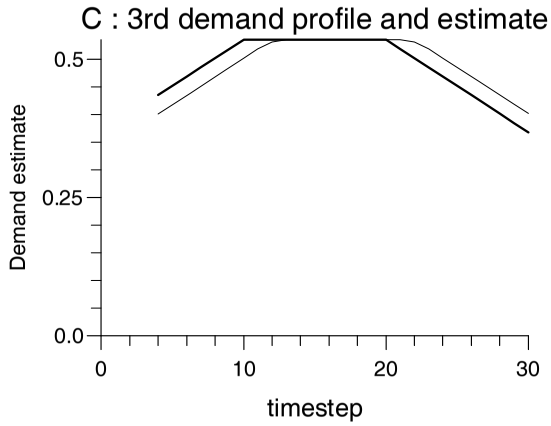

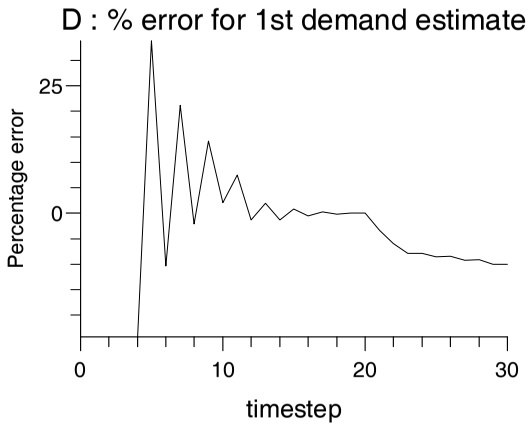

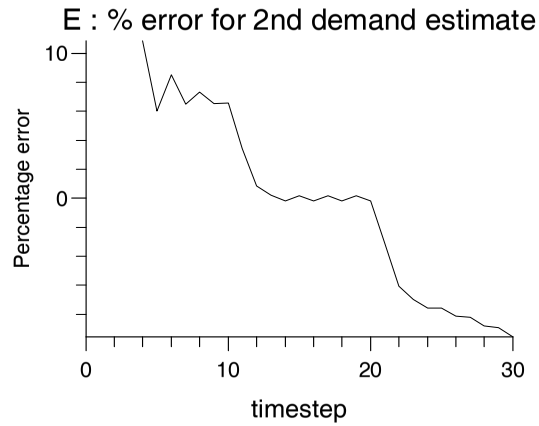

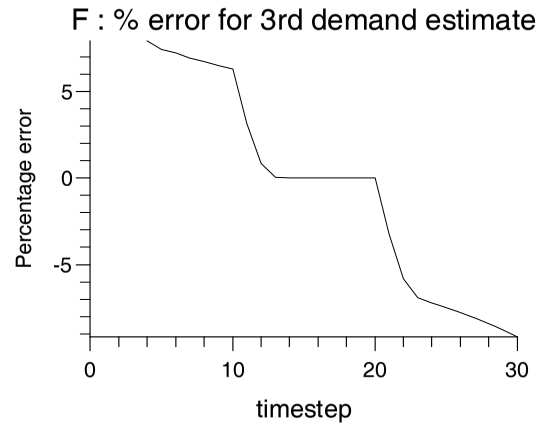

Experiment 6.5

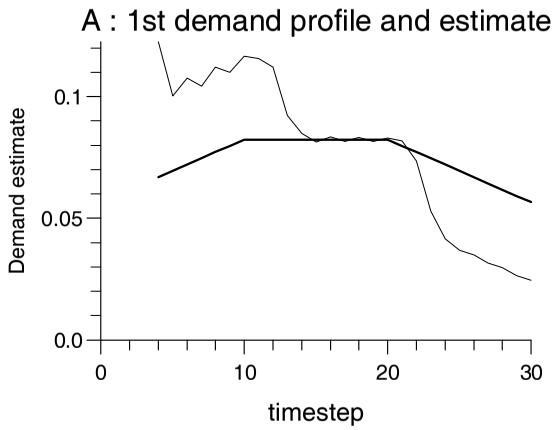

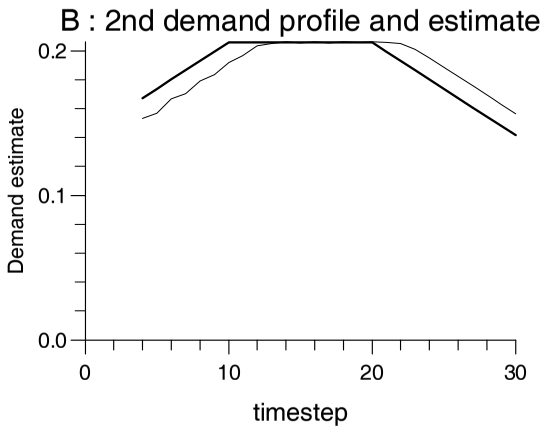

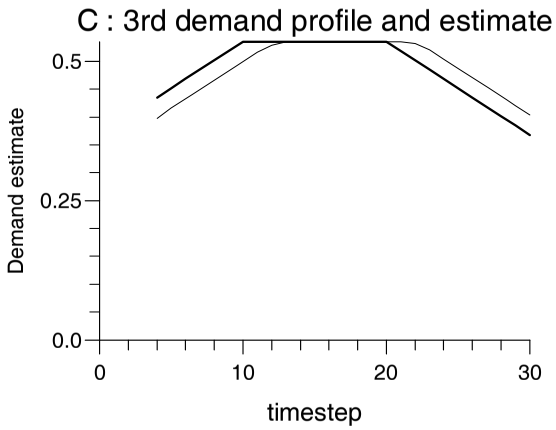

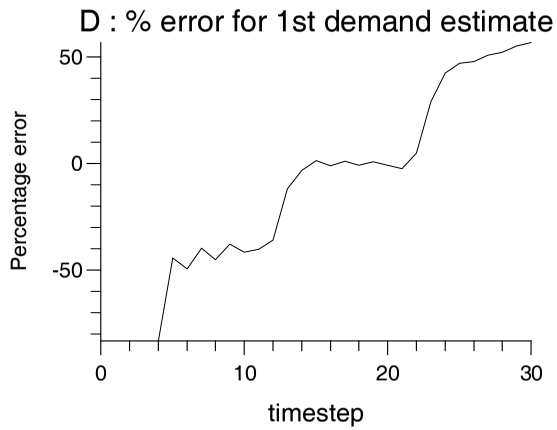

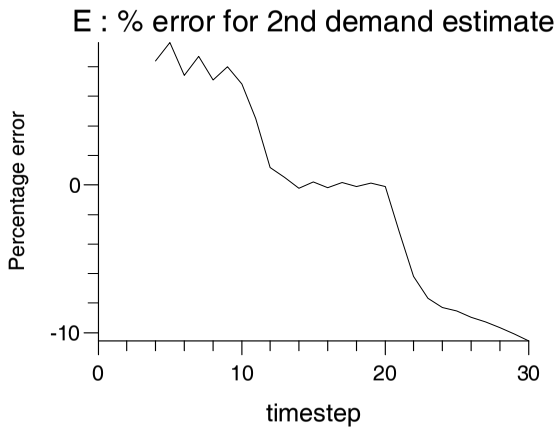

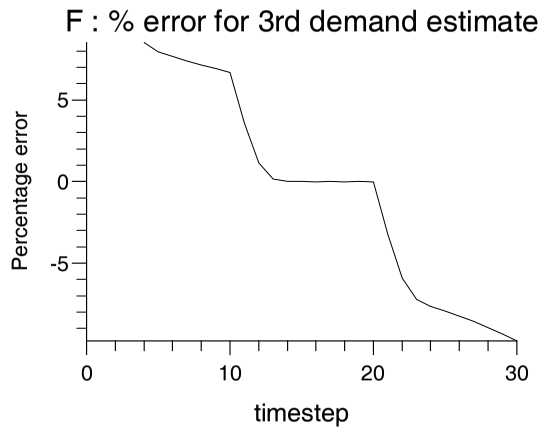

Experiment 6.6

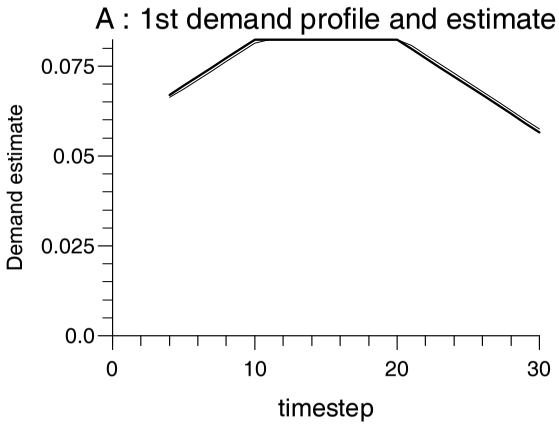

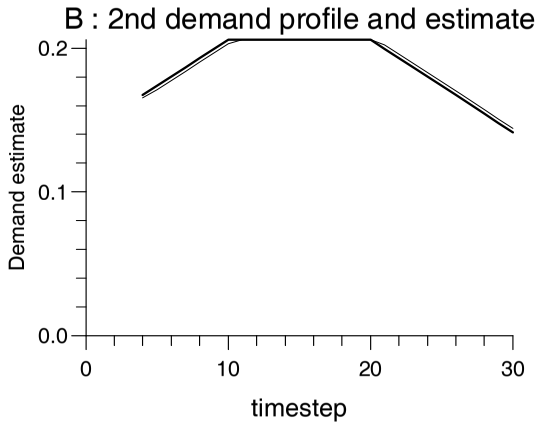

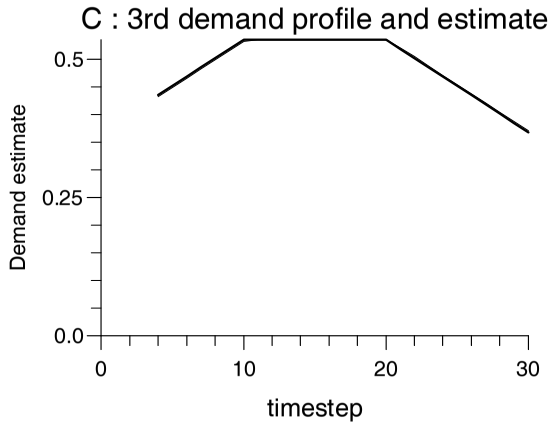

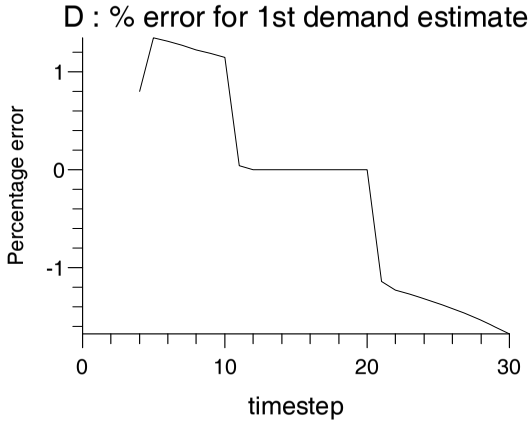

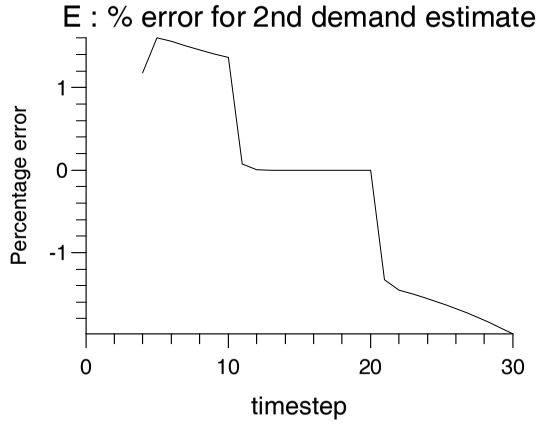

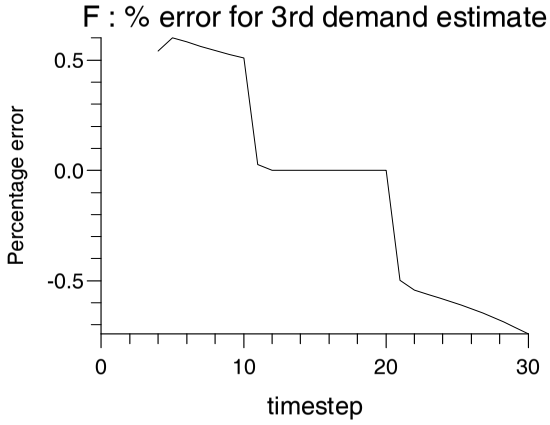

Experiment 6.7

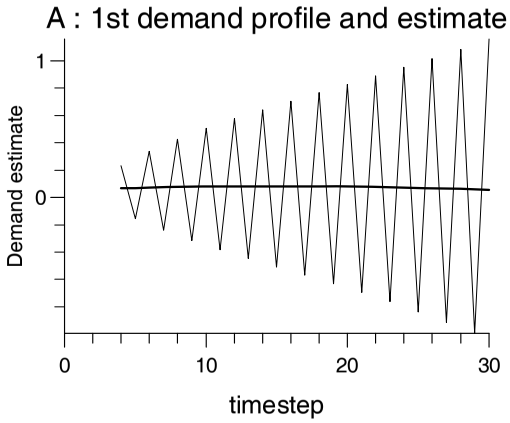

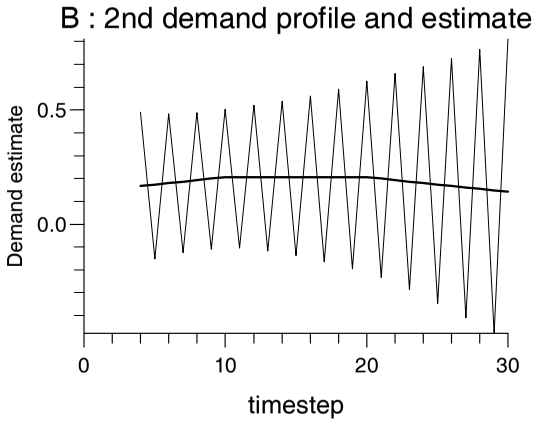

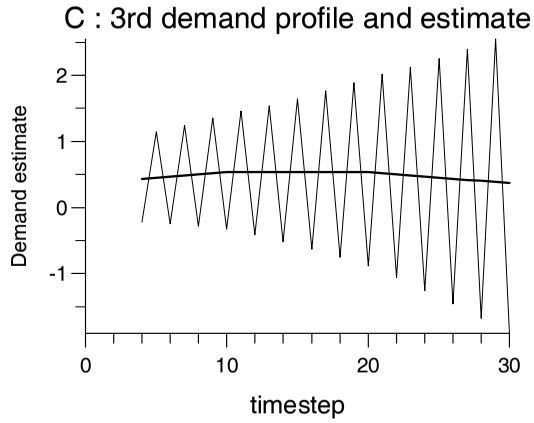

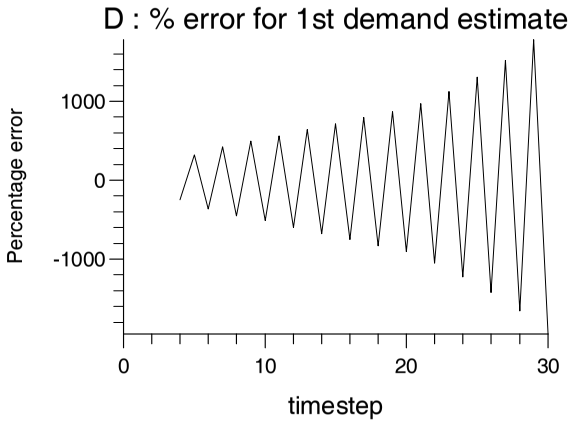

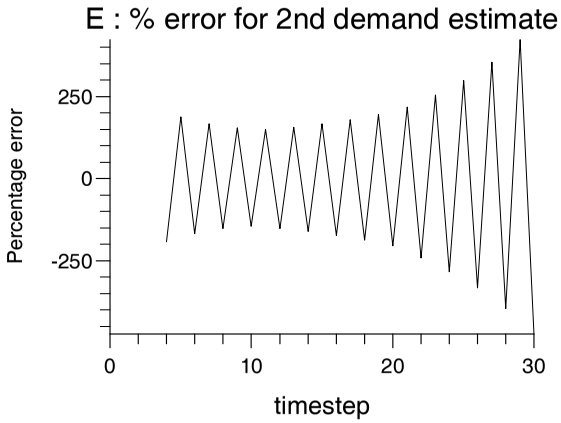

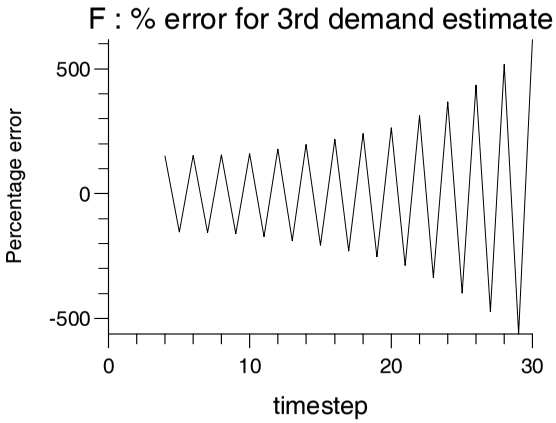

Experiment 6.8

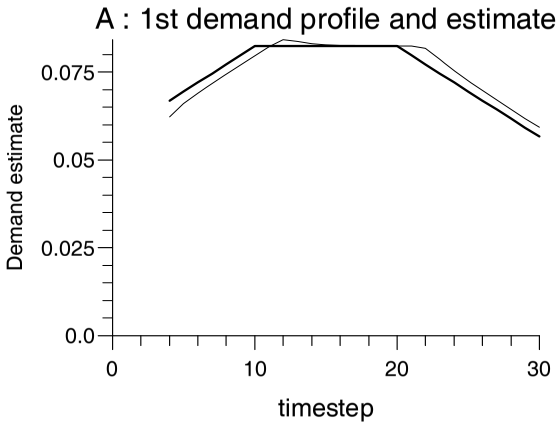

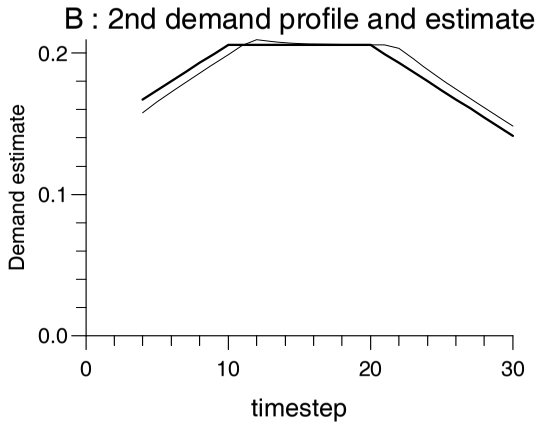

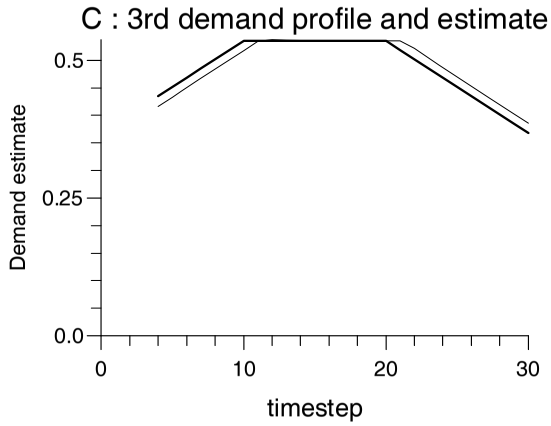

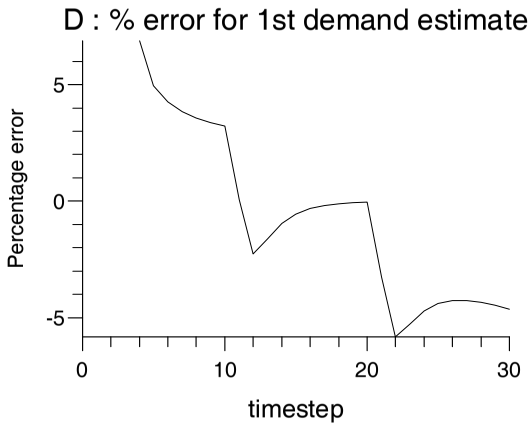

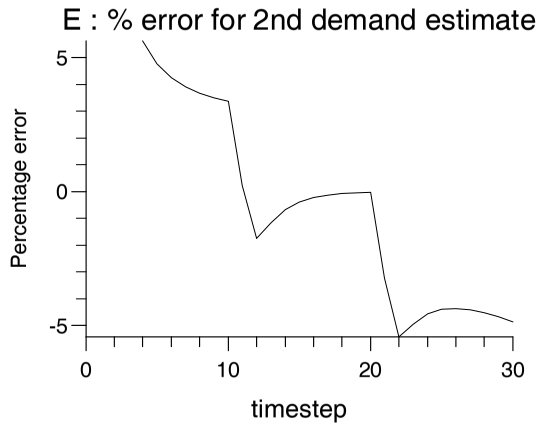

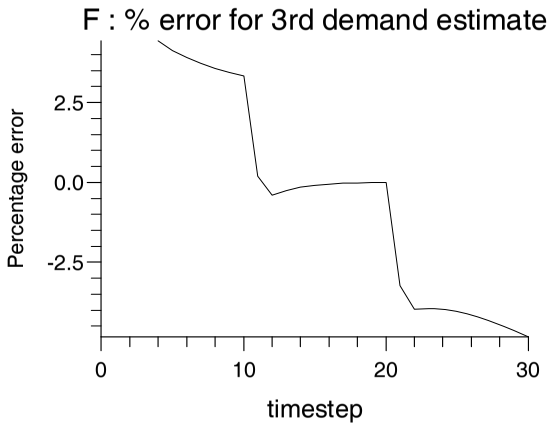

Experiment 6.9

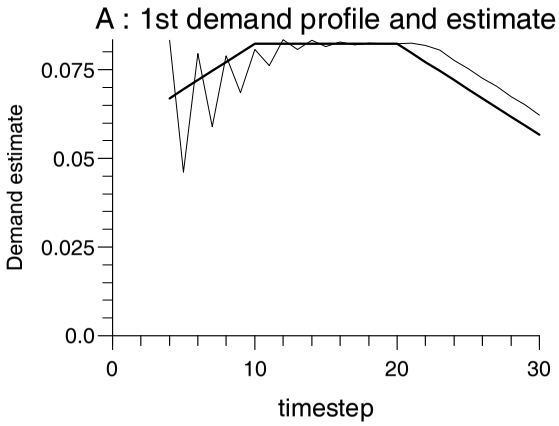

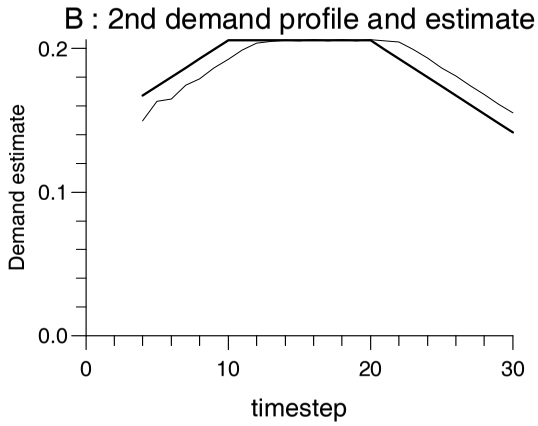

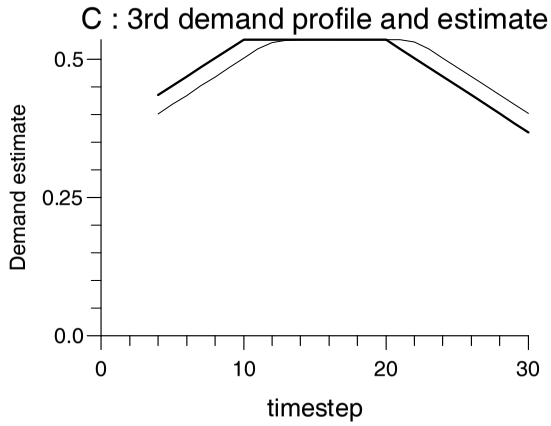

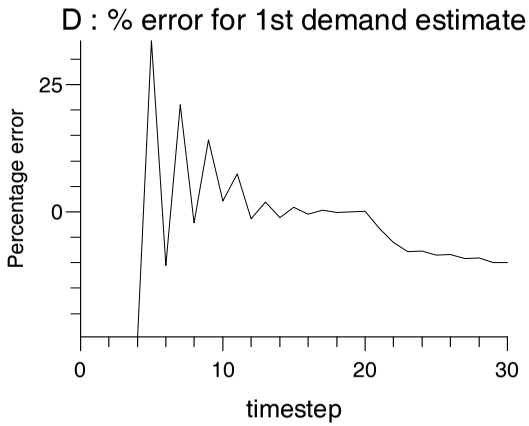

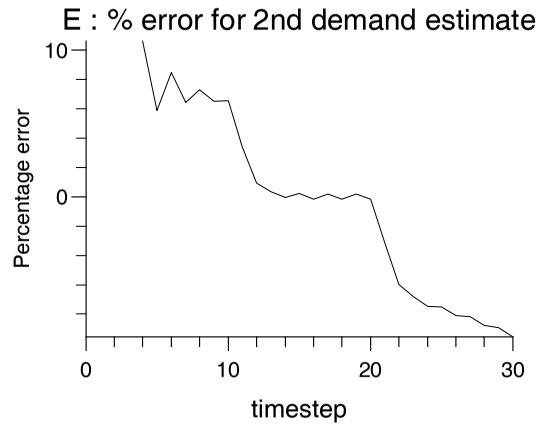

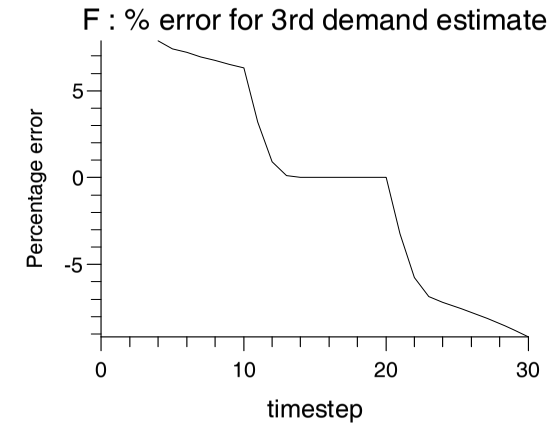

Experiment 6.10

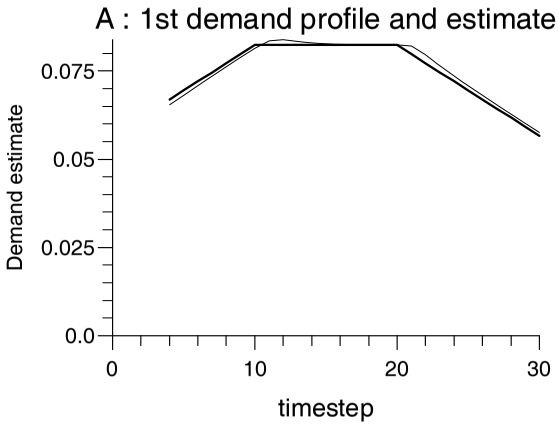

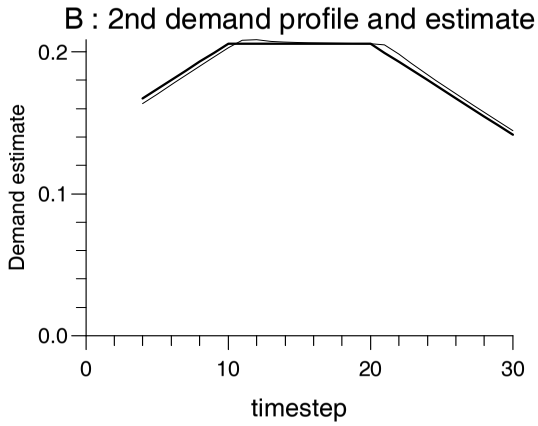

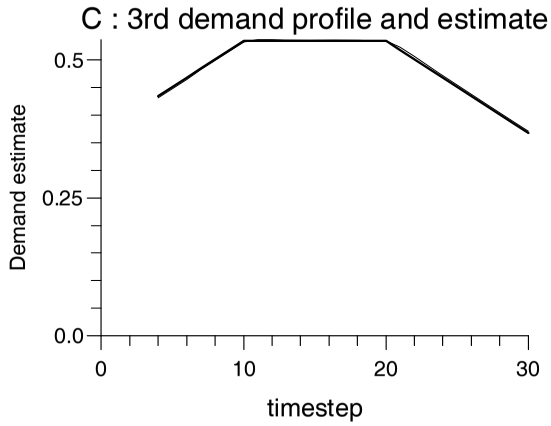

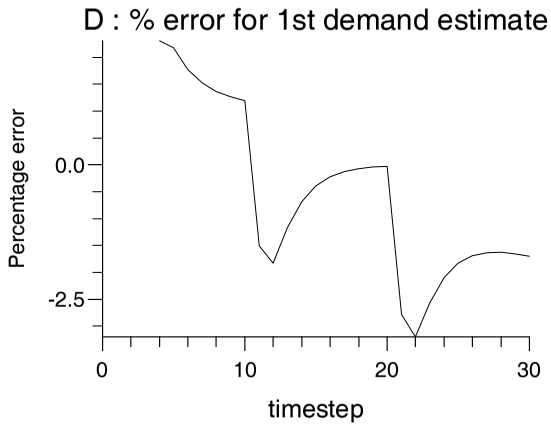

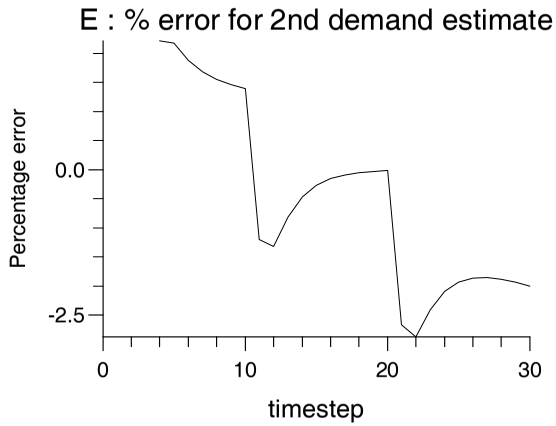

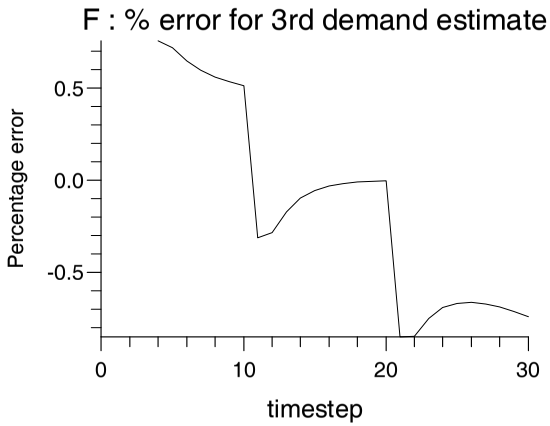

Experiment 6.11

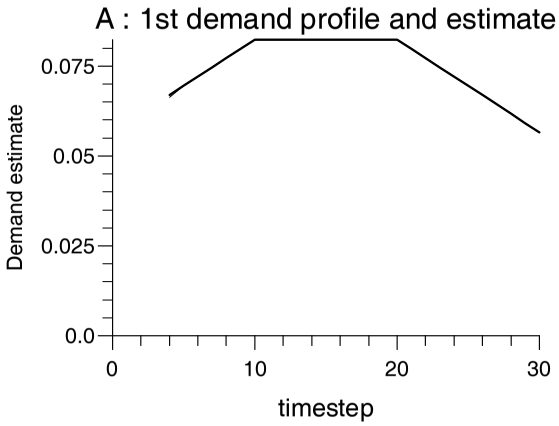

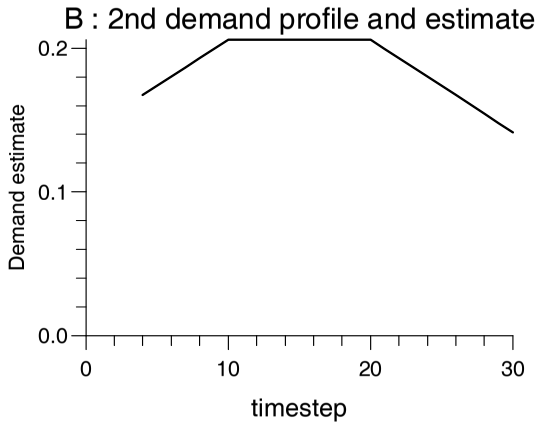

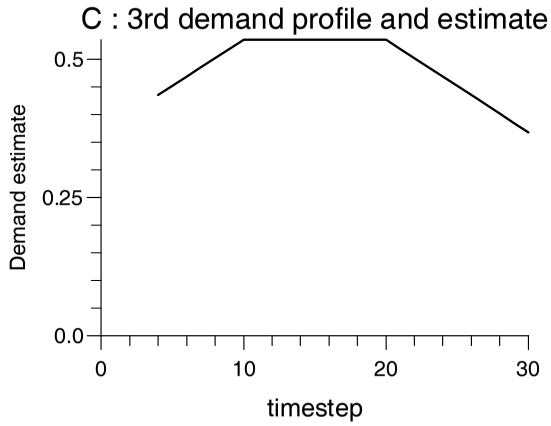

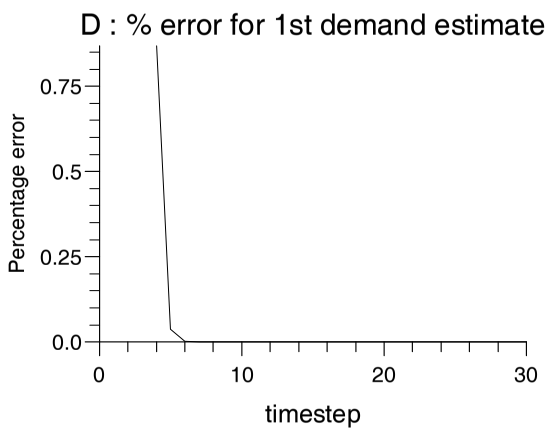

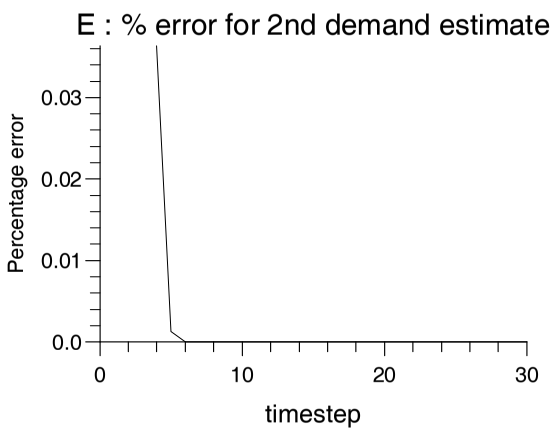

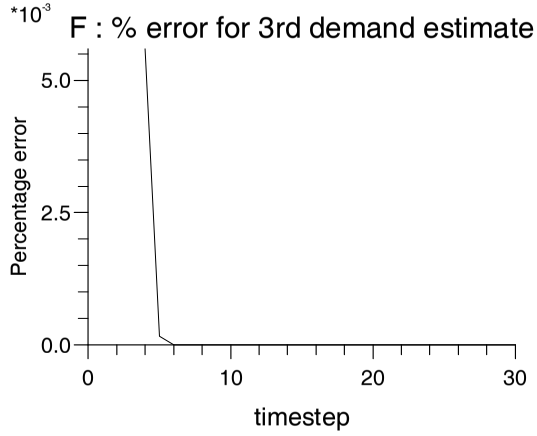

Experiment 6.12

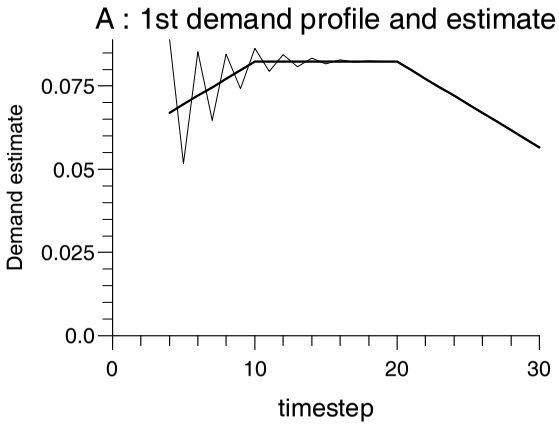

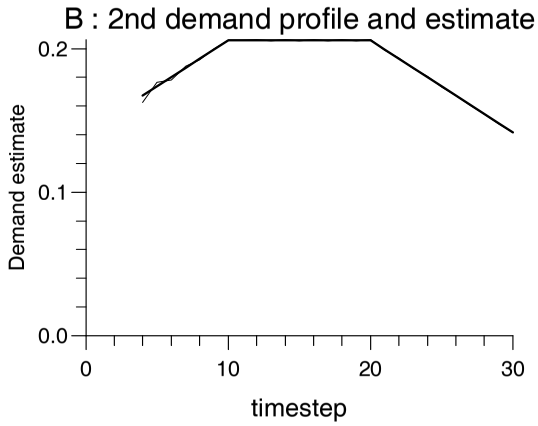

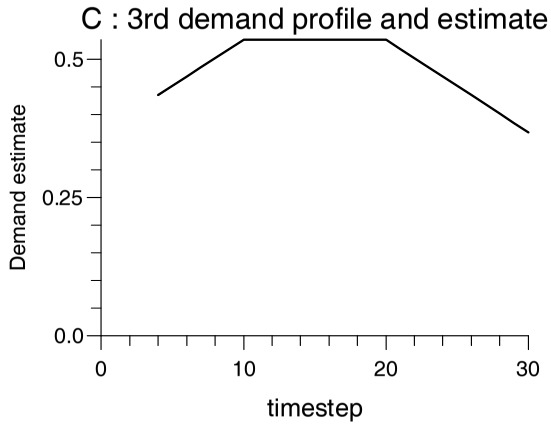

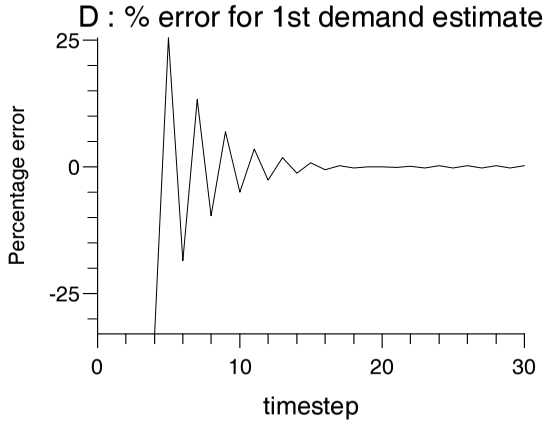

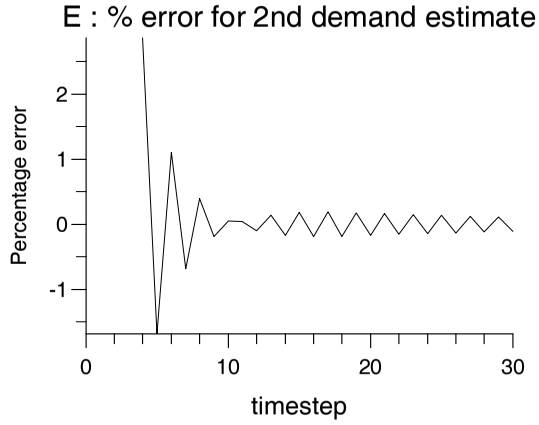

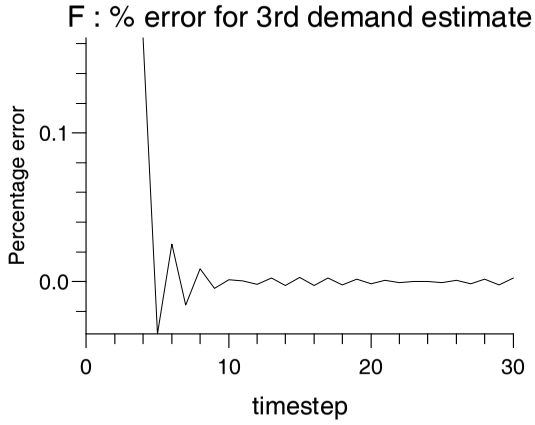

Experiment 6.13

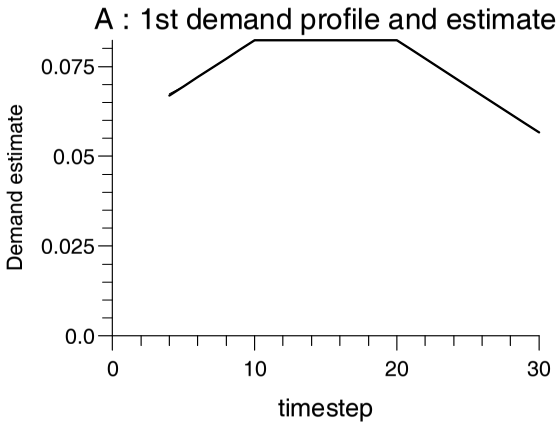

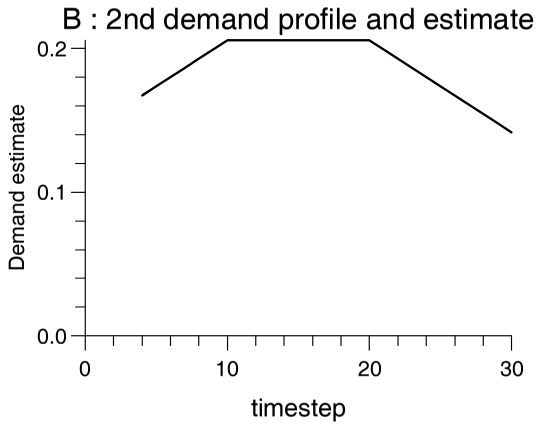

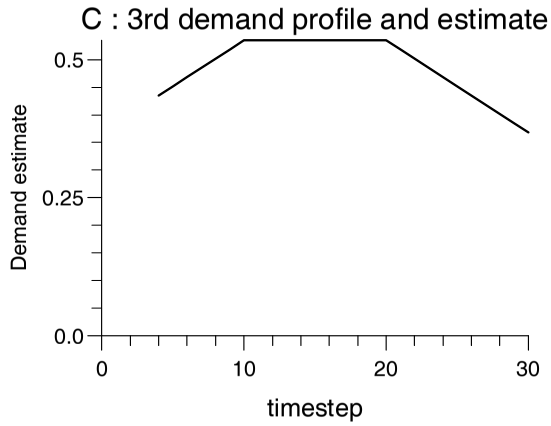

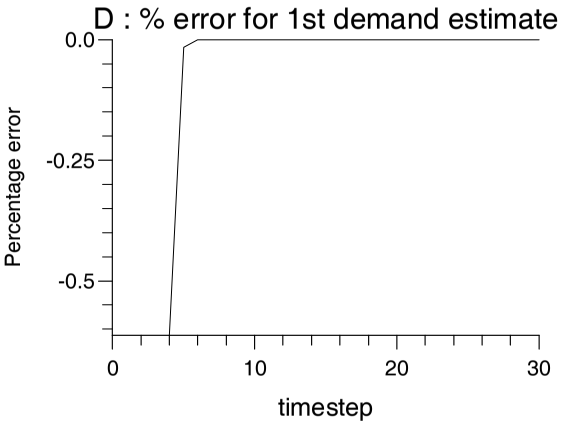

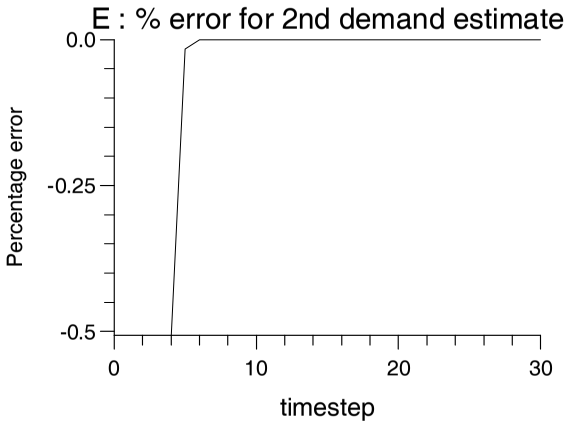

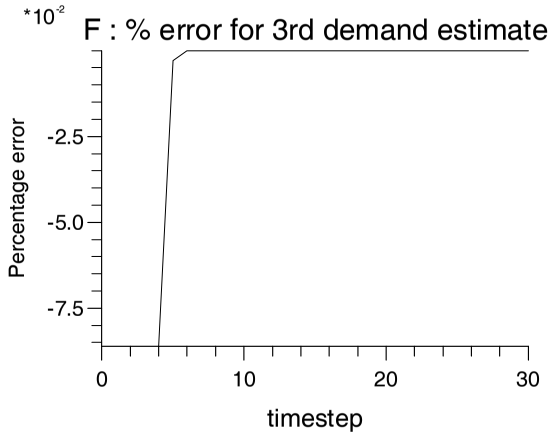

Experiment 6.14

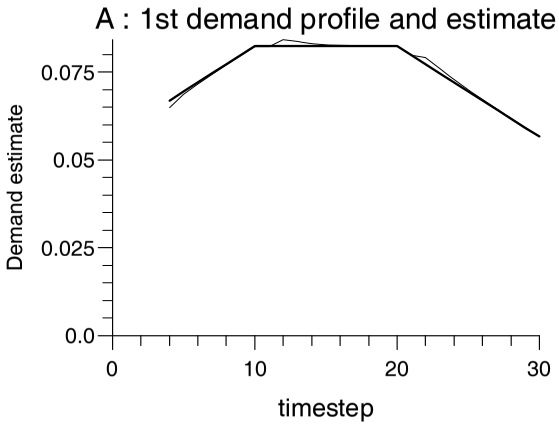

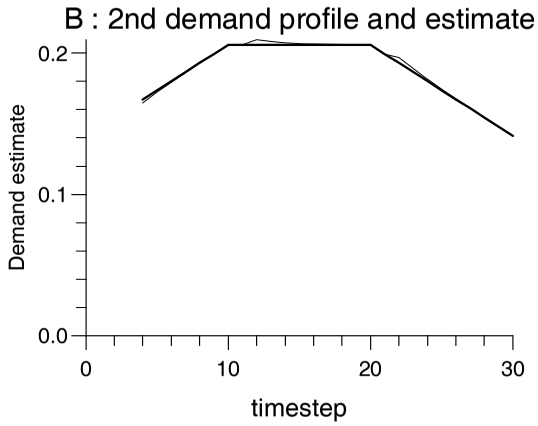

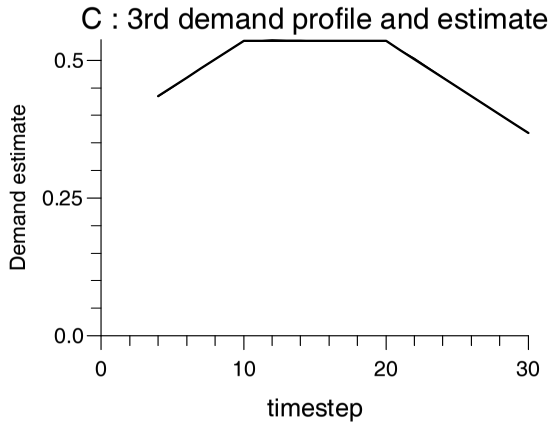

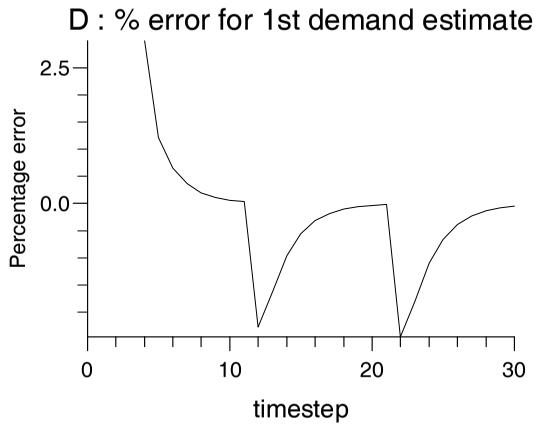

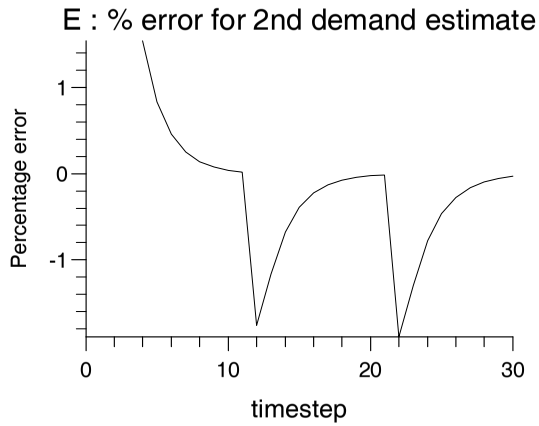

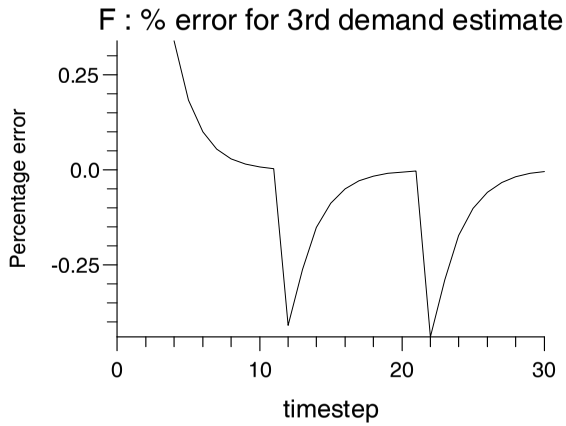

Experiment 6.15

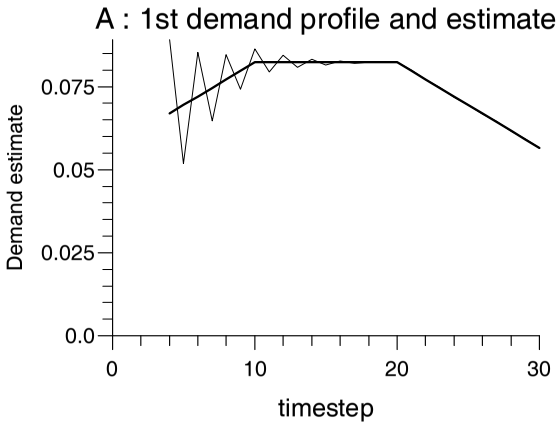

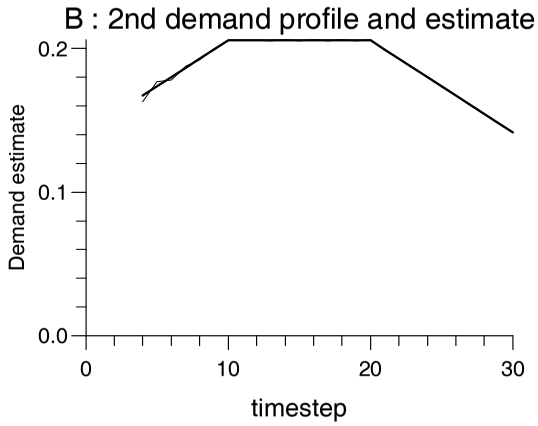

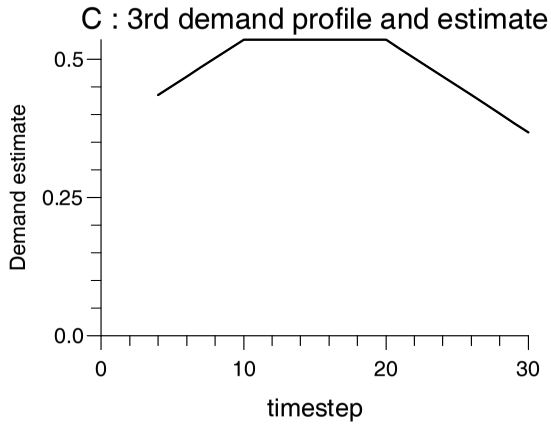

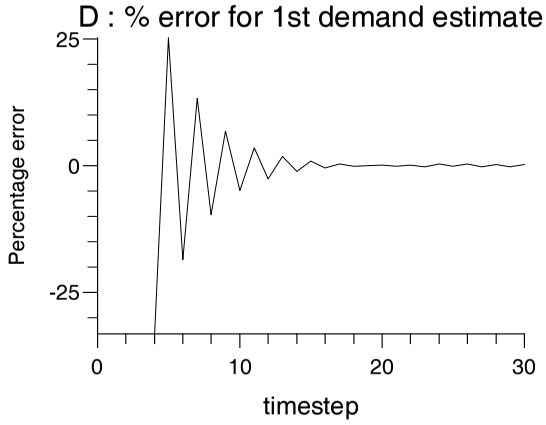

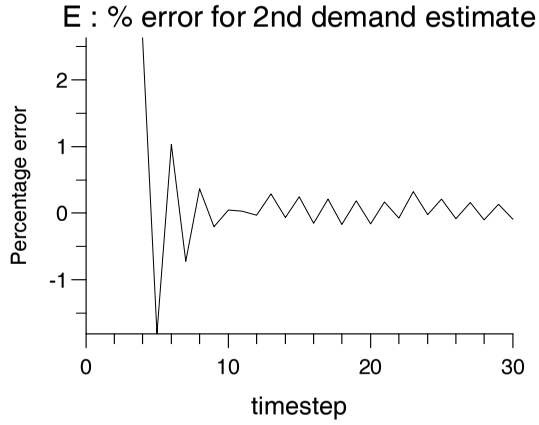

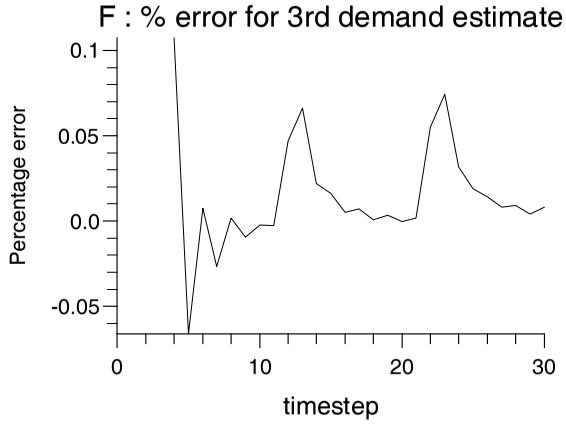

Experiment 6.16

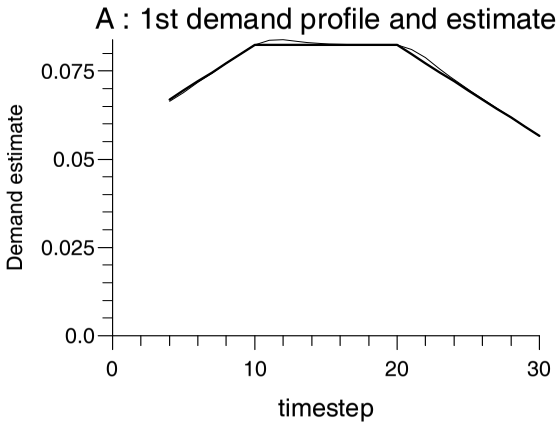

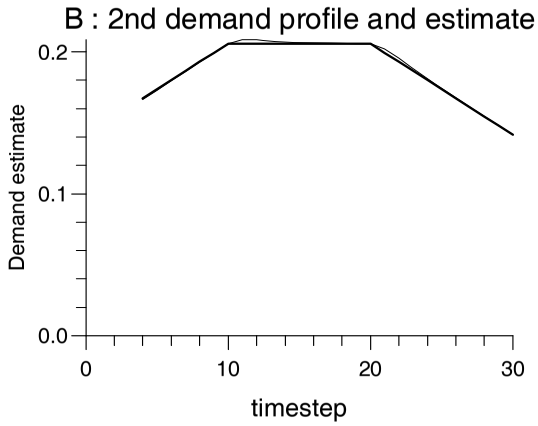

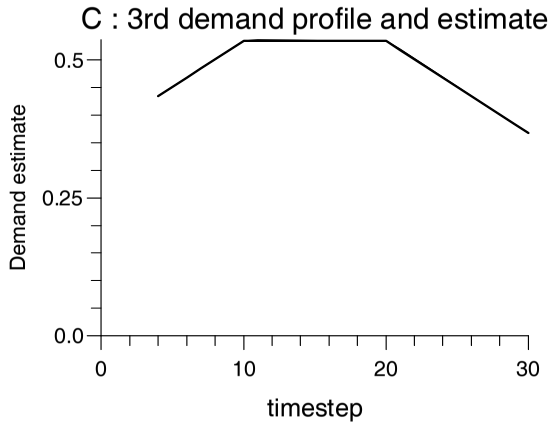

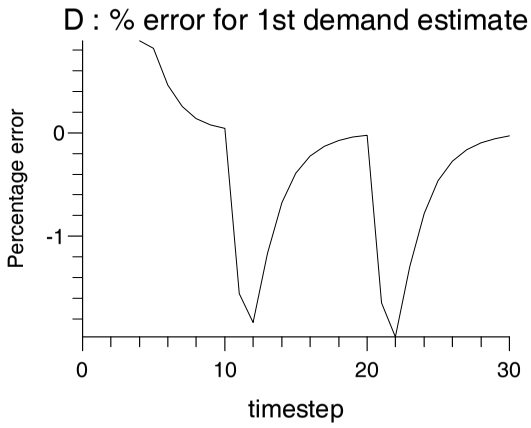

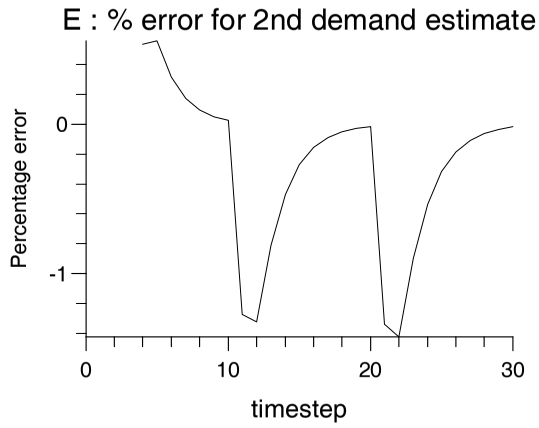

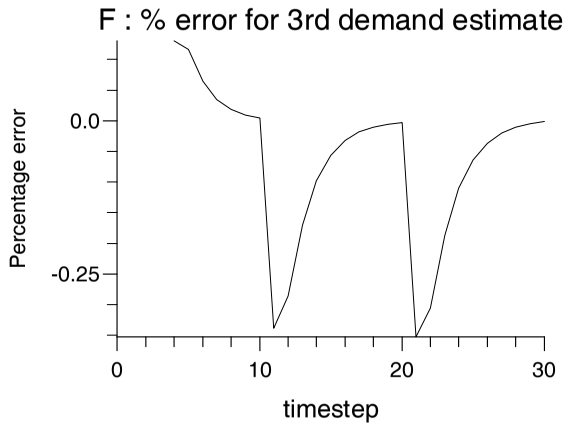

Experiment 6.17

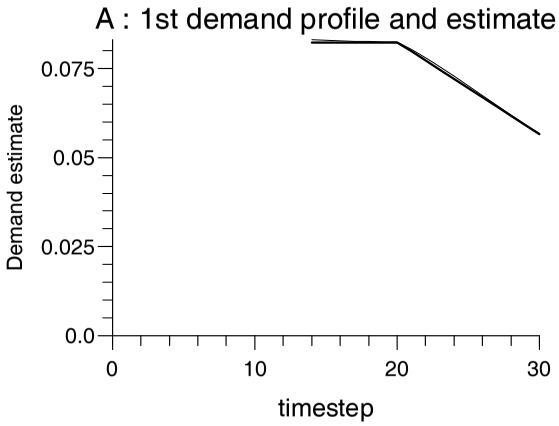

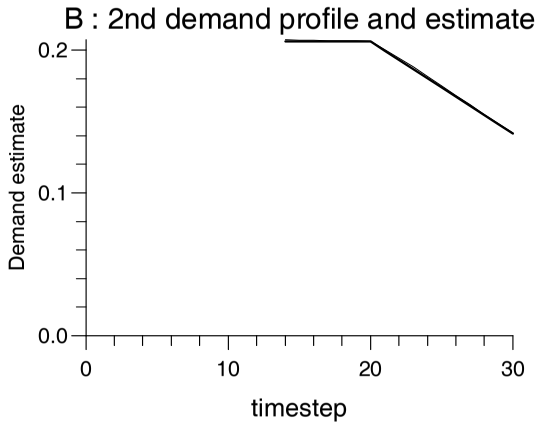

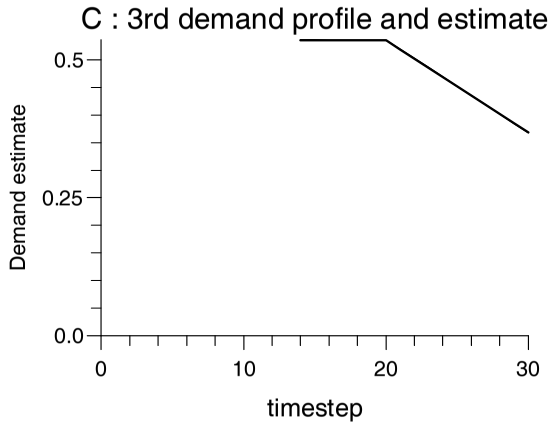

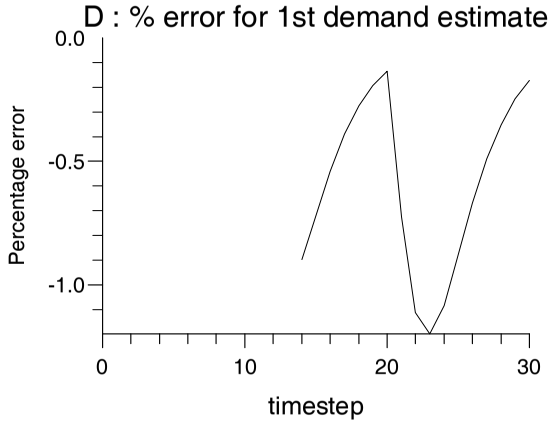

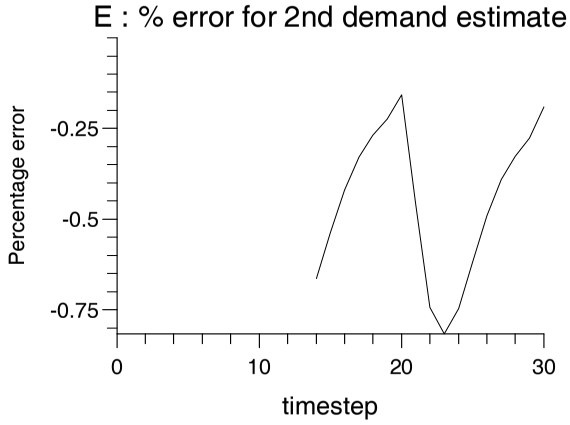

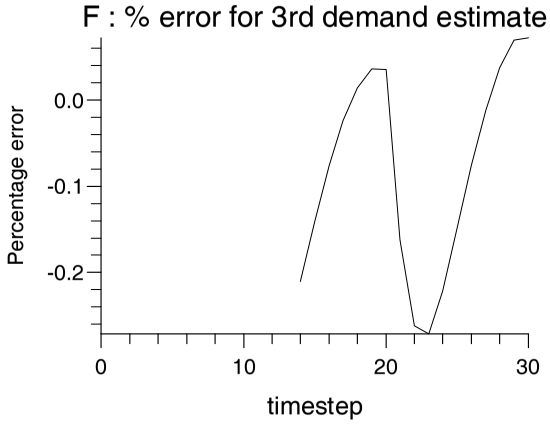

Experiment 6.18

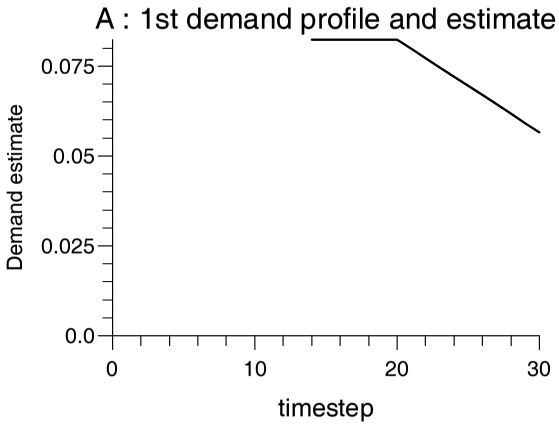

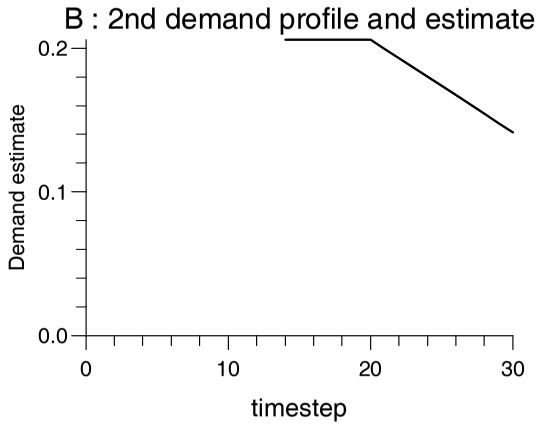

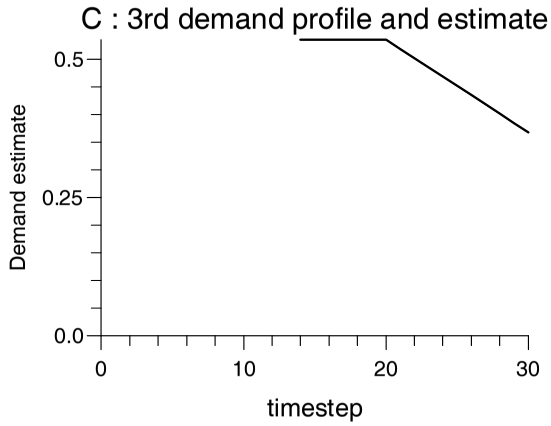

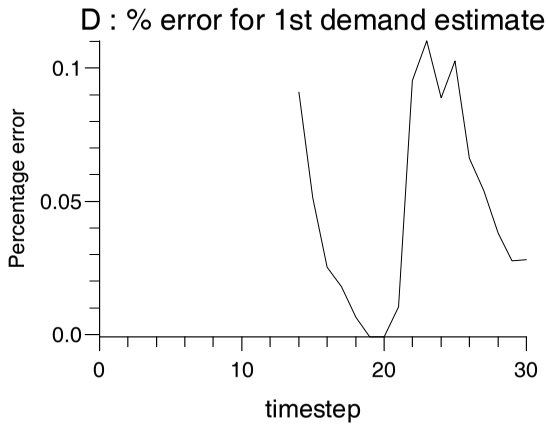

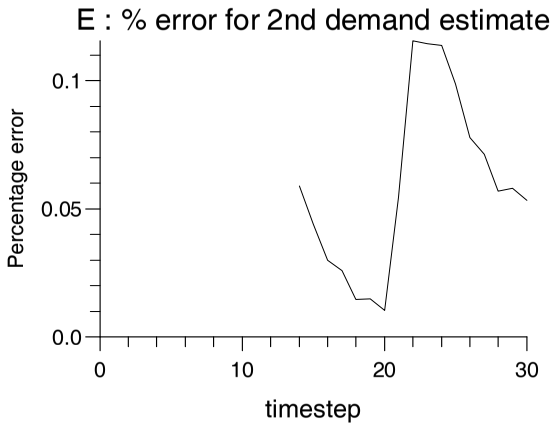

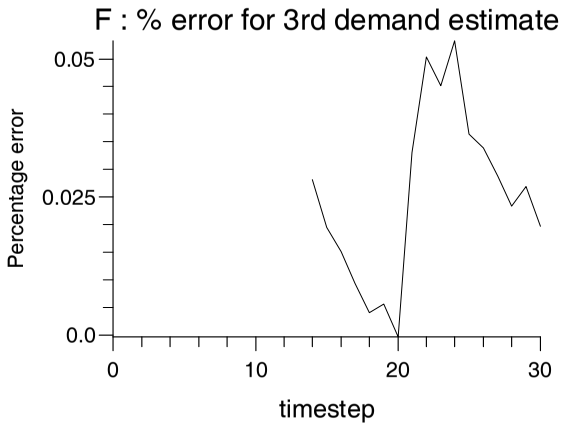

6.4 Discussion

6.4.1 Observer Design A : The Direct Observer

When the weightings, $\tilde{f}_k^{demand\ site}$, were not included in the $\mathcal{M}3$ model, the direct observer gave poor results. However, when the $\tilde{f}_k^{demand\ site}$ were included, for all values of $\theta \in [1/2, 1]$, the state estimate of the direct observer contained no error when data was taken from an $\mathcal{M}0$ model with an identical mesh, and contained only a small amount of error when data was taken from an $\mathcal{M}0$ model with a much finer mesh. Curiously, in contrast to dynamic observer designs, the direct observer gave the most accurate state estimates with $\theta = 1/2$ rather than with $\theta = 1$. The graphs presented begin at timestep 14 due to the need to build up enough timesteps to be able to solve equation (5.4) directly for the state estimate.

The main disadvantage with the direct observer was the large amount of computational work involved.

6.4.2 Observer Design B : The Dynamic Observer Without Feedback at the Current Time-Level

When the weightings, $\tilde{f}_k^{demand\ site}$, were not included in the $\mathcal{M}3$ model, after an initial large error over the first few timesteps characteristic of observer designs, design B observers gave fair estimates of the demand flows when small eigenvalues were assigned. However, these dynamic observers gave estimated profiles for the demands that always lagged behind the true profiles as the observers attempted to continually 'catch up' with the changing flows. This can be understood by considering the un-weighted $\mathcal{M}3$ system

$$E_3 \underline{x}_3(k+1) = A_3 \underline{x}_3(k) + B_3^1 \underline{u}_3(k+1) + B_3^2 \underline{u}(k) \tag{6.24}$$

with discrete measurement of the real pipe system available, corresponding to the following vector of linear combinations of system state variables

$$\underline{y}_3(k) = C_3 \underline{x}_3(k). \tag{6.25}$$

This system (6.24) assumes trivial difference equations for the demand flows of the form

$$d_{k+1}^{demand\ site} = d_k^{demand\ site} \quad for\ all\ k. \tag{6.26}$$

However, if the demand flows are changing then the true equations for the demands become

$$d_{k+1}^{demand\ site} = d_k^{demand\ site} + \tilde{f}_k^{demand\ site} \quad for\ all\ k, \tag{6.27}$$

where $\tilde{f}_k^{demand\ site}$ is a correction term.

If we include these correction terms, $\tilde{f}_k^{demand\ site}$, into the $\mathcal{M}3$ system (6.24), we get the system

$$E_3\underline{x}_3(k+1) = A_3\underline{x}_3(k) + B_3^1\underline{u}_3(k+1) + B_3^2\underline{u}_3(k) + \underline{l}_3(k), \tag{6.28}$$

where $\underline{l}_3(k)$ is a vector containing the $\tilde{f}_k^{demand\ site}$ terms.

The design B dynamic observers were built around the original $\mathcal{M}3$ system (6.24) and had the form

$$E_3\underline{\hat{x}}_3(k+1) = A_3\underline{\hat{x}}_3(k) + B_3^1\underline{u}_3(k+1) + B_3^2\underline{u}_3(k) + G(\underline{y}_3(k) - C_3\underline{\hat{x}}_3(k)). \tag{6.29}$$

If we define the error between the two systems (6.28) and (6.29) at time level k to be

$$\underline{e}(k) = \underline{x}_3(k) - \underline{\hat{x}}_3(k), \tag{6.30}$$

then subtracting equation (6.29) from (6.28) gives

$$E_3\underline{e}(k+1) = (A_3 - GC_3)\underline{e}(k) + \underline{l}_3(k). \tag{6.31}$$

Thus, $\underline{l}_3(k)$ acts as a forcing term on the errors. If the demands are changing, the forcing term $\underline{l}_3(k)$ will be non-zero, giving error in the dynamic observer estimate.

It can be seen that the design B dynamic observer gave much less error with small system eigenvalues than with large system eigenvalues. If the eigenvalues of the observer system (6.29) are small, then so are the eigenvalues of the error system (6.31), and hence the errors damp down more quickly. In fact, whereas the design B dynamic observer with $\theta = 1$ and with large system eigenvalues gave estimated demand profiles that were very crude reflections of the true shapes of these profiles; with smaller system eigenvalues it gave accurate estimates of the shape of the demand profiles, although shifted. Indeed, the first smeared the corners of the demand profile, but the latter did not. However, all demand profiles estimated by design B dynamic observers were slightly shifted.

As θ moved from 1 to 1/2, the errors in the state estimates of the design B dynamic observers with small eigenvalues, seemed to increase. This phenomenon is not understood. However, as θ moved from 1 to 1/2, the assigned observer eigenvalues became more

sensitive. When the eigenstructure assignment algorithm had been used to find a matrix G to assign eigenvalues to the observer system, the values of these observer eigenvalues were then checked by finding the eigenvalues of the matrix $E_3^{-1}(A_3 - GC_3)$. Depending on the computational mesh and the value of θ, the observer eigenvalues sometimes appeared to have moved. This effect was worst for $\theta = 1/2$. Indeed, when large eigenvalues were assigned to the observer with $\theta = 1/2$, the observer became unstable; on checking it was found that not all the eigenvalues had remained within the unit circle. It may be that for $\theta = 1/2$, the $\mathcal{M}3$ system is in some sense 'close' to unobservability. Gaining theoretical understanding of this problem would be worthwhile future research.

Some experiments were run comparing the results from dynamic observers with less robust eigenvalues. For $\theta = 1/2$ (although not for $\theta = 1$), depending on the model parameters, it was sometimes found that the good conditioning of the observer eigenvalues reduced the error in the observer state estimate due to the error in the trivial difference equations (6.2) for the flow demands. It is not understood why the robustness of the observer eigenvalues might help to reduce such error only for $\theta = 1/2$. However, we will now suggest two possible reasons for this phenomenon.

Reason 1

The first possible reason is that the robustness of the eigenvalues means that they are perturbed less by numerical error. Then the robustly assigned eigenvalues remain closer to the origin, and, from both previous discussion above and further argument presented next, the error in the state estimate is reduced. This would explain why this phenomenon was only seen for $\theta = 1/2$, where the sensitivity of the observer eigenvalues became a serious problem.

Reason 2

The following analysis suggests a second possible reason why the robust eigenstructure assignment technique might help to reduce the error introduced into the state estimate by the form of the modelling error present in equations (6.2).

We show that an upper bound on the norm of the error in the state estimate of an $\mathcal{M}3$ model based dynamic observer, caused by modelling error present in equations (6.2), is minimised by minimising

$$cond_F(X) = \|X\|_F \|X^{-1}\|_F$$

where $X = (Y^T E)^{-1}$ is the modal matrix of right eigenvectors of $E_3^{-1}(A_3 - GC_3)$. The eigenstructure assignment technique minimises $\|(Y^T E)^{-1}\|_F$.

From equation (6.31) we can show for any timestep s

$$\underline{e}(s) = [E_3^{-1}(A_3 - GC_3)]^s \underline{e}(0) + \sum_{j=0}^{s-1} [E_3^{-1}(A_3 - GC_3)]^j E_3^{-1} \underline{l}_3(s-1-j). \tag{6.32}$$

Applying basic theory of vector and matrix norms [20] to equation (6.32), we can derive

$$\|\underline{e}(s)\|_2 \leq \|[E_3^{-1}(A_3 - GC_3)]\|_2^s \|\underline{e}(0)\|_2 + \sum_{j=0}^{s-1} \|[E_3^{-1}(A_3 - GC_3)]\|_2^j \|E_3^{-1}\underline{l}_3(s-1-j)\|_2. \tag{6.33}$$

We assume the matrix $E_3^{-1}(A_3 - GC_3)$ has a full set of linearly independent eigenvectors, and from equation (5.9) we have the spectral decomposition

$$E_3^{-1}(A_3 - GC_3) = XDX^{-1}, \tag{6.34}$$

where D is a diagonal matrix of observer eigenvalues, λ_i. Substituting equation (6.34) into equation (6.33) gives

$$\|\underline{e}(s)\|_2 \leq \|[XDX^{-1}]\|_2^s \|\underline{e}(0)\|_2 + \sum_{j=0}^{s-1} \|[XDX^{-1}]\|_2^j \|E_3^{-1}\underline{l}_3(s-1-j)\|_2. \tag{6.35}$$

Applying basic theory of matrix norms to equation (6.35) gives

$$\|\underline{e}(s)\|_2 \leq cond_F^s(X) \|D\|_2^s \|\underline{e}(0)\|_2 + \sum_{j=0}^{s-1} cond_F^j(X) \|D\|_2^j \|E_3^{-1}\underline{l}_3(s-1-j)\|_2. \tag{6.36}$$

Equation (6.36) represents an upper bound on the norm of the error in the state estimate of an $\mathcal{M}3$ model based dynamic observer, caused by modelling error present in equations (6.2). It is obvious this upper bound is minimised by minimising $cond_F(X)$. Also, since

$$\|D\|_2 = MAX\{|\lambda_i|\}$$

we can see that reducing the modulus of $MAX\{|\lambda_i|\}$ will also reduce this upper bound. This may help to explain why reducing the modulus of the eigenvalues assigned to the

observer system helped to reduce the error in the state estimate.

When the weightings, $\tilde{f}_k^{demand\ site}$, were included in the $\mathcal{M}3$ model, the design B dynamic observer state estimates converged perfectly for $\theta = 1$, with both small and large system eigenvalues. Assigning small system eigenvalues to the design B dynamic observers gave faster convergence. However, as θ moved to 1/2, a very small amount of error began to persist in the state estimate.

Lastly, when pressure data was taken from an $\mathcal{M}0$ model constructed upon a much finer mesh, only a small amount of error was introduced in to the observer state estimate.

6.4.3 Observer Design C : The Dynamic Observer With Feedback at the Current Time-Level

In most ways, the design C dynamic observers behaved in a very similar manner to design B dynamic observers, except for increased sensitivity for $\theta = 1/2$. The design C observer became unstable even when it was attempted to assign small eigenvalues; on checking the assigned observer eigenvalues it was found that not all the eigenvalues were within the unit circle. However, with small eigenvalues and $\theta = 1$, the design C dynamic observers seemed to give more accurate state estimates than design B observers when constructed upon $\mathcal{M}3$ models without the weightings, $\tilde{f}_k^{demand\ site}$. The following analysis may suggest why.

The design C dynamic observers were built around the original $\mathcal{M}3$ system (6.24) and had the form

$$E_3\underline{\hat{x}}_3(k+1)+H(\underline{y}_3(k+1)-C_3\underline{\hat{x}}_3(k+1)) = A_3\underline{\hat{x}}_3(k)+B_3^1\underline{u}_3(k+1)+B_3^2\underline{u}_3(k)+G(\underline{y}_3(k)-C_3\underline{\hat{x}}_3(k)). \tag{6.37}$$

If we define the error between the two systems (6.28) and (6.37) at time level k to be

$$\underline{e}(k) = \underline{x}_3(k) - \underline{\hat{x}}_3(k), \tag{6.38}$$

then subtracting equation (6.37) from (6.28) gives

$$(E_3 - HC_3)\underline{e}(k+1) = (A_3 - GC_3)\underline{e}(k) + \underline{l}_3(k). \tag{6.39}$$

As with design B observers, $\underline{l}_3(k)$ acts as a forcing term on the errors. However, the matrix H was chosen to minimise the 2-norm of $(E_3 - HC_3)^{-1}$, and this matrix is implicitly multiplied into the forcing term, $\underline{l}_3(k)$, thus reducing its effects. With $\theta = 1$, in the experiments with dynamic observers the 2-norm of the matrix E_3^{-1} was 1.50, while the 2-norm of $(E_3 - HC_3)^{-1}$ was 0.56; this is believed to explain the improvement in the accuracy of the state estimate when feedback is included at the current time-level.

In an equivalent manner to design B observers, it may be shown that the robust eigenstructure assignment technique might help to reduce the error introduced into the state estimate by the form of the modelling error present in equations (6.2). However, we can also show that an upper bound on the norm of the error in the state estimate is minimised by minimising the 2-norm of $(E_3 - HC_3)^{-1}$.

In a similar way to the derivation of equation (6.32) for the error in the state estimate of design B observers, we may derive the following equation for the error in the state estimate of design C observers. For any timestep s we have

$$\underline{e}(s) = [(E_3 - HC_3)^{-1}(A_3 - GC_3)]^s \underline{e}(0)$$

$$+ \sum_{j=0}^{s-1} [(E_3 - HC_3)^{-1}(A_3 - GC_3)]^j (E_3 - HC_3)^{-1} \underline{l}_3(s-1-j). \qquad (6.40)$$

Applying basic theory of vector and matrix norms to equation (6.40), we can derive

$$\|\underline{e}(s)\|_2 \leq \|(E_3 - HC_3)^{-1}\|_2^s \|(A_3 - GC_3)\|_2^s \|\underline{e}(0)\|_2$$

$$+ \sum_{j=0}^{s-1} \|(E_3 - HC_3)^{-1}\|_2^j \|(A_3 - GC_3)\|_2^j \|(E_3 - HC_3)^{-1}\|_2 \|\underline{l}_3(s-1-j)\|_2. \qquad (6.41)$$

Equation (6.41) represents an upper bound on the norm of the error in the state estimate of a design C observer, caused by modelling error present in equations (6.2). It is obvious this upper bound is minimised by minimising $\|(E_3 - HC_3)^{-1}\|_2$.

If model parameters such as pipe lengths, timesteps, etc. were altered, then the 2-norm of $(E_3 - HC_3)^{-1}$ changed, altering the accuracy of the design C observer state estimates. If the 2-norm of $(E_3 - HC_3)^{-1}$ increased, then the errors in the state estimates increased, and if the 2-norm of $(E_3 - HC_3)^{-1}$ decreased, so did the errors.

When the weightings, $\tilde{f}_k^{demand\ site}$, were included in the $\mathcal{M}3$ model, the design C dynamic observer state estimates converged perfectly for $\theta = 1$.

Lastly, as with design A and B observers, taking pressure data from an $\mathcal{M}0$ model constructed upon a much finer mesh introduced only a small amount of error to the observer state estimate.

Chapter 7

Cycling

Here we introduce a technique, called 'cycling', that can reduce the error introduced into the dynamic observer state estimates by the trivial difference equations (6.2) contained in $\mathcal{M}3$ models. Cycling involves a series of dynamic observers, travelling along the time axis, one after the other. Each dynamic observer uses information about the flow demand profiles given by the previous observer. The technique is made up of the following cycles.

1st Cycle

Firstly we run the usual dynamic observer based upon an $\mathcal{M}3$ model assuming no knowledge about the flow profiles; i.e. with trivial flow equations of the form (6.2). This gives an initial state estimate, $\underline{\hat{x}}_3^1(k)$, for $k = 0, 1, ...$ This is the first cycle.

2nd Cycle

Next we run another dynamic observer making use of the discrete jumps in the demands estimated by the first observer. We assume the $\mathcal{M}3$ model is partitioned according to equation (6.3). Then the second cycle observer estimate, denoted by $\underline{\hat{x}}_3^2(k)$ for $k = 0, 1, ...,$ is calculated from

$$(E_3 - HC_3)\underline{\hat{x}}_3^2(k+1) = (A_3 - GC_3)\underline{\hat{x}}_3^2(k) + B_3^1\underline{u}_3(k+1) + B_3^2\underline{u}_3(k) - H\underline{y}_3(k+1) + G\underline{y}_3(k)$$
$$+ \begin{bmatrix} 0 & 0 \\ 0 & I \end{bmatrix} (\underline{\hat{x}}_3^1(k+1) - \underline{\hat{x}}_3^1(k)) \qquad (7.1)$$

where I is $g \times g$, and where the H matrix is zero for a design B dynamic observer. This gives a new state estimate for $k = 0, 1, ...$

ith Cycle

This process can be repeated for a number of cycles, each time making use of the discrete jumps in the demands estimated by the previous cycle. The *ith* cycle estimate, $\underline{\hat{x}}_3^i(k)$ for $k = 0, 1, ...,$ is calculated from

$$(E_3 - HC_3)\underline{\hat{x}}_3^i(k+1) = (A_3 - GC_3)\underline{\hat{x}}_3^i(k) + B_3^1\underline{u}_3(k+1) + B_3^2\underline{u}_3(k) - H\underline{y}_3(k+1) + G\underline{y}_3(k)$$
$$+ \begin{bmatrix} 0 & 0 \\ 0 & I \end{bmatrix} (\underline{\hat{x}}_3^{i-1}(k+1) - \underline{\hat{x}}_3^{i-1}(k)) \qquad (7.2)$$

where I is $g \times g$, and where the H matrix is zero for a design B dynamic observer. This gives a new state estimate for $k = 0, 1, ...$

Each further cycle is simply another dynamic observer travelling along the time axis, incorporating information from the state estimate of the previous cycle (dynamic observer). It is not immediately obvious how many cycles should be used; it may be that only a second cycle is needed for a significant improvement in the state estimate. A natural question to ask is what happens to the state estimate, $\underline{\hat{x}}_3^i(k)$ for any timestep k, as $i \longrightarrow \infty$. We have the following convergence theorem for cycling based upon a design C observer only.

Theorem 7.1 *When cycling is performed upon a design C observer, for each timestep, k, $\underline{\hat{x}}_3^i(k)$ tends to a limit as more cycles are performed, i.e.*

$$\underline{\hat{x}}_3^i(k) \longrightarrow \underline{\hat{x}}_3(k) \quad as \quad i \longrightarrow \infty,$$

if and only if all the eigenvalues of $(E_3 - HC_3)^{-1}\Upsilon$ are within the unit circle.

Proof

Consider a timestep T. We wish to investigate the convergence of $\underline{\hat{x}}_3^i(k)$ for $k = 1, ..., T$, as the number of cycles increases. Define

$$\underline{z}^i = \begin{bmatrix} \underline{\hat{x}}_3^i(T) \\ \underline{\hat{x}}_3^i(T-1) \\ \\ \vdots \\ \\ \underline{\hat{x}}_3^i(2) \\ \underline{\hat{x}}_3^i(1) \end{bmatrix}.$$

Then from the general cycle equation (7.2), it can be seen $\underline{z}^i$ obeys

$$R\underline{z}^{i+1} = S\underline{z}^i + \underline{v} \tag{7.3}$$

where

$$R = \begin{bmatrix} (E_3 - HC_3) & -(A_3 - GC_3) & & & & \\ & (E_3 - HC_3) & -(A_3 - GC_3) & & & \\ & & \ddots & \ddots & & \\ & & & & (E_3 - HC_3) & -(A_3 - GC_3) \\ & & & & & (E_3 - HC_3) \end{bmatrix},$$

$$S = \begin{bmatrix} \Upsilon & -\Upsilon & & & \\ & \Upsilon & -\Upsilon & & \\ & & \ddots & \ddots & \\ & & & \Upsilon & -\Upsilon \\ & & & & \Upsilon \end{bmatrix},$$

$$\Upsilon = \begin{bmatrix} 0 & 0 \\ 0 & I_g \end{bmatrix},$$

$$\underline{v} = \begin{bmatrix} B_3^1\underline{u}_3(T) + B_3^2\underline{u}_3(T-1) - H\underline{y}_3(T) + G\underline{y}_3(T-1) \\ B_3^1\underline{u}_3(T-1) + B_3^2\underline{u}_3(T-2) - H\underline{y}_3(T-1) + G\underline{y}_3(T-2) \\ \\ \vdots \\ \\ B_3^1\underline{u}_3(2) + B_3^2\underline{u}_3(1) - H\underline{y}_3(2) + G\underline{y}_3(1) \\ B_3^1\underline{u}_3(1) + B_3^2\underline{u}_3(0) - H\underline{y}_3(1) + G\underline{y}_3(0) + (A_3 - GC_3)\underline{\hat{x}}_3(0) - \Upsilon\underline{\hat{x}}_3(0) \end{bmatrix},$$

and $\underline{\hat{x}}_3(0)$ are the observer initial conditions for all cycles. The matrix $R^{-1}S$ is block upper triangular and has square blocks $(E_3 - HC_3)^{-1}\Upsilon$ on its diagonal. The eigenvalues of $R^{-1}S$ are the eigenvalues of the square blocks $(E_3 - HC_3)^{-1}\Upsilon$.

All the eigenvalues of $R^{-1}S$ are within the unit circle if and only if the eigenvalues of $(E_3 - HC_3)^{-1}\Upsilon$ are within the unit circle. Then, system (7.3) converges to a unique limit as the number of cycles increases, and we have

$$\underline{z}^i \longrightarrow \underline{z} \quad as \quad i \longrightarrow \infty.$$

Hence, at each timestep $k = 1, ..., T$, we have

$$\underline{\hat{x}}_3^i(k) \longrightarrow \underline{\hat{x}}_3(k) \quad as \quad i \longrightarrow \infty.$$

If a design B observer is used, by inspection it is obvious that the matrix $E^{-1}\Upsilon$ has multiple eigenvalues equal to 1, and hence the eigenvalues of $R^{-1}S$ are not within the unit circle and system (7.3) is not convergent. □

With the design C observers, we seek to find a matrix H such that $\|(E_3 - HC_3)^{-1}\|_2 < 1$. Since $\|\Upsilon\|_2 = 1$, if $\|(E_3 - HC_3)^{-1}\|_2 < 1$ then $\|(E_3 - HC_3)^{-1}\Upsilon\|_2 < 1$, which implies all the eigenvalues of $(E_3 - HC_3)^{-1}\Upsilon$ are within the unit circle. Then from the previous theorem, the cycling technique is convergent to a unique limit.

We now investigate how the error in the state estimate behaves as the number of cycles increases. Let the true behaviour of the gas network be described by

$$E_3\underline{x}_3(k+1) = A_3\underline{x}_3(k) + B_3^1\underline{u}_3(k+1) + B_3^2\underline{u}_3(k) + \underline{l}_3(k) \tag{7.4}$$

where $\underline{l}_3(k)$ is a vector containing the $\tilde{f}_k^{demand\ site}$ terms.

The general ith cycle (for $i > 1$) is given by equation (7.2). If we define the error between the ith cycle observer estimate and the model (7.4) to be

$$\underline{e}^i(k) = \underline{x}_3(k) - \underline{\hat{x}}_3^i(k) \tag{7.5}$$

then subtracting equation (7.2) from equation (7.4) gives

$$(E_3 - HC_3)\underline{e}^i(k+1) = (A_3 - GC_3)\underline{e}^i(k) + \underline{l}_3(k) - \Upsilon\underline{\hat{x}}_3^{i-1}(k+1) + \Upsilon\underline{\hat{x}}_3^{i-1}(k)$$

which, using equation (7.5), can be rewritten as

$$(E_3-HC_3)\underline{e}^i(k+1) = (A_3-GC_3)\underline{e}^i(k)+\underline{l}_3(k)-\Upsilon[\underline{x}_3(k+1)-\underline{e}^{i-1}(k+1)]+\Upsilon[\underline{x}_3(k)-\underline{e}^{i-1}(k)]. \tag{7.6}$$

Inspection of the structure of the $\mathcal{M}3$ model (7.4) shows

$$\underline{l}_3(k) = \Upsilon\underline{x}_3(k+1) - \Upsilon\underline{x}_3(k). \tag{7.7}$$

Adding equation (7.7) to equation (7.6) gives

$$(E_3 - HC_3)\underline{e}^i(k+1) = (A_3 - GC_3)\underline{e}^i(k) + \Upsilon\underline{e}^{i-1}(k+1) - \Upsilon\underline{e}^{i-1}(k). \tag{7.8}$$

Define

$$\underline{\varepsilon}^i = \begin{bmatrix} \underline{e}^i(T) \\ \underline{e}^i(T-1) \\ \\ \vdots \\ \\ \underline{e}^i(2) \\ \underline{e}^i(1) \end{bmatrix}.$$

Then from equation (7.8), we can see $\underline{\varepsilon}^i$ obeys

$$R\underline{\varepsilon}^{i+1} = S\underline{\varepsilon}^i + \underline{w} \tag{7.9}$$

where the matrices R and S are as previously defined,

$$\underline{w} = \begin{bmatrix} 0 \\ 0 \\ \\ \vdots \\ \\ 0 \\ f(\underline{e}(0)) \end{bmatrix},$$

$\underline{e}(0) = \underline{e}^i(0)$ for all i, is the error in the observer initial conditions for all cycles, and $f(\underline{e}(0)) = [(A_3 - GC_3) - \Upsilon]\underline{e}(0)$. If system (7.9) has its system eigenvalues within the unit circle and is convergent to a limit, $\underline{\varepsilon}$, then this limit satisfies

$$R\underline{\varepsilon} = S\underline{\varepsilon} + \underline{w},$$

i.e.

$$(R - S)\underline{\varepsilon} = \underline{w}. \tag{7.10}$$

Then we can see that

$$\underline{\varepsilon}^i \longrightarrow (R - S)^{-1}\underline{w} \quad as \quad i \longrightarrow \infty,$$

where the matrix $(R-S)$ is invertible since system (7.9) does not have an eigenvalue equal to 1. From the previous analysis, a sufficient condition for this is $\|(E_3 - HC_3)^{-1}\|_2 < 1$. We can see that if the observers are given the correct initial conditions, then $\underline{e}(0)$ is zero and $\underline{\varepsilon}^i$ decays completely away as the number of cycles increases.

However, $\underline{e}(0)$ will most likely not be zero, and this error will propagate with time. It would be difficult to provide a simple analysis of the propagation of such error with time for any arbitrary number of cycles performed. However, for the special case of a design C observer with $\|(E_3 - HC_3)^{-1}\|_2 < 1$ where the cycles are performed to convergence, we can analyse the how the error, $\underline{e}(k)$, in the limit estimate, $\underline{\hat{x}}_3(k)$, propagates with time.

We assume $\|(E_3 - HC_3)^{-1}\|_2 < 1$ and that system (7.9) reaches a steady state, $\underline{\varepsilon}$, after enough cycles. We investigate this steady state. Equation (7.10) can be written out

as

$$\begin{bmatrix} [(E_3 - HC_3) - \Upsilon] & [-(A_3 - GC_3) + \Upsilon] & & & \\ & \ddots & \ddots & & \\ & & & [(E_3 - HC_3) - \Upsilon] & [-(A_3 - GC_3) + \Upsilon] \\ & & & & [(E_3 - HC_3) - \Upsilon] \end{bmatrix} \begin{bmatrix} \underline{e}(T) \\ \underline{e}(T-1) \\ \vdots \\ \underline{e}(2) \\ \underline{e}(1) \end{bmatrix} = \begin{bmatrix} 0 \\ 0 \\ \vdots \\ 0 \\ f(\underline{e}(0)) \end{bmatrix}$$

where

$$\underline{\varepsilon} = [\underline{e}(T)^T, \underline{e}(T-1)^T, ..., \underline{e}(1)^T]^T.$$

By inspection of the above, we find

$$[(E_3 - HC_3) - \Upsilon]\underline{e}(1) = f(\underline{e}(0))$$

and generally

$$[(E_3 - HC_3) - \Upsilon]\underline{e}(k+1) = [(A_3 - GC_3) - \Upsilon]\underline{e}(k) \quad for\ k = 1, ...T-1. \tag{7.11}$$

The matrix $[(E_3 - HC_3) - \Upsilon]$ is full rank since, both $\|(E_3 - HC_3)^{-1}\|_2 < 1$ and $\|\Upsilon\|_2 = 1$ imply $\|(E_3 - HC_3)^{-1}\Upsilon\|_2 < 1$, which implies $(E_3 - HC_3)^{-1}\Upsilon$ has no eigenvalue equal to 1. Thus, if the eigenvalues of system (7.11) are within the unit circle, then

$$\underline{e}(k) \longrightarrow \underline{0} \quad as \quad k \longrightarrow \infty.$$

Ideally, we would like to be able to find feedback matrices H and G such that $\|(E_3 - HC_3)^{-1}\|_2 < 1$ and the eigenvalues of system (7.11) are within the unit circle. In this situation, the cycles may be continued to convergence to a limit, for which the error in the state estimate decays with time. It is shown later that this can be achieved, but not, unfortunately, for $\theta = 1/2$.

It should be noted that when $\|(E_3 - HC_3)^{-1}\|_2 < 1$ and the cycling is performed to convergence, a much cheaper equivalent approach is to solve system (7.3) directly for its limit, $\underline{z}$, from the equation

$$[R - S]\underline{z} = \underline{v}$$

which, by inspection, would involve a new form of observer

$$[(E_3 - HC_3) - \Upsilon]\underline{\hat{x}}(k+1) = [(A_3 - GC_3) - \Upsilon]\underline{\hat{x}}(k) + B_3^1\underline{u}_3(k+1) + B_3^2\underline{u}_3(k) - H\underline{y}_3(k+1) + G\underline{y}_3(k)$$

stepping through time. By inspection of the above system, it is immediately apparant that the trivial difference equations for the flows, and thus the modelling error they contain, have been removed. However, it can be shown that it is not now possible to find feedback matrices G and H to assign arbitrary eigenvalues to this new system. This is further explored in the discussion of the experimental results.

7.1 Experiments

When the $\mathcal{M}0$ model had been running for a while, the pressures at the upstream end and the sites of flow demand were recorded at each timestep and fed into the $\mathcal{M}3$ model-based cycling observers. The flow demands predicted by these techniques were then compared with the true flows used as inputs to the $\mathcal{M}0$ model.

For each experiment, the true flow demand profiles for the demands, $D_k^{A/B}$, $D_k^{B/C}$ and D_k^C are shown as thick lines in Figs. A, B and C respectively and the state estimates for $D_k^{A/B}$, $D_k^{B/C}$ and D_k^C are shown as thin lines. The percentage errors between the state estimates of $D_k^{A/B}$, $D_k^{B/C}$ and D_k^C and their true values are shown in Figs. D, E and F respectively.

In all experiments, data was taken from an $\mathcal{M}0$ model with an identical mesh - both $\mathcal{M}0$ and $\mathcal{M}3$ models have 10 spatial nodes along each pipe.

Two cycles performed

Experiment 7.1) Observer Design B (small eigenvalues) with $\theta = 1$
Experiment 7.2) Observer Design B (small eigenvalues) with $\theta = 0.5$
Experiment 7.3) Observer Design C (small eigenvalues) with $\theta = 1$

Cycles performed to convergence

Experiment 7.4) Observer Design C (small eigenvalues) with $\theta = 1$

Experiment 7.1

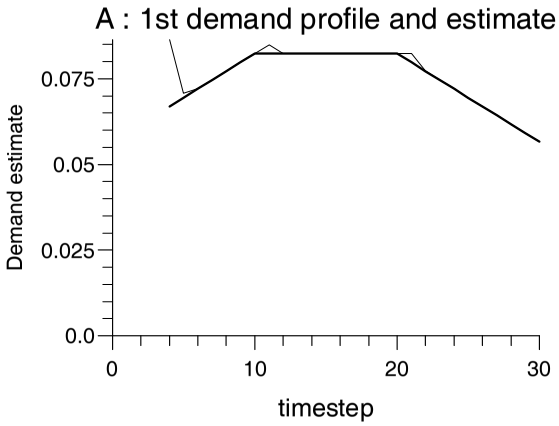

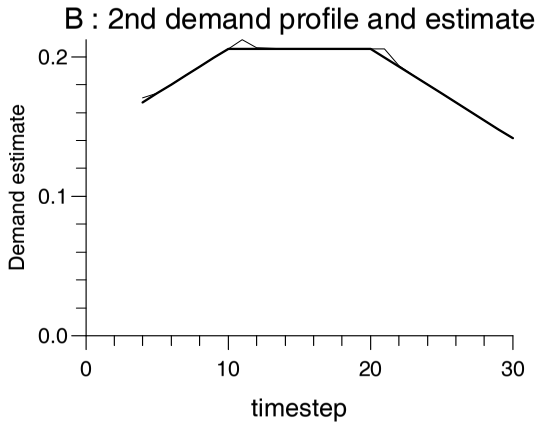

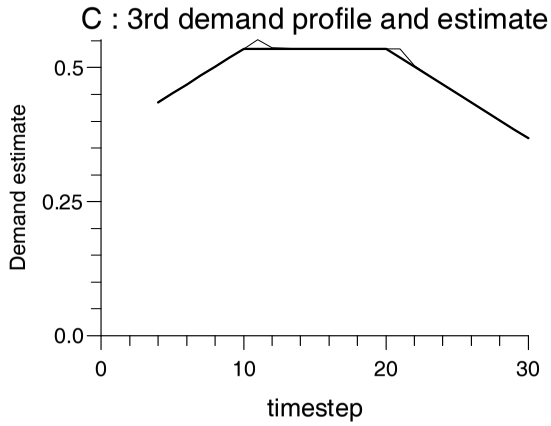

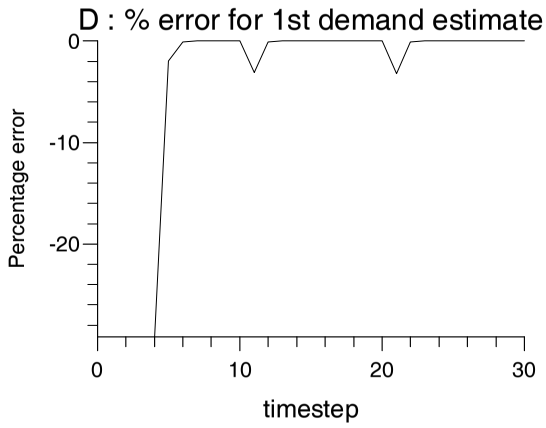

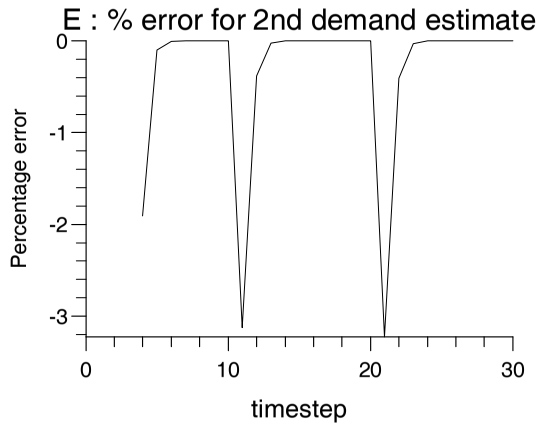

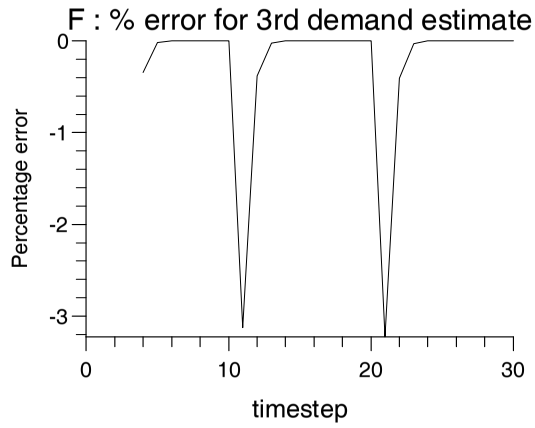

Experiment 7.2

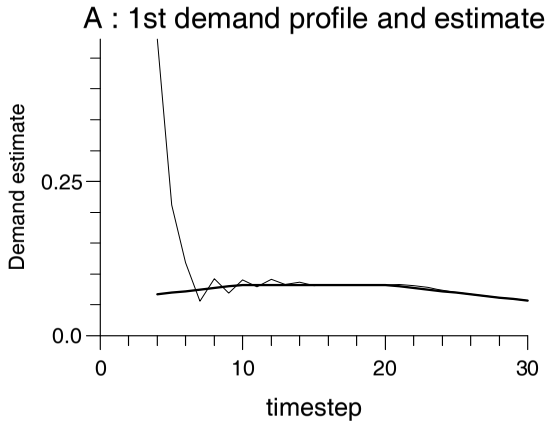

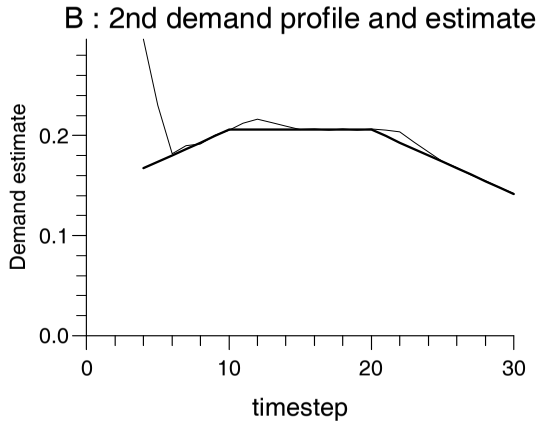

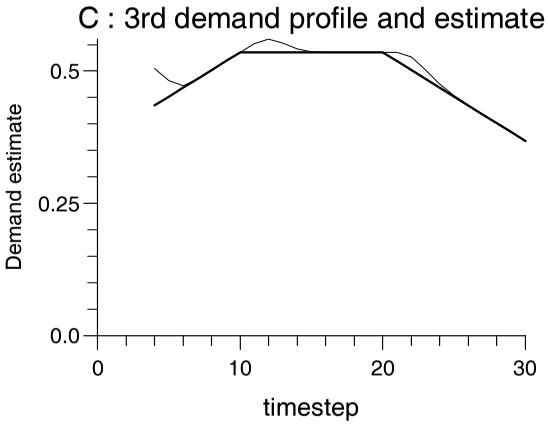

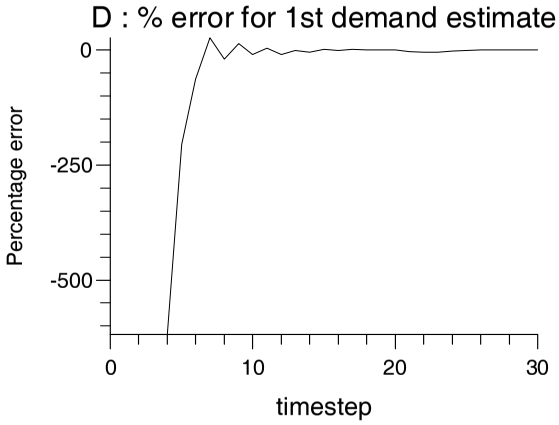

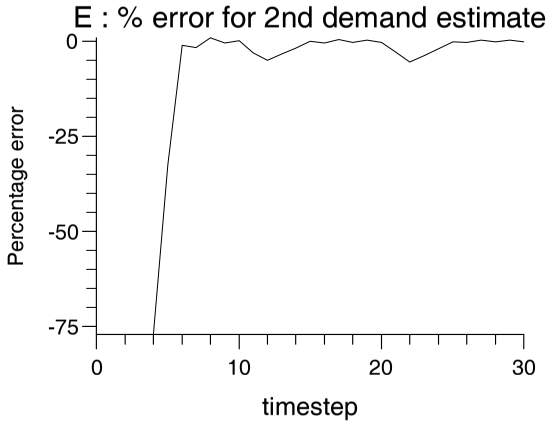

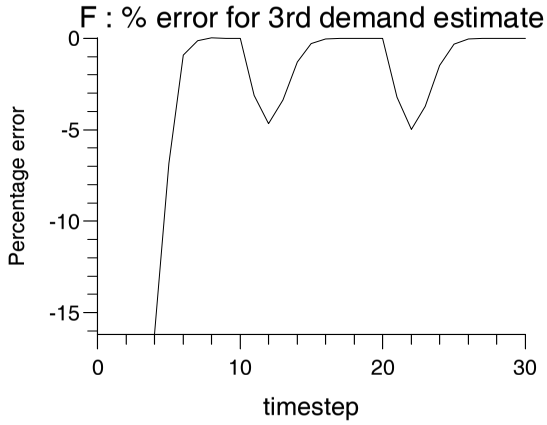

Experiment 7.3

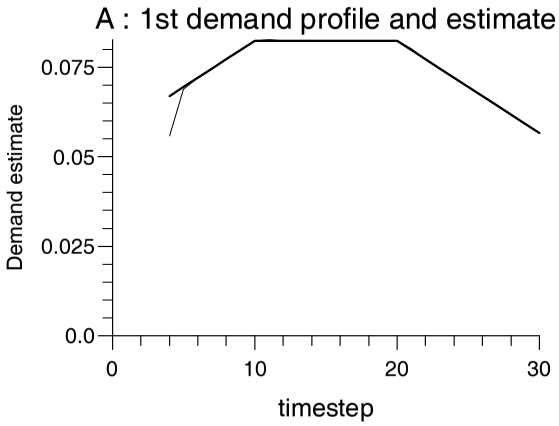

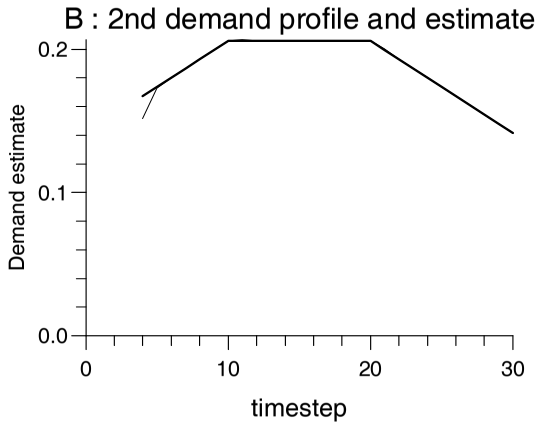

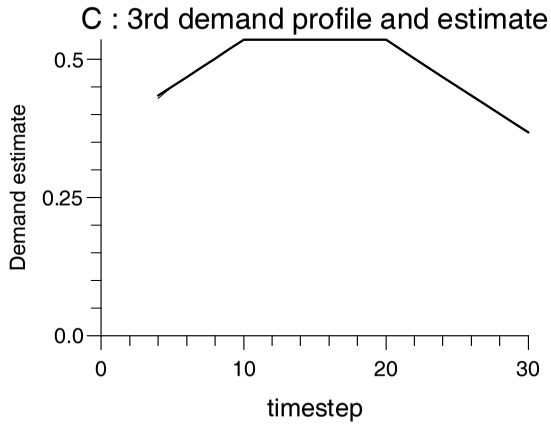

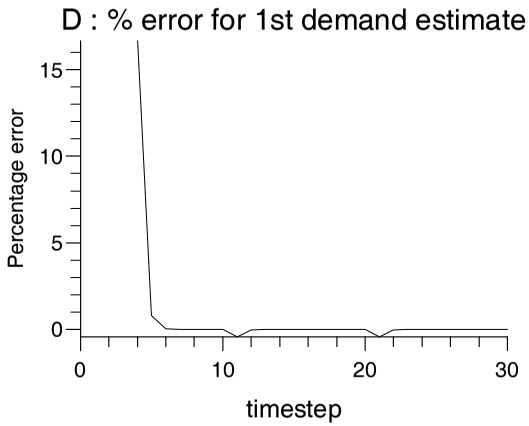

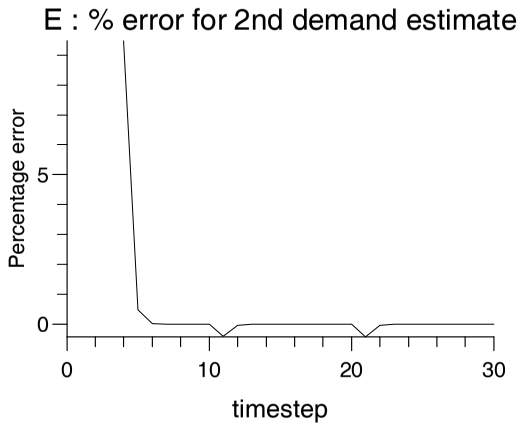

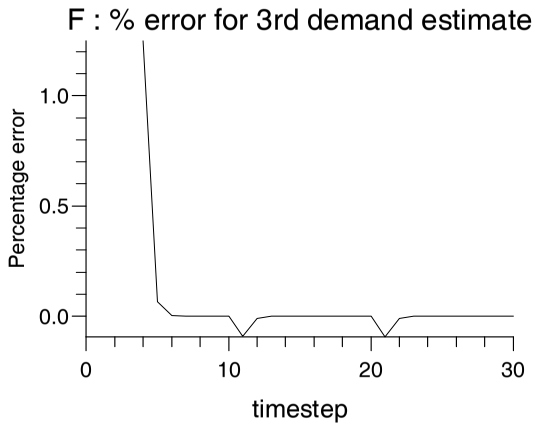

Experiment 7.4

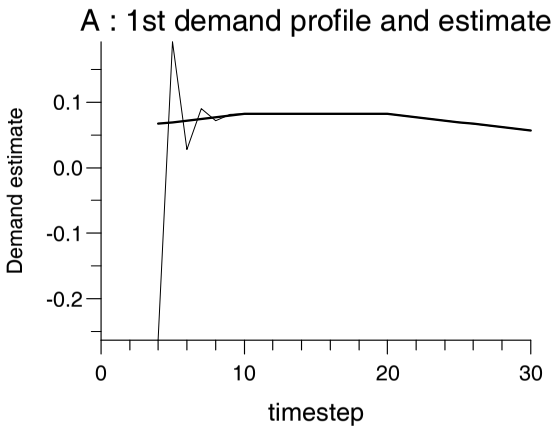

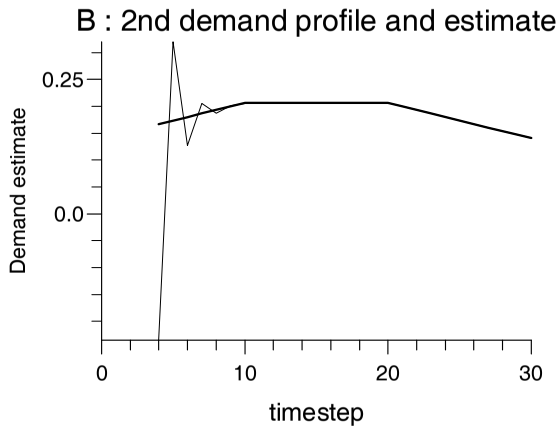

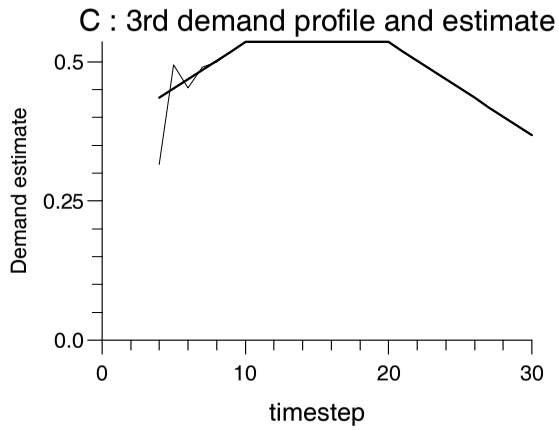

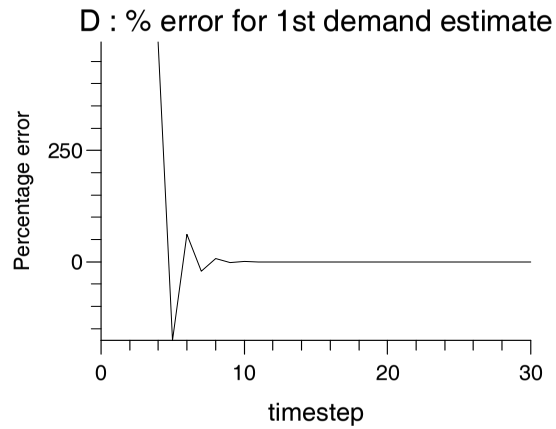

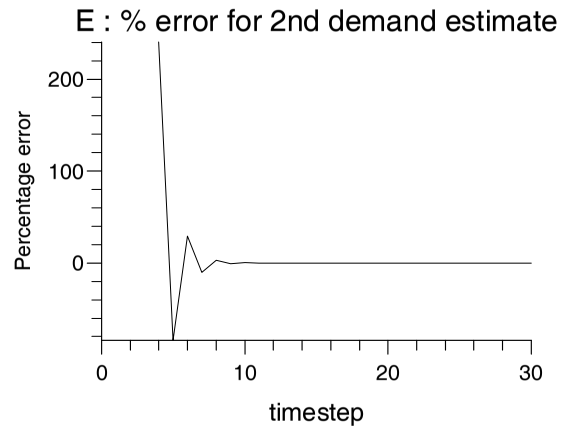

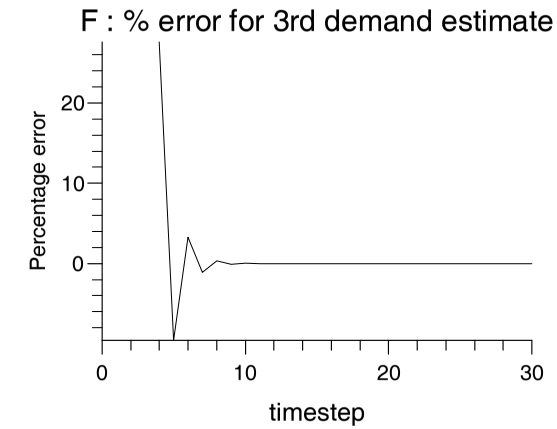

7.2 Discussion

The graphical results of these experiments should be compared to the graphical results of the previous chapter.

Regarding the '2 cycle' experiments, 7.1 to 7.3, only with the design C observer, was the state estimate much improved over the entire flow profile. However, with the design B observer, there was significant improvement in the state estimate of certain parts of the flow profiles from the second cycle. The second cycles seemed to perform badly where the gradient of the flow profile changed sharply, but significantly improved those parts of the flow profiles for which the demand jumps, $\tilde{f}_k^{demand\ site}$, were constant. This is not yet understood, but it may be that it would be possible to determine periods in the day where those parts of the flow profiles would respond well to a second cycle.

Regarding the 'many-cycle' experiment, 7.4, the cycling technique was found to be convergent only when a design C observer was being used. This behaviour can be explained by noting that with the design C observer, with $\theta = 1$, we had $\|(E_3 - HC_3)^{-1}\|_2 = 0.56 < 1$, and hence, as the previous analysis showed, the cycling technique was convergent. Without feedback at the current time-level being incorporated into the basic dynamic observer design, this convergence was lost.

The error in the design C observer state estimates, was seen to be very significantly reduced by cycling to convergence for $\theta = 1$. Indeed, the error was seen to decay completely away with time. This behaviour can be explained by the following.

When a cycling technique, based upon a design C observer with $\|(E_3 - HC_3)^{-1}\|_2 < 1$, converged, we showed that the error in the state estimate obeyed equation (7.11)

$$[(E_3 - HC_3) - \Upsilon]\underline{e}(k+1) = [(A_3 - GC_3) - \Upsilon]\underline{e}(k).$$

If we assume the $\mathcal{M}3$ model is arranged according to equation (6.3), and that the base $\mathcal{M}0$ model is arranged according to equation (4.1), then the $\mathcal{M}3$ model may be written

as

$$\begin{bmatrix} E' & E'' & -B^{1''} \\ 0 & 0 & I \end{bmatrix} \begin{bmatrix} \underline{p}_1(k+1) \\ \underline{p}_2(k+1) \\ \underline{d}(k+1) \end{bmatrix} = \begin{bmatrix} A' & A'' & B^{2''} \\ 0 & 0 & I \end{bmatrix} \begin{bmatrix} \underline{p}_1(k) \\ \underline{p}_2(k) \\ \underline{d}(k) \end{bmatrix}$$
$$+ \begin{bmatrix} B^{1'} \\ 0 \end{bmatrix} \underline{p}_3(k+1) + \begin{bmatrix} B^{2'} \\ 0 \end{bmatrix} \underline{p}_3(k).$$

Then system (7.11) may be written as

$$\begin{bmatrix} E' & E''-H_1 & -B^{1''} \\ 0 & -H_2 & 0 \end{bmatrix} \begin{bmatrix} \underline{p}_{1_{err}}(k+1) \\ \underline{p}_{2_{err}}(k+1) \\ \underline{d}_{err}(k+1) \end{bmatrix} = \begin{bmatrix} A' & A''-G_1 & B^{2''} \\ 0 & -G_2 & 0 \end{bmatrix} \begin{bmatrix} \underline{p}_{1_{err}}(k) \\ \underline{p}_{2_{err}}(k) \\ \underline{d}_{err}(k) \end{bmatrix}$$

where H_1, H_2, G_1 and G_2 are matrix blocks arising from the feedback matrices. $\underline{p}_{1_{err}}(k)$, $\underline{p}_{2_{err}}(k)$ and $\underline{d}_{err}(k)$ are the errors in the state estimates of $\underline{p}_1(k)$, $\underline{p}_2(k)$ and $\underline{d}(k)$ respectively.

We can rearrange the above system to

$$\begin{bmatrix} E' & -B^{1''} & E''-H_1 \\ 0 & 0 & -H_2 \end{bmatrix} \begin{bmatrix} \underline{p}_{1_{err}}(k+1) \\ \underline{d}_{err}(k+1) \\ \underline{p}_{2_{err}}(k+1) \end{bmatrix} = \begin{bmatrix} A' & B^{2''} & A''-G_1 \\ 0 & 0 & -G_2 \end{bmatrix} \begin{bmatrix} \underline{p}_{1_{err}}(k) \\ \underline{d}_{err}(k) \\ \underline{p}_{2_{err}}(k) \end{bmatrix}$$

which can be written in the form

$$\begin{bmatrix} E_2 & E''-H_1 \\ 0 & -H_2 \end{bmatrix} \begin{bmatrix} \underline{x}_{2_{err}}(k+1) \\ \underline{p}_{2_{err}}(k+1) \end{bmatrix} = \begin{bmatrix} A_2 & A''-G_1 \\ 0 & -G_2 \end{bmatrix} \begin{bmatrix} \underline{x}_{2_{err}}(k) \\ \underline{p}_{2_{err}}(k) \end{bmatrix}$$

where

$$\underline{x}_{2_{err}}(k) = \begin{bmatrix} \underline{p}_{1_{err}}(k) \\ \underline{d}_{err}(k) \end{bmatrix},$$

and the matrices E_2 and A_2 are identical to the corresponding $\mathcal{M}2$ system matrices. By inspection of the above system, for any value of θ, the set of eigenvalues of the above error system contains the eigenvalues of the corresponding $\mathcal{M}2$ system. We have shown that the eigenvalues of an $\mathcal{M}2$ system are within the unit circle for $1/2 < \theta \leq 1$, but not for $\theta = 1/2$. This helps to explain the experimental results: when $1/2 < \theta \leq 1$ the error $\underline{e}(k)$ decayed with time, and when $\theta = 1/2$ the error did not appear to decay.

By inspection of the above system, the remaining eigenvalues of the error system are given by the blocks H_2 and G_2; and for the error to decay, these eigenvalues would also

need to be within the unit circle.

How best to use the cycling technique is still not understood. When the cycling technique is not convergent, we can still get some improvement in the state estimate of certain parts of the flow profiles from a second cycle. The second cycle seemed to improve significantly those parts of the flow profiles for which the demand jumps, $\tilde{f}_k^{demand\ site}$, were constant. This might be particularly useful for a design B observer with $\theta = 1/2$, since for $\theta = 1/2$, the corresponding $\mathcal{M}2$ model has multiple eigenvalues equal to -1, and is not asymptotically stable.

The most significant improvement in the state estimate came when the cycling technique was convergent. When the cycling technique was based upon a design C dynamic observer with $1/2 < \theta \leq 1$, the error introduced into the state estimate by the difference equations (6.2) decayed completely away as the number of cycles increased. However, from the above analysis, we see that the decay of the error with time is governed by the eigenvalues of the corresponding $\mathcal{M}2$ system. In fact, for a suitable choice of feedback matrices, H and G, (i.e. with $H_1 = E''$ and $G_1 = A''$) we can show that the cycling technique, cycling to convergence, is directly equivalent to the corresponding $\mathcal{M}2$ system. A worthwhile area of future research would be to determine how the extra freedom available in the choice of H and G may be used to improve the performance of the cycling technique over the corresponding $\mathcal{M}2$ system.

Chapter 8

The Effects of Pressure Measurement Bias on $\mathcal{M}1$ and $\mathcal{M}2$ Models, and $\mathcal{M}3$ Model Based Observers

It may be the case that the pressure measurements at the sites of flow demand are subject to a constant bias, i.e. instead of using a true value for $\underline{p}_2(k)$, we drive the models and observers with

$$\underline{p}_{2_{measured}}(k) = \underline{p}_2(k) + \underline{b} \tag{8.1}$$

where $\underline{b}$ represents a vector of biases, constant with time. These constant biases will introduce error into the state estimates of the different estimation techniques. This is a serious problem for flow demand estimation due to the sensitivity of the flow demand variables to perturbations in the pressures.

We denote the corrupted model and observer state estimates by $\underline{x}_{est}(k)$ where

$$\underline{x}_{est}(k) = \underline{x}(k) + \underline{x}_{err}(k)$$

and $\underline{x}_{err}(k)$ is the error introduced into the state estimate due to the measurement bias. Similarly we specifically denote the corrupted state estimates of $\underline{p}_1(k)$, $\underline{p}_2(k)$ and $\underline{d}(k)$ by

$$\underline{p}_{1_{est}}(k) = \underline{p}_1(k) + \underline{p}_{1_{err}}(k),$$

$$\underline{p}_{2_{est}}(k) = \underline{p}_2(k) + \underline{p}_{2_{err}}(k),$$

$$\underline{d}_{est}(k) = \underline{d}(k) + \underline{d}_{err}(k)$$

respectively, where $\underline{p}_{1_{err}}(k)$, $\underline{p}_{2_{err}}(k)$ and $\underline{d}_{err}(k)$ are the errors introduced into these state estimates due to the measurement bias.

For each estimation technique, we seek to find $\underline{p}_{1_{err}}(k)$, $\underline{p}_{2_{err}}(k)$ and $\underline{d}_{err}(k)$, and show these errors are asymptotically the same for all estimation techniques. We also show that, whilst the relative errors in the pressure estimates are acceptable, the relative errors in the flow demand estimates may be very large.

8.1 $\mathcal{M}1$ Models

Consider the $\mathcal{M}1$ model (3.3). If the $\mathcal{M}1$ model is driven by $[\underline{u}_1(k) + \underline{u}_{1_{bias}}]$ where $\underline{u}_1(k)$ is the vector of 'true' pressures and $\underline{u}_{1_{bias}}$ is a vector resulting solely from the unknown constant biases of equation (8.1), then the actual model run is

$$E_1\underline{x}_{1_{est}}(k+1) = A_1\underline{x}_{1_{est}}(k) + B_1^1[\underline{u}_1(k+1) + \underline{u}_{1_{bias}}] + B_1^2[\underline{u}_1(k) + \underline{u}_{1_{bias}}]. \tag{8.2}$$

From the $\mathcal{M}1$ model equation (3.2), equation (8.2) may be written as

$$\mathcal{E}_{1,1}\underline{p}_{1_{est}}(k+1) = \mathcal{A}_{1,1}\underline{p}_{1_{est}}(k) - \mathcal{E}_{1,2}[\underline{p}_2(k+1) + \underline{b}] + \mathcal{B}_{1,1}^1\underline{p}_3(k+1) + \mathcal{A}_{1,2}[\underline{p}_2(k) + \underline{b}] + \mathcal{B}_{1,1}^2\underline{p}_3(k). \tag{8.3}$$

If equation (3.2) is subtracted from equation (8.3), we derive

$$\mathcal{E}_{1,1}\underline{p}_{1_{err}}(k+1) = \mathcal{A}_{1,1}\underline{p}_{1_{err}}(k) - \mathcal{E}_{1,2}\underline{b} + \mathcal{A}_{1,2}\underline{b}. \tag{8.4}$$

System (8.4) describes how the state estimate error, $\underline{p}_{1_{err}}(k)$, due to constant measurement bias behaves, and we investigate this now.

Since we have proved the $\mathcal{M}1$ system (3.3) is asymptotically stable for $1/2 \leq \theta \leq 1$, then so is system (8.4) which has the same system matrices. Since the input to system (8.4) is constant, the system reaches a steady state given by

$$\mathcal{E}_{1,1}\underline{p}_{1_{err}} = \mathcal{A}_{1,1}\underline{p}_{1_{err}} - \mathcal{E}_{1,2}\underline{b} + \mathcal{A}_{1,2}\underline{b},$$

i.e.

$$(\mathcal{E}_{1,1} - \mathcal{A}_{1,1})\underline{p}_{1_{err}} = (-\mathcal{E}_{1,2} + \mathcal{A}_{1,2})\underline{b}. \tag{8.5}$$

If we arrange the pressure variables in the state vector in their order along the pipe network, i.e. in the following way

$$\underline{x}_1(k) = [p^1_{1,k}, p^1_{2,k}, ..., p^1_{s^1-1,k}, p^2_{1,k}, p^2_{2,k}, ..., p^2_{s^2-1,k}, ..., p^g_{1,k}, p^g_{2,k}...., p^g_{s^g-1,k}]^T,$$

where each general pipe z has $s^z + 1$ nodes (including end nodes), then the matrix $(\mathcal{E}_{1,1} - \mathcal{A}_{1,1})$ takes the form

$$(\mathcal{E}_{1,1} - \mathcal{A}_{1,1}) = \begin{bmatrix} [\mathrm{E}^1 - \mathrm{A}^1] & & & & \\ & [\mathrm{E}^2 - \mathrm{A}^2] & & & \\ & & \ddots & & \\ & & & [\mathrm{E}^{g-1} - \mathrm{A}^{g-1}] & \\ & & & & [\mathrm{E}^g - \mathrm{A}^g] \end{bmatrix}$$

and system (8.5) consists of g disjoint subsystems of the form

$$[\mathrm{E}^z - \mathrm{A}^z]\underline{x}^z_{err} = \underline{l}^z. \tag{8.6}$$

Each system (8.6) contains $s^z - 1$ scalar equations

$$2r^z\Omega^z_i\Gamma^z_i p^z_{i_{err}} = r^z\Omega^z_i\Gamma^z_{i-1}p^z_{i-1_{err}} + r^z\Omega^z_i\Gamma^z_{i+1}p^z_{i+1_{err}} \tag{8.7}$$

for $i = 1, ..., s^z - 1$, where $p^z_{i_{err}}$ represents the asymptotic steady state error contained in the $\mathcal{M}1$ model state estimate of $p^z_{i,k}$ due to pressure measurement bias. In the first and last equations of each system (8.6), $p^z_{0_{err}}$ and $p^z_{s^z_{err}}$ represent the normalised measurement biases at the upstream and downstream ends of the general pipe z respectively. These biases are contained in the vector $\underline{l}^z$.

Each i^{th} equation of system (8.6) is divided by $r^z\Omega^z_i$ to give $s^z - 1$ scalar equations of the form

$$2\Gamma^z_i p^z_{i_{err}} = \Gamma^z_{i-1}p^z_{i-1_{err}} + \Gamma^z_{i+1}p^z_{i+1_{err}}. \tag{8.8}$$

If we had a maximum value for $\Gamma^z_i p^z_{i_{err}}$ occur internally along the pipe, i.e. for $i = 1, ..., s^z - 1$, then for that particular *internal* node, say node j where $1 \leq j \leq s^z - 1$, we would have

$$\Gamma^z_j p^z_{j_{err}} \geq \Gamma^z_i p^z_{i_{err}} \quad for\ 0 \leq i \leq s^z. \tag{8.9}$$

From equation (8.8) we have

$$2\Gamma_j^z p_{j_{err}}^z = \Gamma_{j-1}^z p_{j-1_{err}}^z + \Gamma_{j+1}^z p_{j+1_{err}}^z. \tag{8.10}$$

Equation (8.10) combined with inequality (8.9) implies

$$\Gamma_{j-1}^z p_{j-1_{err}}^z = \Gamma_j^z p_{j_{err}}^z$$

$$\Gamma_{j+1}^z p_{j+1_{err}}^z = \Gamma_j^z p_{j_{err}}^z.$$

We can continue in this way to show that all the $\Gamma_i^z p_{i_{err}}^z$ are equal for $i = 0, ..., s^z$. So if we had a maximum value for $\Gamma_i^z p_{i_{err}}^z$ occur internally along the pipe, i.e. for $i = 1, ..., s^z - 1$, then for that particular *internal* node, say node j, we would have

$$\Gamma_j^z p_{j_{err}}^z = \Gamma_0^z p_{0_{err}}^z = \Gamma_{s^z}^z p_{s_{err}^z}^z. \tag{8.11}$$

Hence

$$\Gamma_i^z p_{i_{err}}^z \leq MAX(\Gamma_0^z p_{0_{err}}^z, \Gamma_{s^z}^z p_{s_{err}^z}^z) \quad for\ i = 1, ..., s^z - 1. \tag{8.12}$$

By considering a minimum value for $\Gamma_i^z p_{i_{err}}^z$ occurring along the pipe, we can similarly derive

$$\Gamma_i^z p_{i_{err}}^z \geq MIN(\Gamma_0^z p_{0_{err}}^z, \Gamma_{s^z}^z p_{s_{err}^z}^z) \quad for\ i = 1, ..., s^z - 1. \tag{8.13}$$

From bounds (8.12) and (8.13) we have for a general pipe z

$$MIN[\frac{\Gamma^{z-1/z} b^{z-1/z}}{\Gamma_i^z}, \frac{\Gamma^{z/z+1} b^{z/z+1}}{\Gamma_i^z}] \leq p_{i_{err}}^z \leq MAX[\frac{\Gamma^{z-1/z} b^{z-1/z}}{\Gamma_i^z}, \frac{\Gamma^{z/z+1} b^{z/z+1}}{\Gamma_i^z}] \ for\ any\ node\ i. \tag{8.14}$$

where we have denoted the upstream and downstream normalised measurement biases, $p_{0_{err}}^z$ and $p_{s_{err}^z}^z$, by $b^{z-1/z}$ and $b^{z/z+1}$ respectively. Equation (8.14) represents bounds on the constant errors in the normalised state estimate of the pressures along a general pipe z, due to measurement bias. It can be seen that the estimate errors depend only on the measurement biases at the two ends of the particular pipe z.

If we assume the measurement biases are not greater than 1 bar or less than -1 bar, then we have

$$-1 \leq b^{z-1/z} N_p \leq 1 \quad and \quad -1 \leq b^{z/z+1} N_p \leq 1. \tag{8.15}$$

However, for a typical gas network we would have

$$35 \ bar \leq True \ pressure \leq 70 \ bar. \tag{8.16}$$

Multiplying inequality (8.14) by N_p, and combining with inequalities (8.15) and (8.16), gives

$$\left| \frac{Error \ in \ pressure \ estimate}{True \ pressure} \right| \leq 1/35 \times MAX[\frac{\Gamma^{z-1/z}}{\Gamma_i^z}, \frac{\Gamma^{z/z+1}}{\Gamma_i^z}] \quad for \ node \ i \ of \ pipe \ z. \tag{8.17}$$

If the Γ^s do not vary greatly along each pipe, then we can see that the pressure estimates will not be completely swamped by the error introduced by measurement bias.

We now examine the asymptotic steady error in the state estimate of the flow demands due to pressure measurement bias. As an $\mathcal{M}1$ model is run, the normalised inline flow perturbations at the ends of each pipe section are estimated by applying a forwards or backwards difference discretisation of equation (2.13), i.e. for a general pipe z, at an upstream pipe end, we would have

$$q^z_{0,k_{est}} = -\epsilon^z_3(\Gamma^z_1 p^z_{1,k_{est}} - \Gamma^z_0 p^z_{0,k_{est}})/\delta x^z \tag{8.18}$$

and at a downstream pipe end, we would have

$$q^z_{s^z,k_{est}} = -\epsilon^z_3(\Gamma^z_{s^z} p^z_{s^z,k_{est}} - \Gamma^z_{s^z-1} p^z_{s^z-1,k_{est}})/\delta x^z. \tag{8.19}$$

To estimate the demand flow at a pipe junction, we use

$$d^{z/z+1}_{k_{est}} = q^z_{s^z,k_{est}} - q^{z+1}_{0,k_{est}}. \tag{8.20}$$

However, the terms $p^z_{1,k_{est}}$, $p^z_{0,k_{est}}$, $p^z_{s^z,k_{est}}$ and $p^z_{s^z-1,k_{est}}$ now contain error due to the measurement bias. Hence, the flow estimates, $q^z_{0,k_{est}}$, $q^z_{s^z,k_{est}}$ and $d^{z/z+1}_{k_{est}}$ also contain error due to the measurement bias.

If we subtract equations (3.4), (3.5) and (3.6) from equations (8.18), (8.19) and (8.20) respectively, and assume the errors in the pressure estimates due to measurement bias have reached a steady state, we derive

$$q^z_{0_{err}} = -\epsilon^z_3(\Gamma^z_1 p^z_{1_{err}} - \Gamma^z_0 p^z_{0_{err}})/\delta x^z, \tag{8.21}$$

$$q^z_{s^z_{err}} = -\epsilon^z_3(\Gamma^z_{s^z} p^z_{s^z_{err}} - \Gamma^z_{s^z-1} p^z_{s^z-1_{err}})/\delta x^z \tag{8.22}$$

and

$$d^{z/z+1}_{err} = q^z_{s^z_{err}} - q^{z+1}_{0_{err}} \tag{8.23}$$

respectively, where $q^z_{0_{err}}$, $q^z_{s^z_{err}}$ and $d^{z/z+1}_{err}$ are the steady errors due to measurement bias in the estimates of $q^z_{0,k}$, $q^z_{s^z,k}$ and $d^{z/z+1}_k$ respectively.

Next we examine the solution to the $s^z - 1$ scalar equations (8.8) in order to derive an explicit formula for $q^z_{0_{err}}$ and $q^z_{s^z_{err}}$ in terms of the measurement biases $b^{z-1/z}$ and $b^{z/z+1}$. For a general pipe z, let

$$\eta^z = \Gamma^z_1 p^z_{1_{err}} - \Gamma^z_0 p^z_{0_{err}}. \tag{8.24}$$

The first scalar equation from the system of scalar equations (8.8) is

$$-\Gamma^z_0 p^z_{0_{err}} + 2\Gamma^z_1 p^z_{1_{err}} - \Gamma^z_2 p^z_{2_{err}} = 0. \tag{8.25}$$

Combining equation (8.25) with equation (8.24) gives

$$\eta^z = \Gamma^z_2 p^z_{2_{err}} - \Gamma^z_1 p^z_{1_{err}}. \tag{8.26}$$

We can continue to show for pipe z

$$\Gamma^z_{i+1} p^z_{i+1_{err}} - \Gamma^z_i p^z_{i_{err}} = \eta^z \quad for\ i = 0, ..., s^z - 1. \tag{8.27}$$

Substituting equation (8.27) into equation (8.21) and equation (8.22) gives

$$q^z_{0_{err}} = q^z_{s^z_{err}} = -\epsilon^z_3 \eta^z/\delta x^z. \tag{8.28}$$

However, adding all s^z equations of the form (8.27) i.e for $i = 0, ..., s^z - 1$, gives

$$\Gamma^z_{s^z} p^z_{s^z_{err}} - \Gamma^z_0 p^z_{0_{err}} = s^z \eta^z. \tag{8.29}$$

Rearranging equation (8.29) gives

$$\eta^z = (\Gamma^z_{s^z} p^z_{s^z_{err}} - \Gamma^z_0 p^z_{0_{err}})/s^z. \tag{8.30}$$

Substituting equation (8.30) into equation (8.28) and using $s^z \delta x^z = 1$, gives

$$q^z_{0_{err}} = q^z_{s^z_{err}} = -\epsilon^z_3(\Gamma^{z/z+1} b^{z/z+1} - \Gamma^{z-1/z} b^{z-1/z}). \tag{8.31}$$

The estimates of the flow demands can be shown to be more sensitive than the estimates of the pressures to measurement bias. If we assume the real gas network is operating in a fairly steady state, then system (3.2) also reaches a steady state. Then in a similar way as for equation (8.31), we can derive

$$q_0^z = q_{s^z}^z = -\epsilon_3^z(\Gamma^{z/z+1}p^{z/z+1} - \Gamma^{z-1/z}p^{z-1/z}) \tag{8.32}$$

where q_0^z, $q_{s^z}^z$, $p^{z-1/z}$ and $p^{z/z+1}$ are the steady states of $q_{0,k}^z$, $q_{s^z,k}^z$, $p_{0,k}^z$ and $p_{s^z,k}^z$ respectively. We assume we have a small inline flow in pipe section z and that we have linearised about $\mathcal{Q}^z = 0$, then from equations (8.31), (8.32) we may derive

$$\frac{Error\ in\ normalised\ pipe\ end\ flow\ estimate}{Correct\ normalised\ pipe\ end\ flow} = \frac{q_{0_{err}}^z}{q_0^z} = \frac{q_{s_{err}^z}^z}{q_{s^z}^z} = \frac{\Gamma^{z/z+1}b^{z/z+1} - \Gamma^{z-1/z}b^{z-1/z}}{\Gamma^{z/z+1}p^{z/z+1} - \Gamma^{z-1/z}p^{z-1/z}}.$$

Using inequality (8.15), we have that $|b^{z/z+1} - b^{z/z-1}|$ may be as large as $2/N_p$. However, in a typical gas network, we would usually have a pressure drop of less than 3 bar along the pipe, and for a very small flow, $|\Gamma^{z/z+1}p^{z/z+1} - \Gamma^{z-1/z}p^{z-1/z}|$ may be very small indeed. Hence, we can see that for a small flow, we may well have

$$\left|\frac{Error\ in\ pipe\ end\ flow\ estimate}{Correct\ pipe\ end\ flow}\right| > 1. \tag{8.33}$$

Small demand flows at the junctions can be seen to have the same sensitivity problem as the inline flows at the pipe ends. We assume there is a small junction flow demand at the pipe junction $z/z+1$, and that we have linearised about $\mathcal{Q}^{z/z+1} = 0$. In which case, from equations (3.6) and (8.23), we have

$$\frac{Error\ in\ normalised\ junction\ flow\ estimate}{Correct\ normalised\ junction\ flow} = \frac{d_{err}^{z/z+1}}{d^{z/z+1}} = \frac{q_{s_{err}^z}^z - q_{0_{err}}^{z+1}}{q_{s^z}^z - q_0^{z+1}}$$

where $d^{z/z+1}$ is the steady state of $d_k^{z/z+1}$. If the true junction flow demand, $d^{z/z+1}$, is very small, then $q_{s^z}^z \approx q_0^{z+1}$, and hence it can be seen that we could have

$$\left|\frac{Error\ in\ junction\ flow\ estimate}{Correct\ junction\ flow}\right| > 1. \tag{8.34}$$

8.2 $\mathcal{M}2$ Models

Consider the $\mathcal{M}2$ system (4.3). If the $\mathcal{M}2$ model is driven by $[\underline{u}_2(k) + \underline{u}_{2_{bias}}]$ where $\underline{u}_2(k)$ is the vector of 'true' pressures and $\underline{u}_{2_{bias}}$ is a vector resulting solely from the unknown constant biases of equation (8.1), then the actual model run is

$$E_2 \underline{x}_{2_{est}}(k+1) = A_2 \underline{x}_{2_{est}}(k) + B_2^1[\underline{u}_2(k+1) + \underline{u}_{2_{bias}}] + B_2^2[\underline{u}_2(k) + \underline{u}_{2_{bias}}]. \tag{8.35}$$

If the base $\mathcal{M}0$ model is arranged and partitioned as in equation (3.1), system (8.35) then has the form

$$\begin{bmatrix} \mathcal{E}_{1,1} & 0 \\ \mathcal{E}_{2,1} & -\mathcal{B}^1_{2,2} \end{bmatrix} \begin{bmatrix} \underline{p}_{1_{est}}(k+1) \\ \underline{d}_{est}(k+1) \end{bmatrix} = \begin{bmatrix} \mathcal{A}_{1,1} & 0 \\ \mathcal{A}_{2,1} & \mathcal{B}^2_{2,2} \end{bmatrix} \begin{bmatrix} \underline{p}_{1_{est}}(k) \\ \underline{d}_{est}(k) \end{bmatrix} + \begin{bmatrix} \mathcal{B}^1_{1,1} & -\mathcal{E}_{1,2} \\ 0 & -\mathcal{E}_{2,2} \end{bmatrix} \begin{bmatrix} \underline{p}_3(k+1) \\ \underline{p}_2(k+1) + \underline{b} \end{bmatrix}$$
$$+ \begin{bmatrix} \mathcal{B}^2_{1,1} & \mathcal{A}_{1,2} \\ 0 & \mathcal{A}_{2,2} \end{bmatrix} \begin{bmatrix} \underline{p}_3(k) \\ \underline{p}_2(k) + \underline{b} \end{bmatrix}. \tag{8.36}$$

If equation (4.4) is subtracted from equation (8.36), we derive

$$\begin{bmatrix} \mathcal{E}_{1,1} & 0 \\ \mathcal{E}_{2,1} & -\mathcal{B}^1_{2,2} \end{bmatrix} \begin{bmatrix} \underline{p}_{1_{err}}(k+1) \\ \underline{d}_{err}(k+1) \end{bmatrix} = \begin{bmatrix} \mathcal{A}_{1,1} & 0 \\ \mathcal{A}_{2,1} & \mathcal{B}^2_{2,2} \end{bmatrix} \begin{bmatrix} \underline{p}_{1_{err}}(k) \\ \underline{d}_{err}(k) \end{bmatrix} + \begin{bmatrix} \mathcal{B}^1_{1,1} & -\mathcal{E}_{1,2} \\ 0 & -\mathcal{E}_{2,2} \end{bmatrix} \begin{bmatrix} 0 \\ \underline{b} \end{bmatrix}$$
$$+ \begin{bmatrix} \mathcal{B}^2_{1,1} & \mathcal{A}_{1,2} \\ 0 & \mathcal{A}_{2,2} \end{bmatrix} \begin{bmatrix} 0 \\ \underline{b} \end{bmatrix}. \tag{8.37}$$

System (8.37) describes how the state estimate error, $[\underline{p}^T_{1_{err}}(k)\ ,\ \underline{d}^T_{err}(k)]^T$, due to constant measurement bias behaves, and we investigate this now.

Since we have proved the $\mathcal{M}2$ system (4.3) is asymptotically stable for $1/2 < \theta \leq 1$, then so is system (8.37) which has the same system matrices. Since the input vector, of system (8.37) is constant, the system reaches a steady state given by

$$\begin{bmatrix} (\mathcal{E}_{1,1} - \mathcal{A}_{1,1}) & 0 \\ (\mathcal{E}_{2,1} - \mathcal{A}_{2,1}) & (-\mathcal{B}^1_{2,2} - \mathcal{B}^2_{2,2}) \end{bmatrix} \begin{bmatrix} \underline{p}_{1_{err}} \\ \underline{d}_{err} \end{bmatrix} = \begin{bmatrix} \mathcal{B}^1_{1,1} & -\mathcal{E}_{1,2} \\ 0 & -\mathcal{E}_{2,2} \end{bmatrix} \begin{bmatrix} \underline{0} \\ \underline{b} \end{bmatrix}$$
$$+ \begin{bmatrix} \mathcal{B}^2_{1,1} & \mathcal{A}_{1,2} \\ 0 & \mathcal{A}_{2,2} \end{bmatrix} \begin{bmatrix} \underline{0} \\ \underline{b} \end{bmatrix}. \tag{8.38}$$

Thus we see that $\underline{p}_{1_{err}}$ is given by the top $n - g$ rows of the above system, i.e.

$$(\mathcal{E}_{1,1} - \mathcal{A}_{1,1})\underline{p}_{1_{err}} = (-\mathcal{E}_{1,2} + \mathcal{A}_{1,2})\underline{b}$$

which is identical to equation (8.5) for the $\mathcal{M}1$ model. $\underline{d}_{err}$ is then given by the last g rows of system (8.38), which correspond to the $g-1$ connectivity equations, and the single downstream flow boundary equation.

We denote the corrupted state estimates of the downstream flow of the last pipe $q^g_{s^g,k}$, and the demand flow $d^{z/z+1}_k$ at the general pipe junction $z/z+1$, by

$$q^g_{s^g,k_{est}} = q^g_{s^g,k} + q^g_{s^g,k_{err}}$$

$$d^{z/z+1}_{k_{est}} = d^{z/z+1}_k + d^{z/z+1}_{k_{err}}$$

respectively, where $q^g_{s^g,k_{err}}$ and $d^{z/z+1}_{k_{err}}$ are the errors introduced into these state estimates by measurement bias.

The single downstream flow boundary equation for the last pipe g is given by equation (2.19). Hence, the last row of system (8.37) contains the following scalar equation for $q^g_{s^g,k_{err}}$

$$-2\theta\Omega^g_{s^g} r^g \Gamma^g_{s^g-1} p^g_{s^g-1,k+1_{err}} + (1+2\theta\Omega^g_{s^g} r^g \Gamma^g_{s^g}) p^g_{s^g,k+1_{err}} + (2\theta\Omega^g_{s^g} r^g \delta x^g/\epsilon^g_3) q^g_{s^g,k+1_{err}} =$$

$$2(1-\theta)\Omega^g_{s^g} r^g \Gamma^g_{s^g-1} p^g_{s^g-1,k_{err}} + (1-2(1-\theta)\Omega^g_{s^g} r^g \Gamma^g_{s^g}) p^g_{s^g,k_{err}} - (2(1-\theta)\Omega^g_{s^g} r^g \delta x^g/\epsilon^g_3) q^g_{s^g,k_{err}}.$$

Thus, the last row of system (8.38) contains the following scalar equation for $q^g_{s^g_{err}}$

$$-2\Omega^g_{s^g} r^g \Gamma^g_{s^g-1} p^g_{s^g-1_{err}} + 2\Omega^g_{s^g} r^g \Gamma^g_{s^g} p^g_{s^g_{err}} + (2\Omega^g_{s^g} r^g \delta x^g/\epsilon^g_3) q^g_{s^g_{err}} = 0$$

and dividing through by $2\Omega^g_{s^g} r^g$ and rearranging gives

$$q^g_{s^g_{err}} = -\epsilon^g_3 (\Gamma^g_{s^g} p^g_{s^g_{err}} - \Gamma^g_{s^g-1} p^g_{s^g-1_{err}})/\delta x^g \tag{8.39}$$

which is identical to equation (8.22) with $z=g$, which gives the error in the downstream flow estimate of an $\mathcal{M}1$ model. Hence, we have shown that, asymptotically, the error in the downstream flow estimate of an $\mathcal{M}2$ model is equal to the error in the downstream flow estimate of an $\mathcal{M}1$ model.

The $g-1$ connectivity equations for the general pipe section $z/z+1$ are given by equation (2.23). Hence, the last g rows of system (8.37) contain $g-1$ scalar equations for the variables, $d^{z/z+1}_{k_{err}}$, of the form

$$-(\Phi^{z/z+1}\epsilon^z_3 \Gamma^z_{s^z-1}\theta/\delta x^z) p^z_{s^z-1,k+1_{err}} + (1+\Phi^{z/z+1}\epsilon^z_3 \Gamma^{z/z+1}\theta/\delta x^z + \Phi^{z/z+1}\epsilon^{z+1}_3 \Gamma^{z/z+1}\theta/\delta x^{z+1}) p^{z/z+1}_{k+1_{err}}$$

$$-(\Phi^{z/z+1}\epsilon^{z+1}_3 \Gamma^{z+1}_1 \theta/\delta x^{z+1}) p^{z+1}_{1,k+1_{err}} + \Phi^{z/z+1}\theta d^{z/z+1}_{k+1_{err}} =$$

$$(\Phi^{z/z+1}\epsilon^z_3 \Gamma^z_{s^z-1}(1-\theta)/\delta x^z) p^z_{s^z-1,k_{err}} + (1-\Phi^{z/z+1}\epsilon^z_3 \Gamma^{z/z+1}(1-\theta)/\delta x^z - \Phi^{z/z+1}\epsilon^{z+1}_3 \Gamma^{z/z+1}(1-\theta)/\delta x^{z+1}) p^{z/z+1}_{k_{err}}$$

$$+(\Phi^{z/z+1}\epsilon_3^{z+1}\Gamma_1^{z+1}(1-\theta)/\delta x^{z+1})p_{1,k_{err}}^{z+1} - \Phi^{z/z+1}(1-\theta)d_{k_{err}}^{z/z+1}.$$

Thus, the last g rows of system (8.38) contain $g-1$ scalar equations of the following form for the variables, $d_{err}^{z/z+1}$

$$-(\Phi^{z/z+1}\epsilon_3^z\Gamma_{s^z-1}^z/\delta x^z)p_{s^z-1_{err}}^z + (\Phi^{z/z+1}\epsilon_3^z\Gamma^{z/z+1}/\delta x^z + \Phi^{z/z+1}\epsilon_3^{z+1}\Gamma^{z/z+1}/\delta x^{z+1})p_{err}^{z/z+1}$$

$$-(\Phi^{z/z+1}\epsilon_3^{z+1}\Gamma_1^{z+1}/\delta x^{z+1})p_{1_{err}}^{z+1} + \Phi^{z/z+1}d_{err}^{z/z+1} = 0$$

and dividing through by $\Phi^{z/z+1}$ and rearranging gives

$$d_{err}^{z/z+1} = \{-\epsilon_3^z(\Gamma^{z/z+1}p_{err}^{z/z+1} - \Gamma_{s^z-1}^z p_{s^z-1_{err}}^z)/\delta x^z\} - \{-\epsilon_3^{z+1}(\Gamma_1^{z+1}p_{1_{err}}^{z+1} - \Gamma^{z/z+1}p_{err}^{z/z+1})/\delta x^{z+1}\}. \quad (8.40)$$

Returning again to the equations governing the errors in the flow estimates of an $\mathcal{M}1$ model, if we substitute equations (8.21) and (8.22) into equation (8.23), then we derive an equation which gives the error in a junction flow estimate of an $\mathcal{M}1$ model, and which is identical to equation (8.40). Hence, we have shown the asymptotic errors in the junction flow estimates of an $\mathcal{M}2$ model are equal to the asymptotic errors in the junction flow estimates of an $\mathcal{M}1$ model.

8.3 Observers Constructed Upon $\mathcal{M}3$ Models

We show that the error due to measurement bias introduced into state estimate of the direct observer, and the asymptotic steady error introduced into a dynamic observer, constructed upon $\mathcal{M}3$ models, are both equal to the asymptotic error introduced into an $\mathcal{M}2$ model. We assume the observers are constructed upon un-weighted $\mathcal{M}3$ models (6.4); however, the same results may be obtained for weighted $\mathcal{M}3$ models (6.23) by incorporating the vector of weightings, $\underline{l}_3(k)$, into the analysis.

If the $\mathcal{M}2$ model is arranged and partitioned according to equation (4.2), then equation (8.35) may be written in the form

$$\begin{bmatrix} E' & -B^{1''} \end{bmatrix} \begin{bmatrix} \underline{p}_{1_{est}}(k+1) \\ \underline{d}_{est}(k+1) \end{bmatrix} = \begin{bmatrix} A' & B^{2''} \end{bmatrix} \begin{bmatrix} \underline{p}_{1_{est}}(k) \\ \underline{d}_{est}(k) \end{bmatrix} + \begin{bmatrix} B^{1'} & -E'' \end{bmatrix} \begin{bmatrix} \underline{p}_3(k+1) \\ \underline{p}_2(k+1) + \underline{b} \end{bmatrix}$$

$$+ \begin{bmatrix} B^{2'} & A'' \end{bmatrix} \begin{bmatrix} \underline{p}_3(k) \\ \underline{p}_2(k) + \underline{b} \end{bmatrix}. \quad (8.41)$$

If equation (4.2) is subtracted from equation (8.41), we derive

$$\begin{bmatrix} E' & -B^{1''} \end{bmatrix} \begin{bmatrix} \underline{p}_{1_{err}}(k+1) \\ \underline{d}_{err}(k+1) \end{bmatrix} = \begin{bmatrix} A' & B^{2''} \end{bmatrix} \begin{bmatrix} \underline{p}_{1_{err}}(k) \\ \underline{d}_{err}(k) \end{bmatrix} - E''\underline{b} + A''\underline{b}. \quad (8.42)$$

System (8.42) is equivalent to system (8.37) and describes how the state estimate error due to constant measurement bias behaves. As explained previously for system (8.37), system (8.42) reaches a steady state given by

$$\left[\begin{array}{cc} [E' - A'] & [-B^{1''} - B^{2''}] \end{array}\right] \left[\begin{array}{c} \underline{p}_{1_{err}} \\ \underline{d}_{err} \end{array}\right] = -E''\underline{b} + A''\underline{b}. \tag{8.43}$$

We show that the error due to measurement bias introduced into the state estimate of a direct observer and the asymptotic state estimate of a dynamic observer, constructed upon $\mathcal{M}3$ models, is given by an equation identical to equation (8.43).

8.3.1 The Direct Observer

Consider a direct observer (5.4), constructed upon an $\mathcal{M}3$ model (6.4). We assume the right hand side of equation (5.4) is formed from $\underline{u}_3(k)$ and $[\underline{y}_3(k) + \underline{b}]$, where $\underline{b}$ is the vector of unknown constant biases from equation (8.1). The actual observer run is

$$\Theta\underline{\mathcal{X}}_{est} = \underline{\Delta} + \underline{\Delta}_{bias}. \tag{8.44}$$

where $\underline{\Delta}_{bias}$ is a vector resulting solely from the biases $\underline{b}$. Θ is the matrix

$$\left[\begin{array}{cccccccccc} A_3 & -E_3 & 0 & 0 & . & . & . & . & . \\ 0 & A_3 & -E_3 & 0 & 0 & . & . & . & . \\ 0 & 0 & A_3 & -E_3 & 0 & 0 & . & . & . \\ : & : & : & : & : & : & : & : & : \\ : & : & : & : & : & : & : & : & : \\ C_3 & 0 & 0 & 0 & . & . & . & . & . \\ 0 & C_3 & 0 & 0 & . & . & . & . & . \\ 0 & 0 & C_3 & 0 & . & . & . & . & . \\ 0 & 0 & 0 & C_3 & . & . & . & . & . \\ : & : & : & : & : & : & : & : & : \\ : & : & : & : & : & : & : & : & : \end{array}\right],$$

$$\underline{\mathcal{X}}^T_{est} = \{\underline{\hat{x}}_{3_{est}}(k)^T, \underline{\hat{x}}_{3_{est}}(k+1)^T, \underline{\hat{x}}_{3_{est}}(k+2)^T, ...\underline{\hat{x}}_{3_{est}}(k+n-1)^T\},$$

where $\underline{\hat{x}}_{3_{est}}(k)$ is the observer estimate for $\underline{x}_3(k)$,

$$\{\underline{\Delta} + \underline{\Delta}_{bias}]^T = \{-(B^1_3\underline{u}_3(k+1) + B^2_3\underline{u}_3(k))^T, -(B^1_3\underline{u}_3(k+2) + B^2_3\underline{u}_3(k+1))^T,$$

$$...., -(B^1_3\underline{u}_3(k+n-1) + B^2_3\underline{u}_3(k+n-2))^T,$$

$$[\underline{y}_3(k)+\underline{b}]^T, [\underline{y}_3(k+1)+\underline{b}]^T, ..., [\underline{y}_3(k+n-1)+\underline{b}]^T\},$$

and n is the number of timesteps over which equation (8.44) is solved.

If equation (5.4) is subtracted from equation (8.44), we derive

$$\Theta\underline{\mathcal{X}}_{err} = \underline{\Delta}_{bias}. \tag{8.45}$$

where

$$\underline{\mathcal{X}}^T_{err} = \{\underline{\widehat{x}}_{3_{err}}(k)^T, \underline{\widehat{x}}_{3_{err}}(k+1)^T, \underline{\widehat{x}}_{3_{err}}(k+2)^T, ...\underline{\widehat{x}}_{3_{err}}(k+n-1)^T\},$$

$\underline{\widehat{x}}_{3_{err}}(k)$ is the error due to measurement bias in the observer estimate for $\underline{x}_3(k)$, and

$$\underline{\Delta}^T_{bias} = \{\underline{0}^T, \underline{0}^T, ..., \underline{0}^T, \underline{b}^T, \underline{b}^T, ...\underline{b}^T\}.$$

We observe that system (5.4) is the usual direct observer constructed upon an $\mathcal{M}3$ model. As shown previously in chapter 5, if the underlying $\mathcal{M}3$ model accurately describes the behaviour of the gas network, system (5.4) will give the true state of the gas network. Then system (8.45) describes how the state estimate error, $\underline{\mathcal{X}}_{err}$, due to constant measurement bias behaves.

Since the $\mathcal{M}3$ model (6.4) with measurements (6.5) is completely observable, if the the scalar equations of system (8.45) are consistent with each other the matrix Θ will have a large enough rank to completely determine a unique solution for $\underline{\mathcal{X}}_{err}$. The unique solution is found from the following.

By inspection of system (8.45), it can be seen that a solution must behave according to

$$E_3\underline{\widehat{x}}_{3_{err}}(k+1) = A_3\underline{\widehat{x}}_{3_{err}}(k) \tag{8.46}$$

with constraints

$$C_3\underline{\widehat{x}}_{3_{err}}(k) = \underline{\widehat{p}}_{2_{err}}(k) = \underline{b}. \tag{8.47}$$

We investigate a steady solution, $\underline{\widehat{x}}_{3_{err}} = \underline{\widehat{x}}_{3_{err}}(k)$ for all k, given by equations (8.47) and

$$E_3\underline{\widehat{x}}_{3_{err}} = A_3\underline{\widehat{x}}_{3_{err}}. \tag{8.48}$$

Assuming the $\mathcal{M}3$ model is arranged and partitioned as in equation (6.3), and assuming the base $\mathcal{M}0$ system is arranged and partitioned according to equation (4.1), then

equation (8.48) can be written in the form

$$\begin{bmatrix} [E' - A'] & [E'' - A''] & [-B^{1''} - B^{2''}] \\ 0 & 0 & 0 \end{bmatrix} \begin{bmatrix} \underline{\widehat{p}}_{1_{err}} \\ \underline{\widehat{p}}_{2_{err}} \\ \underline{\widehat{d}}_{err} \end{bmatrix} = \underline{0}. \tag{8.49}$$

Combining systems (8.47) and (8.49) gives

$$\begin{bmatrix} [E' - A'] & [E'' - A''] & [-B^{1''} - B^{2''}] \\ 0 & I & 0 \end{bmatrix} \begin{bmatrix} \underline{\widehat{p}}_{1_{err}} \\ \underline{\widehat{p}}_{2_{err}} \\ \underline{\widehat{d}}_{err} \end{bmatrix} = \begin{bmatrix} \underline{0} \\ \underline{b} \end{bmatrix}. \tag{8.50}$$

A unique consistent solution to system (8.50) can be found as follows. The last g rows of system (8.50) give

$$\underline{\widehat{p}}_{2_{err}} = \underline{b}.$$

Then the top n rows of system (8.50) give

$$\begin{bmatrix} [E' - A'] & [-B^{1''} - B^{2''}] \end{bmatrix} \begin{bmatrix} \underline{\widehat{p}}_{1_{err}} \\ \underline{\widehat{d}}_{err} \end{bmatrix} = -E''\underline{b} + A''\underline{b}$$

which is identical to equation (8.43).

Hence, the error introduced into the $\mathcal{M}3$ model-based direct observer state estimate due to the constant measurement bias of equation (8.1), is identical to the asymptotic error introduced into the state estimate of $\mathcal{M}2$ models, which in turn is identical to the asymptotic error introduced into the state estimate of $\mathcal{M}1$ models.

8.3.2 The Dynamic Observers

Consider a dynamic observer, (5.5) or (5.25), constructed upon an $\mathcal{M}3$ model (6.4). If the observer is driven by $\underline{u}_3(k)$ and $[\underline{y}_3(k) + \underline{b}]$, where $\underline{u}_3(k)$ and $\underline{y}_3(k)$ are vectors of 'true' pressures, and $\underline{b}$ is a vector resulting solely from the unknown constant biases of equation (8.1), then the actual observer run is

$$\begin{aligned}(E_3 - HC_3)\underline{\widehat{x}}_{3_{est}}(k+1) = (A_3 - GC_3)\underline{\widehat{x}}_{3_{est}}(k) + B_3^1\underline{u}_3(k+1) + B_3^2\underline{u}_3(k) \\ - H[\underline{y}_3(k+1) + \underline{b}] + G[\underline{y}_3(k) + \underline{b}],\end{aligned} \tag{8.51}$$

where the matrix H may be zero for design B dynamic observers.

If equation (5.25) is subtracted from equation (8.51), we derive

$$(E_3 - HC_3)\underline{\hat{x}}_{3_{err}}(k+1) = (A_3 - GC_3)\underline{\hat{x}}_{3_{err}}(k) - H\underline{b} + G\underline{b}. \tag{8.52}$$

We observe that system (5.25) is the usual dynamic observer constructed upon an $\mathcal{M}3$ model. As shown previously in chapter 5, if the underlying $\mathcal{M}3$ model accurately describes the behaviour of the gas network, system (5.25) will tend asymptotically to the true state of the gas network. Then system (8.52) describes how the state estimate error, $\underline{\hat{x}}_{3_{err}}(k)$, due to constant measurement bias behaves.

Since the original observer system is assigned eigenvalues within the unit circle, system (8.52) also has its eigenvalues within the unit circle and is asymptotically stable. Also, since the input to system (8.52), $-H\underline{b} + G\underline{b}$, is constant, the system tends with time to a steady state, $\underline{\hat{x}}_{3_{err}}$, given by

$$[(E_3 - HC_3) - (A_3 - GC_3)]\underline{\hat{x}}_{3_{err}} = -H\underline{b} + G\underline{b}. \tag{8.53}$$

Assuming the $\mathcal{M}3$ model is arranged and partitioned as in equation (6.3), and the base $\mathcal{M}0$ system is arranged and partitioned according to equation (4.1), then equation (8.53) can be written in the form

$$\begin{bmatrix} [E' - A'] & [E'' - H_1 - A'' + G_1] & [-B^{1''} - B^{2''}] \\ 0 & -H_2 + G_2 & 0 \end{bmatrix} \begin{bmatrix} \underline{\hat{p}}_{1_{err}} \\ \underline{\hat{p}}_{2_{err}} \\ \underline{\hat{d}}_{err} \end{bmatrix} = \begin{bmatrix} -H_1 + G_1 \\ -H_2 + G_2 \end{bmatrix} \underline{b} \tag{8.54}$$

where H_1, H_2, G_1 and G_2 are the matrix blocks arising from the feedback matrices.

Since system (8.52) does not have an eigenvalue equal to 1, the matrix $[(E_3 - HC_3) - (A_3 - GC_3)]$ must be full rank, and so the square matrix block $(-H_2 + G_2)$ is full rank also. Then it can be seen that the bottom g rows of system (8.54) give

$$\underline{\hat{p}}_{2_{err}} = \underline{b}. \tag{8.55}$$

Substituting equation (8.55) into the top $n - g$ rows of system (8.54) gives

$$\begin{bmatrix} [E' - A'] & [-B^{1''} - B^{2''}] \end{bmatrix} \begin{bmatrix} \underline{\hat{p}}_{1_{err}} \\ \underline{\hat{d}}_{err} \end{bmatrix} = -E''\underline{b} + A''\underline{b}$$

which is identical to equation (8.43).

Hence, the asymptotic error in the $\mathcal{M}3$ model-based dynamic observer due to the constant measurement bias of equation (8.1), is identical to both the error introduced into the state estimate of a direct observer and the asymptotic error introduced into the state estimate of $\mathcal{M}2$ models, which in turn is identical to the asymptotic error introduced into the state estimate of $\mathcal{M}1$ models.

8.4 Experiments

As the $\mathcal{M}0$ model was run, the pressures at the upstream end and the sites of flow demand were recorded at each timestep. The pressure measurements at the three flow demand sites, A/B, B/C and C, were then corrupted by constant biases of 1 bar, -1 bar and 1 bar respectively. These corrupted pressures were then fed into the $\mathcal{M}1$ and $\mathcal{M}2$ models, and $\mathcal{M}3$ model based observers. The flow demands predicted by these estimation techniques were then compared with the true flows used as inputs to the $\mathcal{M}0$ model.

For each experiment, the true flow demand profiles for the demands, $D_k^{A/B}$, $D_k^{B/C}$ and D_k^C are shown as thick lines in Figs. A, B and C respectively, and the state estimates for $D_k^{A/B}$, $D_k^{B/C}$ and D_k^C are shown as thin lines. The percentage errors between the state estimates of $D_k^{A/B}$, $D_k^{B/C}$ and D_k^C and their true values are shown in Figs. D, E and F respectively.

The $\mathcal{M}3$ model based observers include the exact values of the weightings, $\tilde{f}_k^{demand\ site}$, in the trivial flow demand difference equations so that the effects of the measurement biases may be observed without other forms of error present.

Data taken from $\mathcal{M}0$ model with identical mesh - $\mathcal{M}0$, $\mathcal{M}1$, $\mathcal{M}2$ and $\mathcal{M}3$ models have 10 spatial nodes along each pipe.

Experiment 8.1) $\mathcal{M}1$ Model with $\theta = 1$

Experiment 8.2) $\mathcal{M}2$ Model with $\theta = 1$

Experiment 8.3) Observer Design B (small eigenvalues) with $\theta = 0.5$

Experiment 8.4) Observer Design C (small eigenvalues) with $\theta = 1$

Data taken from $\mathcal{M}0$ model with identical mesh - $\mathcal{M}0$ and $\mathcal{M}3$ models have 5 spatial nodes along each pipe.

Experiment 8.5) Observer Design A with $\theta = 0.5$

Experiment 8.1

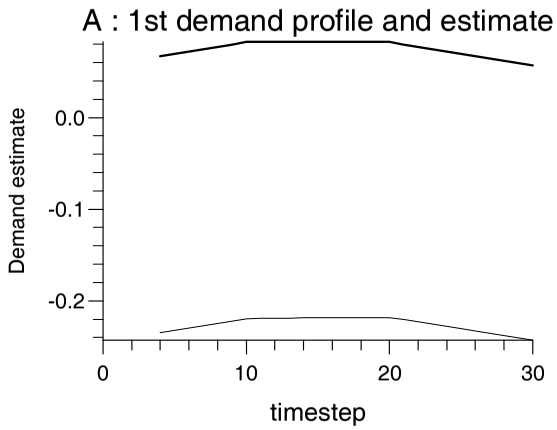

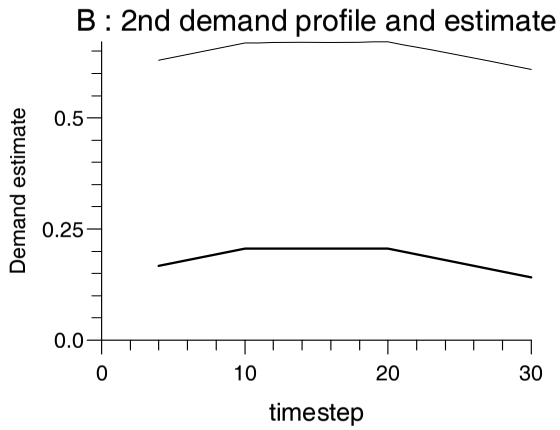

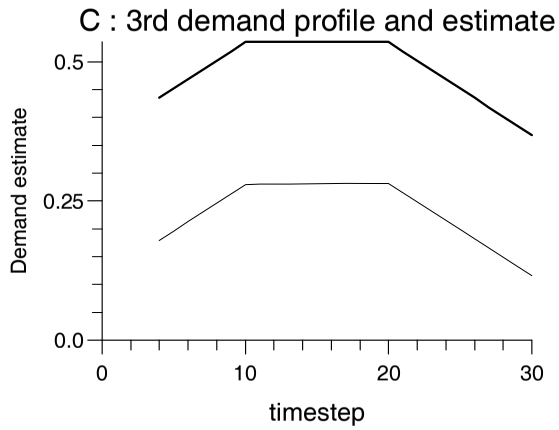

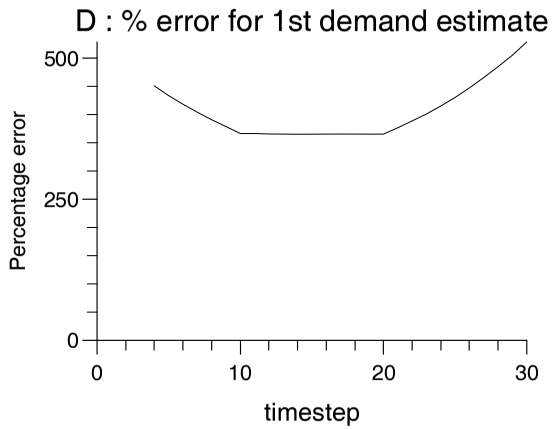

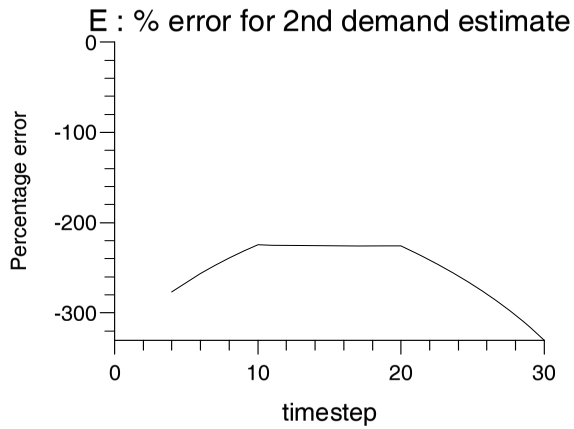

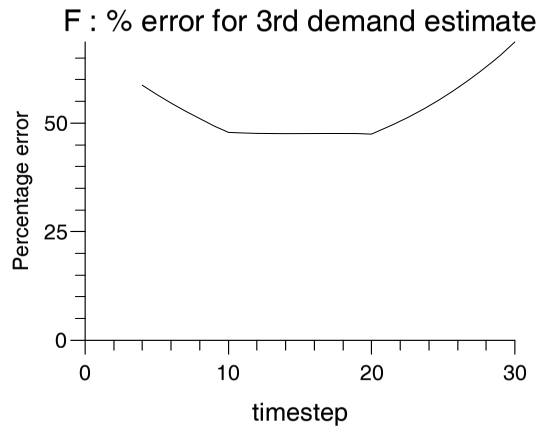

Experiment 8.2

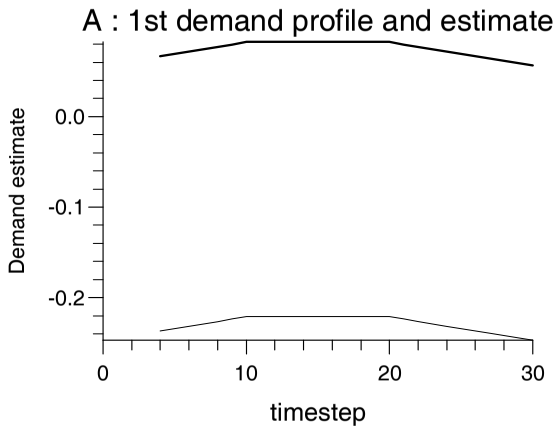

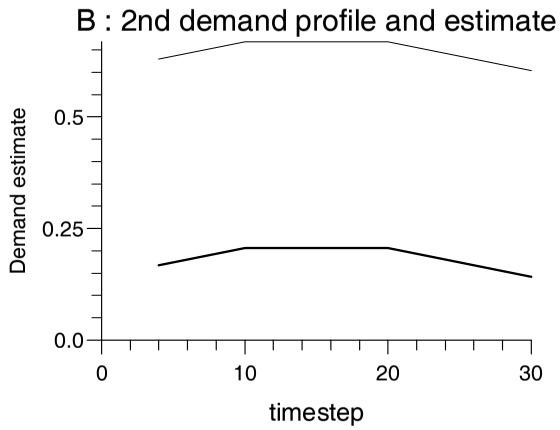

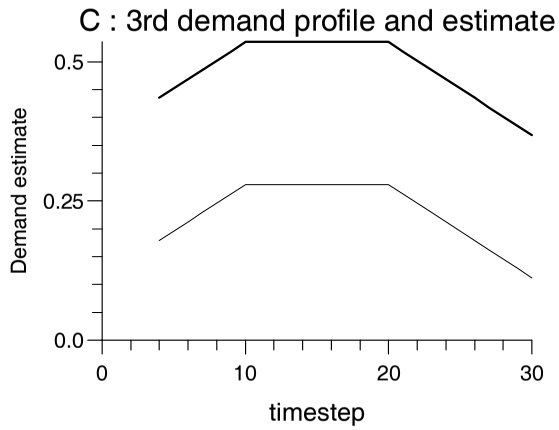

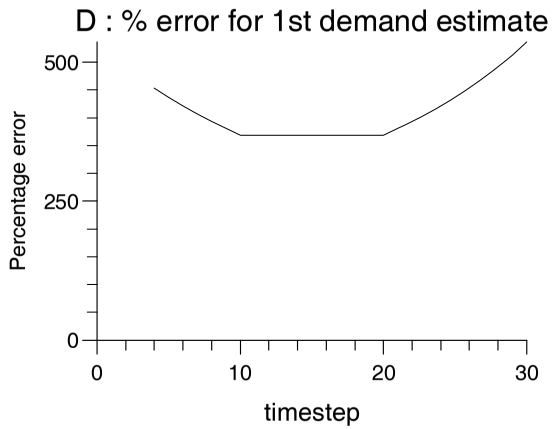

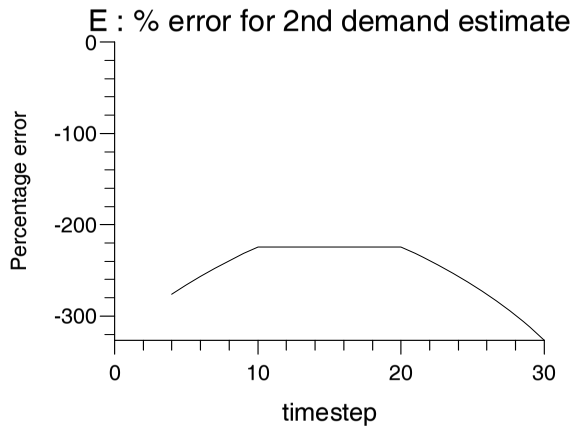

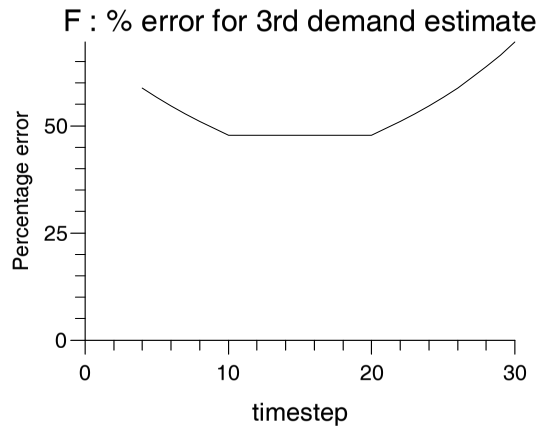

Experiment 8.3

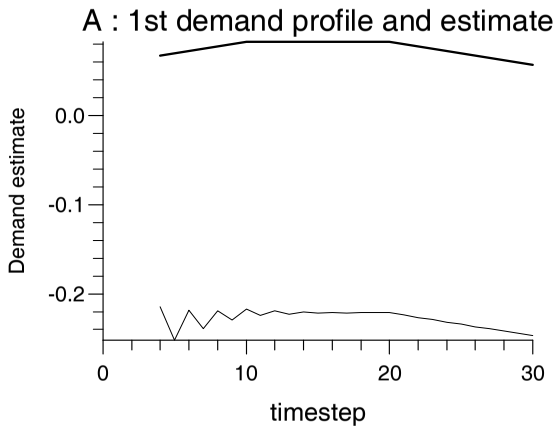

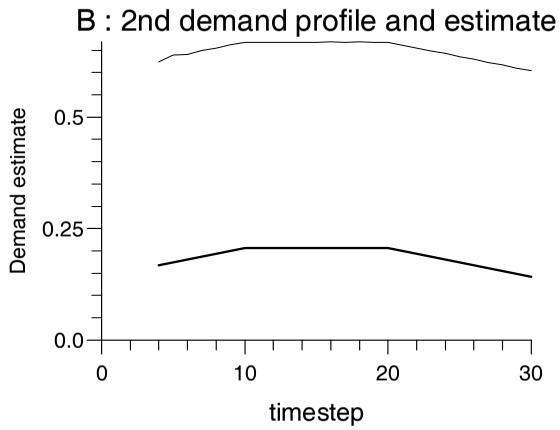

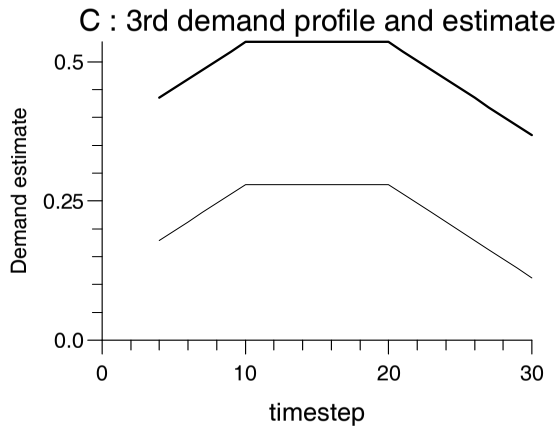

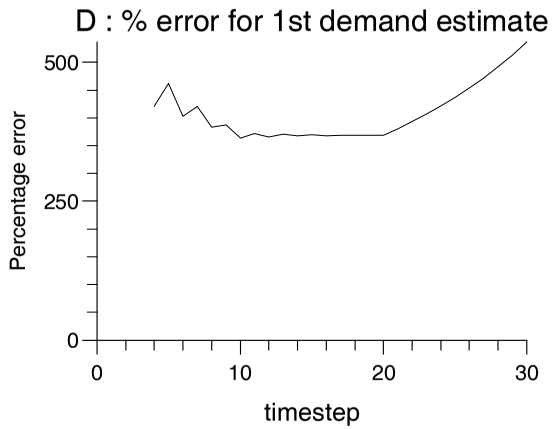

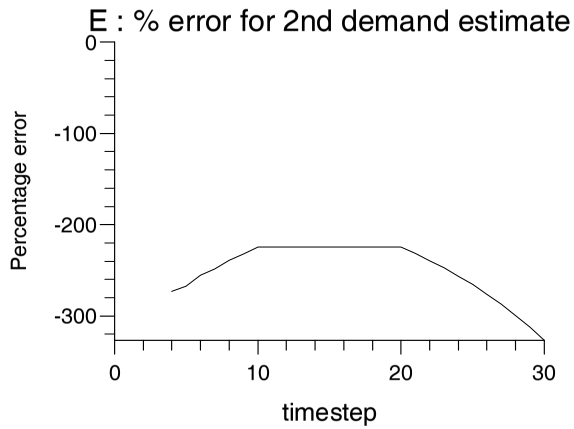

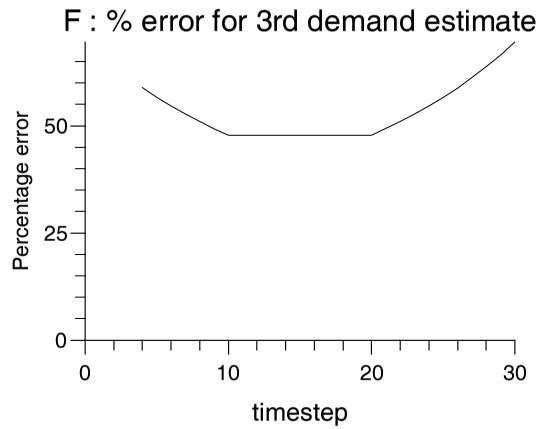

Experiment 8.4

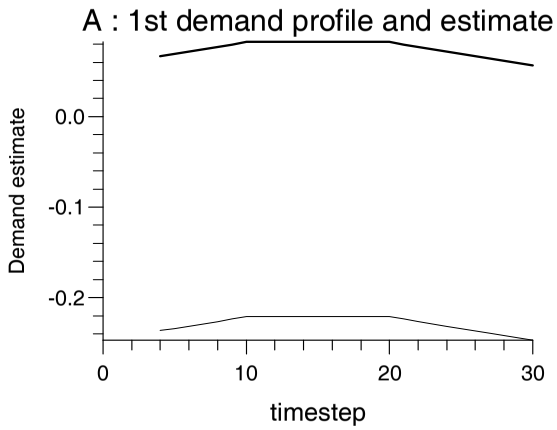

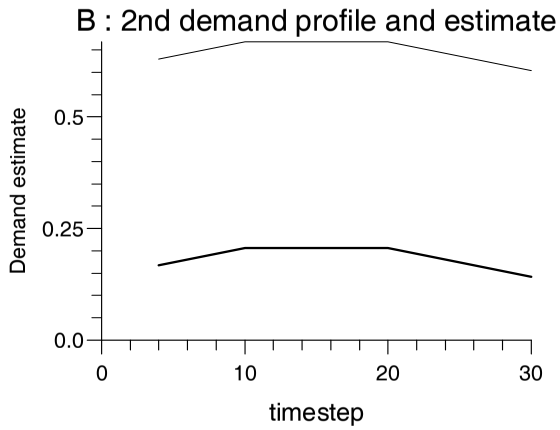

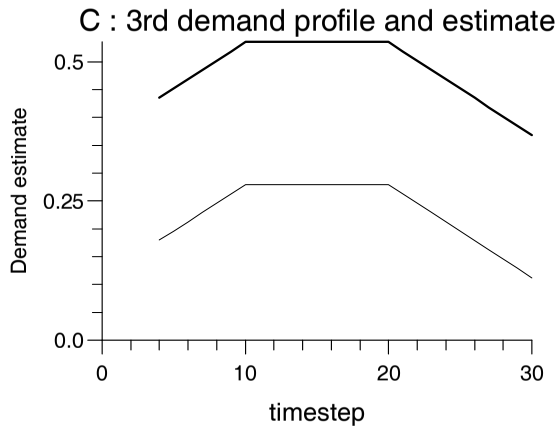

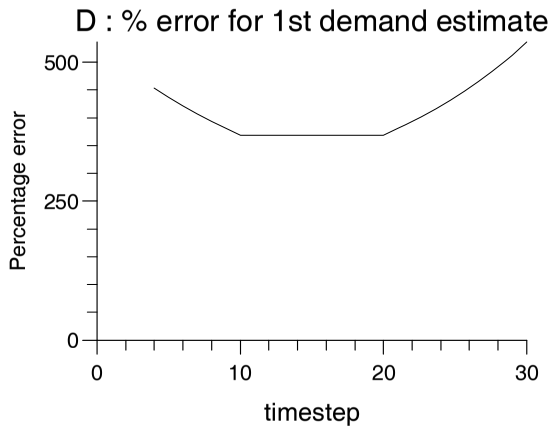

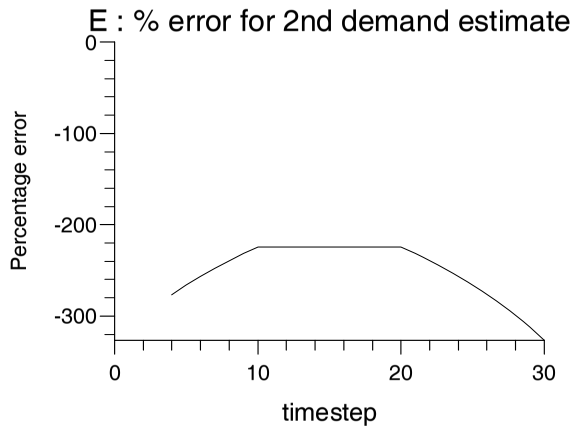

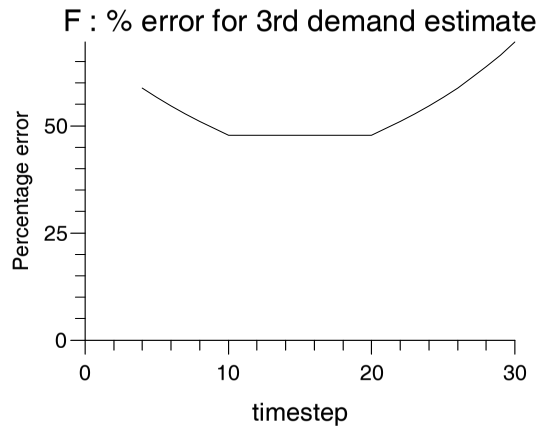

Experiment 8.5

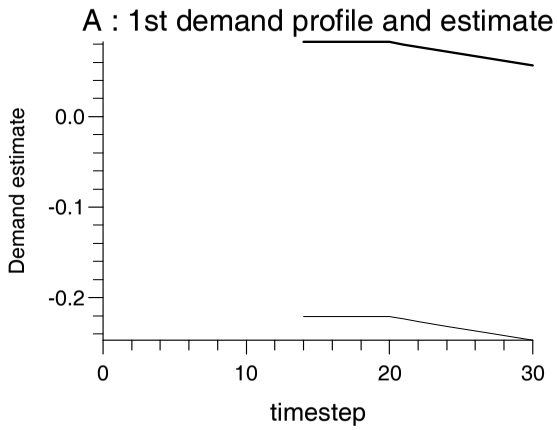

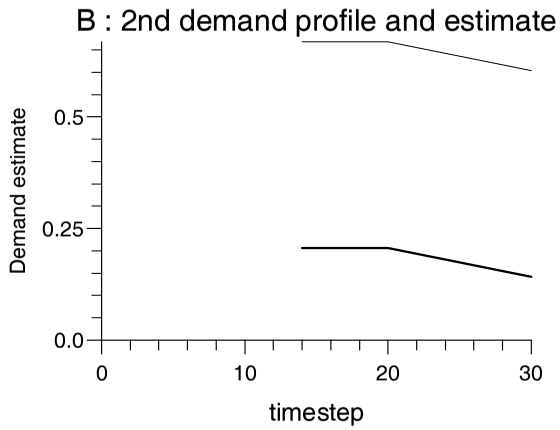

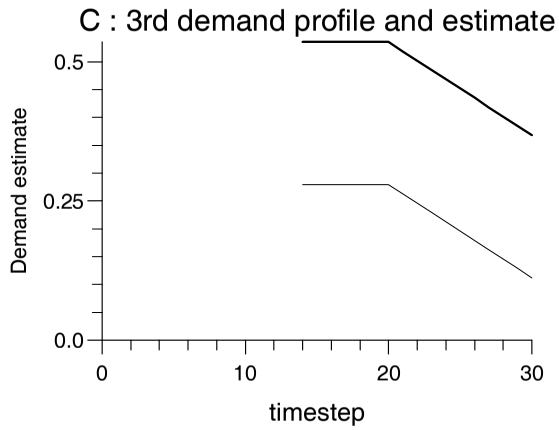

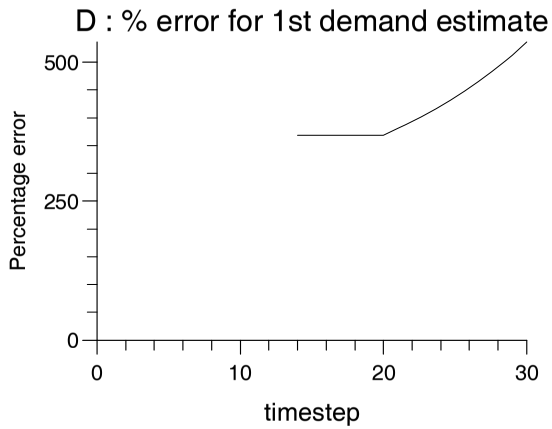

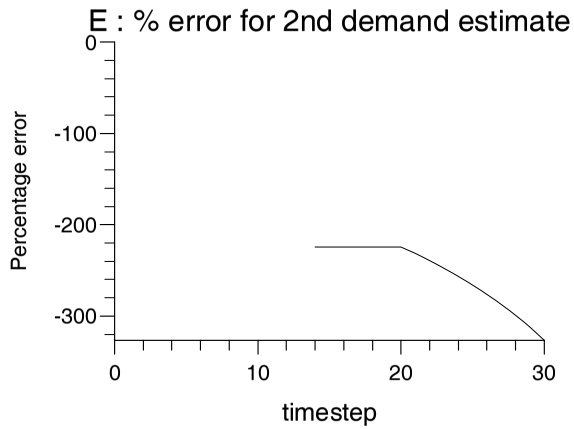

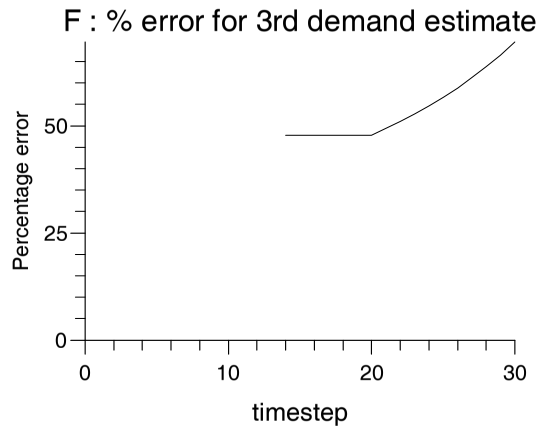

8.5 Discussion

The estimates of the flow demands, from all of the flow estimation techniques, were completely swamped by the error introduced by pressure measurement bias. Hence, a technique must be found to deal with such measurement biases. One approach would be to consider such biases as sensor faults and investigate fault diagnosis techniques [33]. Another approach, described in [34], tries to incorporate the biases into the existing model state vector and construct an observer upon such an augmented model. However, we can show that any such techniques will not work with the $\mathcal{M}1$, $\mathcal{M}2$ or $\mathcal{M}3$ models presented so far; and that an entirely new model will be required to filter out the adverse effects of measurement bias. From the preceding analysis contained in this chapter, it can be seen that, when running an $\mathcal{M}1$ or $\mathcal{M}2$ model, or any type of observer based upon an $\mathcal{M}3$ model, any time series of pressure inputs and measurements which have been corrupted by any set of constant pressure sensor biases, are perfectly consistent with some unique times series of $\mathcal{M}1$, $\mathcal{M}2$ or $\mathcal{M}3$ system states with no pressure input or measurement biases, which will be the actual state estimates given (asymptotically, in the case of a dynamic observer). Hence, as long as the biases are not so gross that these new $\mathcal{M}1$, $\mathcal{M}2$ or $\mathcal{M}3$ system states are unphysical, the biases will be undetectable.

Firstly, we consider $\mathcal{M}1$ and $\mathcal{M}2$ models. Assuming some initial conditions, any time series of bias corrupted pressure inputs, $\underline{p}_3(k)$ and $\underline{p}_{2_{measured}}(k) = \underline{p}_2(k) + \underline{b}$, will be perfectly consistent with either the unique times series of $\mathcal{M}1$ system states given by equation (8.2), or the unique times series of $\mathcal{M}2$ system states given by equation (8.35), where the unbiased $\mathcal{M}1$ and $\mathcal{M}2$ input pressures would be assumed to be $\underline{p}_3(k)$ and $(\underline{p}_2(k) + \underline{b})$. These unique $\mathcal{M}1$ and $\mathcal{M}2$ system states would obviously be the actual state estimates given by the $\mathcal{M}1$ and $\mathcal{M}2$ models.

Next, we consider $\mathcal{M}3$ models. Assume the true state of the gas network is given by an $\mathcal{M}3$ model

$$E_3\underline{x}_3(k+1) = A_3\underline{x}_3(k) + B_3^1\underline{u}_3(k+1) + B_3^2\underline{u}_3(k) \tag{8.56}$$

where

$$C_3\underline{x}_3(k) = \underline{p}_2(k)$$

for some initial conditions. In the preceding analysis of this chapter, it was shown that the error in the direct observer estimate was given by a steady $\mathcal{M}3$ model sequence

$$E_3\underline{\hat{x}}_{3_{err}}(k+1) = A_3\underline{\hat{x}}_{3_{err}}(k) \tag{8.57}$$

consistent with constraints

$$C_3\underline{\hat{x}}_{3_{err}}(k) = \underline{\hat{p}}_{2_{err}}(k) = \underline{b}, \tag{8.58}$$

and that the asymptotic error in the dynamic observer estimate was identical. If we add system (8.57) to system (8.56), we derive the following system

$$E_3\underline{x}_{3_{est}}(k+1) = A_3\underline{x}_{3_{est}}(k) + B_3^1\underline{u}_3(k+1) + B_3^2\underline{u}_3(k) \tag{8.59}$$

which is consistent with biased pressure measurements

$$\underline{y}_{3_{est}}(k) = C_3\underline{x}_{3_{est}}(k) = \underline{p}_2(k) + \underline{b},$$

where $\underline{x}_{3_{est}}(k) = \underline{x}_3(k) + \underline{\hat{x}}_{3_{err}}(k)$. Hence, any time series of bias corrupted pressure measurements, $\underline{p}_{2_{measured}}(k) = \underline{p}_2(k) + \underline{b}$, will be perfectly consistent with the unique times series of $\mathcal{M}3$ system states given by equation (8.59), where the unbiased input and measurement pressures are assumed to be $\underline{p}_3(k)$ and $(\underline{p}_2(k) + \underline{b})$ respectively.

From the previous analysis of this chapter, the estimate of a direct observer, and the asymptotic estimate of a dynamic observer will be given by $\underline{x}_3(k) + \underline{\hat{x}}_{3_{err}}$, i.e. by $\underline{x}_{3_{est}}(k)$ of system (8.59).

In the next chapter we investigate a new model variation that is able to estimate the pressure measurement biases by incorporating information about the time-profiles of the flow demands in a different manner to weighted $\mathcal{M}3$ models.

Chapter 9

Measurement Bias and $\mathcal{M}4$ Models

It may be the case that the pressure measurements at the sites of flow demand are subject to a constant bias, i.e.

$$\underline{y}(k) = \underline{p}_2(k) + \underline{b}(k) \tag{9.1}$$

where $\underline{b}(k)$ is a g dimensional vector of constant measurement biases. This is a serious problem for flow demand estimation and these pressure measurement biases need also to be estimated.

The g measurement biases are assumed to obey

$$\underline{b}(k+1) = \underline{b}(k). \tag{9.2}$$

To try to estimate these biases, we construct a new model variation, which we denote by $\mathcal{M}4$. As with the construction of the earlier $\mathcal{M}3$ model, we start from a base $\mathcal{M}0$ model. As before we first incorporate the input variables, $\underline{d}(k)$, into the state vector, but this time the $\mathcal{M}4$ models assume trivial difference equations for the flow demands of the form

$$flow\ demand_{k+1}^{demand\ site} = w_k^{demand\ site} \times flow\ demand_k^{demand\ site}$$

where the $w_k^{demand\ site}$ are estimated from other measured flow demands. After normalisation, we would have

$$normalised\ flow\ demand_{k+1}^{demand\ site} = w_k^{demand\ site} \times normalised\ flow\ demand_k^{demand\ site},$$

that is, we would have

$$\mathcal{Q}^{demand\ site} + d_{k+1}^{demand\ site} = w_k^{demand\ site} \times (\mathcal{Q}^{demand\ site} + d_k^{demand\ site}). \tag{9.3}$$

Hence, the normalised and linearised gas network $\mathcal{M}4$ models now contain difference equations of the form

$$d_{k+1}^{demand\ site} \;=\; w_k^{demand\ site} \times d_k^{demand\ site} \;+\; (w_k^{demand\ site} - 1) \times \mathcal{Q}^{demand\ site}. \qquad (9.4)$$

These scalar equations may be written together as the following sub-system of the $\mathcal{M}4$ model

$$\underline{d}(k+1) \;=\; W(k)\underline{d}(k) \;+\; (W(k) - I)\underline{q}$$

where $W(k)$ is a diagonal block containing time-varying profile coefficients, $w_k^{demand\ site}$, and $\underline{q}$ is a vector containing the steady flow demands, $\mathcal{Q}^{demand\ site}$, about which the gas network model is linearised. The term on the far right, $(W(k) - I)\underline{q}$, is included on the right hand side of the $\mathcal{M}4$ system as shown below.

Next we incorporate the measurement biases into the new state vector, and incorporate the trivial difference equations (9.2) into the system.

Assuming the base $\mathcal{M}0$ model is arranged and partitioned as in equation (4.1), then the new $n + 2g$ dimensional $\mathcal{M}4$ system has the form

$$\begin{bmatrix} E_0 & -B^{1''} & 0 \\ 0 & I & 0 \\ 0 & 0 & I \end{bmatrix} \begin{bmatrix} \underline{x}_0(k+1) \\ \underline{d}(k+1) \\ \underline{b}(k+1) \end{bmatrix} = \begin{bmatrix} A_0 & B^{2''} & 0 \\ 0 & W(k) & 0 \\ 0 & 0 & I \end{bmatrix} \begin{bmatrix} \underline{x}_0(k) \\ \underline{d}(k) \\ \underline{b}(k) \end{bmatrix}$$

$$+ \begin{bmatrix} B^{1'} \\ 0 \\ 0 \end{bmatrix} \underline{p}_3(k+1) + \begin{bmatrix} B^{2'} \\ 0 \\ 0 \end{bmatrix} \underline{p}_3(k) + \begin{bmatrix} 0 \\ (W(k) - I)\underline{q} \\ 0 \end{bmatrix} \qquad (9.5)$$

which can be expressed in the general descriptor system form

$$E_4\underline{x}_4(k+1) = A_4(k)\underline{x}_4(k) + B_4^1\underline{u}_4(k+1) + B_4^2\underline{u}_4(k) + \underline{l}_4(k) \qquad (9.6)$$

where the system matrix $A_4(k)$ is time-varying. It should be noted that the Hautus condition has been shown to be necessary and sufficient for the complete observability of *time-invariant* systems only.

For such an $\mathcal{M}4$ model, the only pressure input required is the upstream pressure (assumed known). The g pressure plus bias measurements of the real gas network at

the sites of flow demand are not needed as inputs to the $\mathcal{M}4$ model, and are, in fact, measurements of its state variables

$$\underline{y}_4(k) = C_4\underline{x}_4(k), \tag{9.7}$$

available for use in a direct or dynamic observer.

9.1 Theorems

In this section, we firstly prove that the matrix E_4 of an $\mathcal{M}4$ model is full rank if $\theta > 0$. Secondly, we prove certain conditions to be sufficient to guarantee the assignability of eigenvalues to the observer at a particular timestep. In fact, we show that for $1/2 \leq \theta \leq 1$, if at a particular timestep, the diagonal elements of $W(k)$ are not equal to either 1 or to any of the eigenvalues of the corresponding $\mathcal{M}2$ model, then at that timestep the Hautus condition holds for the $\mathcal{M}4$ model (9.6). Finally, we show the necessity of the new $\mathcal{M}4$ model form of the profile difference equations for the flow demands. It is shown that if the profile difference equations of an $\mathcal{M}4$ model are replaced by the $\mathcal{M}3$ model profile difference equations, then the Hautus condition never holds at any timestep k.

Theorem 9.1 *If $\theta > 0$, the E_4 matrix of an $\mathcal{M}4$ model is full rank.*

Proof

E_4 is $(n+2g)\times(n+2g)$ and takes the form

$$E_4 = \begin{bmatrix} E_0 & -B^{1''} & 0 \\ 0 & I & 0 \\ 0 & 0 & I \end{bmatrix}$$

where I is $g\times g$.

By construction, since we have already shown E_0 is invertible if $\theta > 0$, E_4^{-1} is $(n+2g)\times(n+2g)$ and takes the form

$$E_4^{-1} = \begin{bmatrix} E_0^{-1} & E_0^{-1}B^{1''} & 0 \\ 0 & I & 0 \\ 0 & 0 & I \end{bmatrix}$$

where I is $g \times g$.

Hence, the E_4 matrix of an $\mathcal{M}4$ model is full rank. $\square$

Theorem 9.2 *For $1/2 \leq \theta \leq 1$, if at a particular timestep the diagonal elements of $W(k)$ are not equal either to 1 or to any of the eigenvalues of the corresponding $\mathcal{M}2$ model, then at that timestep the Hautus condition holds for the $\mathcal{M}4$ model (9.6).*

Proof

By inspection, at any particular timestep, k, the eigenvalues of an $\mathcal{M}4$ system consist of the n eigenvalues of the base $\mathcal{M}0$ system, g eigenvalues equal to the g variables $w_k^{demand\ site}$, and g eigenvalues equal to 1. Hence, the eigenvalues of the $\mathcal{M}4$ system are real.

The Hautus condition holds for the $\mathcal{M}4$ system if and only if for all $\mu \in \mathbf{R}$

$$(A_4(k) - \mu E_4)\underline{v} = \underline{0} \tag{9.8}$$

$$C_4 \underline{v} = \underline{0} \tag{9.9}$$

$$\Longleftrightarrow$$

$$\underline{v} = \underline{0} \tag{9.10}$$

where $\underline{v} \in \mathbf{R}^{n+2g}$.

Equation (9.10) $\Longrightarrow$ equations (9.8), (9.9) trivially.

Equations (9.8), (9.9) and (9.10) can be expressed in the following way. The Hautus condition holds for the $\mathcal{M}4$ system if and only if for all $\mu \in \mathbf{R}$

$$(A_0 - \mu E_0)\underline{v}_n + (B^{2''} - \mu(-B^{1''}))\underline{v}_g = \underline{0} \tag{9.11}$$

$$(W(k) - \mu I)\underline{v}_g = \underline{0} \tag{9.12}$$

$$(1 - \mu)\underline{\tilde{v}}_g = \underline{0} \tag{9.13}$$

$$C_0 \underline{v}_n + \underline{\tilde{v}}_g = \underline{0} \tag{9.14}$$

$$\Longleftrightarrow$$

$$\underline{v}_n = \underline{0} \ , \ \underline{v}_g = \underline{0} \ , \ \underline{\tilde{v}}_g = \underline{0} \tag{9.15}$$

where $\underline{v} = [\underline{v}_n^T, \underline{v}_g^T, \underline{\tilde{v}}_g^T]^T$, and $\underline{v}_n \in \mathbf{R}^n$, $\underline{v}_g \in \mathbf{R}^g$, $\underline{\tilde{v}}_g \in \mathbf{R}^g$.

We firstly consider the case where $\mu \neq 1$.

Equation (9.13) implies $\underline{\tilde{v}}_g = \underline{0}$.

Substituting $\underline{\tilde{v}}_g = \underline{0}$ into equation (9.14) gives

$$C_0 \underline{v}_n = \underline{0}. \tag{9.16}$$

If $\mu \neq w_k^{demand\ site}$ for all flow demands, equation (9.12) gives $\underline{v}_g = \underline{0}$.

Substituting $\underline{v}_g = \underline{0}$ into equation (9.11) gives

$$(A_0 - \mu E_0)\underline{v}_n = \underline{0}. \tag{9.17}$$

Since the original $\mathcal{M}0$ system is completely observable for $\theta > 0$, we have for all $\mu \in \mathbf{R}$

$$(A_0 - \mu E_0)\underline{v}_n = \underline{0} \ \ , \ \ C_0 \underline{v}_n = \underline{0} \iff \underline{v}_n = \underline{0}. \tag{9.18}$$

Equations (9.16), (9.17) and (9.18) give $\underline{v}_n = \underline{0}$.

Hence we have $\underline{v} = \underline{0}$.

If $\mu = w_k^{demand\ site}$ for any flow demands, we consider the base $\mathcal{M}0$ system partitioned according to equation (4.1). Then equation (9.11) can be written as the following system of n equations for the $n + g$ dimensional vector $[\underline{v}_{n-g}^T, \underline{\hat{v}}_g^T, \underline{v}_g^T]^T$

$$[(A' - \mu E') \quad (A'' - \mu E'') \quad (B^{2''} - \mu(-B^{1''}))] \begin{bmatrix} \underline{v}_{n-g} \\ \underline{\hat{v}}_g \\ \underline{v}_g \end{bmatrix} = \underline{0} \tag{9.19}$$

where

$$\underline{v}_n = \begin{bmatrix} \underline{v}_{n-g} \\ \underline{\hat{v}}_g \end{bmatrix}$$

and $\underline{v}_{n-g} \in \mathbf{R}^{n-g}$ and $\underline{\hat{v}}_g \in \mathbf{R}^g$.

Equation (9.16) zeros the elements of $\underline{v}_n$ corresponding to the measured pressures at the sites of flow demand; i.e. equation (9.16) zeros $\underline{\hat{v}}_g$. Removing $\underline{\hat{v}}_g$ from system (9.19) gives the system

$$[(A' - \mu E') \quad (B^{2''} - \mu(-B^{1''}))] \begin{bmatrix} \underline{v}_{n-g} \\ \underline{v}_g \end{bmatrix} = \underline{0}. \tag{9.20}$$

However, the system matrices of an $\mathcal{M}2$ model corresponding to the base $\mathcal{M}0$ model have the form

$$E_2 = [E' \quad -B^{1''}]$$

$$A_2 = [A' \quad B^{2''}].$$

So system (9.20) has the form

$$(A_2 - \mu E_2) \begin{bmatrix} \underline{v}_{n-g} \\ \underline{v}_g \end{bmatrix} = \underline{0}. \tag{9.21}$$

If we assume $\mu = w_k^{demand\ site}$ is not equal to an eigenvalue of the corresponding $\mathcal{M}2$ system, $(A_2 - \mu E_2)$ is full rank, and hence system (9.21) implies

$$\begin{bmatrix} \underline{v}_{n-g} \\ \underline{v}_g \end{bmatrix} = \underline{0}.$$

Hence we have $\underline{v} = \underline{0}$.

We secondly consider the case where $\mu = 1$.

Since we are assuming none of the $w_k^{demand\ site}$ are equal to 1, equation (9.12) gives $\underline{v}_g = \underline{0}$.

Substituting $\underline{v}_g = \underline{0}$ into equation (9.11) gives

$$(A_0 - \mu E_0)\underline{v}_n = \underline{0}.$$

Since we have shown for $1/2 \leq \theta \leq 1$, that all the eigenvalues of the original $\mathcal{M}0$ system have modulus less than 1, the above equation with $\mu = 1$ implies $\underline{v}_n = \underline{0}$.

Substituting $\underline{v}_n = \underline{0}$ into equation (9.14) gives $\underline{\tilde{v}}_g = \underline{0}$.

Hence we have $\underline{v} = \underline{0}$.

Hence, we have the result; equations (9.8), (9.9) $\Longrightarrow$ equation (9.10).

Hence, for $1/2 \leq \theta \leq 1$, if at a particular timestep the diagonal elements of $W(k)$ are not equal either to 1 or to any of the eigenvalues of the corresponding $\mathcal{M}2$ model, then at that timestep the Hautus condition will hold for the $\mathcal{M}4$ model (9.6). $\Box$

We construct dynamic observers for such an $\mathcal{M}4$ system by finding a new feedback matrix, $G(k)$, at each timestep to assign eigenvalues within the unit circle. Since, the matrix $A_4(k)$ is time-varying, assigning eigenvalues within the unit circle is not necessarily sufficient to cause the observer to converge asymptotically. However, if the dynamics of the real system are quite slow, from [15], it follows that assigning sufficiently small eigenvalues may well give convergence.

We can find the feedback matrix $G(k)$ to assign observer eigenvalues arbitrarily at each timestep k when the Hautus condition holds, and the above theorem implies the Hautus condition does not hold for only a few specific values of the coefficients w_k^{node}. At these particular timesteps we can run the simple $\mathcal{M}4$ model i.e. without the observer feedback terms $G(\underline{y}(k) - C\underline{x}(k))$ or $H(\underline{y}(k+1) - C\underline{x}(k+1))$. However, alternatively, it may be possible to choose θ to place the eigenvalues of the corresponding $\mathcal{M}2$ system away from likely values of the coefficients w_k^{node}, which for slowly varying flow demands should be close to 1.

Lastly, in this theory section we show why the new $\mathcal{M}4$ model form of trivial difference equation (9.4) for the flow demands is neccessary in order to estimate the measurement biases. We have the following theorem.

Theorem 9.3 *If the trivial difference equations*

$$d_{k+1}^{demand\ site} = w_k^{demand\ site} \times d_k^{demand\ site} + (w_k^{demand\ site} - 1) \times \mathcal{Q}^{demand\ site}$$

of an $\mathcal{M}4$ model are replaced by the $\mathcal{M}3$ model difference equations

$$d_{k+1}^{demand\ site} = d_k^{demand\ site} + \tilde{f}_k^{demand\ site} \quad for\ all\ k,$$

then the Hautus condition never holds at any timestep k.

Proof

If we had incorporated the previous $\mathcal{M}3$ model form of difference equation (6.22) into $\mathcal{M}4$ models, the $\mathcal{M}4$ system matrices would have been identical except that for the matrix block $W(k)$, we would have had $W(k) = I$ for all timesteps k. Thus, the matrices E_4 and A_4 would have had the form

$$E_4 = \begin{bmatrix} E_0 & -B^{1''} & 0 \\ 0 & I & 0 \\ 0 & 0 & I \end{bmatrix}$$

and

$$A_4 = \begin{bmatrix} A_0 & B^{2''} & 0 \\ 0 & I & 0 \\ 0 & 0 & I \end{bmatrix}.$$

The Hautus condition holds for this alternative $\mathcal{M}4$ system if and only if for all $\mu \in \mathbf{R}$

$$(A_4 - \mu E_4)\underline{v} = \underline{0} \tag{9.22}$$

$$C_4\underline{v} = \underline{0} \tag{9.23}$$

$$\Longleftrightarrow$$

$$\underline{v} = \underline{0} \tag{9.24}$$

where $\underline{v} \in \mathbf{R}^{n+2g}$.

We combine systems (9.22) and (9.23) into the following system

$$\begin{bmatrix} (A_4 - \mu E_4) \\ C_4 \end{bmatrix} \underline{v} = \underline{0}. \tag{9.25}$$

For $\mu = 1$, from the above structures for A_4 and E_4, we can see that $(A_4 - \mu E_4)$ has rank at most n, whilst C_4 has rank g. Hence, the matrix

$$\begin{bmatrix} (A_4 - \mu E_4) \\ C_4 \end{bmatrix}$$

has at most rank $n + g$, and, by the 'rank + nullity' theorem [14], [27], system (9.25) admits non-zero solutions for $\underline{v}$. Hence, the Hautus condition does not hold. □

9.2 Experiments

As the $\mathcal{M}0$ model was run, the pressures at the upstream end and the sites of flow demand were recorded at each timestep. The pressure measurements at the three flow demand sites, A/B, B/C and C, were then corrupted by constant biases of 1 bar, -1 bar and 1 bar respectively. These corrupted pressures were then fed into both design A and design B observers constructed upon an $\mathcal{M}4$ model. For the design B dynamic observer, the feedback matrix, G, was recalculated at each timestep, and the assigned eigenvalues were spread evenly in the interval $(0, 0.1)$. Experiments with design C observers are not presented since design C observers constructed upon $\mathcal{M}4$ models were found to behave similarly to design B observers. The flow demands predicted by the observers were then compared with the true flows used as inputs to the $\mathcal{M}0$ model. For experiments 9.1 to 9.3, the $\mathcal{M}0$ model simulating a gas network was identical to the $\mathcal{M}0$ model upon which the $\mathcal{M}4$ model was constructed. For experiments 9.4 to 9.8, the $\mathcal{M}0$ model simulating a gas network had a much finer discretisation (in both space and time) than the $\mathcal{M}4$ model.

In all experiments, the $\mathcal{M}4$ models were given the exact values of the profile coefficients, $w_k^{demand\ site}$, calculated from the flow demand inputs to the $\mathcal{M}0$ model.

For each experiment, the true flow demand profiles for the demands, $D_k^{A/B}$, $D_k^{B/C}$ and D_k^C are shown as thick lines in Figs. A, B and C respectively, and the state estimates for $D_k^{A/B}$, $D_k^{B/C}$ and D_k^C are shown as thin lines. The percentage errors between the state estimates of $D_k^{A/B}$, $D_k^{B/C}$ and D_k^C and their true values are shown in Figs. D, E and F respectively.

Data taken from $\mathcal{M}0$ model with identical mesh - both $\mathcal{M}0$ and $\mathcal{M}4$ models have 10 spatial nodes along each pipe.

Experiment 9.1) Observer Design B with $\theta = 1$

Experiment 9.2) Observer Design B with $\theta = 0.75$

Experiment 9.3) Observer Design B with $\theta = 0.5$

Data taken from $\mathcal{M}0$ model with much finer mesh - $\mathcal{M}4$ model has 5 spatial nodes along each pipe.

Experiment 9.4) Observer Design A with $\theta = 1$

Experiment 9.5) Observer Design A with $\theta = 0.75$

Experiment 9.6) Observer Design A with $\theta = 0.5$

Data taken from $\mathcal{M}0$ model with much finer mesh - $\mathcal{M}4$ model has 10 spatial nodes along each pipe.

Experiment 9.7) Observer Design B with $\theta = 1$

Experiment 9.8) Observer Design B with $\theta = 0.75$

Experiment 9.1

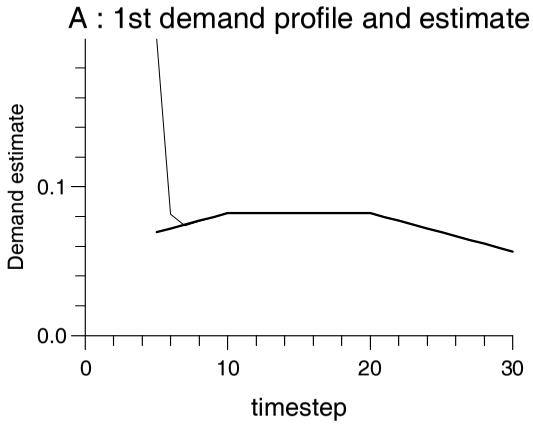

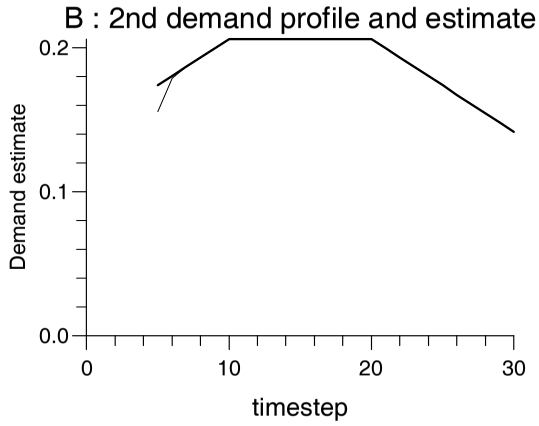

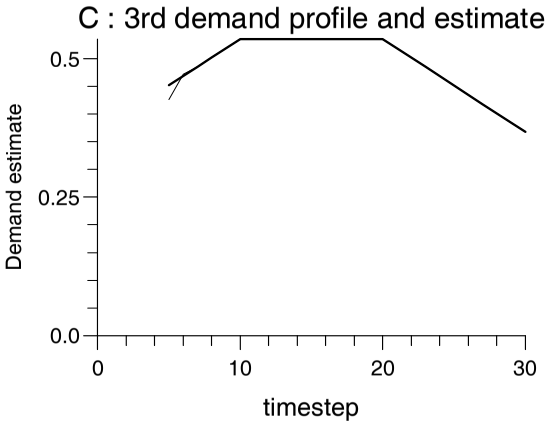

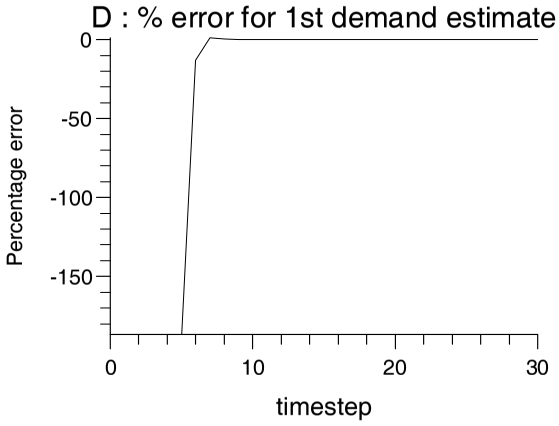

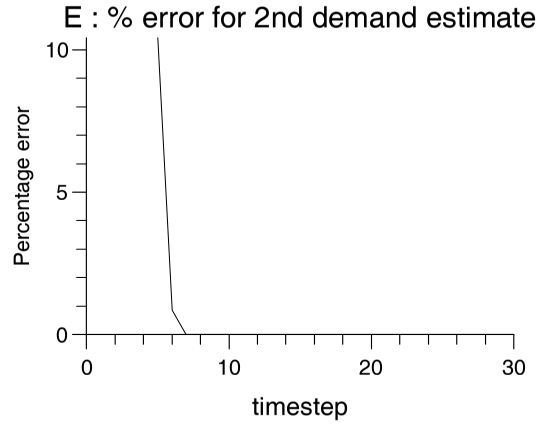

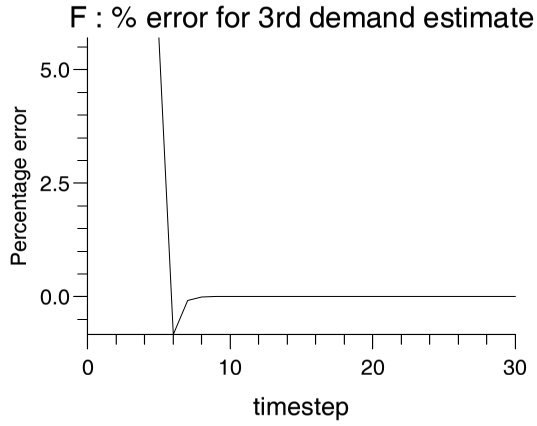

Experiment 9.2

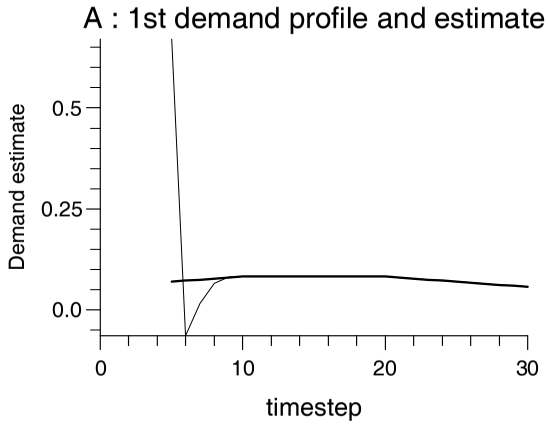

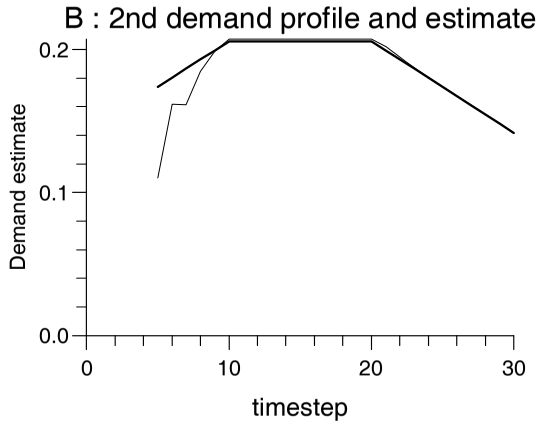

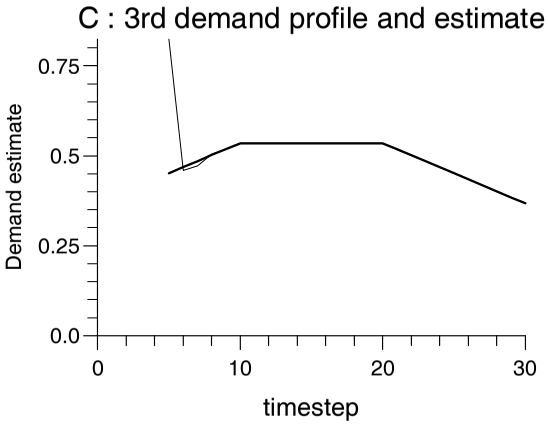

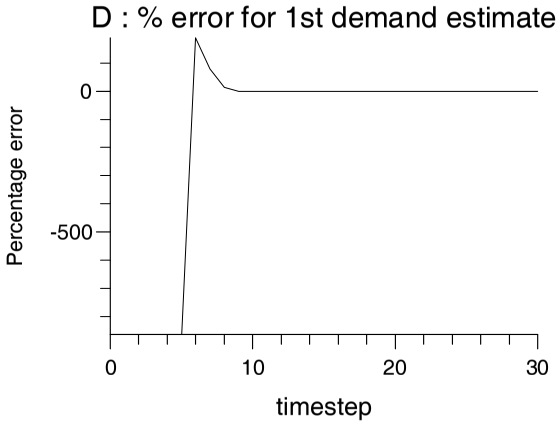

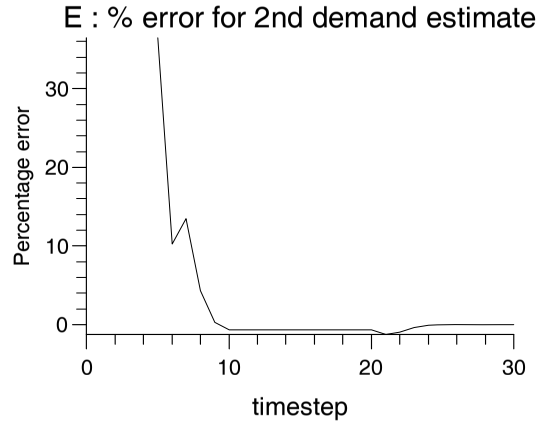

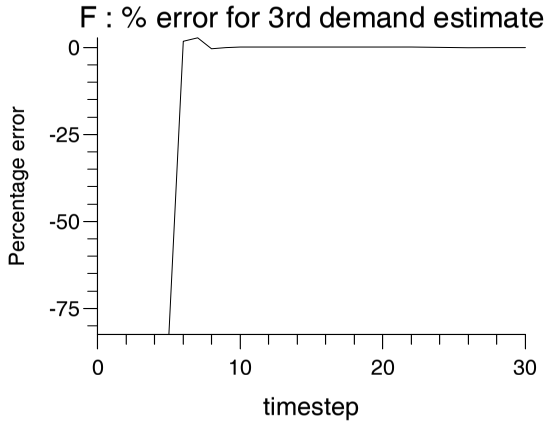

Experiment 9.3

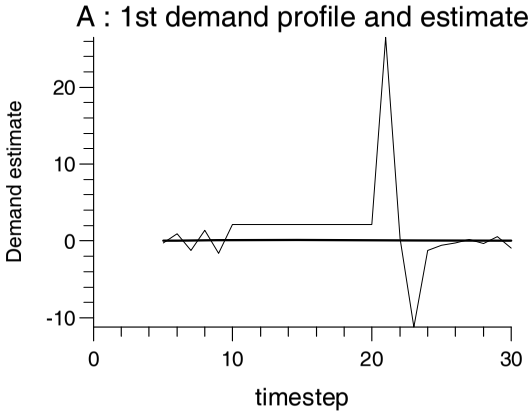

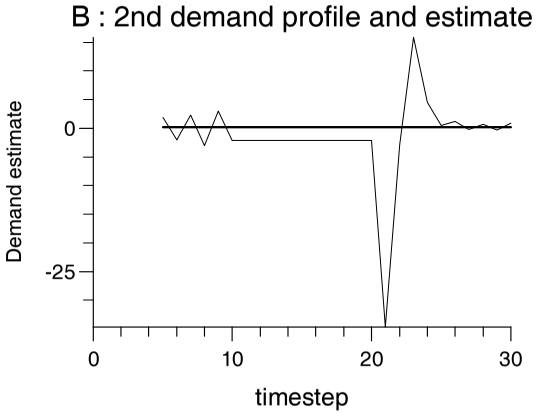

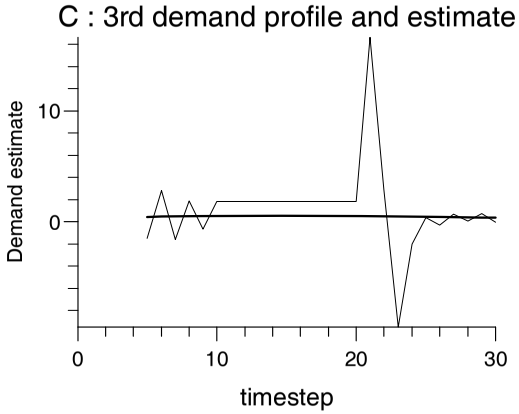

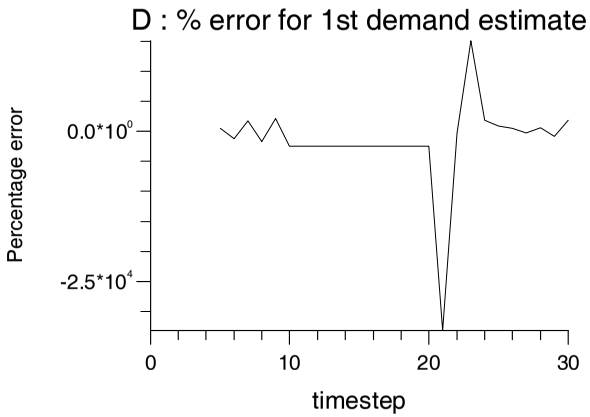

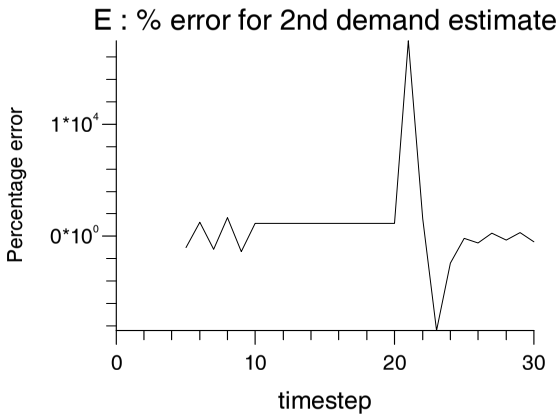

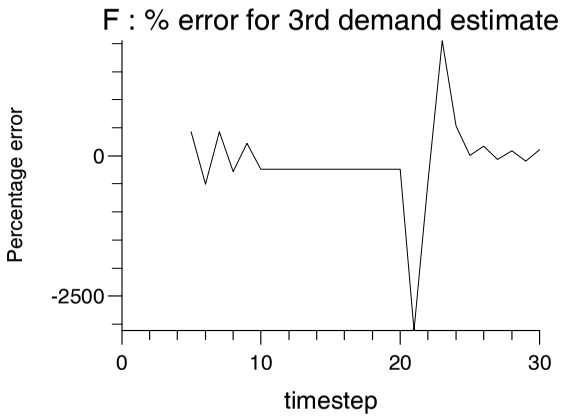

Experiment 9.4

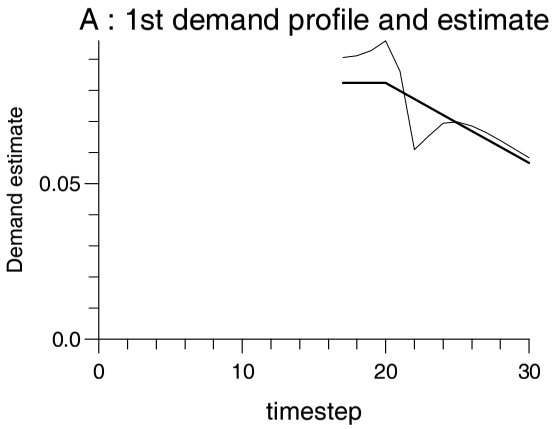

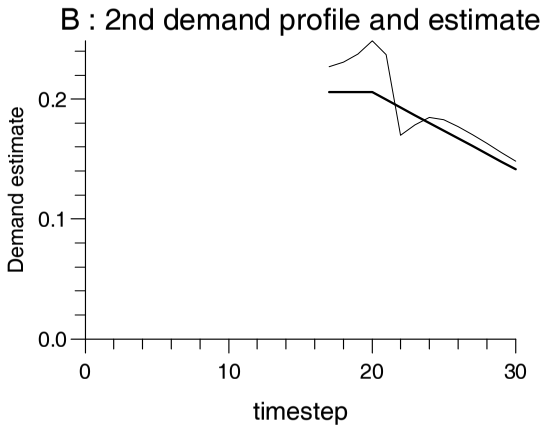

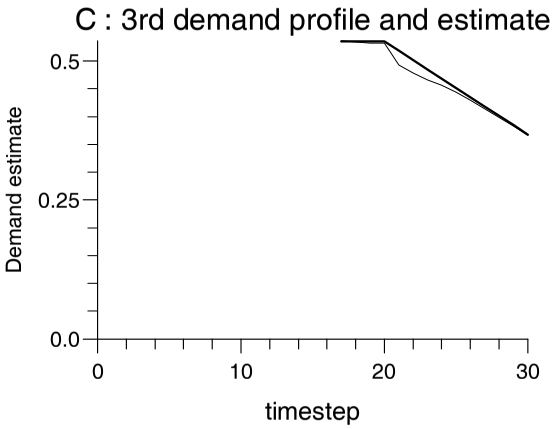

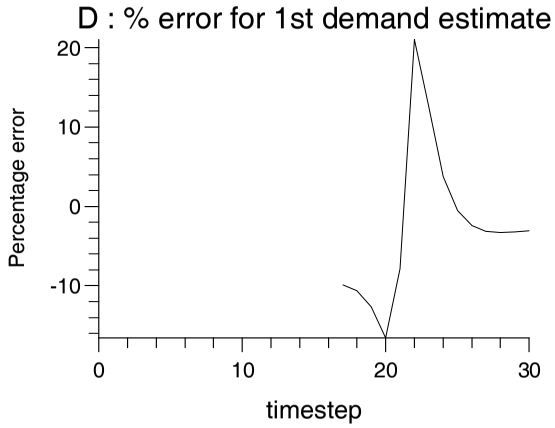

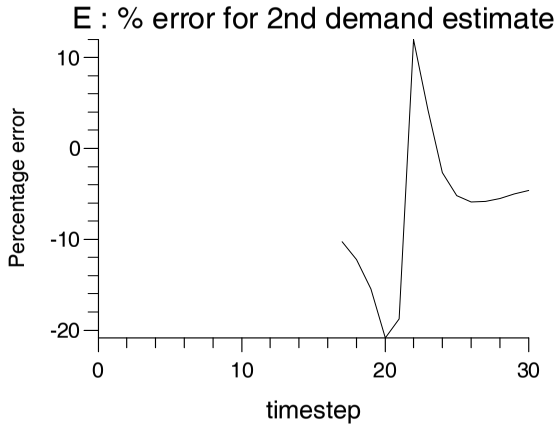

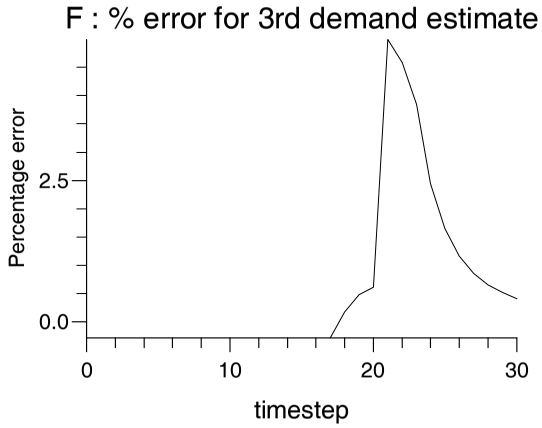

Experiment 9.5

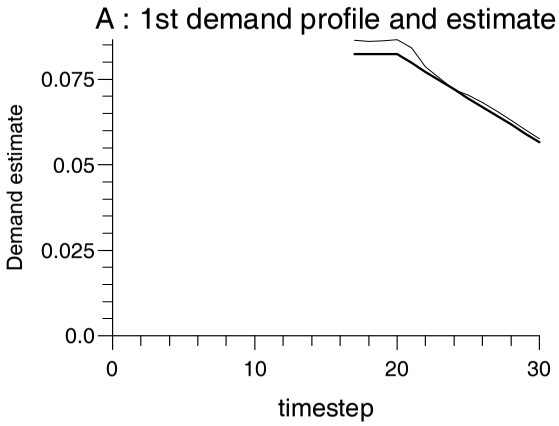

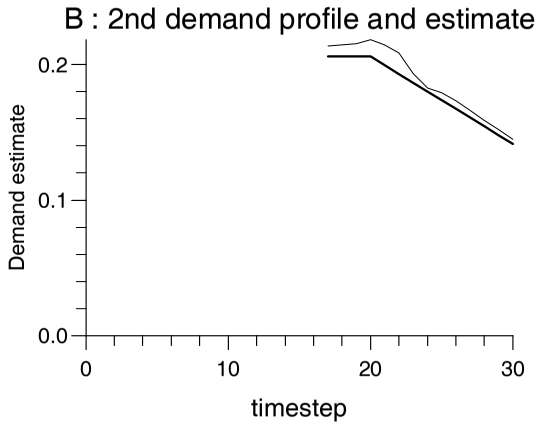

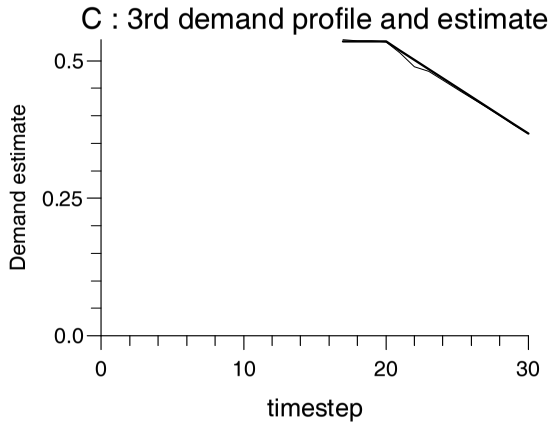

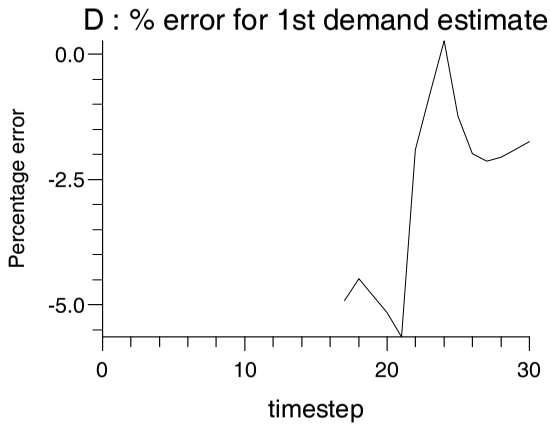

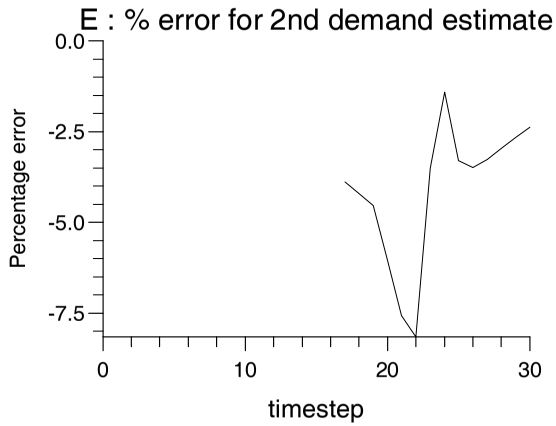

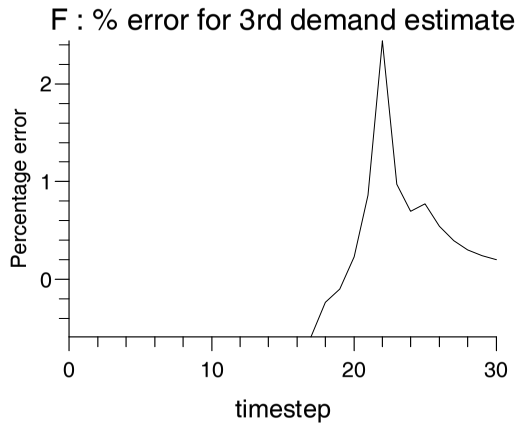

Experiment 9.6

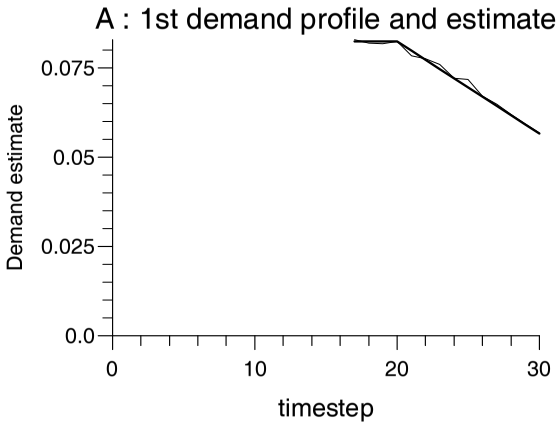

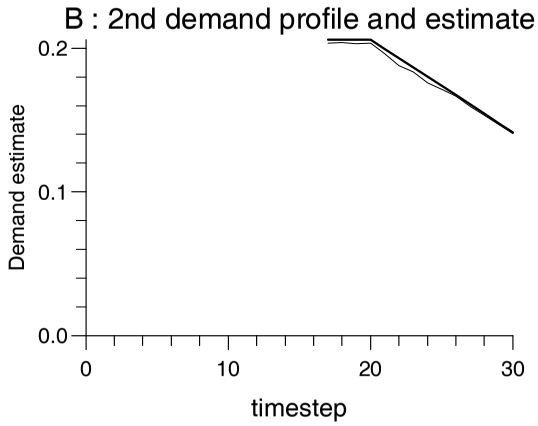

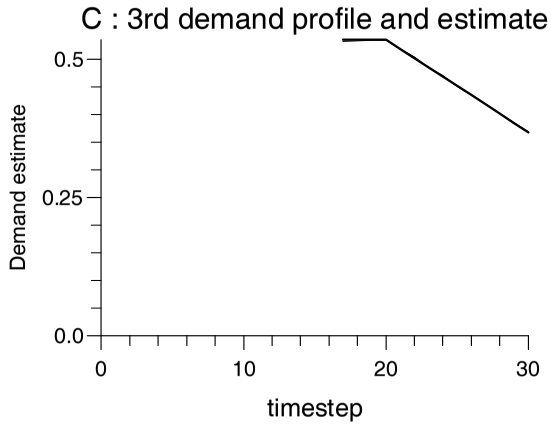

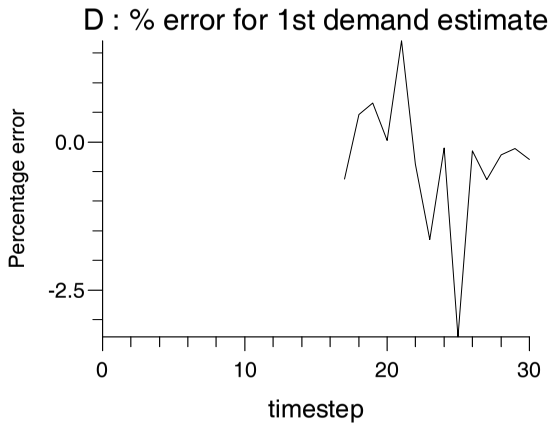

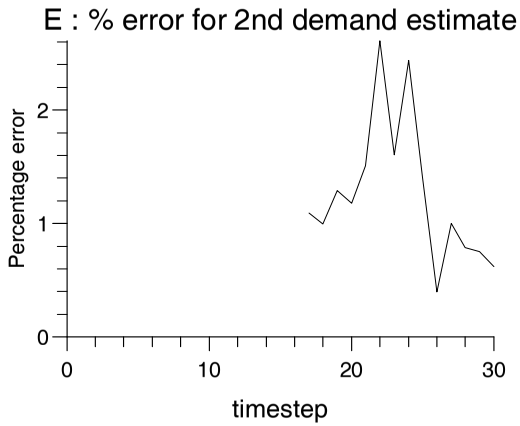

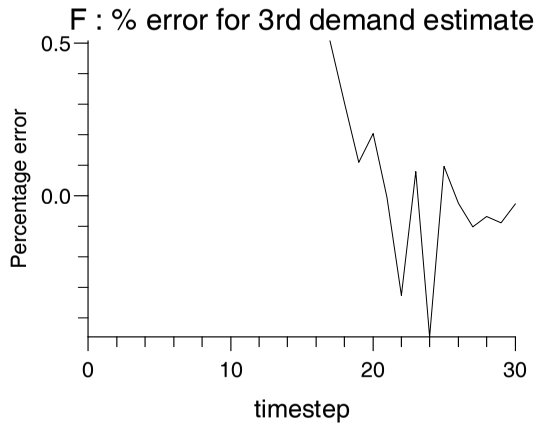

Experiment 9.7

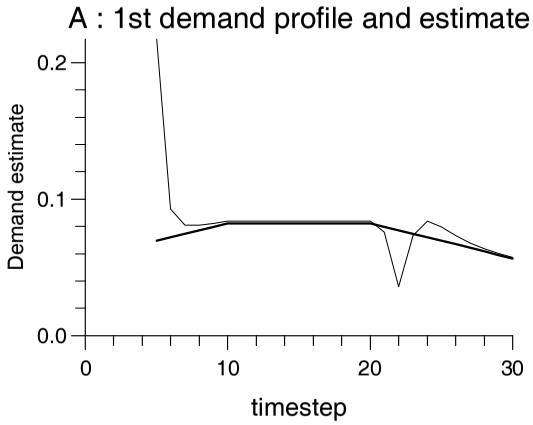

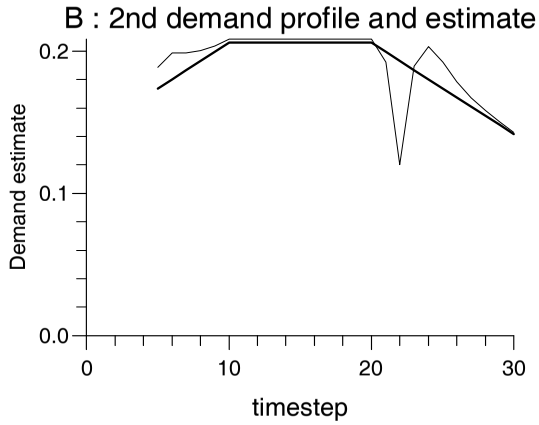

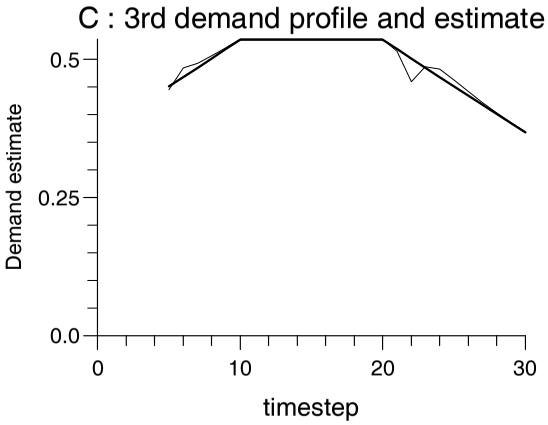

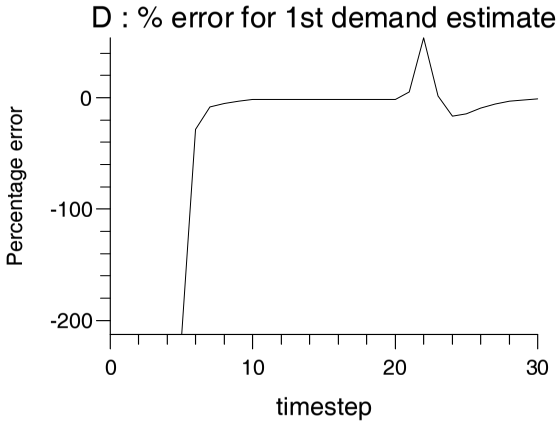

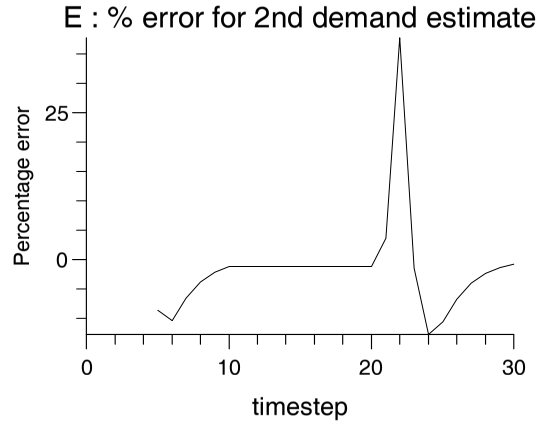

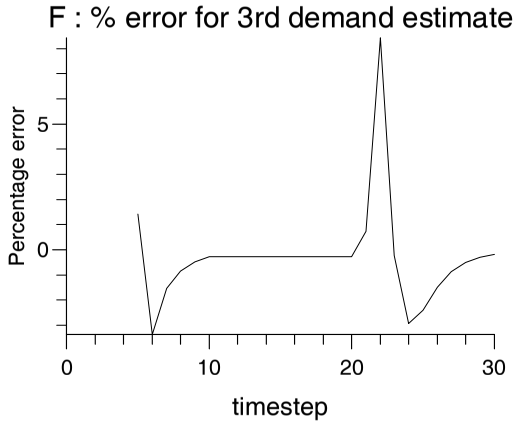

Experiment 9.8

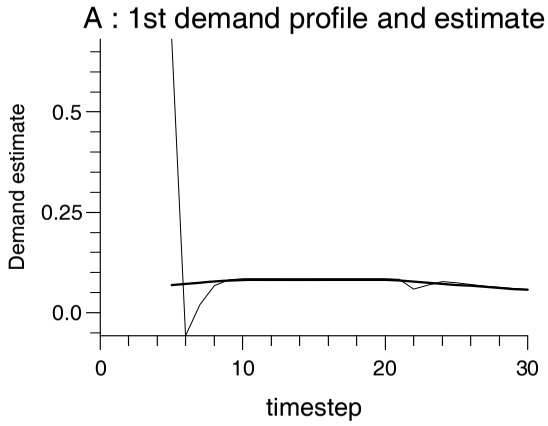

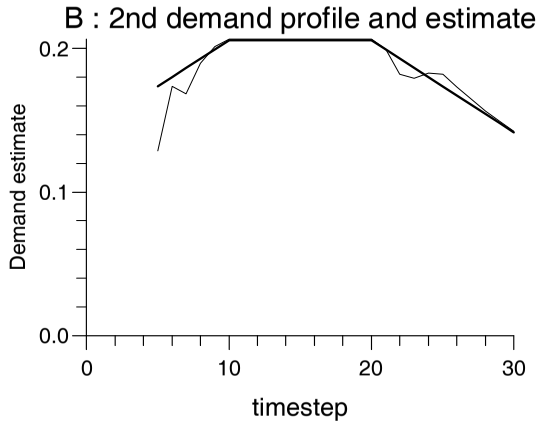

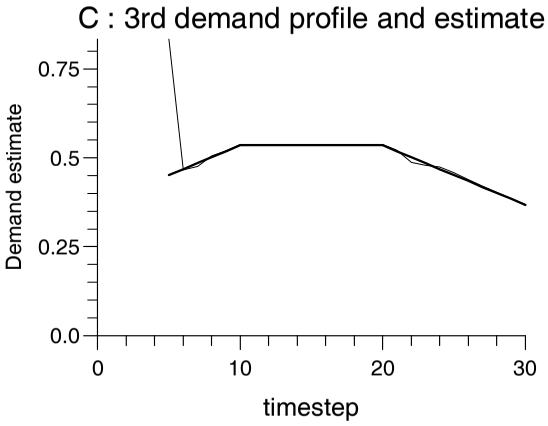

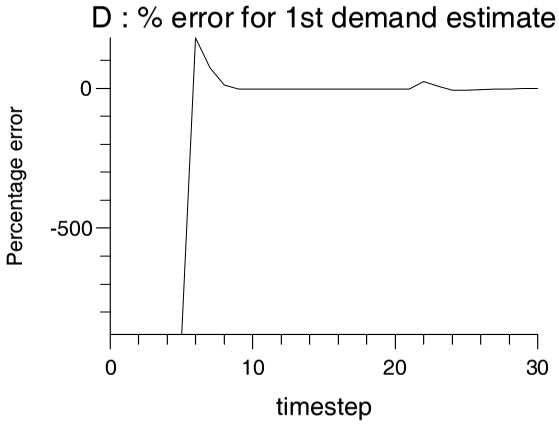

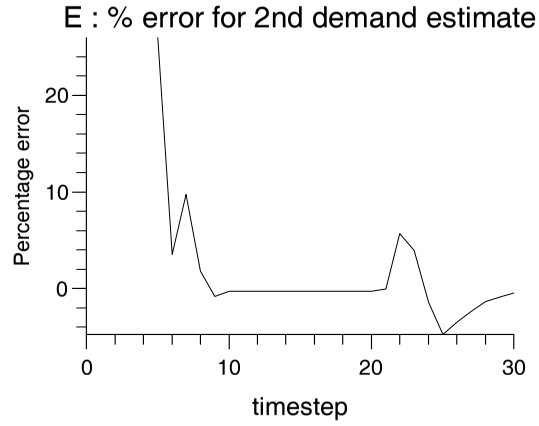

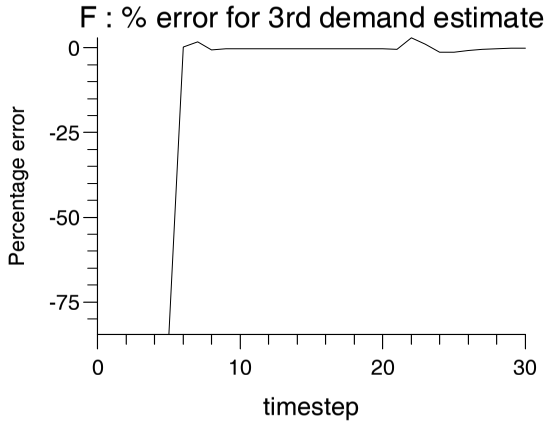

9.3 Discussion

The chosen flow profile was a severe test for the observers due to the long central period for which the flow demands remained constant. For this period the feedback was omitted from the dynamic observer leaving the simple $\mathcal{M}4$ model.

When data was taken from an $\mathcal{M}0$ model with an identical mesh, the direct observer gave perfect state estimates for all timesteps (although these graphs are ommitted), for all values of $\theta \in [1/2, 1]$. However, if fewer spatial nodes were used, the direct observer could fail during the period for which the flows remained constant. Increasing the number of spatial nodes increased the dimension of the $\mathcal{M}4$ model, and hence, the number of timesteps over which equation (5.4) was solved. This helped to give equation (5.4) a large enough rank to be solved for a unique solution over these difficult regions of the flow profiles.

With data taken from an identical mesh, the dynamic observer converged successfully with time for $\theta = 1$ and $\theta = 3/4$, but not for $\theta = 1/2$. As θ moved from 1 to 1/2, the assigned observer eigenvalues became more sensitive in a similar way to $\mathcal{M}3$ model based dynamic observers. Indeed, on checking the assigned observer eigenvalues, it was found that all eigenvalues were within the unit circle when $\theta = 1$ but not when $\theta = 1/2$. It may be that for $\theta = 1/2$, the $\mathcal{M}4$ system is in some sense 'close' to losing the Hautus condition. Gaining theoretical understanding of this problem would be worthwhile future research. For the dynamic observer, it was also noted that the eigenvalues of the system needed to be not only within the unit circle, but much closer to the origin before there was convergence. Since the observer has time-varying system matrices, assigning eigenvalues within the unit circle is not sufficient for asymptotic stability, and hence convergence. From [15], sufficiently small eigenvalues need to be assigned before there is convergence.

Unfortunately, we have no theoretical guarantee of the observability of the time-varying $\mathcal{M}4$ system, or of the performance of the direct and dynamic observers constructed upon such models. This would be a worthwhile area of future research, for which some useful references would be [41], [26], [6], [7], [15].

When data was taken from an $\mathcal{M}0$ model with a much finer discretisation, both di-

rect and dynamic observers behaved poorly for $\theta = 1$. Direct and dynamic observers constructed upon $\mathcal{M}4$ models are in some sense more sensitive to modelling (and measurement) error than previous estimation techniques investigated in this thesis. From various experiments performed, it was seen that the error present in the state estimates generally seems to have the following form. The error seems to decrease over periods when the profile coefficients, $w_k^{demand\ site}$, are constant, but increase suddenly when there is a sudden change in the values of $w_k^{demand\ site}$. This is not understood, but it may be the case that an alternative observer design could help to reduce such error. Perhaps an observer that switched between the different models, $\mathcal{M}3$ and $\mathcal{M}4$, at certain times of day could be designed to estimate the biases, where the $\mathcal{M}4$ model based observer would run over certain 'favourable' timesteps only. Then these estimates of the biases may be kept while an $\mathcal{M}3$ model based observer is run over periods where an $\mathcal{M}4$ model based observer would fail.

However, as θ moved from 1 to 1/2, the error introduced by taking data from a finer mesh was reduced. For $\theta = 1/2$, the dynamic observer failed due to the sensitivity of the observer eigenvalues; however, the direct observer coped very well indeed.

In the next chapter, we look at the problem of pressure measurement noise. Experimental results show clearly the extra sensitivity of $\mathcal{M}4$ models, the flow state estimates of which are completely swamped by the error introduced by measurement noise. To deal with this problem, we examine two simple smoothing techniques, and derive two final model variations, $\mathcal{M}5$ and $\mathcal{M}6$, to deal with the problem of the sensitivity of the flow demand estimates. $\mathcal{M}5$ and $\mathcal{M}6$ models have only a single total flow demand perturbation state variable that is the sum of all the individual demand flow perturbation variables. Such models are less sensitive to pressure measurement noise.

Chapter 10

White Noise, Flow Integration Smoothing Techniques, $\mathcal{M}5$ and $\mathcal{M}6$ Models.

All pressure measurements taken from gas networks are subject to white noise, which is assumed to have a Gaussian distribution with mean 0 bar and standard deviation 0.1 bar [11], [38]. Due to the sensitivity of small flow demand estimates to pressure measurement perturbations, this is a major problem and we now look at filtering/smoothing techniques. We avoid Kalman filters due to their unexceptional performance in [17], [40], [35], and instead examine two simple smoothing techniques that are computationally cheap, but very effective. These two smoothing techniques make use of the known flow demand profiles; the first technique is based on difference equations of the form (6.22), and the second technique is based on difference equations of the form (9.4). We also derive two final model variations, $\mathcal{M}5$ and $\mathcal{M}6$, to deal with the problem of the sensitivity of small flow demand estimates. $\mathcal{M}5$ and $\mathcal{M}6$ models have only a single total flow demand perturbation state variable that is the sum of all the individual demand flow perturbation variables. Such models are less sensitive to pressure measurement noise. $\mathcal{M}5$ models are based on difference equations of the form (6.22), and give quite acceptable flow demand estimates when measurement noise is present. However, $\mathcal{M}5$ models cannot cope with measurement bias. Hence, $\mathcal{M}6$ models are developed, which are based on difference equations of the form (9.4), which can also estimate biases.

N.B. Up until now, in experiments throughout this thesis, the flows at demand sites A/B, B/C and C were in the ratio 2:5:13. However, in this chapter a few indicated experiments will also be run with the flows in the ratio 20:1:79. This will be important in demonstrating the differing effects of pressure measurement noise on the estimates of flow demands of considerably different magnitude.

10.1 The Effects of White Noise on the State Estimation Techniques Presented So Far

In this section, we examine experimentally how the presence of white noise in the pressure measurements affects the flow demand estimates of the various model and observer techniques.

10.1.1 Experiments

In the following experiments, the models and observers were tested using the same flow profiles as used previously throughout this thesis, which we call *profile a*. For *profile a*, the flow demands were initially increasing linearly, then constant, and then decreasing linearly. However, the experiments with $\mathcal{M}4$ model based observers are repeated with new profiles, which we shall call *profile b*. For *profile b*, the flow demands were initially decreasing linearly, then increasing linearly, and then decreasing linearly again. *Profile a* was a servere test for the $\mathcal{M}4$ model based observers due to the long central period for which the flow demands remained constant. *Profile b*, does not have any period for which the flow profile coefficients, $w_k^{demand\ site}$ are 1.

As the $\mathcal{M}0$ model was run, the pressures at the upstream end and the sites of flow demand were recorded at each timestep. The pressure measurements at the three flow demand sites, A/B, B/C and C, were then corrupted by white noise with a Gaussian distribution with mean 0 bar and standard deviation 0.1 bar. At each timestep, the measurement noise errors were independent of the measurement noise errors at other timesteps. For the experiments with $\mathcal{M}4$ model based observers, the pressure measurements at the three flow demand sites, A/B, B/C and C, were then corrupted by constant

biases of 1 bar, -1 bar and 1 bar respectively. These corrupted pressures were then fed into the $\mathcal{M}1$ and $\mathcal{M}2$ models, and $\mathcal{M}3$ and $\mathcal{M}4$ model based observers. The flow demands predicted by these estimation techniques were then compared with the true flows used as inputs to the $\mathcal{M}0$ model.

The $\mathcal{M}3$ and $\mathcal{M}4$ model based observers incorporated the exact values of the weightings, $\tilde{f}_k^{demand\ site}$, and profile coefficients, $w_k^{demand\ site}$, respectively.

For each experiment, the true flow demand profiles for the demands, $D_k^{A/B}$, $D_k^{B/C}$ and D_k^C are shown as thick lines in Figs. A, B and C respectively, and the state estimates for $D_k^{A/B}$, $D_k^{B/C}$ and D_k^C are shown as thin lines. The percentage errors between the state estimates of $D_k^{A/B}$, $D_k^{B/C}$ and D_k^C and their true values are shown in Figs. D, E and F respectively.

Data taken from $\mathcal{M}0$ model with identical mesh

All experiments were based on models with 10 spatial nodes per pipe, except for experiments 10.3, 10.6 and 10.8 (direct observers), which were based on models with 5 spatial nodes per pipe. For all experiments, the flow demands were in the ratio 2:5:13.

Experiment 10.1) $\mathcal{M}1$ Model with $\theta = 1$ (*flow profile a*)

Experiment 10.2) $\mathcal{M}2$ Model with $\theta = 1$ (*flow profile a*)

Experiment 10.3) ($\mathcal{M}3$ model) Observer Design A with $\theta = 0.5$ (*flow profile a*)

Experiment 10.4) ($\mathcal{M}3$ model) Observer Design B (small eigenvalues) with $\theta = 1$ (*flow profile a*)

Experiment 10.5) ($\mathcal{M}3$ model) Observer Design C (small eigenvalues) with $\theta = 1$ (*flow profile a*)

Experiment 10.6) ($\mathcal{M}4$ model) Observer Design A with $\theta = 0.5$ (*flow profile a*)

Experiment 10.7) ($\mathcal{M}4$ model) Observer Design B with $\theta = 1$ (*flow profile a*)

Experiment 10.8) ($\mathcal{M}4$ model) Observer Design A with $\theta = 0.5$ (*flow profile b*)

Experiment 10.9) ($\mathcal{M}4$ model) Observer Design B with $\theta = 1$ (*flow profile b*)

Experiment 10.1

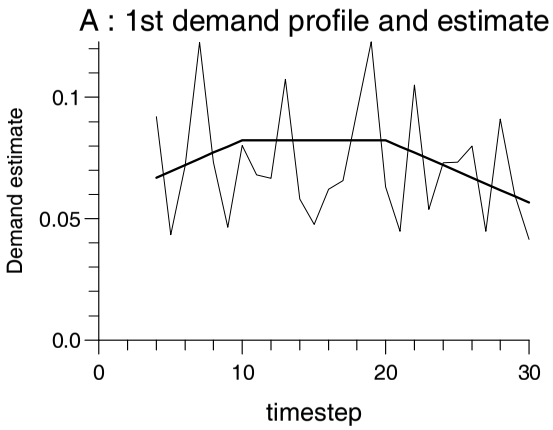

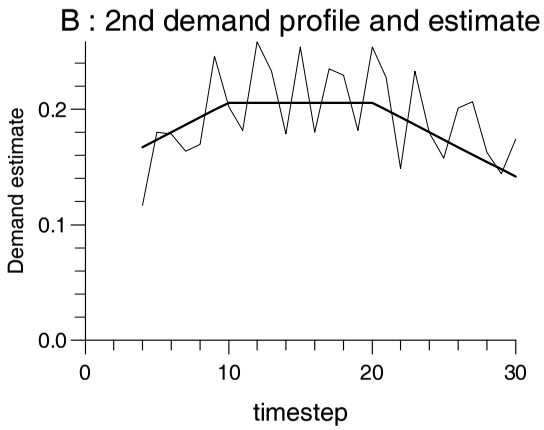

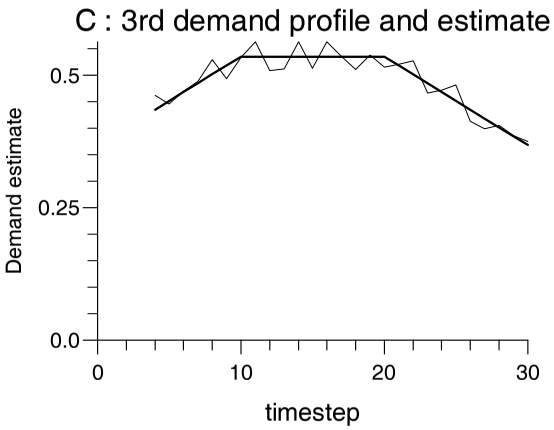

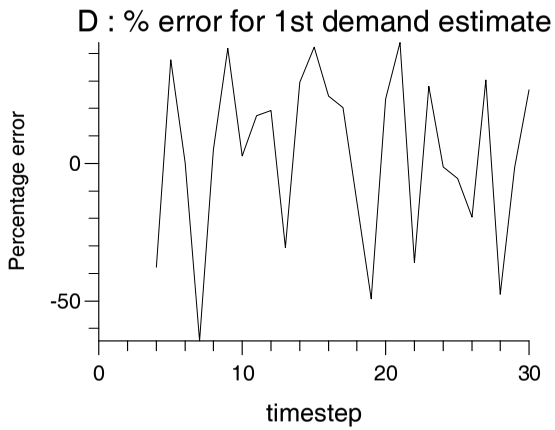

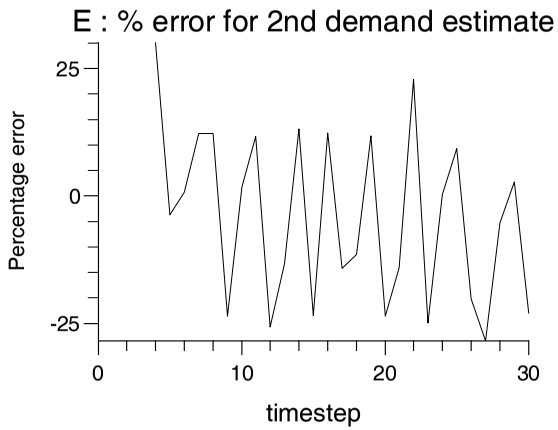

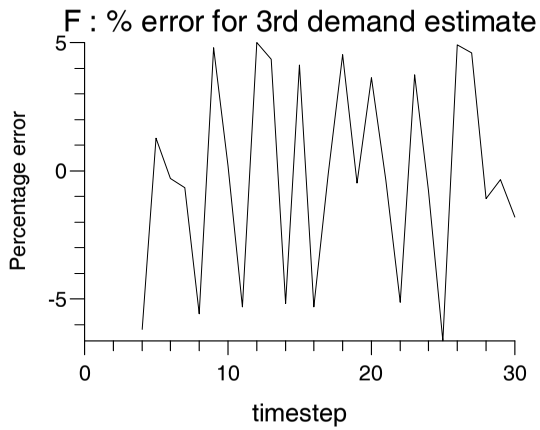

Experiment 10.2

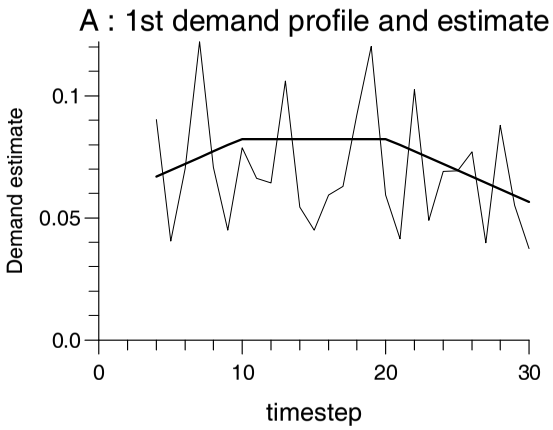

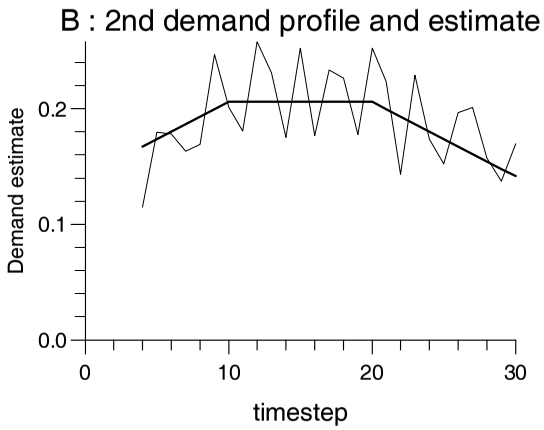

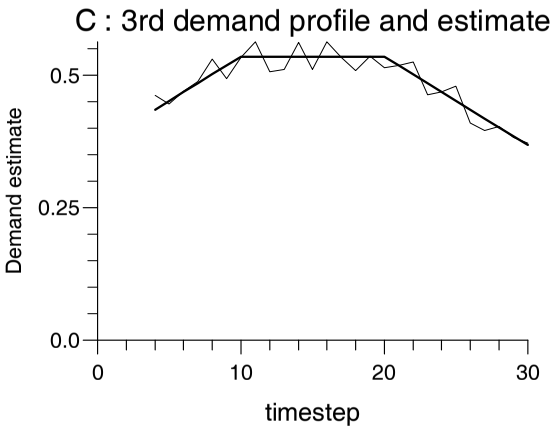

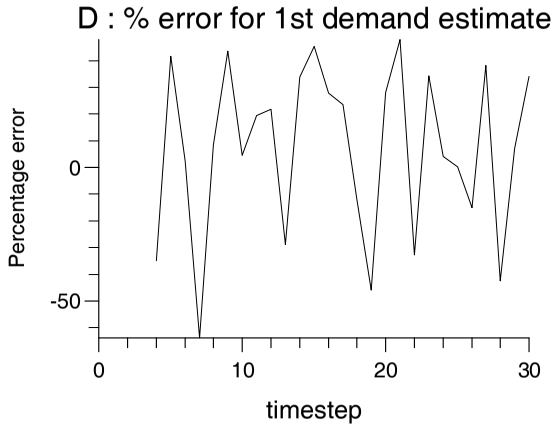

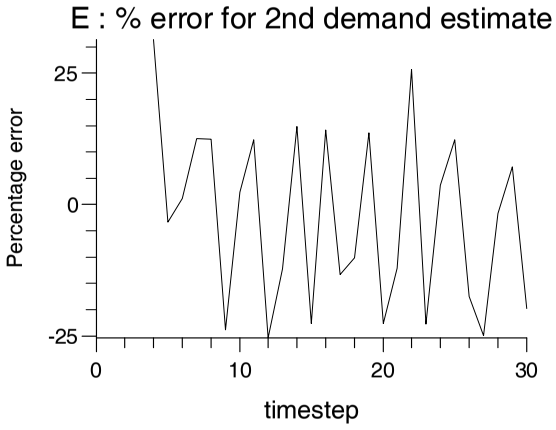

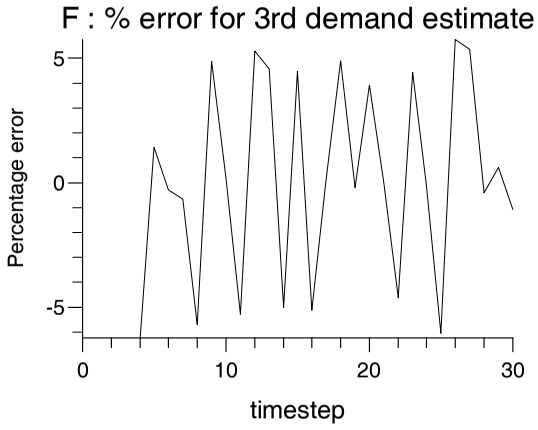

Experiment 10.3

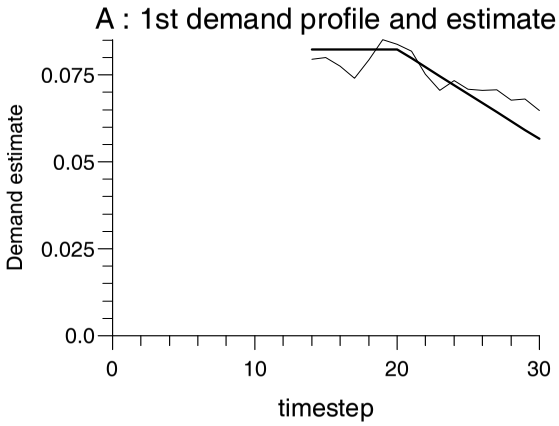

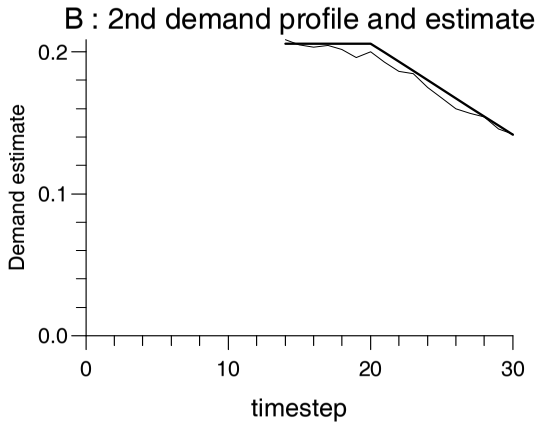

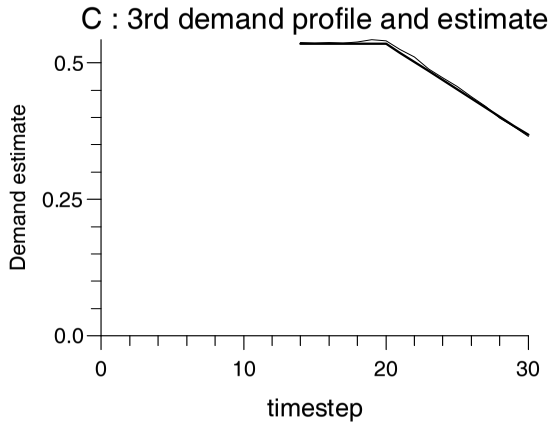

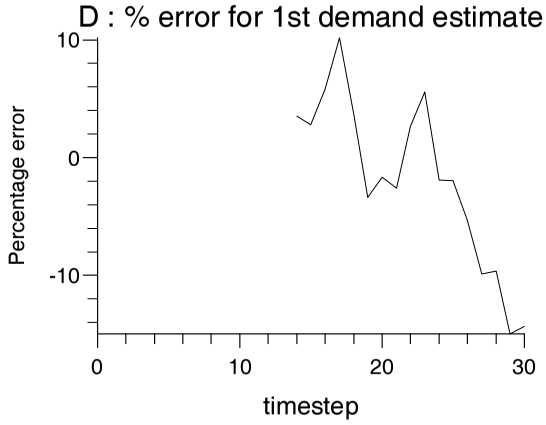

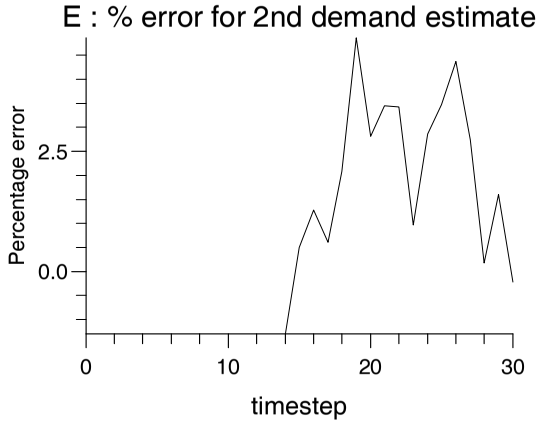

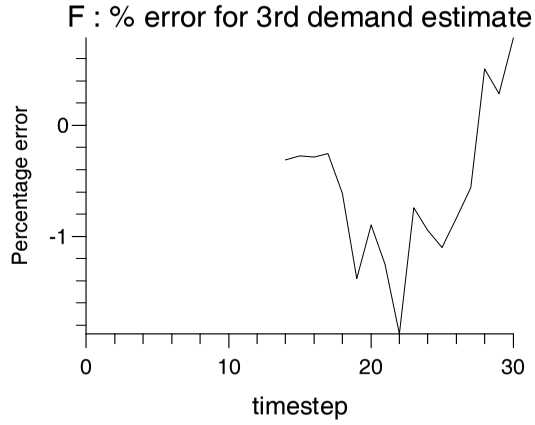

Experiment 10.4

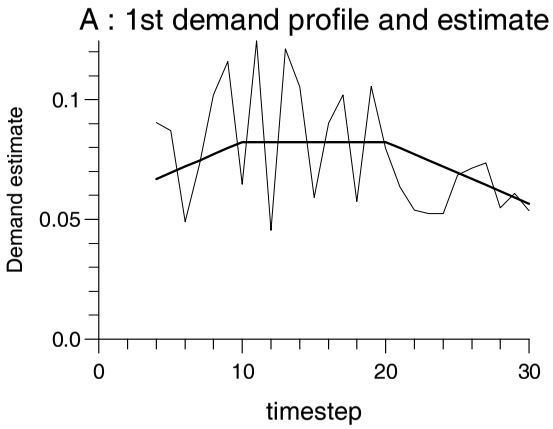

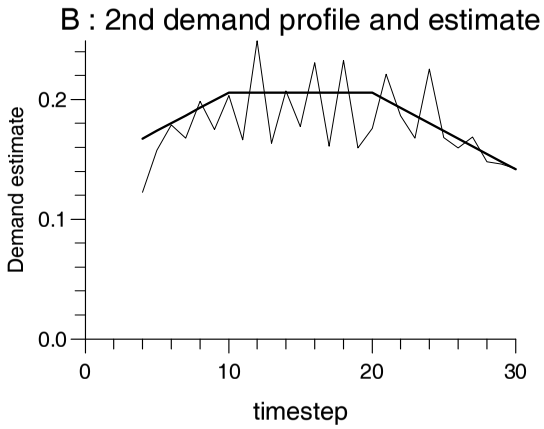

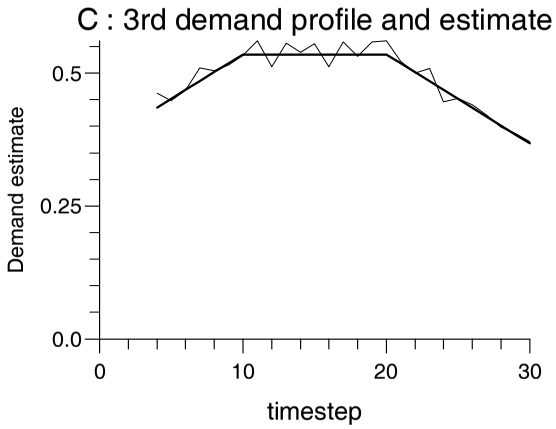

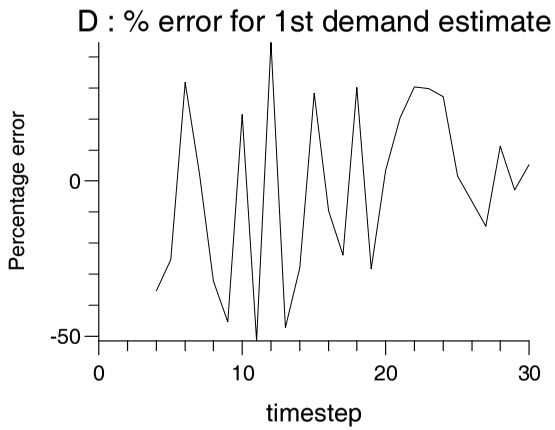

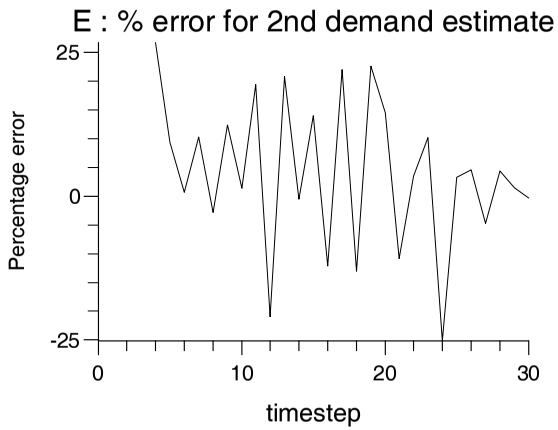

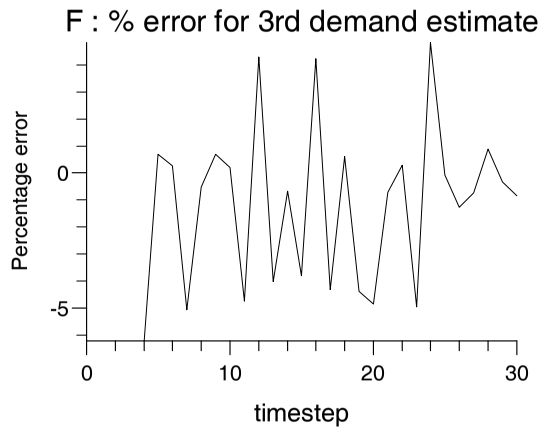

Experiment 10.5

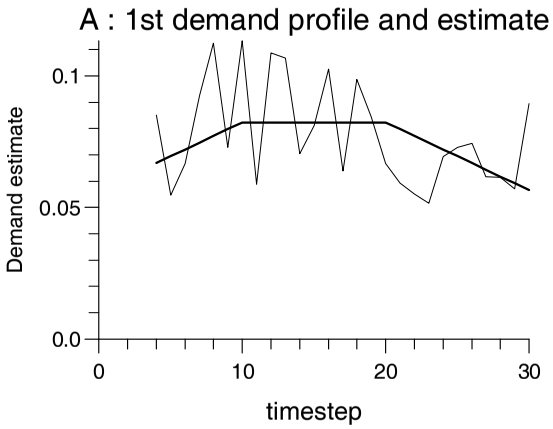

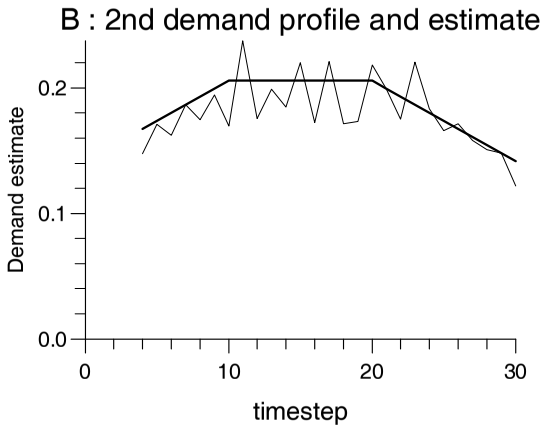

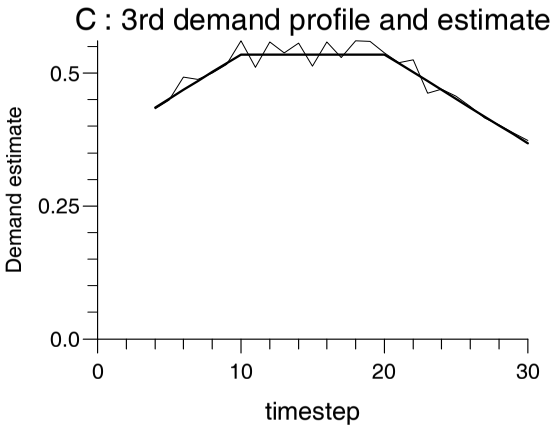

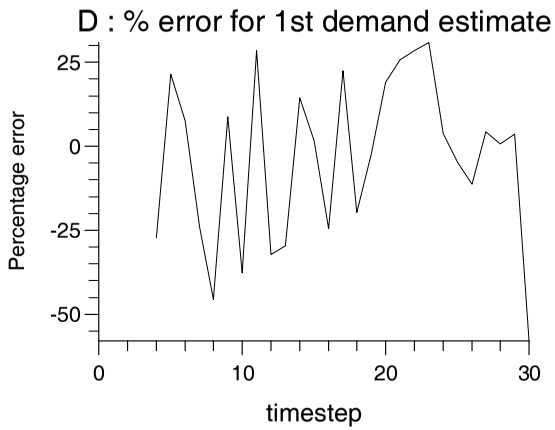

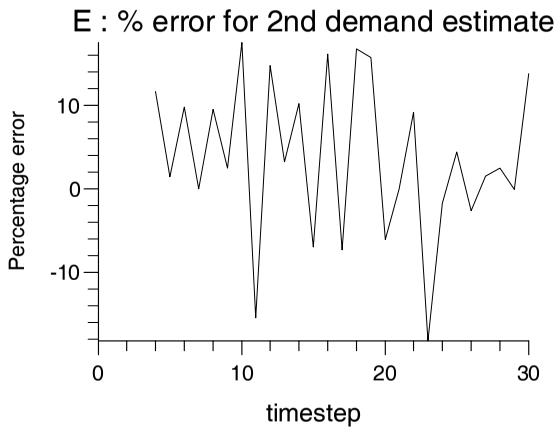

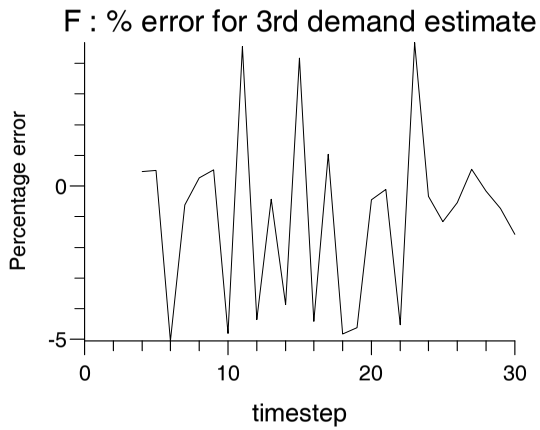

Experiment 10.6

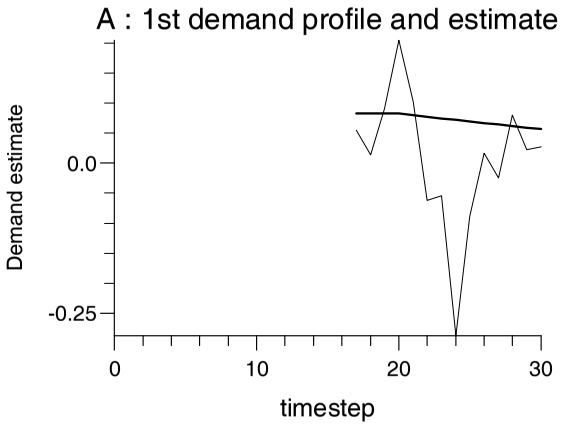

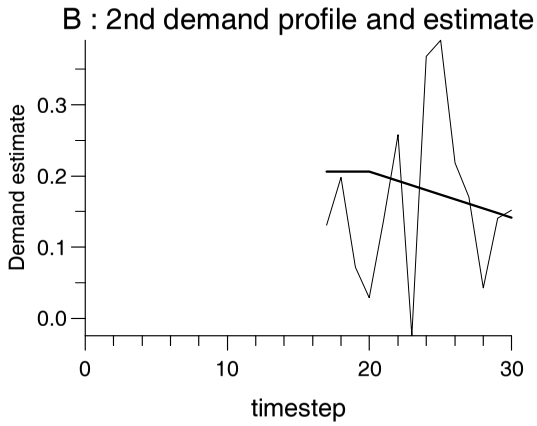

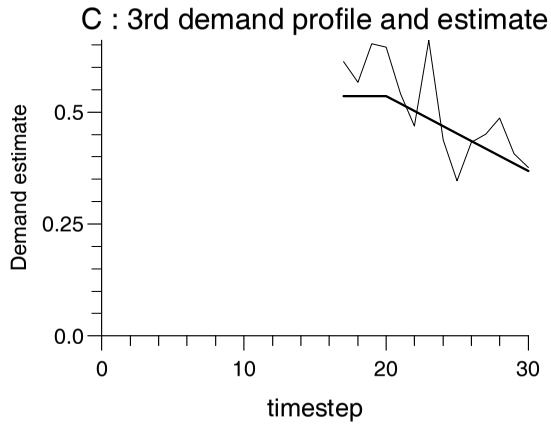

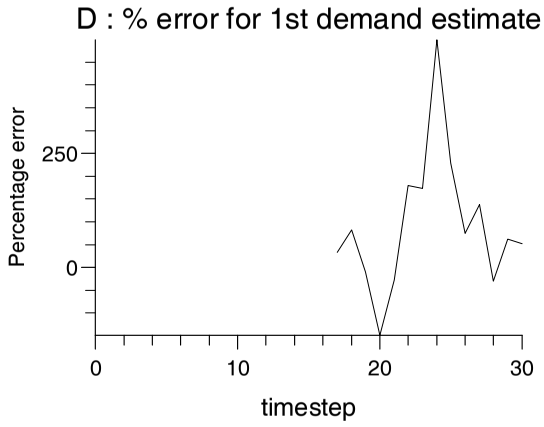

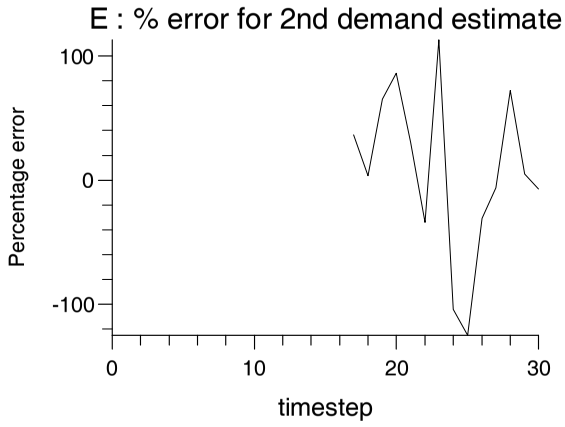

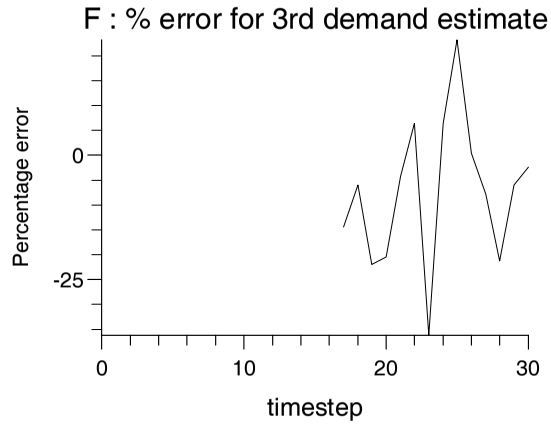

Experiment 10.7

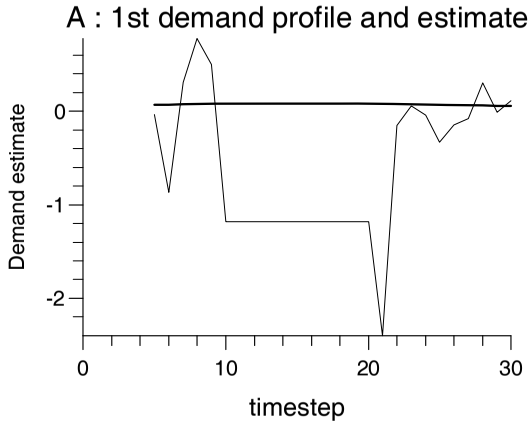

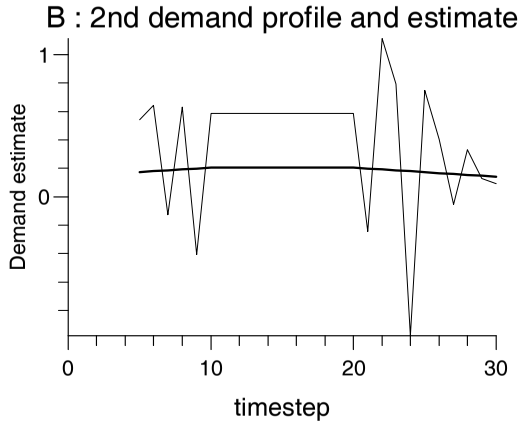

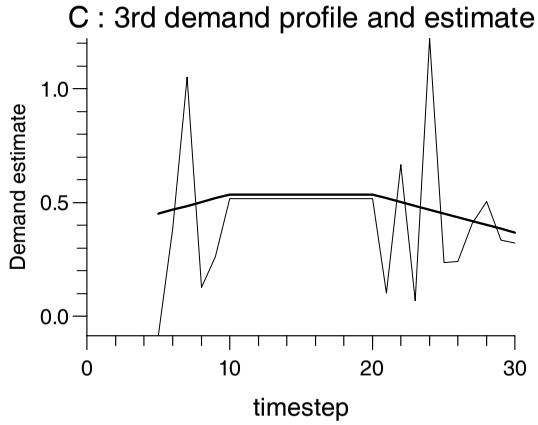

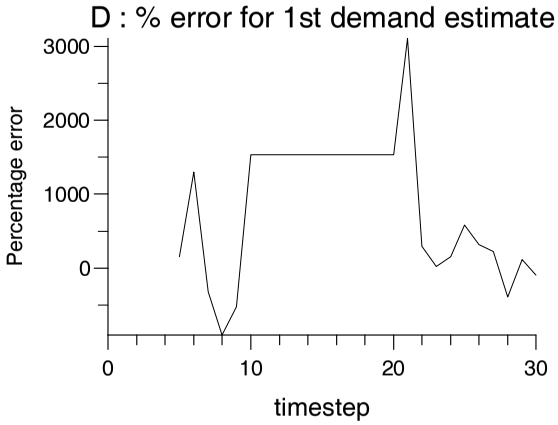

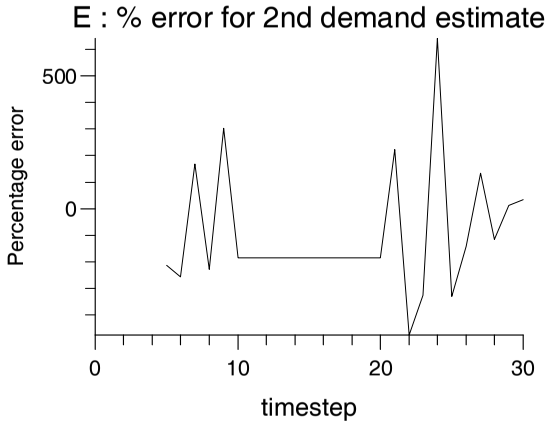

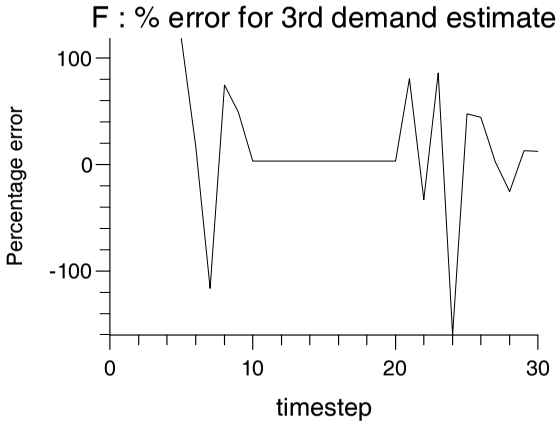

Experiment 10.8

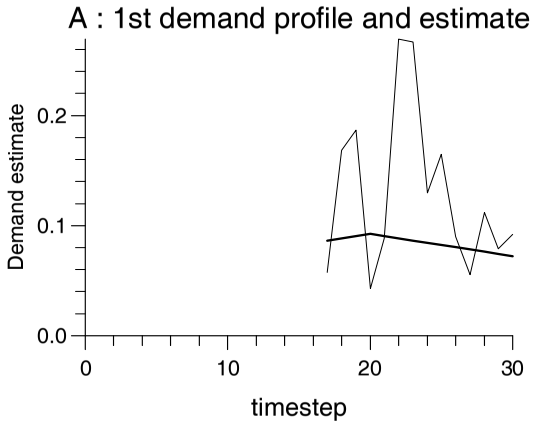

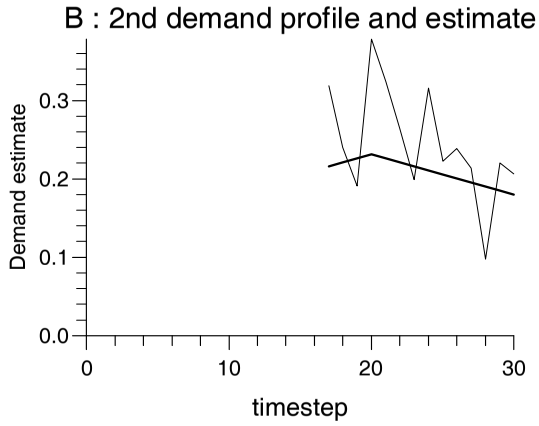

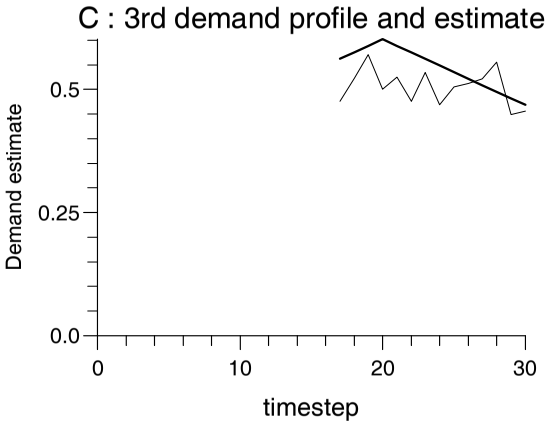

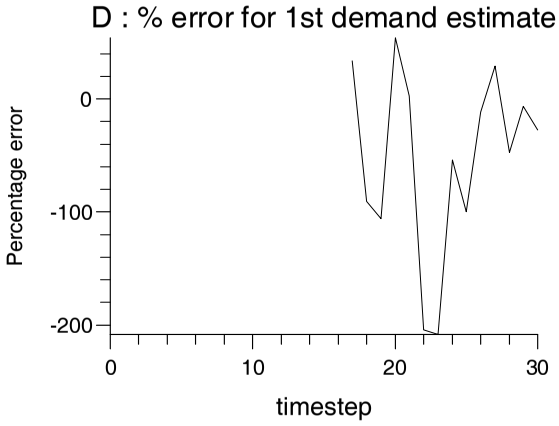

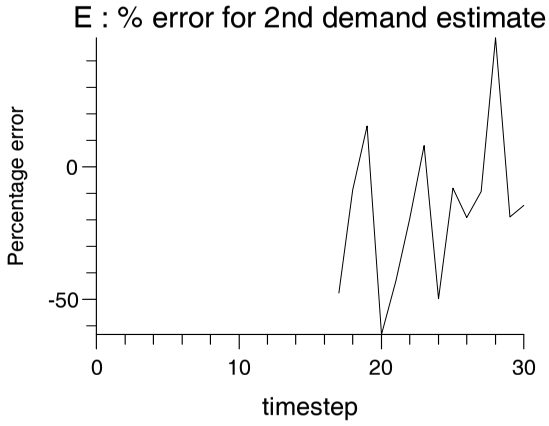

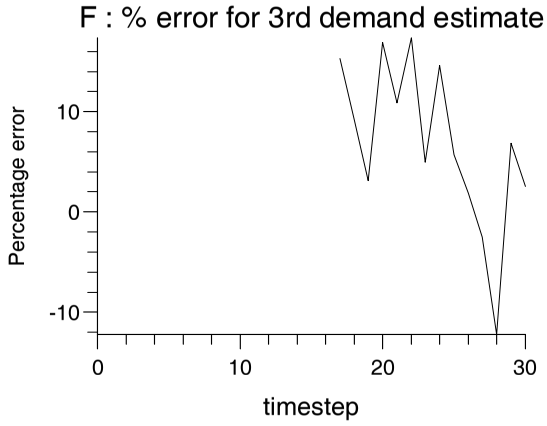

Experiment 10.9

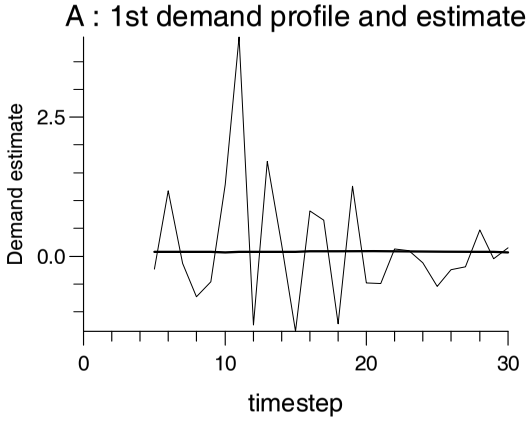

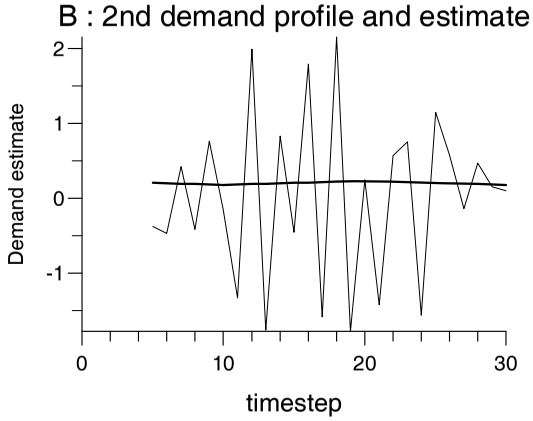

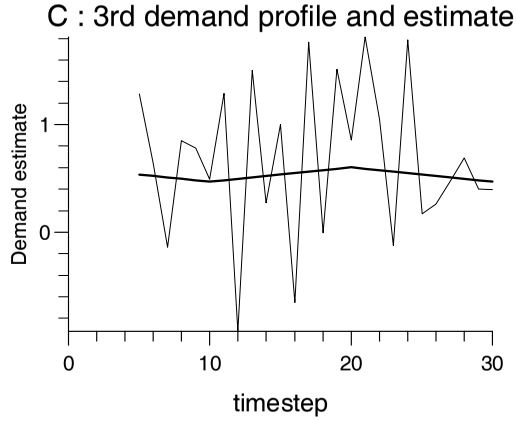

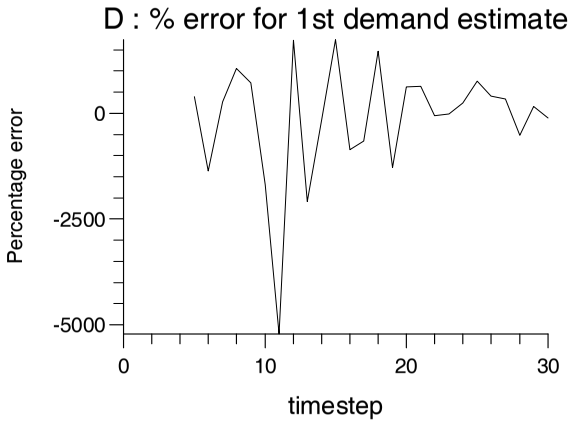

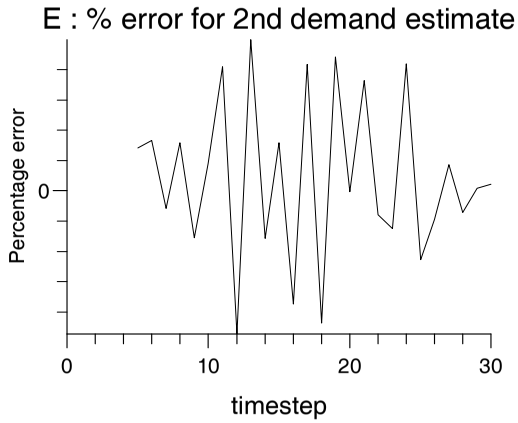

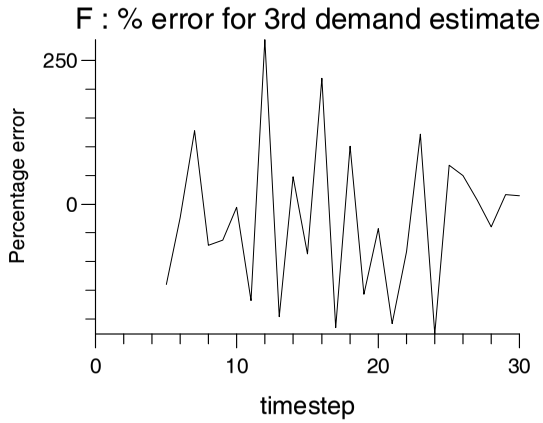

10.1.2 Discussion

For all estimation techniques, the smaller the flow demand, the more badly affected they were by the pressure measurement noise. Of the estimation techniques that did not estimate measurement bias, only direct observers based upon $\mathcal{M}3$ models gave acceptable estimates of the larger flow demands. However, these are computationally expensive, and a robust dynamic observer is really needed. Regarding bias estimating techniques, both direct and dynamic $\mathcal{M}4$ model based observers were particularly sensitive to measurement noise, and no improvement was found for any value of θ. Also, the choice of flow profile did not seem to greatly affect the dynamic $\mathcal{M}4$ model based observer, although, the direct observer seemed to give more accurate flow estimates with *profile b*.

We will now investigate two smoothing techniques that help to reduce significantly the error in the flow demand state estimates due to measurement noise. These smoothing techniques are based on the two types of trivial difference equation used in $\mathcal{M}3$ and $\mathcal{M}4$ models respectively.

10.2 The $\mathcal{M}3$ Flow Integration Smoothing Technique

It is possible to use the known profiles of the flow demands to smooth the profiles of the flow demand estimates corrupted by pressure measurement noise. For the $\mathcal{M}3$ flow integration smoothing technique, we use trivial difference equations for the flow demand perturbations of the form (6.22). An $\mathcal{M}3$ model based observer is run continuously. Over any time interval, $k = r, ..., s$, (say one hour), for each demand the estimated flow perturbation at each time step is integrated, that is, for each flow demand we find $\sum_{k=r}^{s} \widehat{d}_k^{demand\ site}$, where $\widehat{d}_k^{demand\ site}$ is our noise contaminated estimate of $d_k^{demand\ site}$.

Since

$$\widehat{d}_k^{demand\ site} = d_k^{demand\ site} + e_k$$

where e_k is some varying error due to noisy inputs to the observer, we have that

$$\sum_{k=r}^{s} \widehat{d}_k^{demand\ site} = \sum_{k=r}^{s} d_k^{demand\ site} + \sum_{k=r}^{s} e_k.$$

Since the assigned observer eigenvalues are asymptotically stable, we would expect that in the sum $\sum_{k=r}^{s} e_k$, the individual e_k cancel out to some extent, and that

$$\frac{\sum_{k=r}^{s} \widehat{d}_k^{demand\ site}}{\sum_{k=r}^{s} d_k^{demand\ site}} \longrightarrow 1 \quad as\ s-r \longrightarrow \infty. \tag{10.1}$$

Some attempt was made to provide a statistical proof of equation (10.1), but this was not achieved. Future theoretical investigation of the validity of equation (10.1), would be worthwhile, and a useful reference for this would be [12] p.30. Assuming equation (10.1) holds, if the time period $k = r, ..., s$ is large enough, $\sum_{k=r}^{s} \widehat{d}_k^{demand\ site}$ is a good estimate of $\sum_{k=r}^{s} d_k^{demand\ site}$.

If, after a large time period, $k = r, ..., s$, we assume we have a good estimate of $\sum_{k=r}^{s} d_k^{demand\ site}$, then we can find $d_r^{demand\ site}$ from the following.

From the definition of the flow demand profile jumps, $\tilde{f}_k^{demand\ site}$, it can be seen that for any timestep k

$$d_k^{demand\ site} = d_r^{demand\ site} + \sum_{j=r}^{k-1} \tilde{f}_j^{demand\ site} \qquad if\ k > r$$

from which we can derive

$$\sum_{k=r}^{s} d_k^{demand\ site} = (s-r+1) d_r^{demand\ site} + \sum_{k=r+1}^{s} (\sum_{j=r}^{k-1} \tilde{f}_j^{demand\ site}),$$

i.e.

$$d_r^{demand\ site} = \frac{(\sum_{k=r}^{s} d_k^{demand\ site}) - \sum_{k=r+1}^{s} (\sum_{j=r}^{k-1} \tilde{f}_j^{demand\ site})}{(s-r+1)}.$$

Once $\sum_{k=r}^{s} \widehat{d}_k^{demand\ site}$ is calculated, it may be used as an estimate for $\sum_{k=r}^{s} d_k^{demand\ site}$. $d_r^{demand\ site}$ may then be estimated from the above equation. From $d_r^{demand\ site}$, we can compute $d_k^{demand\ site}$ for all k from the difference equations (6.22).

10.2.1 Experiments

The $\mathcal{M}3$ flow integration smoothing technique was not found to work well with direct observers. Hence, only experiments with dynamic observers are presented here.

Experiments 10.4 and 10.5 were repeated as experiments 10.10 and 10.11, respectively, this time applying the $\mathcal{M}3$ flow integration smoothing technique to timesteps 10 to 30. Hence, only results for these timesteps are presented.

Experiment 10.10

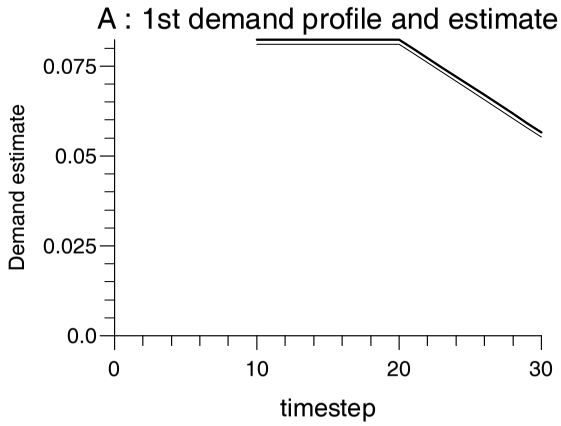

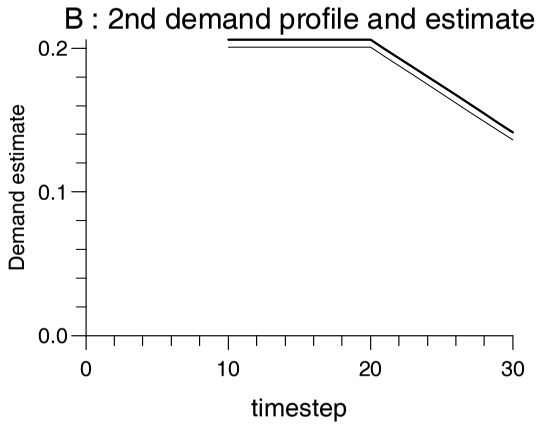

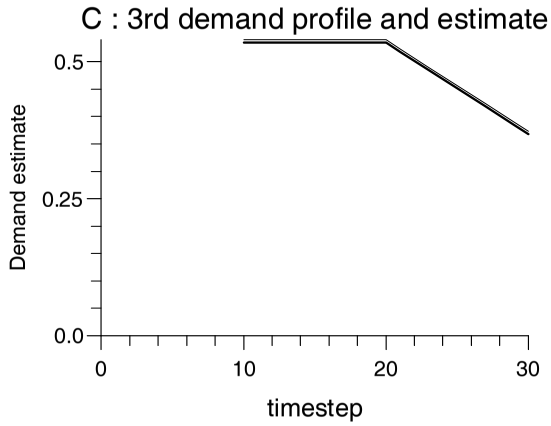

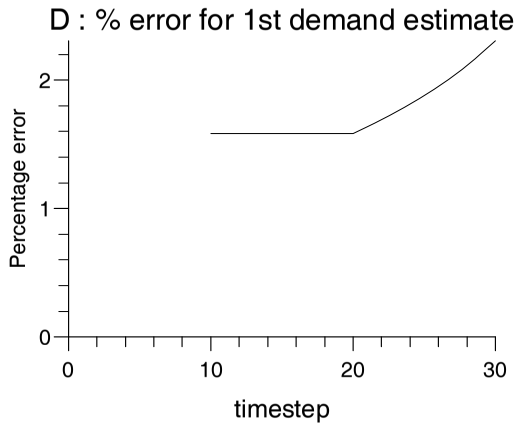

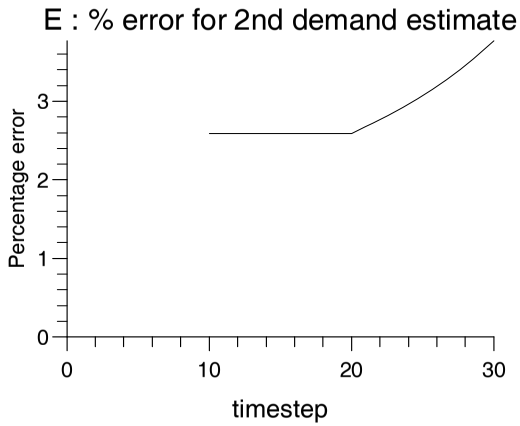

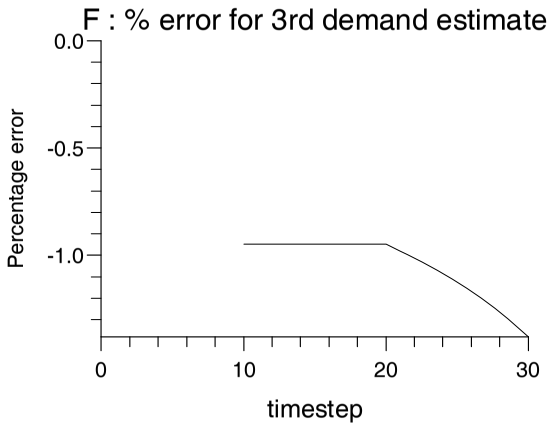

Experiment 10.11

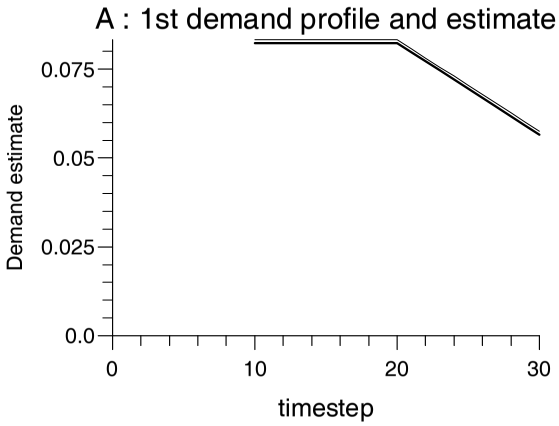

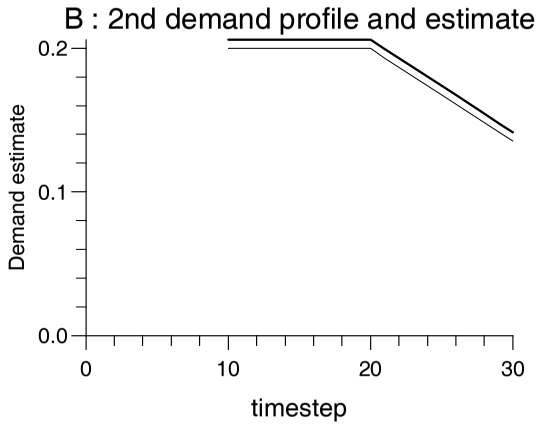

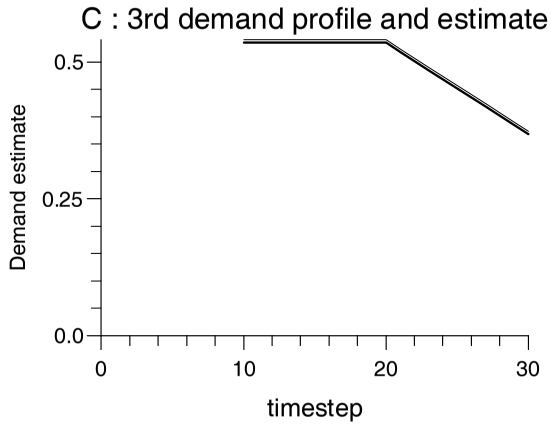

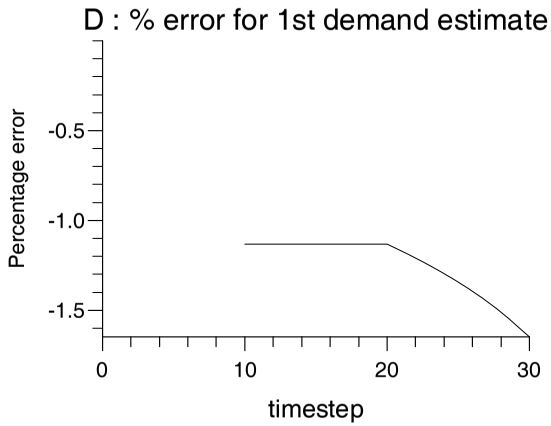

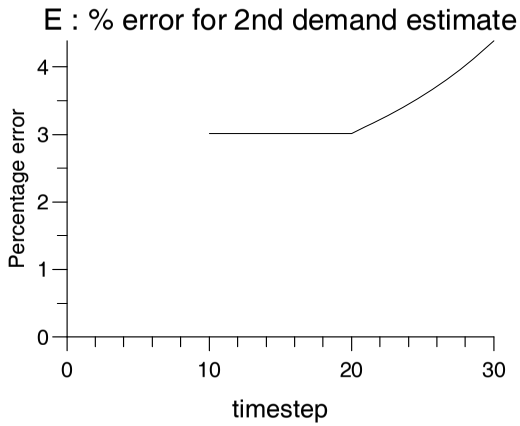

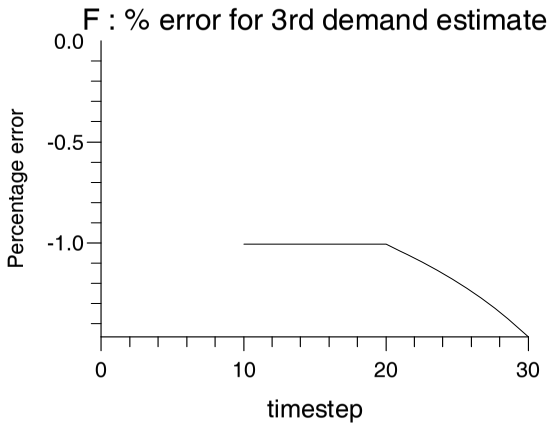

10.2.2 Discussion

It can be readily seen that the $\mathcal{M}3$ flow integration smoothing technique significantly reduces the error, due to pressure measurement noise, in the flow demand estimates of $\mathcal{M}3$ model based dynamic observers. Also, the smoothing technique maintains the true 'shapes' of the profiles, but with the measurement noise causing such estimated profiles to be shifted up or down the flow demand axis.

Although it was not investigated experimentally, the $\mathcal{M}3$ flow integration smoothing technique could be implemented as a filtering technique for each current time-level. At each new timestep, s, the smoothing process would be carried out over some timesteps, $k = r, ..., s$, to give a filtered estimate for the current time-level s. This would be a more useful approach, and the effectiveness of such an $\mathcal{M}3$ flow integration filtering technique would be worth exploring.

10.3 The $\mathcal{M}4$ Flow Integration Smoothing Technique

For the $\mathcal{M}4$ flow integration smoothing technique, we use trivial difference equations for the flow demand perturbations of the form (9.3). An $\mathcal{M}4$ model based observer is run continuously. Over some time interval, $k = r, ..., s$, (say one hour), for each demand the estimated flow perturbation at each time step is integrated, that is, for each flow demand, we find $\sum_{k=r}^{s} \widehat{d}_k^{demand\ site}$, where $\widehat{d}_k^{demand\ site}$ is our noise contaminated estimate of $d_k^{demand\ site}$. As explained previously, we expect that if the time period $k = r, ..., s$ is large enough, then $\sum_{k=r}^{s} \widehat{d}_k^{demand\ site}$ will be a good estimate of $\sum_{k=r}^{s} d_k^{demand\ site}$.

Firstly, it is obvious that

$$\begin{aligned} Total\ normalised\ integrated\ flow &= \sum_{k=r}^{s} (d_k^{demand\ site} + \mathcal{Q}^{demand\ site}) \\ &= (s - r + 1)\mathcal{Q}^{demand\ site} + \sum_{k=r}^{s} d_k^{demand\ site}. \end{aligned} \tag{10.2}$$

Secondly, from equation (9.3) it can be seen that

$$Total\ normalised\ integrated\ flow = (d_r^{demand\ site} + \mathcal{Q}^{demand\ site})$$

$$\times(1 + w_r^{demand\ site} + w_r^{demand\ site} w_{r+1}^{demand\ site} + ... + \prod_{k'=r}^{s-1} w_{k'}^{demand\ site})$$

$$= (d_r^{demand\ site} + \mathcal{Q}^{demand\ site})(1 + \sum_{k=r}^{s-1}(\prod_{k'=r}^{k} w_{k'}^{demand\ site}))$$

$$= d_r^{demand\ site}(1+\sum_{k=r}^{s-1}(\prod_{k'=r}^{k} w_{k'}^{demand\ site})) + \mathcal{Q}^{demand\ site}(1+\sum_{k=r}^{s-1}(\prod_{k'=r}^{k} w_{k'}^{demand\ site})). \tag{10.3}$$

Combining equations (10.2) and (10.3) gives

$$d_r^{demand\ site} = \frac{(s-r+1)\mathcal{Q}^{demand\ site} + \sum_{k=r}^{s} d_k^{demand\ site}}{(1 + \sum_{k=r}^{s-1}(\prod_{k'=r}^{k} w_{k'}^{demand\ site}))} - \mathcal{Q}^{demand\ site}.$$

Once $\sum_{k=r}^{s} \widehat{d}_k^{demand\ site}$ is calculated, it may be used as an estimate for $\sum_{k=r}^{s} d_k^{demand\ site}$. $d_r^{demand\ site}$ may then be estimated from the above equation. From $d_r^{demand\ site}$, we can compute $d_k^{demand\ site}$ for all k from the difference equations (9.4).

10.3.1 Experiments

The $\mathcal{M}4$ flow integration smoothing technique was not found to work well with direct observers. Hence, only an experiment with a design B observer is presented here (the smoothing technique worked equally well with a design C observer).

Experiment 10.9 was repeated as experiment 10.12, this time applying the $\mathcal{M}4$ flow integration smoothing technique to timesteps 10 to 30. Hence, only results for these timesteps are presented.

Experiment 10.12

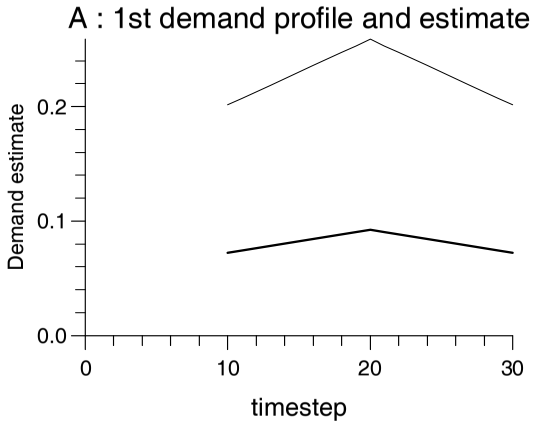

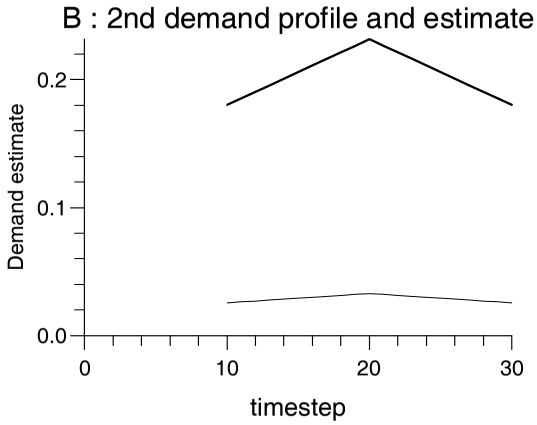

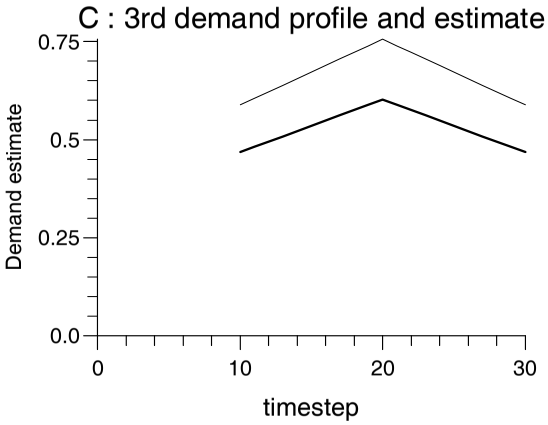

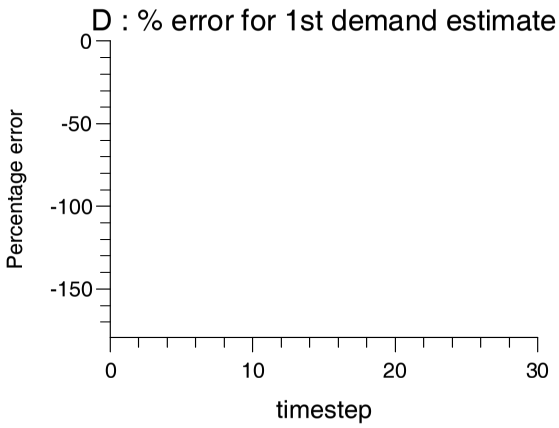

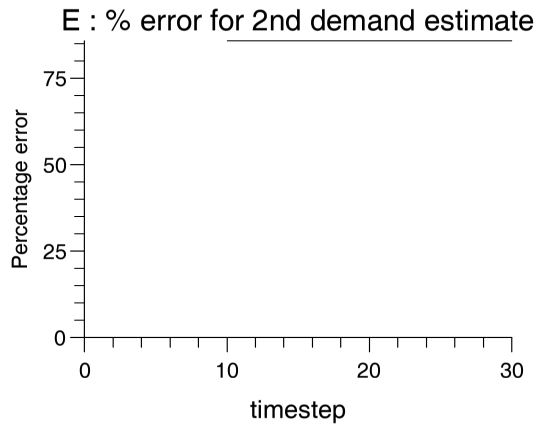

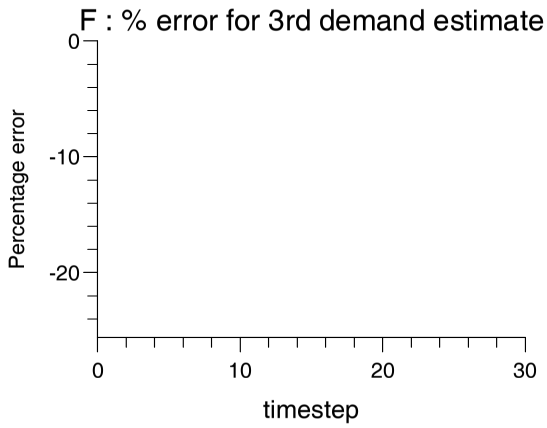

10.3.2 Discussion

For Figs. D and F, the graphs coincide with the axes.

It can be readily seen that the $\mathcal{M}4$ flow integration smoothing technique significantly reduces the error, due to pressure measurement noise, in the flow demand estimates of $\mathcal{M}4$ model based dynamic observers. However, the error is still very large indeed.

In a similar way to the $\mathcal{M}3$ flow integration smoothing technique, the $\mathcal{M}4$ flow integration smoothing technique may be implemented as a filter for each current time-level. Although an $\mathcal{M}4$ flow integration filtering technique was not investigated experimentally, the performance of such a technique would be worth exploring.

The $\mathcal{M}3$ and $\mathcal{M}4$ models still contain the underlying sensitivity of the small flow demands to pressure measurement perturbations. For this reason we next examine two new model variations, $\mathcal{M}5$ and $\mathcal{M}6$ models, for which the estimates of small flow demands from observers constructed upon such models are significantly less sensitive.

10.4 The $\mathcal{M}5$ Model

Due to the sensitivity of the previous models to pressure measurement noise, we now investigate a new model variation, denoted by $\mathcal{M}5$, which has only a single total flow demand perturbation state variable that is the sum of all the individual demand flow perturbation variables. We consider the g scalar equations of the form (6.22). If we add these g equations together we can derive

$$d_{k+1}^{tot} = d_k^{tot} + \tilde{f}_k^{tot} \quad for\ all\ k \tag{10.4}$$

where $d_k^{tot} = \sum_{demand\ site=1}^{g} d_k^{demand\ site}$ and $\tilde{f}_k^{tot} = \sum_{demand\ site=1}^{g} \tilde{f}_k^{demand\ site}$. The $\mathcal{M}5$ models now contain the single state flow variable, d_k^{tot} with a difference equation of the form (10.4), where the sum of weightings, $\tilde{f}_k^{tot}$, is contained in a vector on the right hand side of the system as shown later.

To recover the values of the separate flow demand perturbation variables, $d_k^{demand\ site}$, from d_k^{tot}, the model uses information about the relative magnitudes of the flow demands;

that is, we assume that at each timestep, for each flow demand the ratio, $\alpha_k^{demand\ site}$, is known, where

$$flow\ demand\ _k^{demand\ site} \ = \ \alpha_k^{demand\ site} \times total\ flow\ demand\ _k$$

and $0 \leq \alpha_k^{demand\ site} \leq 1$.

After normalisation, we would have

$$normalised\ flow\ demand\ _k^{demand\ site} \ = \ \alpha_k^{demand\ site} \times normalised\ total\ flow\ demand\ _k,$$

that is, we would have for any particular demand site h (where h may be a junction demand site, $z/z+1$, of general pipes z and $z+1$, or the downstream demand site, g)

$$\mathcal{Q}^h + d_k^h \ = \ \alpha_k^h \times \sum_{demand\ site=1}^{g} (\mathcal{Q}^{demand\ site} + d_k^{demand\ site})$$

and hence

$$d_k^h = \alpha_k^h d_k^{tot} + \alpha_k^h \mathcal{Q}^{tot} - \mathcal{Q}^h \tag{10.5}$$

where $\mathcal{Q}^{tot} = \sum_{demand\ site=1}^{g} \mathcal{Q}^{demand\ site}$.

To form an $\mathcal{M}5$ model, we start from a base $\mathcal{M}0$ model. All the basic difference equations of the form (2.17) remain unchanged in an $\mathcal{M}5$ model. However, the $g-1$ connectivity equations and the single downstream flow boundary equation are altered by the following. The g flow demand perturbation variables are removed from the input vector, summed into a single total flow demand perturbation variable, and then incorporated into the new $\mathcal{M}5$ state vector, that is, the n dimensional $\mathcal{M}0$ state vector $\underline{x}_0(k)$ is augmented to the $n+1$ dimensional $\mathcal{M}5$ state vector

$$\underline{x}_5(k) = \begin{bmatrix} \underline{x}_0(k) \\ d_k^{tot} \end{bmatrix}.$$

The new trivial difference equation (10.4) is then added to form the $\mathcal{M}5$ system. Assuming the base $\mathcal{M}0$ model is arranged and partitioned as in equation (4.1), the new $n+1$ dimensional $\mathcal{M}5$ system has the form

$$\begin{bmatrix} E_0 & \underline{e}(k+1) \\ 0 & 1 \end{bmatrix} \begin{bmatrix} \underline{x}_0(k+1) \\ d_{k+1}^{tot} \end{bmatrix} = \begin{bmatrix} A_0 & \underline{a}(k) \\ 0 & 1 \end{bmatrix} \begin{bmatrix} \underline{x}_0(k) \\ d_k^{tot} \end{bmatrix} + \begin{bmatrix} B^{1'} \\ 0 \end{bmatrix} \underline{p}_3(k+1) + \begin{bmatrix} B^{2'} \\ 0 \end{bmatrix} \underline{p}_3(k)$$

$$+\begin{bmatrix} \underline{v}(k+1) \\ 0 \end{bmatrix} + \begin{bmatrix} \underline{v}(k) \\ \tilde{f}_k^{tot} \end{bmatrix} \tag{10.6}$$

where the vectors $\underline{e}(k+1)$ and $\underline{a}(k)$ contain only the time-varying coefficients linking the total flow variable, d_k^{tot}, with the new forms of the $g-1$ connectivity equations and the single downstream flow boundary equation. Likewise, the vectors $\underline{v}(k+1)$ and $\underline{v}(k)$ contain only elements associated with the g flow equations. These elements of $\underline{e}(k+1)$, $\underline{a}(k)$, $\underline{v}(k+1)$ and $\underline{v}(k)$ are now determined by considering the new forms of the flow equations in $\mathcal{M}5$ models.

The original general 'connectivity equation' between two pipe sections z and $z+1$ is given by (2.23). For an $\mathcal{M}5$ model, equation (10.5) is substituted into equation (2.23) to give

$$\begin{aligned}
&-(\Phi^{z/z+1}\epsilon_3^z\Gamma^z_{s^z-1}\theta/\delta x^z)p^z_{s^z-1,k+1} + (1+\Phi^{z/z+1}\epsilon_3^z\Gamma^{z/z+1}\theta/\delta x^z + \Phi^{z/z+1}\epsilon_3^{z+1}\Gamma^{z/z+1}\theta/\delta x^{z+1})p^{z/z+1}_{k+1} \\
&-(\Phi^{z/z+1}\epsilon_3^{z+1}\Gamma_1^{z+1}\theta/\delta x^{z+1})p^{z+1}_{1,k+1} + \Phi^{z/z+1}\theta(\alpha^{z/z+1}_{k+1}d^{tot}_{k+1} + \alpha^{z/z+1}_{k+1}\mathcal{Q}^{tot} - \mathcal{Q}^{z/z+1}) = \\
&(\Phi^{z/z+1}\epsilon_3^z\Gamma^z_{s^z-1}(1-\theta)/\delta x^z)p^z_{s^z-1,k} + (1-\Phi^{z/z+1}\epsilon_3^z\Gamma^{z/z+1}(1-\theta)/\delta x^z - \Phi^{z/z+1}\epsilon_3^{z+1}\Gamma^{z/z+1}(1-\theta)/\delta x^{z+1})p^{z/z+1}_k \\
&+(\Phi^{z/z+1}\epsilon_3^{z+1}\Gamma_1^{z+1}(1-\theta)/\delta x^{z+1})p^{z+1}_{1,k} - \Phi^{z/z+1}(1-\theta)(\alpha^{z/z+1}_k d^{tot}_k + \alpha^{z/z+1}_k\mathcal{Q}^{tot} - \mathcal{Q}^{z/z+1})
\end{aligned} \tag{10.7}$$

which can be rearranged to

$$\begin{aligned}
&-(\Phi^{z/z+1}\epsilon_3^z\Gamma^z_{s^z-1}\theta/\delta x^z)p^z_{s^z-1,k+1} + (1+\Phi^{z/z+1}\epsilon_3^z\Gamma^{z/z+1}\theta/\delta x^z + \Phi^{z/z+1}\epsilon_3^{z+1}\Gamma^{z/z+1}\theta/\delta x^{z+1})p^{z/z+1}_{k+1} \\
&-(\Phi^{z/z+1}\epsilon_3^{z+1}\Gamma_1^{z+1}\theta/\delta x^{z+1})p^{z+1}_{1,k+1} + \Phi^{z/z+1}\theta\alpha^{z/z+1}_{k+1}d^{tot}_{k+1} = \\
&(\Phi^{z/z+1}\epsilon_3^z\Gamma^z_{s^z-1}(1-\theta)/\delta x^z)p^z_{s^z-1,k} + (1-\Phi^{z/z+1}\epsilon_3^z\Gamma^{z/z+1}(1-\theta)/\delta x^z - \Phi^{z/z+1}\epsilon_3^{z+1}\Gamma^{z/z+1}(1-\theta)/\delta x^{z+1})p^{z/z+1}_k \\
&+(\Phi^{z/z+1}\epsilon_3^{z+1}\Gamma_1^{z+1}(1-\theta)/\delta x^{z+1})p^{z+1}_{1,k} - \Phi^{z/z+1}(1-\theta)\alpha^{z/z+1}_k d^{tot}_k \\
&-\Phi^{z/z+1}\theta(\alpha^{z/z+1}_{k+1}\mathcal{Q}^{tot} - \mathcal{Q}^{z/z+1}) - \Phi^{z/z+1}(1-\theta)(\alpha^{z/z+1}_k\mathcal{Q}^{tot} - \mathcal{Q}^{z/z+1}).
\end{aligned} \tag{10.8}$$

Equation (10.8) represents the new form of the connectivity equation for pipe sections z and $z+1$ used in $\mathcal{M}5$ models. The last two terms of equation (10.8), $-\Phi^{z/z+1}\theta(\alpha^{z/z+1}_{k+1}\mathcal{Q}^{tot} - \mathcal{Q}^{z/z+1})$ and $-\Phi^{z/z+1}(1-\theta)(\alpha^{z/z+1}_k\mathcal{Q}^{tot} - \mathcal{Q}^{z/z+1})$, are contained in the the vectors $\underline{v}(k+1)$ and $\underline{v}(k)$ respectively. The coefficients $\Phi^{z/z+1}\theta\alpha^{z/z+1}_{k+1}$, $-\Phi^{z/z+1}(1-\theta)\alpha^{z/z+1}_k$ of the total flow perturbation variable, $d^{tot}_{timestep}$, are contained in the vectors $\underline{e}(k+1)$ and $\underline{a}(k)$ respectively.

A similar procedure is carried out to obtain the new form of the downstream flow boundary equation. The original downstream flow boundary equation is given by equation (2.19). For an $\mathcal{M}5$ model, equation (10.5) is substituted into equation (2.19) to give

$$-2\theta\Omega^g_{s^g}r^g\Gamma^g_{s^g-1}p_{s^g-1,k+1} + (1+2\theta\Omega^g_{s^g}r^g\Gamma^g_{s^g})p_{s^g,k+1}$$

$$+(2\theta\Omega^g_{s^g}r^g\delta x^g/\epsilon^g_3)(\alpha^{downstream}_{k+1}d^{tot}_{k+1} + \alpha^{downstream}_{k+1}\mathcal{Q}^{tot} - \mathcal{Q}^{downstream}) =$$

$$2(1-\theta)\Omega^g_{s^g}r^g\Gamma^g_{s^g-1}p_{s^g-1,k} + (1-2(1-\theta)\Omega^g_{s^g}r^g\Gamma^g_{s^g})p_{s^g,k}$$

$$-(2(1-\theta)\Omega^g_{s^g}r^g\delta x^g/\epsilon^g_3)(\alpha^{downstream}_{k}d^{tot}_{k} + \alpha^{downstream}_{k}\mathcal{Q}^{tot} - \mathcal{Q}^{downstream}) \qquad (10.9)$$

which can be rearranged to

$$-2\theta\Omega^g_{s^g}r^g\Gamma^g_{s^g-1}p_{s^g-1,k+1} + (1+2\theta\Omega^g_{s^g}r^g\Gamma^g_{s^g})p_{s^g,k+1} + (2\theta\Omega^g_{s^g}r^g\delta x^g/\epsilon^g_3)\alpha^{downstream}_{k+1}d^{tot}_{k+1} =$$

$$2(1-\theta)\Omega^g_{s^g}r^g\Gamma^g_{s^g-1}p_{s^g-1,k} + (1-2(1-\theta)\Omega^g_{s^g}r^g\Gamma^g_{s^g})p_{s^g,k} - (2(1-\theta)\Omega^g_{s^g}r^g\delta x^g/\epsilon^g_3)\alpha^{downstream}_{k}d^{tot}_{k}$$

$$-(2\theta\Omega^g_{s^g}r^g\delta x^g/\epsilon^g_3)(\alpha^{downstream}_{k+1}\mathcal{Q}^{tot} - \mathcal{Q}^{downstream})$$

$$-(2(1-\theta)\Omega^g_{s^g}r^g\delta x^g/\epsilon^g_3)(\alpha^{downstream}_{k}\mathcal{Q}^{tot} - \mathcal{Q}^{downstream}). \qquad (10.10)$$

Equation (10.10) represents the new form of the downstream flow boundary equation used in $\mathcal{M}5$ models. The last two terms of equation (10.10), $-(2\theta\Omega^g_{s^g}r^g\delta x^g/\epsilon^g_3)(\alpha^{downstream}_{k+1}\mathcal{Q}^{tot} - \mathcal{Q}^{downstream})$ and $-(2(1-\theta)\Omega^g_{s^g}r^g\delta x^g/\epsilon^g_3)(\alpha^{downstream}_{k}\mathcal{Q}^{tot} - \mathcal{Q}^{downstream})$, are contained in the vectors $\underline{v}(k+1)$ and $\underline{v}(k)$ respectively. The two coefficients, $(2\theta\Omega^g_{s^g}r^g\delta x^g/\epsilon^g_3)\alpha^{downstream}_{k+1}$ and $-(2(1-\theta)\Omega^g_{s^g}r^g\delta x^g/\epsilon^g_3)\alpha^{downstream}_{k}$, of the total flow perturbation variable, $d^{tot}_{timestep}$, are contained in the vectors $\underline{\epsilon}(k+1)$ and $\underline{a}(k)$ respectively.

One can immediately see that if the ratios between the separate flow demands remain constant with time, i.e., if for all demand sites, h, we have

$$\alpha^h_k = \alpha^h \quad for\ all\ k,$$

then the $\mathcal{M}5$ system matrices, $E_5(k+1)$ and $A_5(k)$ will be time invariant. However, if the ratios, α^h_k change with time, then so will $E_5(k+1)$ and $A_5(k)$.

The above $\mathcal{M}5$ model can be expressed in the general descriptor system form

$$E_5(k+1)\underline{x}_5(k+1) = A_5(k)\underline{x}_5(k) + B^1_5\underline{u}_5(k+1) + B^2_5\underline{u}_5(k) + \underline{l}^1_5(k+1) + \underline{l}^2_5(k). \quad (10.11)$$

For such an $\mathcal{M}5$ model, the only pressure input required is the upstream pressure (assumed known). The g pressure measurements of the real gas network at the sites of flow demand are not needed as inputs to the $\mathcal{M}5$ model, and are, in fact, measurements of its state variables

$$\underline{y}_5(k) = C_5\underline{x}_5(k) \tag{10.12}$$

available for use in a direct or dynamic observer.

10.4.1 Theorems

In this section, we firstly prove that the matrix E_5 of an $\mathcal{M}5$ model is full rank for each timestep k, if $\theta > 0$. We then prove that the Hautus condition holds for the $\mathcal{M}5$ model (10.11) for each timestep k, if $1/2 \leq \theta \leq 1$.

Theorem 10.1 *If $\theta > 0$, the matrix E_5 of an $\mathcal{M}5$ model is full rank for each timestep k.*

Proof

E_5 is $(n+1)\times(n+1)$ and takes the form

$$E_5 = \begin{bmatrix} E_0 & \underline{e}(k+1) \\ 0 & 1 \end{bmatrix}.$$

By construction, since we have already shown E_0 is invertible if $\theta > 0$, E_5^{-1} is $(n+1)\times(n+1)$ and takes the form

$$E_5^{-1} = \begin{bmatrix} E_0^{-1} & -E_0^{-1}\underline{e}(k+1) \\ 0 & 1 \end{bmatrix}.$$

Hence, the matrix E_5 of an $\mathcal{M}5$ model is full rank for each timestep k. □

Theorem 10.2 *If $1/2 \leq \theta \leq 1$, the Hautus condition holds for the $\mathcal{M}5$ model (10.11) for each timestep k.*

Proof

By inspection, the eigenvalues of an $\mathcal{M}5$ system consist of the n eigenvalues of the base $\mathcal{M}0$ system, and 1 eigenvalue equal to 1. Hence, the eigenvalues of the $\mathcal{M}5$ system are real.

We have the Hautus condition for the $\mathcal{M}5$ system if and only if for all $\mu \in \mathbf{R}$

$$(A_5(k) - \mu E_5(k+1))\underline{v} = \underline{0} \tag{10.13}$$

$$C_5\underline{v} = \underline{0} \tag{10.14}$$

$$\Longleftrightarrow$$

$$\underline{v} = \underline{0} \tag{10.15}$$

where $\underline{v} \in \mathbf{R}^{n+1}$.

Equation (10.15) $\Longrightarrow$ equations (10.13), (10.14) trivially.

Equations (10.13), (10.14) and (10.15) can be expressed in the following way. We have the Hautus condition for the $\mathcal{M}5$ system if and only if for all $\mu \in \mathbf{R}$

$$(A_0 - \mu E_0)\underline{v}_n + (\underline{a}(k) - \mu \underline{e}(k+1))\underline{v}_1 = \underline{0} \tag{10.16}$$

$$(1-\mu)\underline{v}_1 = \underline{0} \tag{10.17}$$

$$C_0\underline{v}_n = \underline{0} \tag{10.18}$$

$$\Longleftrightarrow$$

$$\underline{v}_n = \underline{0}\ ,\ \underline{v}_1 = \underline{0} \tag{10.19}$$

where $\underline{v} = [\underline{v}_n^T, \underline{v}_1^T]^T$, and $\underline{v}_n \in \mathbf{R}^n$, $\underline{v}_1 \in \mathbf{R}^1$.

We firstly consider the case where $\mu \neq 1$.

Equation (10.17) implies $\underline{v}_1 = \underline{0}$.

Substituting $\underline{v}_1 = \underline{0}$ into equation (10.16) gives

$$(A_0 - \mu E_0)\underline{v}_n = \underline{0}. \tag{10.20}$$

Since we have shown the original $\mathcal{M}0$ system is observable for $\theta > 0$, we have for all $\mu \in \mathbf{R}$

$$(A_0 - \mu E_0)\underline{v}_n = \underline{0} \;\; , \;\; C_0\underline{v}_n = \underline{0} \; , \iff \underline{v}_n = \underline{0}. \tag{10.21}$$

Equations (10.18), (10.20), (10.21) $\Longrightarrow \underline{v}_n = \underline{0}$.

Hence, we have $\underline{v}_n = \underline{0}$, $\underline{v}_1 = \underline{0}$; and so equations (10.13), (10.14) $\Longrightarrow$ (10.15).

We secondly consider the case where $\mu = 1$.

Equation (10.16) becomes

$$\left[\begin{array}{cc} (A_0 - E_0) & (\underline{a}(k) - \underline{e}(k+1)) \end{array} \right] \left[\begin{array}{c} \underline{v}_n \\ \underline{v}_1 \end{array} \right] = \underline{0}. \tag{10.22}$$

If we assume the $\mathcal{M}0$ model is partitioned according to equation (3.1), then equation (10.22) may be written as

$$\left[\begin{array}{ccc} (\mathcal{A}_{1,1} - \mathcal{E}_{1,1}) & (\mathcal{A}_{1,2} - \mathcal{E}_{1,2}) & \underline{0} \\ (\mathcal{A}_{2,1} - \mathcal{E}_{2,1}) & (\mathcal{A}_{2,2} - \mathcal{E}_{2,2}) & \underline{h}(k) \end{array} \right] \left[\begin{array}{c} \underline{v}_{n-g} \\ \underline{v}_g \\ \underline{v}_1 \end{array} \right] = \underline{0} \tag{10.23}$$

where the vector $\underline{h}(k) \in \mathbf{R}^g$ now contains the g elements of $(\underline{a}(k) - \underline{e}(k+1))$ that correspond to coefficients from the flow equations. Also, $\underline{v}_n = [\underline{v}_{n-g}^T, \underline{v}_g^T]^T$ where $\underline{v}_{n-g} \in \mathbf{R}^{n-g}$ and $\underline{v}_g \in \mathbf{R}^g$.

Equation (10.18) zeros the g elements of $\underline{v}_n$ corresponding to the measured pressures at the sites of flow demand. Hence $\underline{v}_g = \underline{0}$.

Removing $\underline{v}_g$ from system (10.23) gives

$$\left[\begin{array}{cc} (\mathcal{A}_{1,1} - \mathcal{E}_{1,1}) & \underline{0} \\ (\mathcal{A}_{2,1} - \mathcal{E}_{2,1}) & \underline{h}(k) \end{array} \right] \left[\begin{array}{c} \underline{v}_{n-g} \\ \underline{v}_1 \end{array} \right] = \underline{0}. \tag{10.24}$$

From the stability theorem for $\mathcal{M}1$ systems, for $1/2 \leq \theta \leq 1$, 1 is not an eigenvalue of $(\mathcal{E}_{1,1}^{-1}\mathcal{A}_{1,1})$, and hence $(\mathcal{A}_{1,1} - \mathcal{E}_{1,1})$ is full rank. Hence equation (10.24) implies $\underline{v}_{n-g} = \underline{0}$.

The vector $(\underline{a}(k) - \underline{e}(k+1))$ contains $g-1$ elements of the form $-\Phi^{z/z+1}(1-\theta)\alpha_k^{z/z+1} - \Phi^{z/z+1}\theta\alpha_{k+1}^{z/z+1}$ which result from the $g-1$ connectivity equations, and one element of the

form $-(2(1-\theta)\Omega^g_{sg} r^g \delta x^g/\epsilon^g_3)\alpha^{downstream}_k - (2\theta\Omega^g_{sg} r^g \delta x^g/\epsilon^g_3)\alpha^{downstream}_{k+1}$ which results from the downstream flow boundary equation. For $1/2 \leq \theta \leq 1$, it is obvious that both terms in each element of the vector $(\underline{a}(k) - \underline{e}(k+1))$ have the same sign, and that at least one term is always non-zero. Hence, the vector $(\underline{a}(k) - \underline{e}(k+1))$ contains non-zero elements, and hence, the vector $\underline{h}(k)$ also contains non-zero elements. Thus equation (10.24) implies $\underline{v}_1 = \underline{0}$.

Hence, we have $\underline{v}_n = \underline{0}$, $\underline{v}_1 = \underline{0}$; and so equations (10.13), (10.14) $\Longrightarrow$ (10.15).

Hence, for $1/2 \leq \theta \leq 1$, the Hautus condition holds for the $\mathcal{M}5$ model (10.11) for each timestep k. □

If the ratios $\alpha^{demand\ site}_k$ do not vary with time then the $\mathcal{M}5$ system matrices do not vary with time and we have the following corollary.

Corollary 10.1 *For $1/2 \leq \theta \leq 1$, if the ratios, $\alpha^{demand\ site}_k$ do not vary with time, then the $\mathcal{M}5$ model is completely observable.*

When the ratios, $\alpha^{demand\ site}_k$ do not vary with time, we are assured of the complete observability of the $\mathcal{M}5$ model and direct and dynamic observers may be employed for state estimation.

When the ratios, $\alpha^{demand\ site}_k$ do vary with time, and hence the $\mathcal{M}5$ system matrices vary with time, we may employ time-varying versions of the dynamic and direct observers in a similar way to $\mathcal{M}4$ models.

In the following experiments, we abandon direct observers due to their high computational expense, and investigate dynamic observers only.

10.4.2 Experiments

As the $\mathcal{M}0$ model was run, the pressures at the upstream end and the sites of flow demand were recorded at each timestep. For experiments 10.13 to 10.16, there was no pressure measurement noise added. However, for experiments 10.17 to 10.22, the pressure measurements at the three flow demand sites, A/B, B/C and C, were corrupted

by white noise with a Gaussian distribution with mean 0 bar and standard deviation 0.1 bar. These pressures were then fed into the $\mathcal{M}5$ model based observer (or $\mathcal{M}3$ model based observer in experiment 10.21). The eigenvalues assigned to the $\mathcal{M}5$ model based observer were spread evenly in the interval $(0, 0.1)$. The flow demands predicted by this estimation technique were then compared with the true flows used as inputs to the $\mathcal{M}0$ model. For all experiments, the $\mathcal{M}5$ (or $\mathcal{M}3$) model based observer included the exact values of the weightings, $\tilde{f}_k^{demand\ site}$, in the trivial flow demand difference equations. Exact values were also used for the ratios, $\alpha_k^{demand\ site}$. Also, in each experiment the $\mathcal{M}5$ (or $\mathcal{M}3$) model had 10 spatial nodes along each pipe.

For experiments 10.13 to 10.20, *flow profile a* was used with the flows at demand sites A/B, B/C and C in the ratio 2:5:13. For the final two experiments, 10.21 and 10.22, similarly shaped profiles were used, but where the ratio between the demands was changed to 20:1:79. These last experiments demonstrated how $\mathcal{M}5$ models can very significantly improve the state estimates of very small flows in the presence of pressure measurement noise.

For each experiment, the true flow demand profiles for the demands, $D_k^{A/B}$, $D_k^{B/C}$ and D_k^C are shown as thick lines in Figs. A, B and C respectively, and the state estimates for $D_k^{A/B}$, $D_k^{B/C}$ and D_k^C are shown as thin lines. The percentage errors between the state estimates of $D_k^{A/B}$, $D_k^{B/C}$ and D_k^C and their true values are shown in Figs. D, E and F respectively.

The following four experiments do not have measurement noise added.

Data taken from $\mathcal{M}0$ model with identical mesh

Experiment 10.13) ($\mathcal{M}5$ model) Observer Design B with $\theta = 1$

Experiment 10.14) ($\mathcal{M}5$ model) Observer Design B with $\theta = 0.5$

Data taken from $\mathcal{M}0$ model with much finer mesh

Experiment 10.15) ($\mathcal{M}5$ model) Observer Design B with $\theta = 1$

Experiment 10.16) ($\mathcal{M}5$ model) Observer Design B with $\theta = 0.5$

The following two experiments do have measurement noise added.

Data taken from $\mathcal{M}0$ model with identical mesh

Experiment 10.17) ($\mathcal{M}5$ model) Observer Design B with $\theta = 1$

Data taken from $\mathcal{M}0$ model with much finer mesh

Experiment 10.18) ($\mathcal{M}5$ model) Observer Design B with $\theta = 1$

The following four experiments do have measurement noise added, but the $\mathcal{M}3$ flow integration smoothing technique is then applied to the observer estimates of the individual flow demands.

Data taken from $\mathcal{M}0$ model with identical mesh

Experiment 10.19) ($\mathcal{M}5$ model) Observer Design B with $\theta = 1$

Data taken from $\mathcal{M}0$ model with much finer mesh

Experiment 10.20) ($\mathcal{M}5$ model) Observer Design B with $\theta = 1$

Experiment 10.21) ($\mathcal{M}3$ model) Observer Design B (small eigenvalues) with $\theta = 1$ *(New flow ratio 20:1:79)*

Experiment 10.22) ($\mathcal{M}5$ model) Observer Design B with $\theta = 1$ *(New flow ratio 20:1:79)*

Experiment 10.13

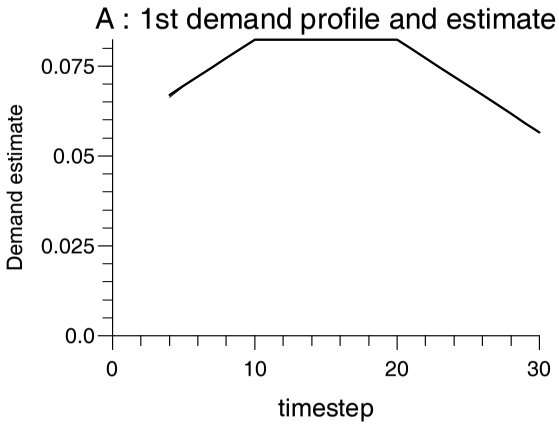

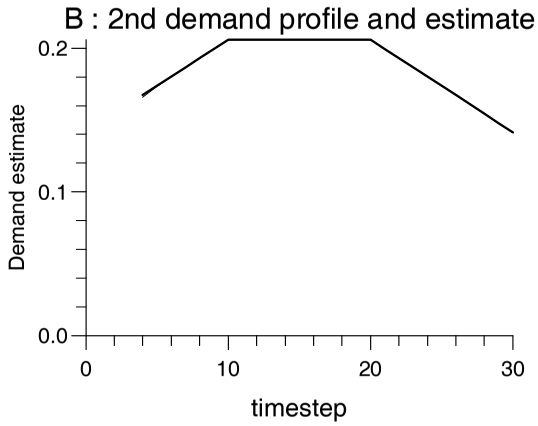

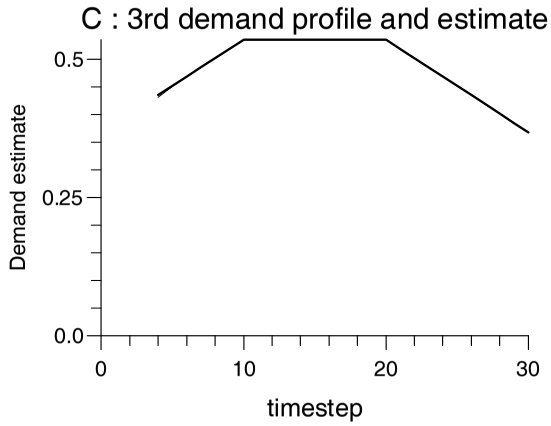

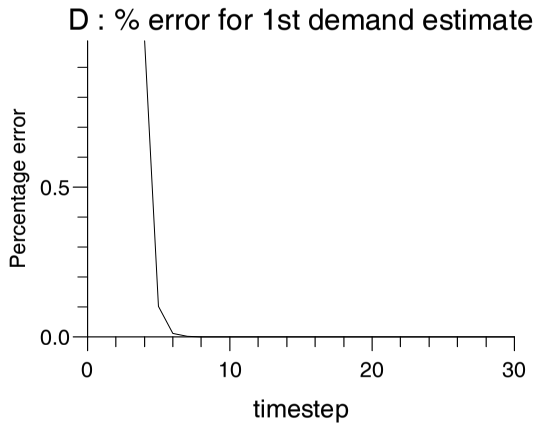

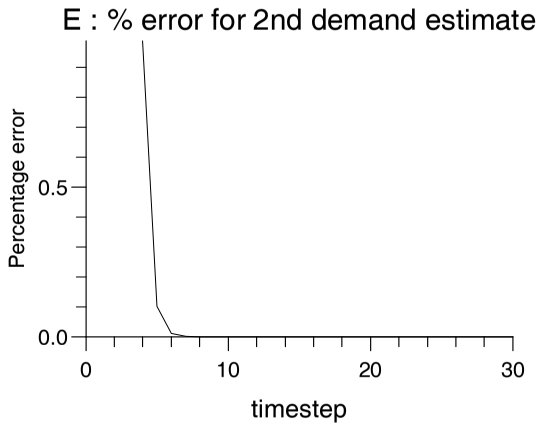

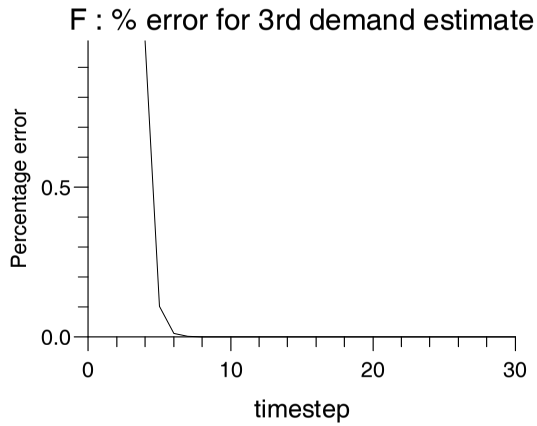

Experiment 10.14

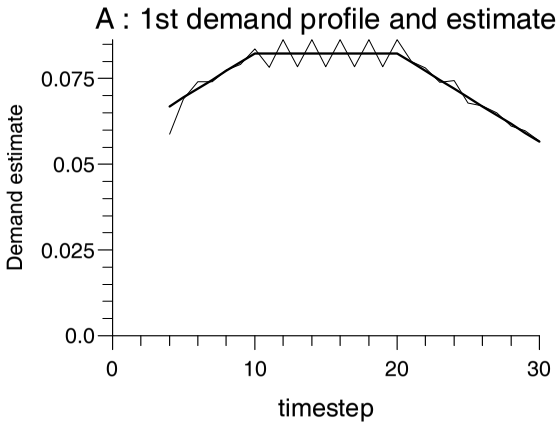

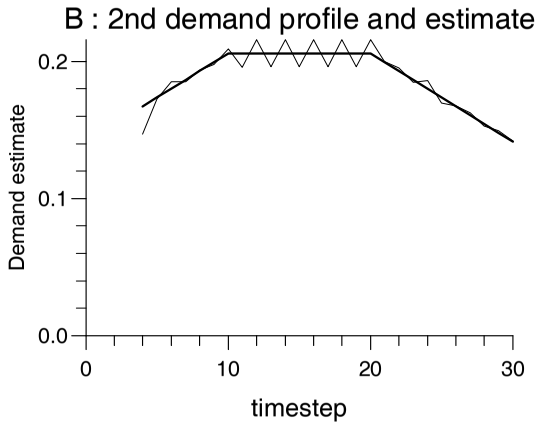

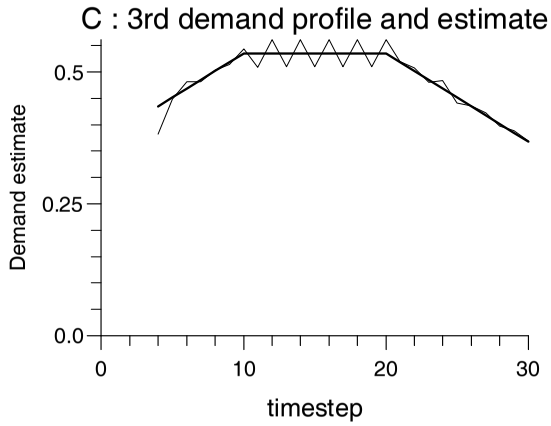

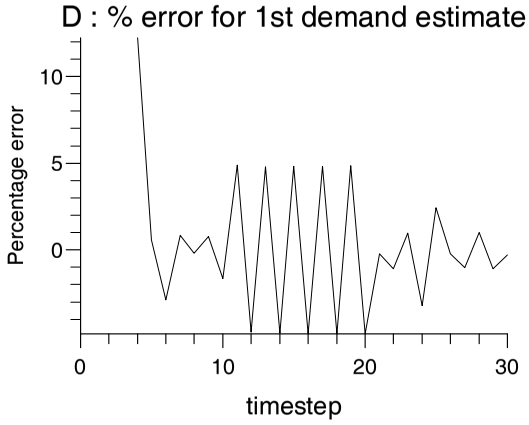

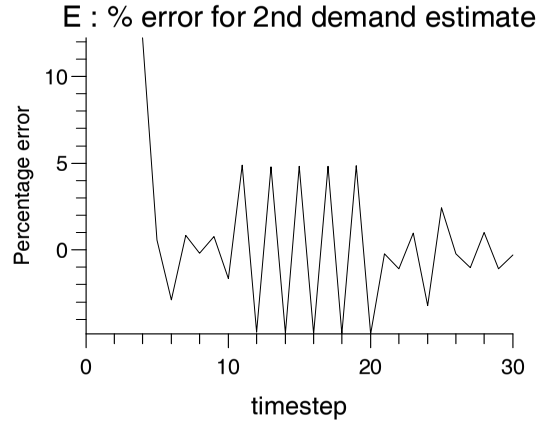

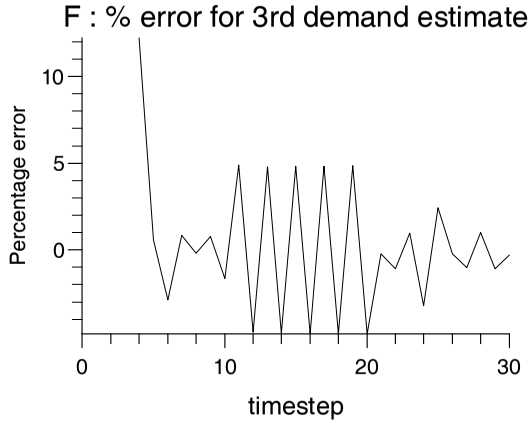

Experiment 10.15

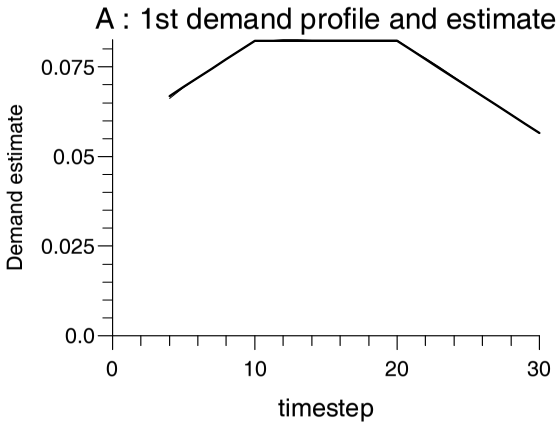

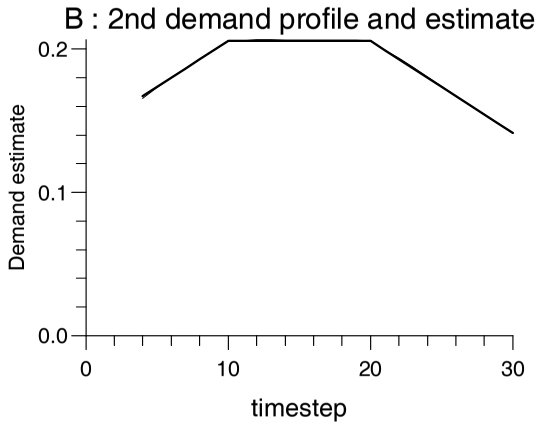

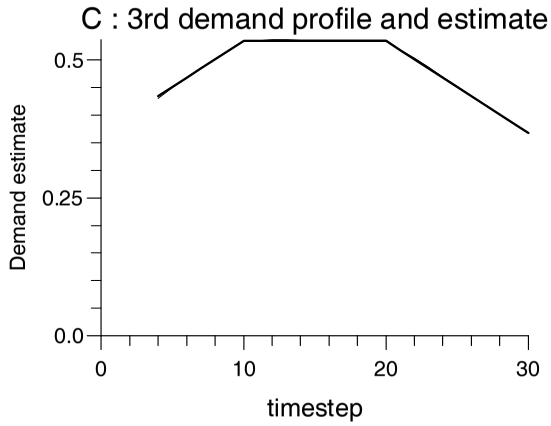

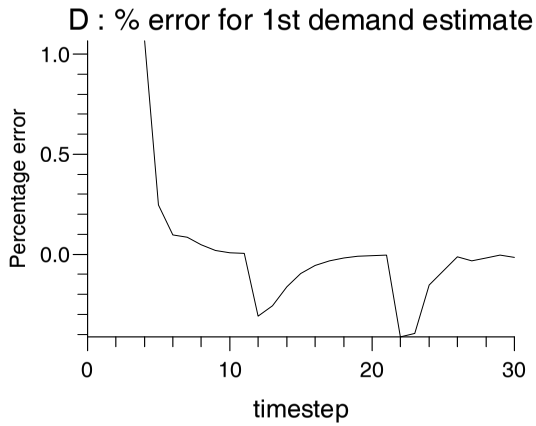

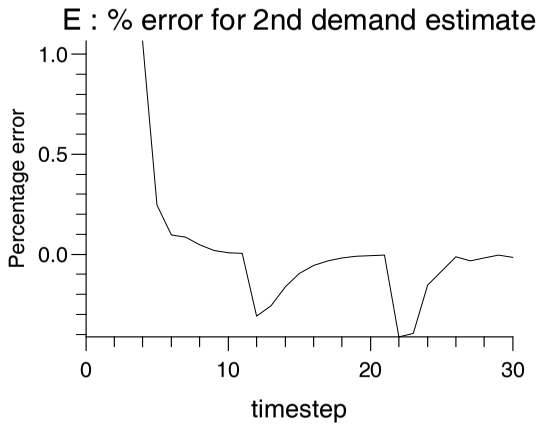

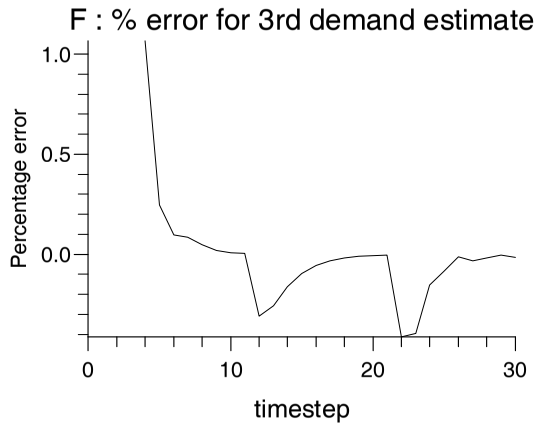

Experiment 10.16

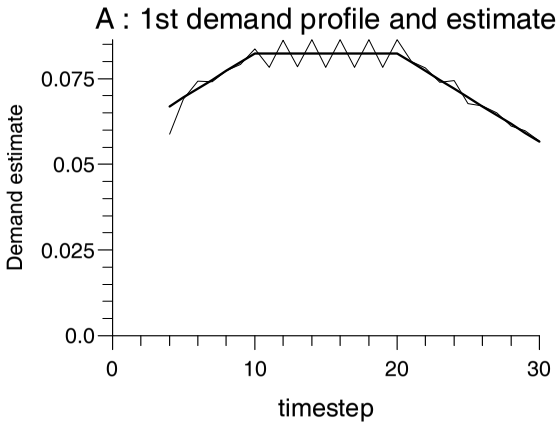

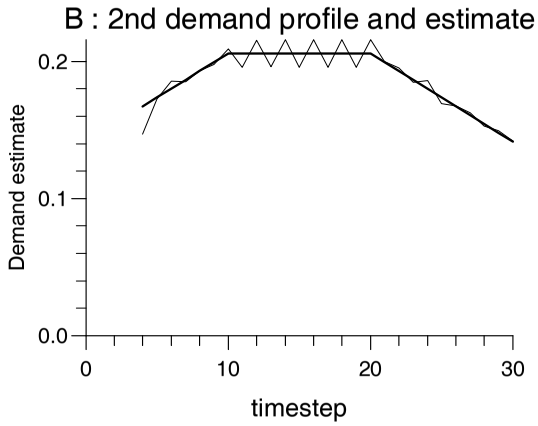

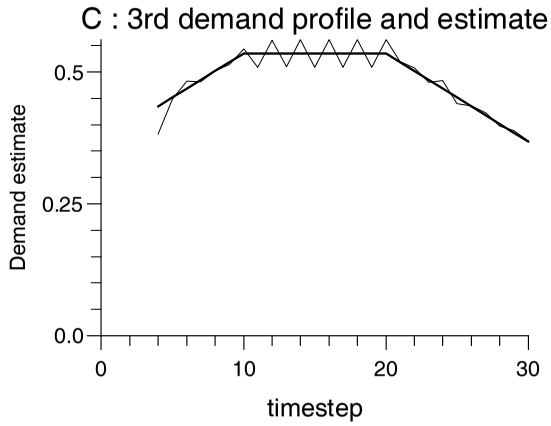

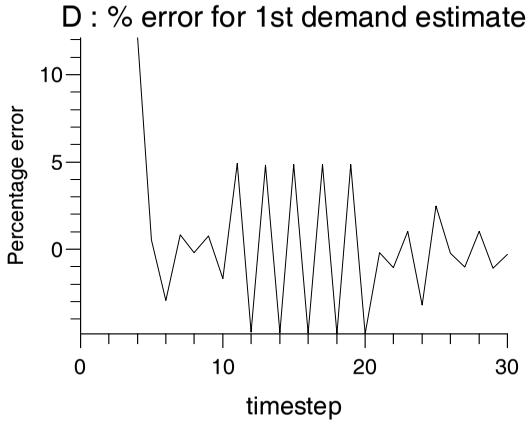

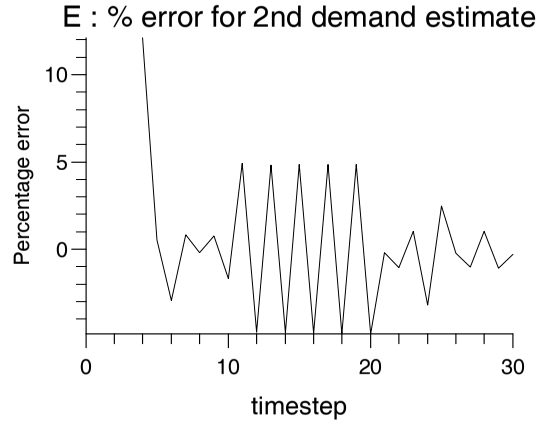

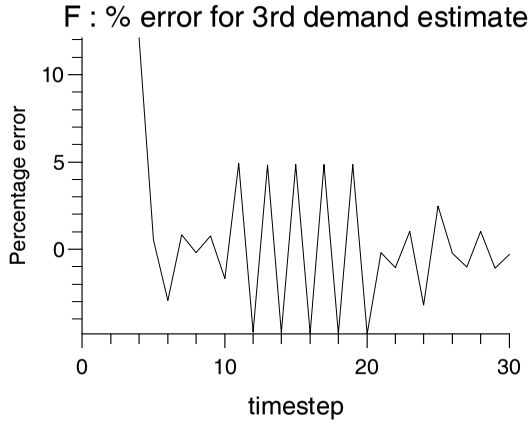

Experiment 10.17

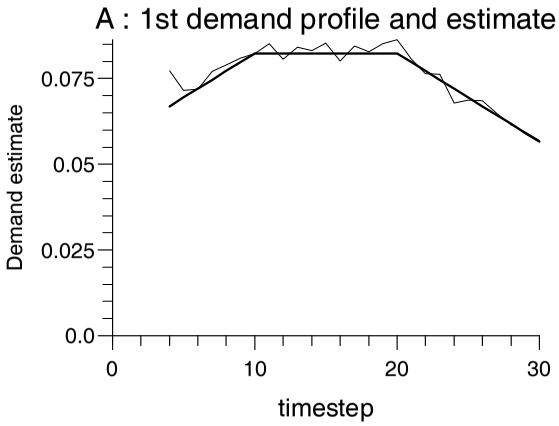

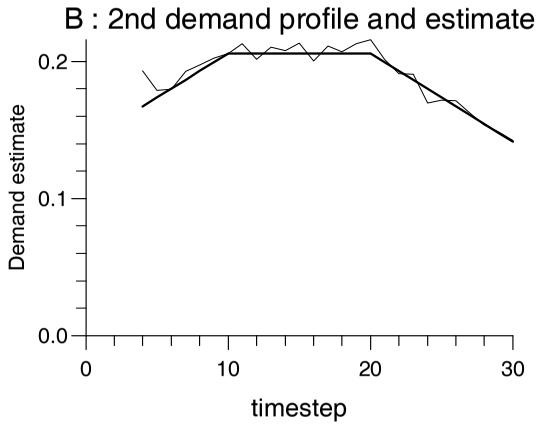

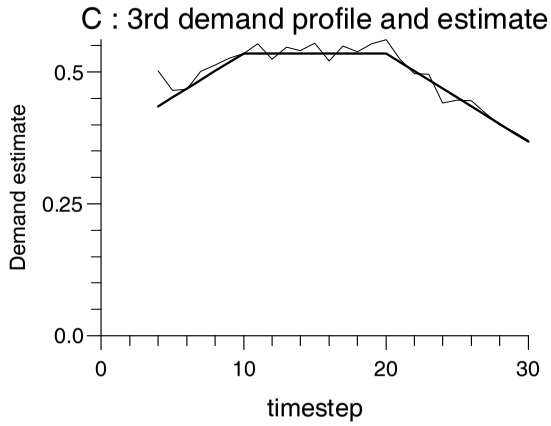

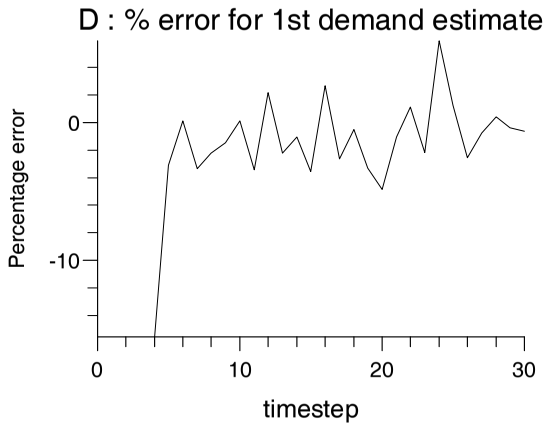

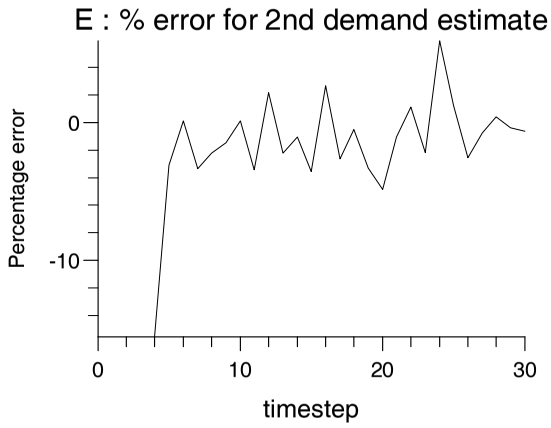

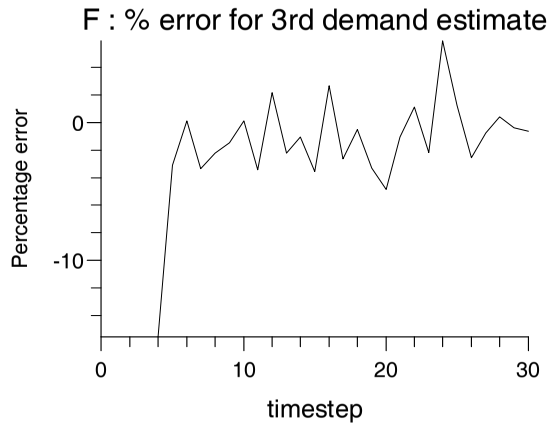

Experiment 10.18

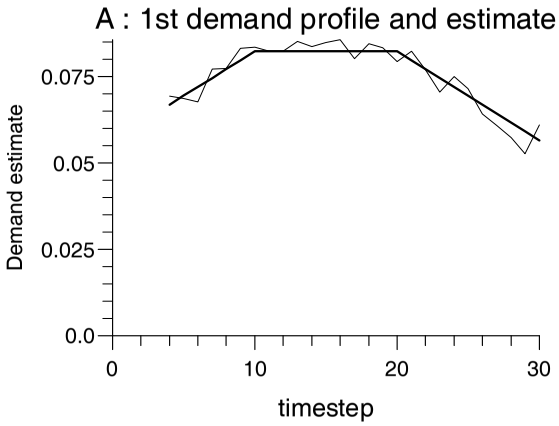

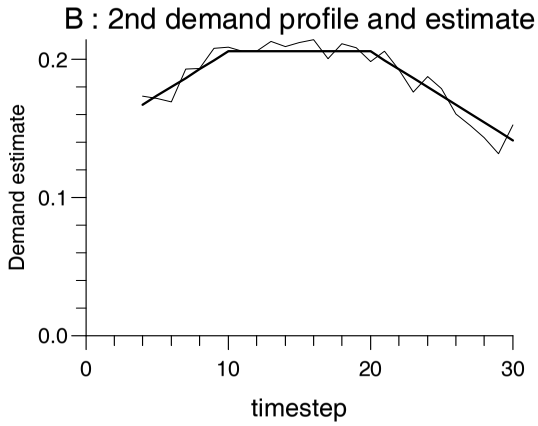

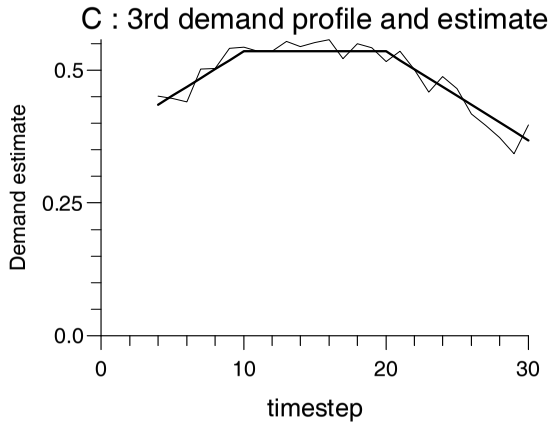

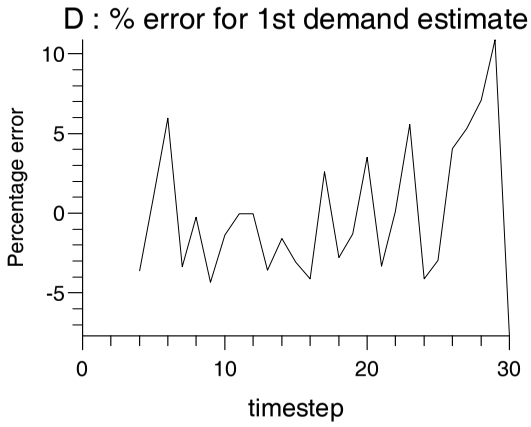

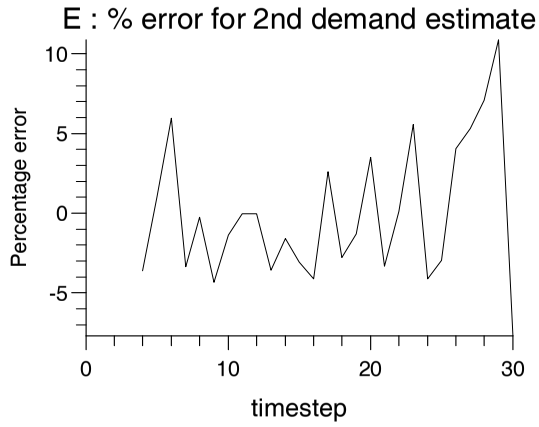

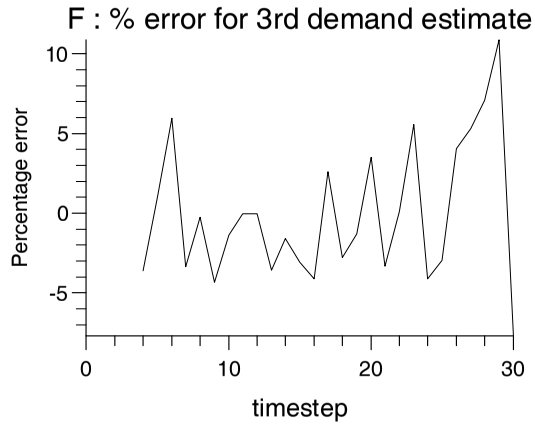

Experiment 10.19

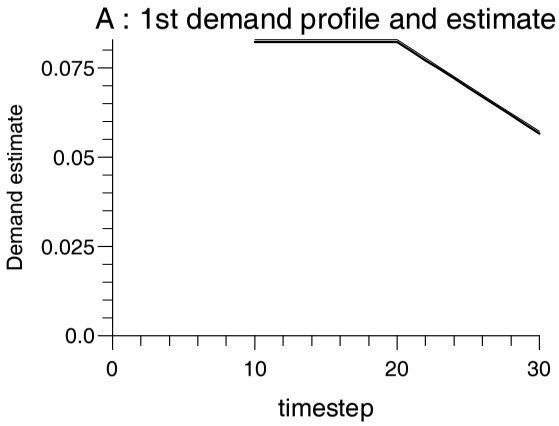

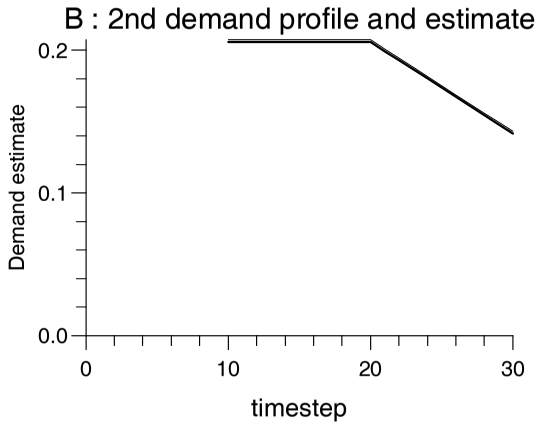

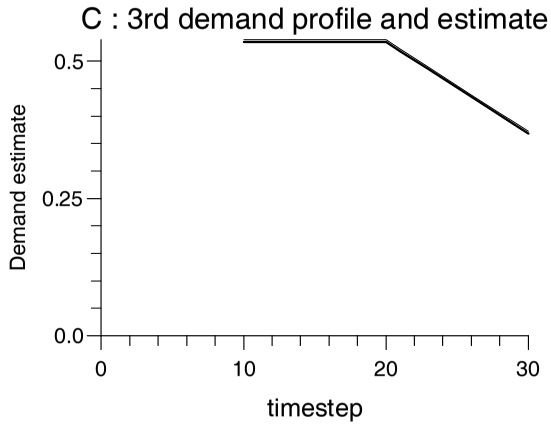

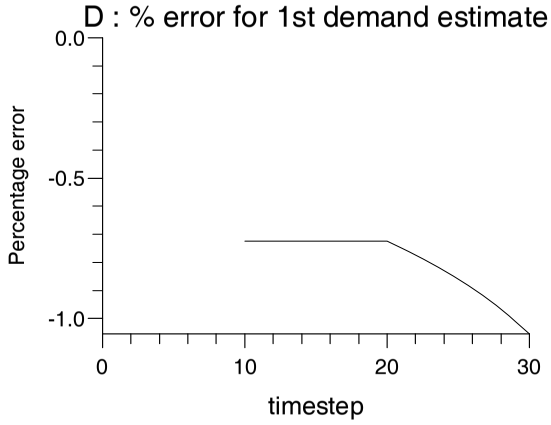

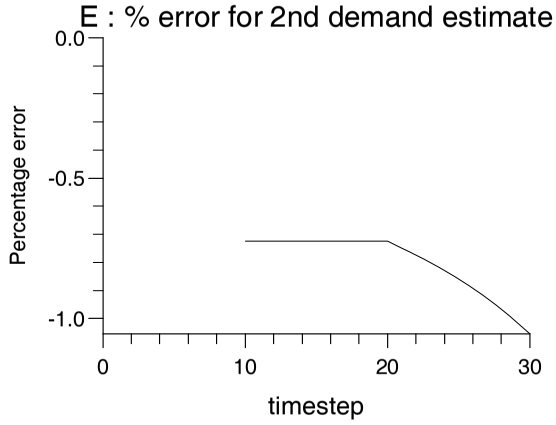

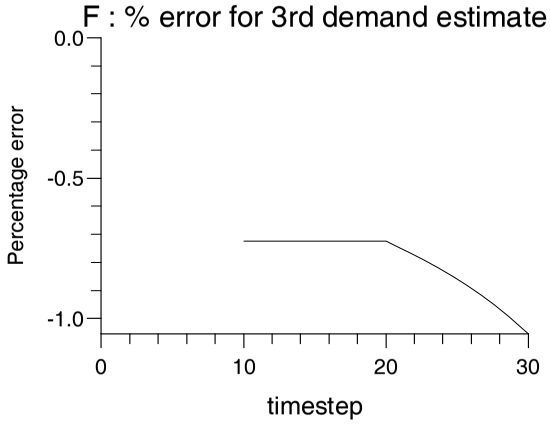

Experiment 10.20

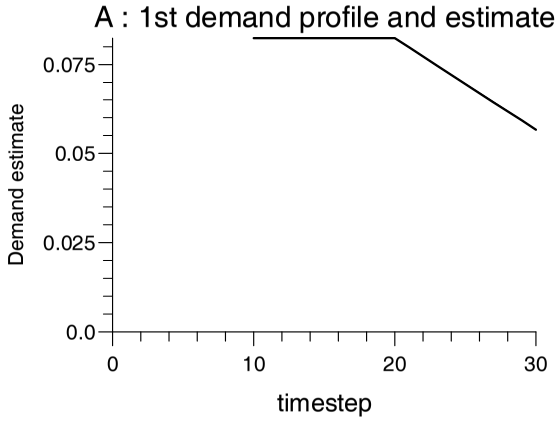

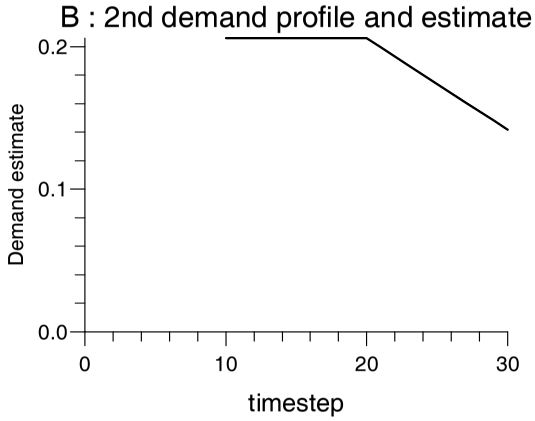

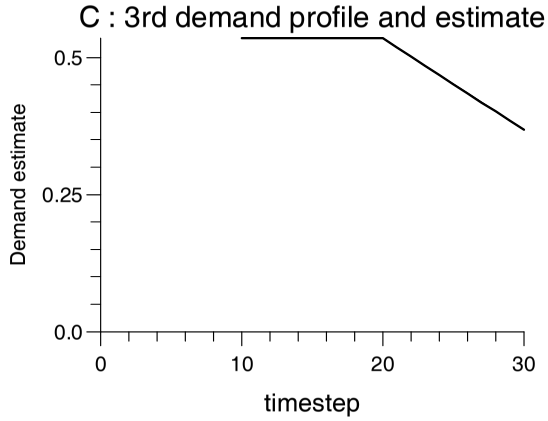

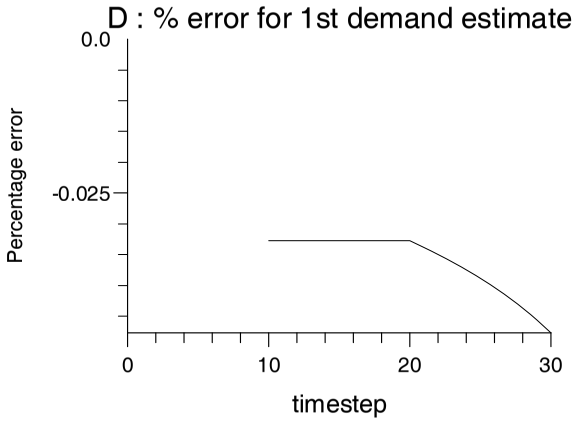

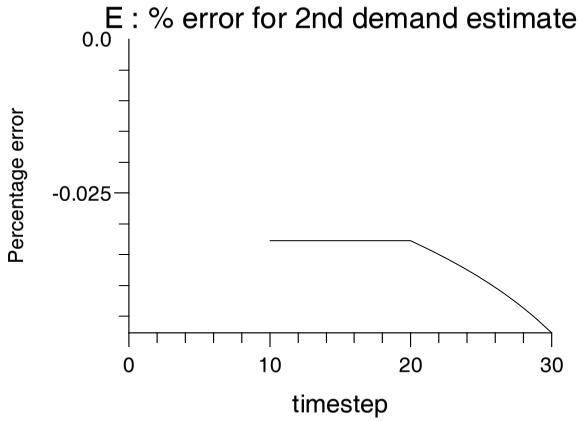

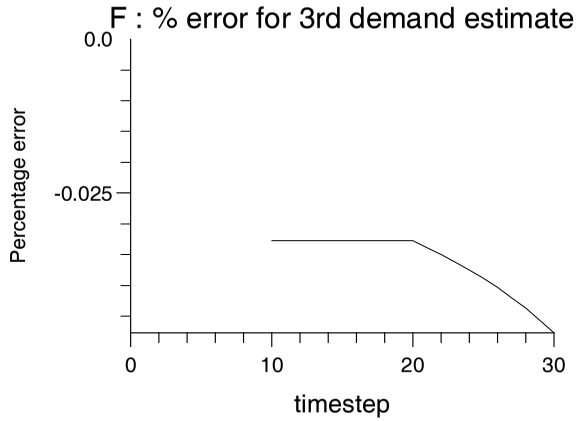

Experiment 10.21

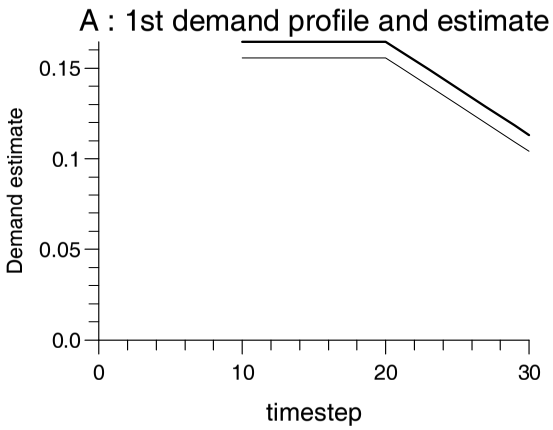

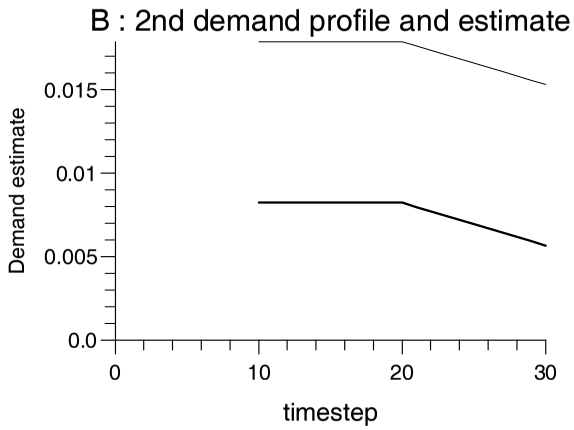

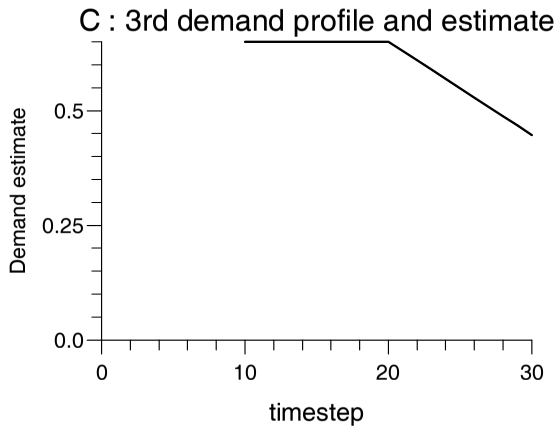

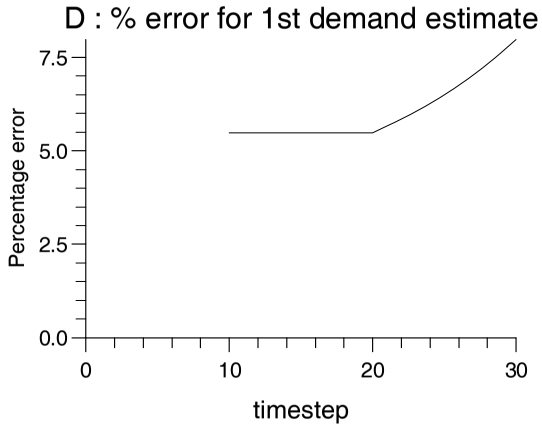

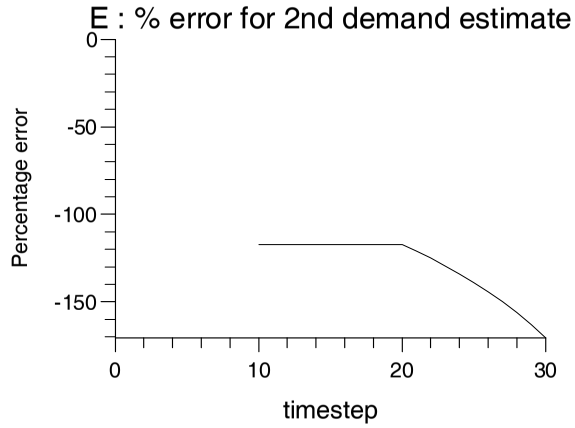

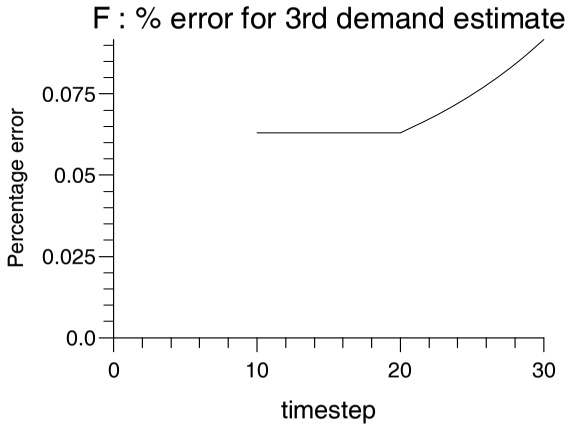

Experiment 10.22

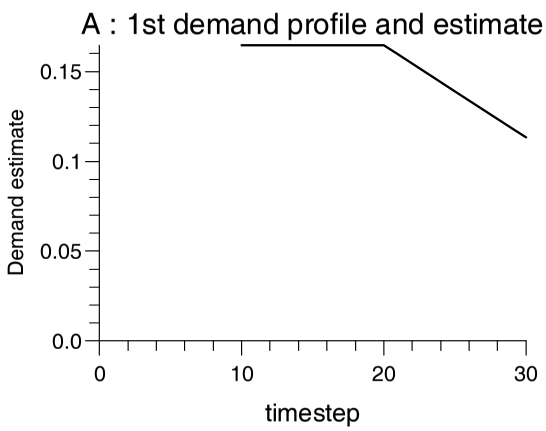

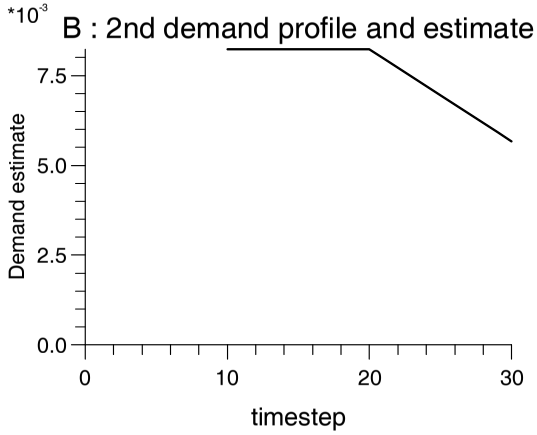

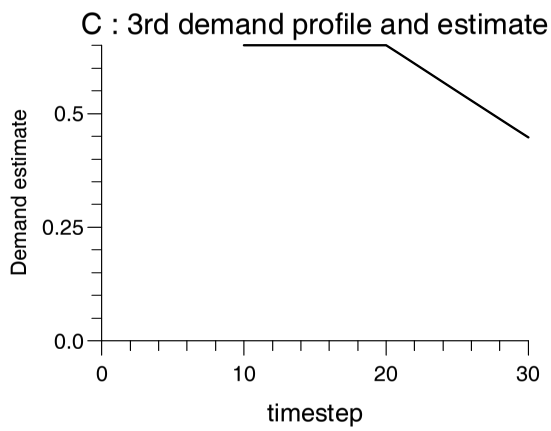

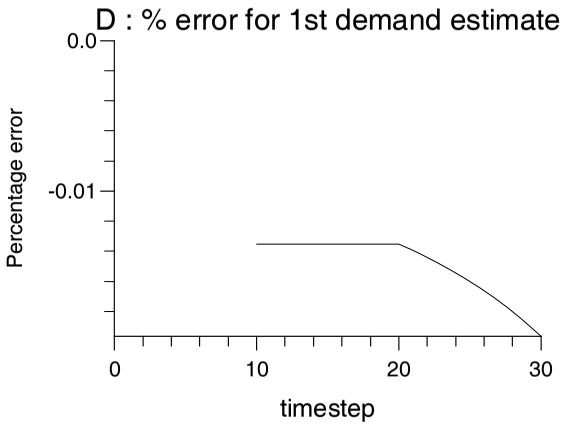

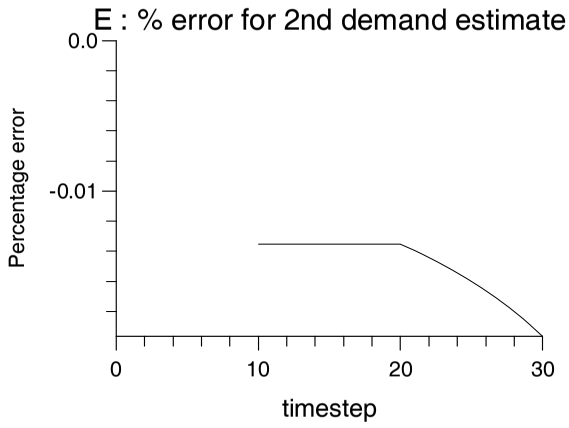

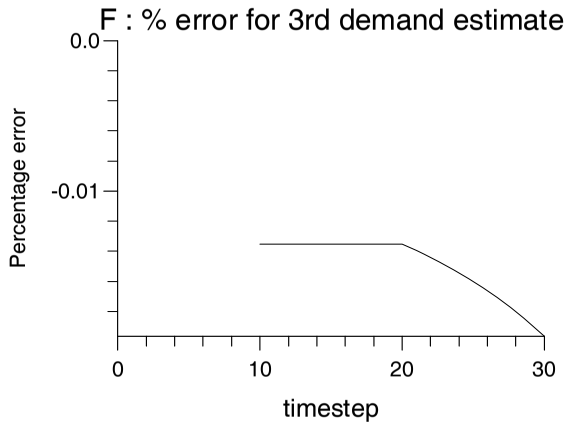

10.4.3 Discussion

When pressure data was taken from an $\mathcal{M}0$ model with an identical mesh, the $\mathcal{M}5$ model based dynamic observer converged perfectly for $\theta = 1$. However, as θ moved close to $1/2$, error began to persist in the state estimate. As θ moved from 1 to $1/2$, the assigned observer eigenvalues became more sensitive in a similar way to dynamic observers based upon $\mathcal{M}3$ and $\mathcal{M}4$ models. As was suggested for these earlier models, it may be that for $\theta = 1/2$, the Hautus condition for the $\mathcal{M}5$ system is close to failing, and theoretical analysis of this would be of value. When pressure data was taken from an $\mathcal{M}0$ model with a much finer mesh, observers based upon $\mathcal{M}5$ models continued to perform well, with little increase in the error in the flow demand estimates.

When pressure measurement noise was added, but no smoothing technique applied, it could be seen that the estimates of the first two small demands contained much less error than with previous model and observer designs. The salient feature of $\mathcal{M}5$ models is their decreased sensitivity to pressure measurement noise. When the $\mathcal{M}3$ flow integration smoothing technique was also applied, the estimates of the flow demands became very good indeed. The last two experiments, 10.21 and 10.22, clearly demonstrate the $\mathcal{M}5$ model's increased accuracy in the estimation of very small flow demands.

Unfortunately, pressure measurements from real gas networks are also subject to constant bias, and $\mathcal{M}5$ models are not able to cope with these. Hence, we now investigate the last model variation of this thesis, the $\mathcal{M}6$ model, that not only has the benefits of a single flow demand state variable, but is also capable of estimating the measurement biases.

10.5 The $\mathcal{M}6$ Model

The estimates of small flow demands from observers based upon $\mathcal{M}5$ models were found to be significantly less sensitive to pressure measurement noise than with previous models. However, $\mathcal{M}5$ model based observers were unable to cope with measurement bias. We now investigate a new model variation, denoted by $\mathcal{M}6$, that also has only a single total flow variable, but which can also estimate the measurement biases. We consider the g

scalar equations of the form (9.4). If we add these g equations together we can derive

$$d_{k+1}^{tot} = \sum_{demand\ site=1}^{g} w_k^{demand\ site} d_k^{demand\ site} + \sum_{demand\ site=1}^{g} (w_k^{demand\ site} - 1)\mathcal{Q}^{demand\ site} \tag{10.25}$$

where $d_k^{tot} = \sum_{demand\ site=1}^{g} d_k^{demand\ site}$ for all k, as before. We can now use equation (10.5) to substitute for each term, $d_k^{demand\ site}$, on the right hand side of equation (10.25) to give

$$d_{k+1}^{tot} = \sum_{demand\ site=1}^{g} w_k^{demand\ site} (\alpha_k^{demand\ site} d_k^{tot} + \alpha_k^{demand\ site} \mathcal{Q}^{tot} - \mathcal{Q}^{demand\ site})$$

$$+ \sum_{demand\ site=1}^{g} (w_k^{demand\ site} - 1)\mathcal{Q}^{demand\ site} \tag{10.26}$$

and rearranging gives

$$d_{k+1}^{tot} = c_k d_k^{tot} + (c_k - 1)\mathcal{Q}^{tot} \tag{10.27}$$

where $c_k = \sum_{demand\ site=1}^{g} w_k^{demand\ site} \alpha_k^{demand\ site}$. The $\mathcal{M}6$ models now contain the single state flow variable, d_k^{tot}, with a difference equation of the form (10.27) where the term $(c_k - 1)\mathcal{Q}^{tot}$ is contained in a vector on the right hand side of the system as shown later.

To form an $\mathcal{M}6$ model, we start from a base $\mathcal{M}0$ model and initially proceed in a similar way to the formation of an $\mathcal{M}5$ model. All the basic difference equations of the form (2.17) remain unchanged in an $\mathcal{M}6$ model. However, the $g-1$ connectivity equations and the single downstream flow boundary equation are altered by the following. The g flow demand perturbation variables are removed from the input vector, summed into a single total flow demand perturbation variable, and then incorporated into the new $\mathcal{M}6$ state vector. The new trivial difference equation (10.27) is then added to form the $\mathcal{M}6$ system.

However, with $\mathcal{M}6$ models we now assume, as we have assumed with $\mathcal{M}4$ models, that the pressure measurements at the sites of flow demand are now subject to a constant bias described by equation (9.1)

$$\underline{y}(k) = \underline{p}_2(k) + \underline{b}(k).$$

The g measurement biases are assumed to obey equation (9.2)

$$\underline{b}(k+1) = \underline{b}(k).$$

The last step in the construction of an $\mathcal{M}6$ model is to incorporate the g measurement biases into the new state vector, and incorporate the trivial difference equations (9.2) into the system.

The new $n+1+g$ dimensional $\mathcal{M}6$ state vector now has the form

$$\underline{x}_6(k) = \begin{bmatrix} \underline{x}_0(k) \\ d_k^{tot} \\ \underline{b}(k) \end{bmatrix}.$$

Assuming the base $\mathcal{M}0$ model is arranged and partitioned as in equation (4.1), the new $n+1+g$ dimensional $\mathcal{M}6$ system has the form

$$\begin{bmatrix} E_0 & \underline{e}(k+1) & 0 \\ 0 & 1 & 0 \\ 0 & 0 & I \end{bmatrix} \begin{bmatrix} \underline{x}_0(k+1) \\ d_{k+1}^{tot} \\ \underline{b}(k+1) \end{bmatrix} = \begin{bmatrix} A_0 & \underline{a}(k) & 0 \\ 0 & c_k & 0 \\ 0 & 0 & I \end{bmatrix} \begin{bmatrix} \underline{x}_0(k) \\ d_k^{tot} \\ \underline{b}(k) \end{bmatrix}$$

$$+ \begin{bmatrix} B^{1'} \\ 0 \\ 0 \end{bmatrix} \underline{p}_3(k+1) + \begin{bmatrix} B^{2'} \\ 0 \\ 0 \end{bmatrix} \underline{p}_3(k) + \begin{bmatrix} \underline{v}(k+1) \\ 0 \\ 0 \end{bmatrix} + \begin{bmatrix} \underline{v}(k) \\ (c_k - 1)\mathcal{Q}^{tot} \\ 0 \end{bmatrix} \tag{10.28}$$

where I is $g \times g$, and where the the construction of the vectors $\underline{e}(k+1)$, $\underline{a}(k)$, $\underline{v}(k+1)$ and $\underline{v}(k)$ is identical to the $\mathcal{M}5$ model. One can immediately see the $\mathcal{M}6$ system matrices, $E_6(k+1)$ and $A_6(k)$ are time-varying.

The above $\mathcal{M}6$ model can be expressed in the general descriptor system form

$$E_6(k+1)\underline{x}_6(k+1) = A_6(k)\underline{x}_6(k) + B_6^1\underline{u}_6(k+1) + B_6^2\underline{u}_6(k) + \underline{l}_6^1(k+1) + \underline{l}_6^2(k). \tag{10.29}$$

For such an $\mathcal{M}6$ model, the only pressure input required is the upstream pressure (assumed known). The g pressure measurements of the real gas network at the sites of flow demand are not needed as inputs to the $\mathcal{M}6$ model, and are, in fact, measurements of its state variables

$$\underline{y}_6(k) = C_6\underline{x}_6(k) \tag{10.30}$$

available for use in a direct or dynamic observer.

10.5.1 Theorems

In this section, it is firstly proved that the matrix E_6 of an $\mathcal{M}6$ model is full rank if $\theta > 0$. Secondly, we prove certain conditions to be sufficient to guarantee the assignability of eigenvalues to the $\mathcal{M}6$ model based dynamic observer at a particular timestep. In fact, we show the following. For $1/2 \leq \theta \leq 1$, if at a particular timestep the coefficients, c_k, are not equal to 1, or to any of the eigenvalues of the corresponding $\mathcal{M}1$ model, or to $-((1-\theta)\alpha_k^{demand\ site})/(\theta\alpha_{k+1}^{demand\ site})$ for at least one demand site, then at that timestep the Hautus condition holds for the $\mathcal{M}6$ system (10.29).

Theorem 10.1 *If $\theta > 0$, the matrix E_6 of an $\mathcal{M}6$ model is full rank.*

Proof

E_6 is $(n+1+g)\times(n+1+g)$ and takes the form

$$E_6 = \begin{bmatrix} E_0 & \underline{e}(k+1) & 0 \\ 0 & 1 & 0 \\ 0 & 0 & I \end{bmatrix}.$$

By construction, since we have already shown E_0 is invertible for $\theta > 0$, E_6^{-1} is $(n+1+g)\times(n+1+g)$ and takes the form

$$E_6^{-1} = \begin{bmatrix} E_0^{-1} & -E_0^{-1}\underline{e}(k+1) & 0 \\ 0 & 1 & 0 \\ 0 & 0 & I \end{bmatrix}.$$

Hence, the matrix E_6 of an $\mathcal{M}6$ model is full rank. □

Theorem 10.2 *For $1/2 \leq \theta \leq 1$, if at a particular timestep the coefficients, c_k, are not equal to 1, or to any of the eigenvalues of the corresponding $\mathcal{M}1$ model, or to $-((1-\theta)\alpha_k^{demand\ site})/(\theta\alpha_{k+1}^{demand\ site})$ for at least one demand site, then at that timestep the Hautus condition holds for the $\mathcal{M}6$ system (10.29).*

Proof

By inspection, at any particular timestep k, the eigenvalues of an $\mathcal{M}6$ system consist of the n eigenvalues of the base $\mathcal{M}0$ system, 1 eigenvalue equal to c_k, and g eigenvalues equal to 1. Hence, the eigenvalues of the $\mathcal{M}6$ system are real.

We have the Hautus condition for the $\mathcal{M}6$ system if and only if for all $\mu \in \mathbf{R}$

$$(A_6(k) - \mu E_6(k+1))\underline{v} = \underline{0} \tag{10.31}$$

$$C_6\underline{v} = \underline{0} \tag{10.32}$$

$$\Longleftrightarrow$$

$$\underline{v} = \underline{0} \tag{10.33}$$

where $\underline{v} \in \mathbf{R}^{n+1+g}$.

Equation (10.33) $\Longrightarrow$ equations (10.31), (10.32) trivially.

Equations (10.31), (10.32) and (10.33) can be expressed in the following way. We have the Hautus condition for the $\mathcal{M}6$ system if and only if for all $\mu \in \mathbf{R}$

$$(A_0 - \mu E_0)\underline{v}_n + (\underline{a}(k) - \mu \underline{e}(k+1))\underline{v}_1 = \underline{0} \tag{10.34}$$

$$(c_k - \mu)\underline{v}_1 = \underline{0} \tag{10.35}$$

$$(1 - \mu)\underline{v}_g = \underline{0} \tag{10.36}$$

$$C_0\underline{v}_n + \underline{v}_g = \underline{0} \tag{10.37}$$

$$\Longleftrightarrow$$

$$\underline{v}_n = \underline{0}\ ,\ \underline{v}_1 = \underline{0}\ ,\ \underline{v}_g = \underline{0} \tag{10.38}$$

where $\underline{v} = [\underline{v}_n^T, \underline{v}_1^T, \underline{v}_g^T]^T$, and $\underline{v}_n \in \mathbf{R}^n$, $\underline{v}_1 \in \mathbf{R}^1$, $\underline{v}_g \in \mathbf{R}^g$.

We firstly consider the case where $\mu = 1$.

If $c_k \neq 1$, equation (10.35) implies $\underline{v}_1 = \underline{0}$.

Substituting $\underline{v}_1 = \underline{0}$ into equation (10.34) gives

$$(A_0 - \mu E_0)\underline{v}_n = \underline{0}.$$

Since the $\mathcal{M}0$ stability theorem shows 1 is not an eigenvalue of the $\mathcal{M}0$ system for $1/2 \leq \theta \leq 1$, the above equation implies $\underline{v}_n = \underline{0}$.

Substituting $\underline{v}_n = \underline{0}$ into equation (10.37) gives $\underline{v}_g = \underline{0}$.

Hence we have $\underline{v} = \underline{0}$.

We secondly consider the case where $\mu \neq 1$.

Equation (10.36) implies $\underline{v}_g = \underline{0}$.

Substituting $\underline{v}_g = \underline{0}$ into equation (10.37) gives

$$C_0\underline{v}_n = \underline{0}. \tag{10.39}$$

If $\mu \neq c_k$, equation (10.35) implies $\underline{v}_1 = \underline{0}$.

Substituting $\underline{v}_1 = \underline{0}$ into equation (10.34) gives

$$(A_0 - \mu E_0)\underline{v}_n = \underline{0}. \tag{10.40}$$

Since the original $\mathcal{M}0$ system is completely observable for $\theta > 0$, we have for all $\mu \in \mathbf{R}$

$$(A_0 - \mu E_0)\underline{v}_n = \underline{0} \quad , \quad C_0\underline{v}_n = \underline{0} \; , \iff \underline{v}_n = \underline{0}. \tag{10.41}$$

Equations (10.39), (10.40) and (10.41) imply $\underline{v}_n = \underline{0}$.

Hence $\underline{v} = \underline{0}$.

If $\mu = c_k$, equation (10.34) becomes

$$\left[\begin{array}{cc} (A_0 - c_k E_0) & (\underline{a}(k) - c_k \underline{e}(k+1)) \end{array} \right] \left[\begin{array}{c} \underline{v}_n \\ \underline{v}_1 \end{array} \right] = \underline{0}. \tag{10.42}$$

If we assume the $\mathcal{M}0$ model is partitioned according to equation (3.1), then equation (10.42) may be written as

$$\begin{bmatrix} (\mathcal{A}_{1,1} - c_k\mathcal{E}_{1,1}) & (\mathcal{A}_{1,2} - c_k\mathcal{E}_{1,2}) & \underline{0} \\ (\mathcal{A}_{2,1} - c_k\mathcal{E}_{2,1}) & (\mathcal{A}_{2,2} - c_k\mathcal{E}_{2,2}) & \underline{\tilde{h}}(k) \end{bmatrix} \begin{bmatrix} \underline{v}_{n-g} \\ \underline{\tilde{v}}_g \\ \underline{v}_1 \end{bmatrix} = \underline{0} \qquad (10.43)$$

where the vector $\underline{\tilde{h}}(k) \in \mathbf{R}^g$ now contains the g elements of $(\underline{a}(k) - c_k\underline{e}(k+1))$ that correspond to coefficients from the flow equations. Also, $\underline{v}_n = [\underline{v}_{n-g}^T, \underline{\tilde{v}}_g^T]^T$ where $\underline{v}_{n-g} \in \mathbf{R}^{n-g}$ and $\underline{\tilde{v}}_g \in \mathbf{R}^g$.

Equation (10.39) zeros the g elements of $\underline{v}_n$ corresponding to the measured pressures at the sites of flow demand. Hence $\underline{\tilde{v}}_g = \underline{0}$.

Removing $\underline{\tilde{v}}_g$ from system (10.43) gives

$$\begin{bmatrix} (\mathcal{A}_{1,1} - c_k\mathcal{E}_{1,1}) & \underline{0} \\ (\mathcal{A}_{2,1} - c_k\mathcal{E}_{2,1}) & \underline{\tilde{h}}(k) \end{bmatrix} \begin{bmatrix} \underline{v}_{n-g} \\ \underline{v}_1 \end{bmatrix} = \underline{0}. \qquad (10.44)$$

If c_k is not an eigenvalue of the corresponding $\mathcal{M}1$ system, then $(\mathcal{A}_{1,1} - c_k\mathcal{E}_{1,1})$ is full rank. Hence equation (10.44) implies $\underline{v}_{n-g} = \underline{0}$.

The vector $(\underline{a}(k) - c_k\underline{e}(k+1))$ contains $g-1$ elements of the form $-\Phi^{z/z+1}(1-\theta)\alpha_k^{z/z+1} - c_k\Phi^{z/z+1}\theta\alpha_{k+1}^{z/z+1}$ which result from the $g-1$ connectivity equations, and one element of the form $-(2(1-\theta)\Omega_{sg}^g r^g \delta x^g/\epsilon_3^g)\alpha_k^{downstream} - c_k(2\theta\Omega_{sg}^g r^g \delta x^g/\epsilon_3^g)\alpha_{k+1}^{downstream}$ which results from the downstream flow boundary equation. It can be seen that if the coefficients, c_k, are not equal to $-((1-\theta)\alpha_k^{demand\ site})/(\theta\alpha_{k+1}^{demand\ site})$ for at least one demand site, then the vector $(\underline{a}(k) - c_k\underline{e}(k+1))$ contains at least one non-zero element.

If the vector $(\underline{a}(k) - c_k\underline{e}(k+1))$ contains at least one non-zero element, then the vector $\underline{\tilde{h}}(k)$ will also contain that non-zero element. Then equation (10.44) implies $\underline{v}_1 = \underline{0}$.

Hence $\underline{v} = \underline{0}$.

Hence, for $1/2 \leq \theta \leq 1$, if at a particular timestep the coefficients, c_k, are not equal to 1, or to any of the eigenvalues of the corresponding $\mathcal{M}1$ model, or to $-((1-\theta)\alpha_k^{demand\ site})/(\theta\alpha_{k+1}^{demand\ site})$ for at least one demand site, then at that timestep the Hautus condition holds for the $\mathcal{M}6$ system (10.29). □

From the above theorem, we expect the Hautus condition to hold for the $\mathcal{M}6$ model almost always. However, in an equivalent way to $\mathcal{M}4$ models, it is interesting to note that θ may be chosen to exert some control over the discrete values of the coefficients, c_k, for which the theorem does not guarantee the Hautus condition to hold for the $\mathcal{M}6$ system.

10.5.2 Experiments

As the $\mathcal{M}0$ model was run, the pressures at the upstream end and the sites of flow demand were recorded at each timestep. For experiments 10.23 to 10.25, there was no pressure measurement noise added. However, for experiments 10.26 to 10.31, the pressure measurements at the three flow demand sites, A/B, B/C and C, were corrupted by white noise with a Gaussian distribution with mean 0 bar and standard deviation 0.1 bar. The pressure measurements at the three flow demand sites, A/B, B/C and C, were then corrupted by constant biases of 1 bar, -1 bar and 1 bar respectively. These corrupted pressures were then fed into the $\mathcal{M}6$ model based observer (or $\mathcal{M}4$ model based observer in experiment 10.30). The eigenvalues assigned to the $\mathcal{M}6$ model based observer were spread evenly in the interval $(0, 0.1)$. The flow demands predicted by this estimation technique were then compared with the true flows used as inputs to the $\mathcal{M}0$ model. In all experiments, perfect values were used for the profile coefficients, $w_k^{demand\ site}$, and the ratios, $\alpha_k^{demand\ site}$. Also in each experiment the $\mathcal{M}6$ (or $\mathcal{M}4$) model had 10 spatial nodes along each pipe.

For experiments 10.23 to 10.29, *flow profile a* was used with the flows at demand sites A/B, B/C and C in the ratio 2:5:13. For the final two experiments, 10.30 and 10.31, similarly shaped profiles were used, but where the ratio between the demands was changed to 20:1:79. These last experiments demonstrated how $\mathcal{M}6$ models can very significantly improve the state estimates of very small flows in the presence of pressure measurement noise.

For each experiment, the true flow demand profiles for the demands, $D_k^{A/B}$, $D_k^{B/C}$ and D_k^C are shown as thick lines in Figs. A, B and C respectively, and the state estimates for $D_k^{A/B}$, $D_k^{B/C}$ and D_k^C are shown as thin lines. The percentage errors between the state

estimates of $D_k^{A/B}$, $D_k^{B/C}$ and D_k^C and their true values are shown in Figs. D, E and F respectively.

The following three experiments do not have measurement noise added.

Data taken from $\mathcal{M}0$ model with identical mesh

Experiment 10.23) ($\mathcal{M}6$ model) Observer Design B with $\theta = 1$

Experiment 10.24) ($\mathcal{M}6$ model) Observer Design B with $\theta = 0.5$

Data taken from $\mathcal{M}0$ model with much finer mesh

Experiment 10.25) ($\mathcal{M}6$ model) Observer Design B with $\theta = 1$

The following two experiments do have measurement noise added.

Data taken from $\mathcal{M}0$ model with identical mesh

Experiment 10.26) ($\mathcal{M}6$ model) Observer Design B with $\theta = 1$

Data taken from $\mathcal{M}0$ model with much finer mesh

Experiment 10.27) ($\mathcal{M}6$ model) Observer Design B with $\theta = 1$

The following four experiments do have measurement noise added, but the $\mathcal{M}4$ flow integration smoothing technique is then applied.

Data taken from $\mathcal{M}0$ model with identical mesh

Experiment 10.28) ($\mathcal{M}6$ model) Observer Design B with $\theta = 1$

Data taken from $\mathcal{M}0$ model with much finer mesh

Experiment 10.29) ($\mathcal{M}6$ model) Observer Design B with $\theta = 1$

Experiment 10.30) ($\mathcal{M}4$ model) Observer Design B with $\theta = 1$ *(New flow ratio 20:1:79)*

Experiment 10.31) ($\mathcal{M}6$ model) Observer Design B with $\theta = 1$ *(New flow ratio 20:1:79)*

Experiment 10.23

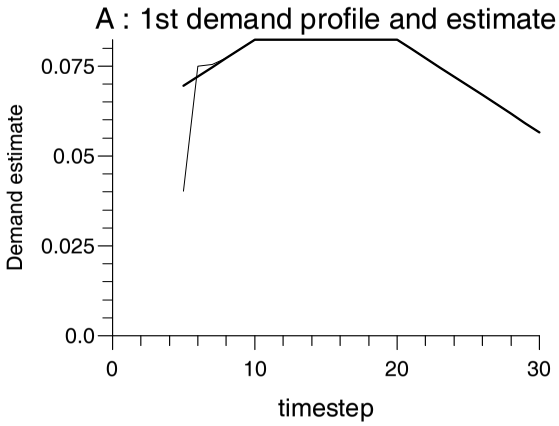

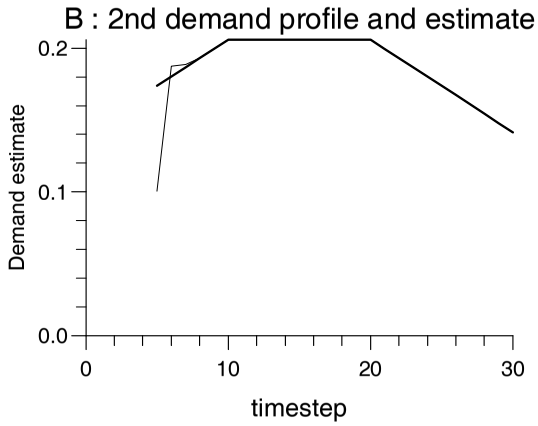

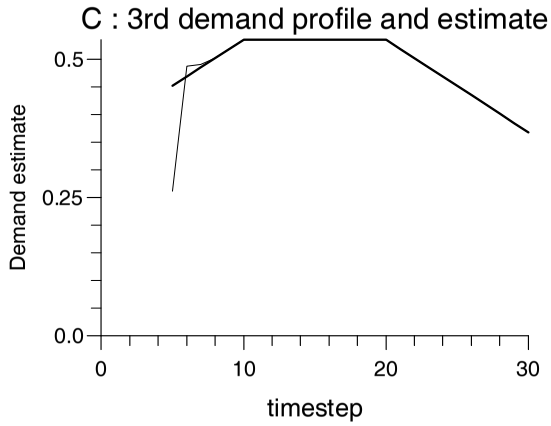

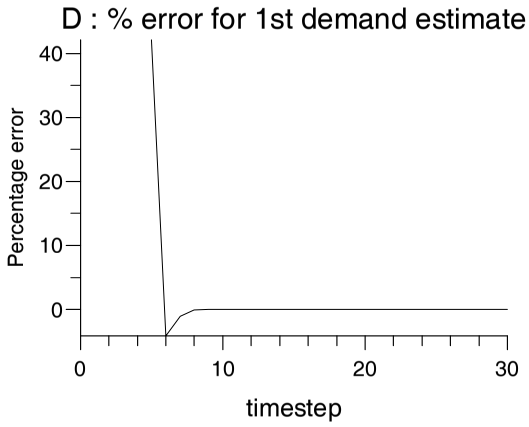

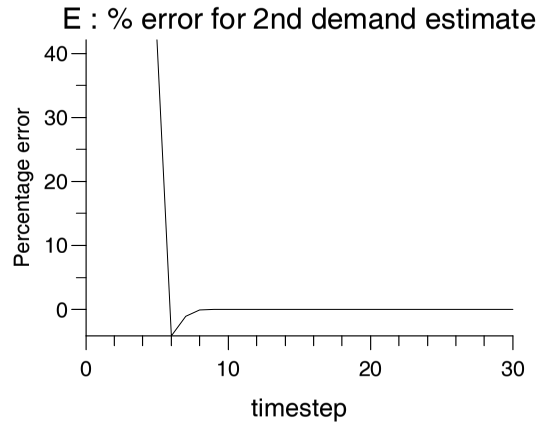

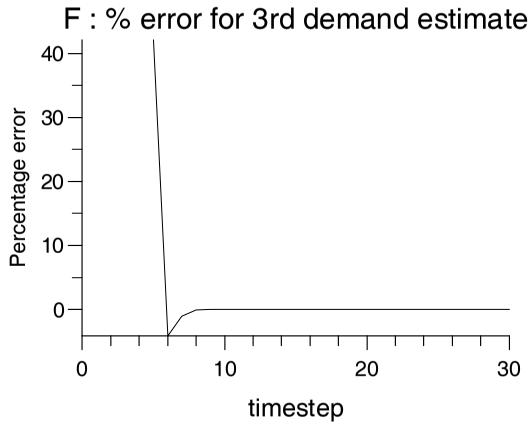

Experiment 10.24

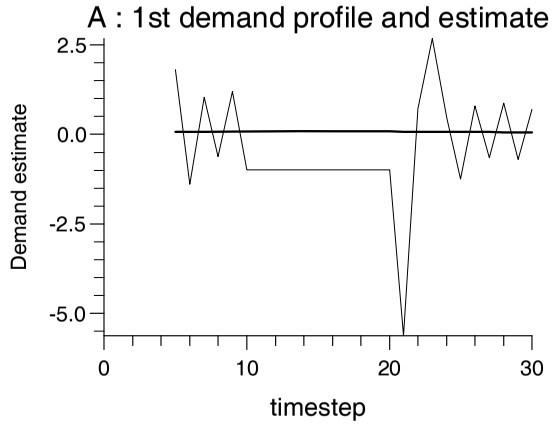

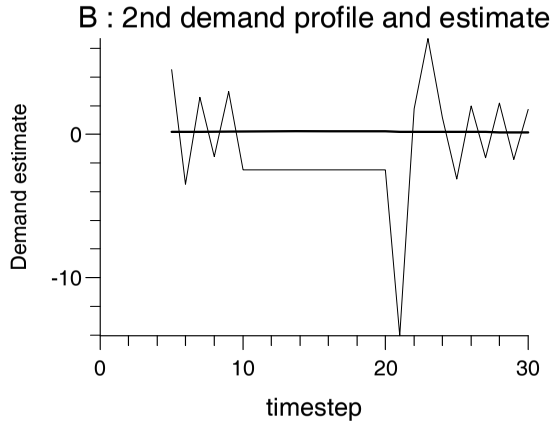

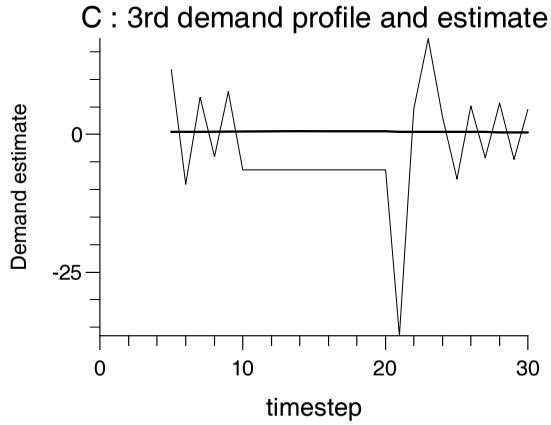

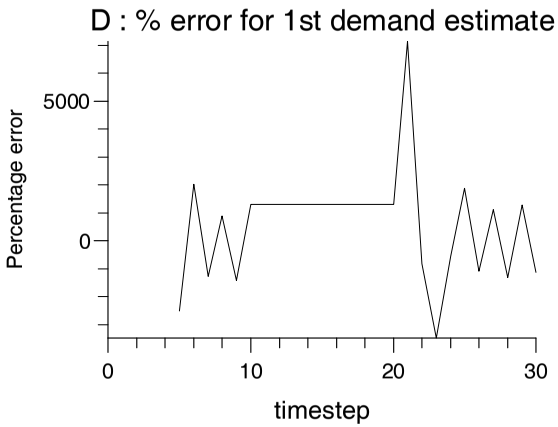

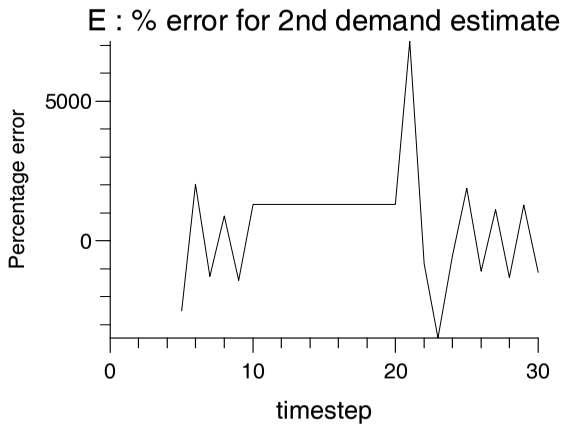

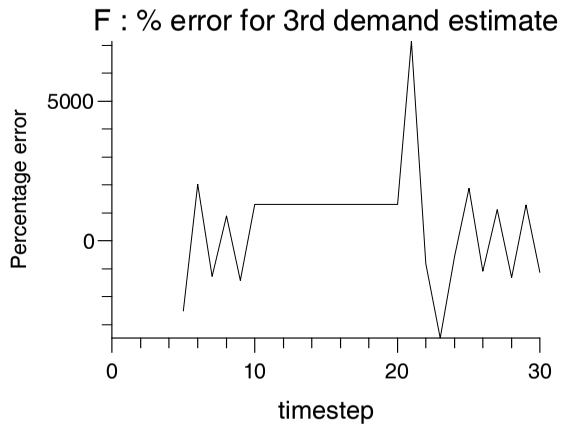

Experiment 10.25

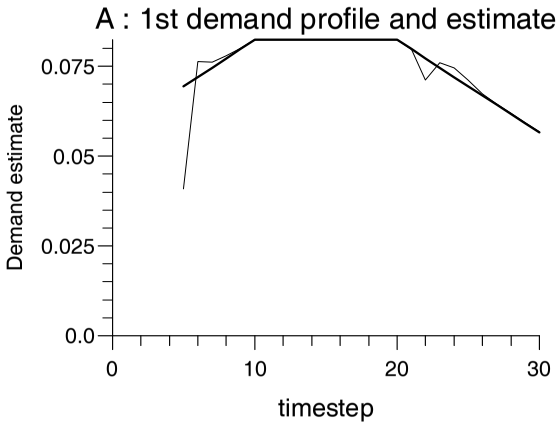

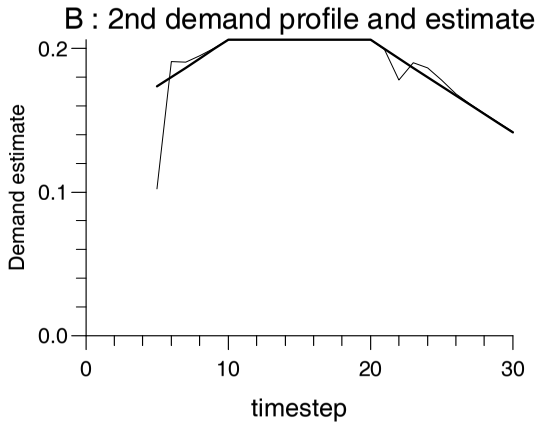

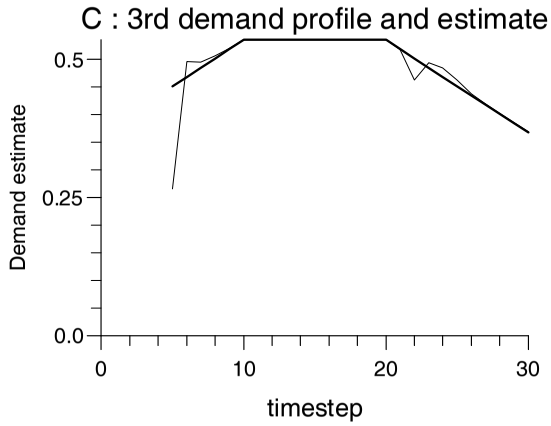

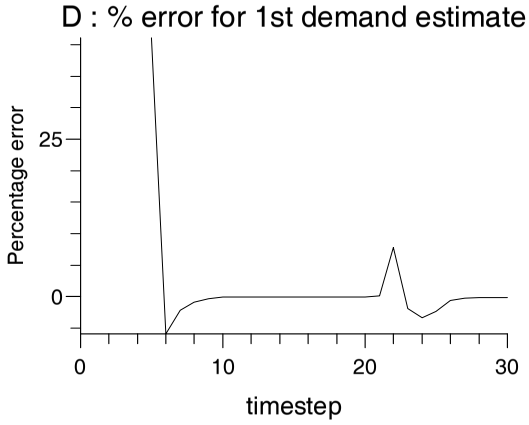

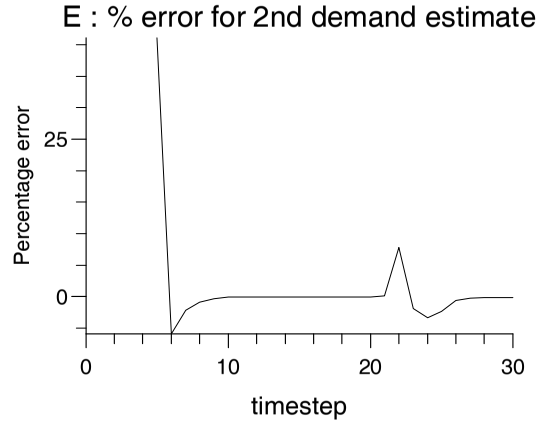

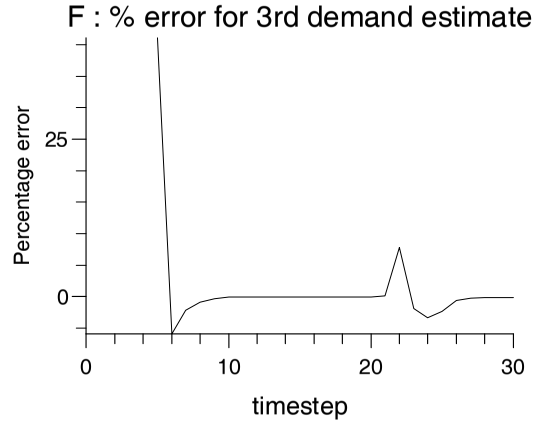

Experiment 10.26

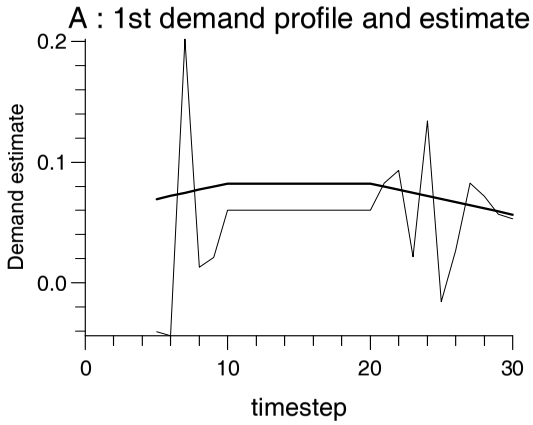

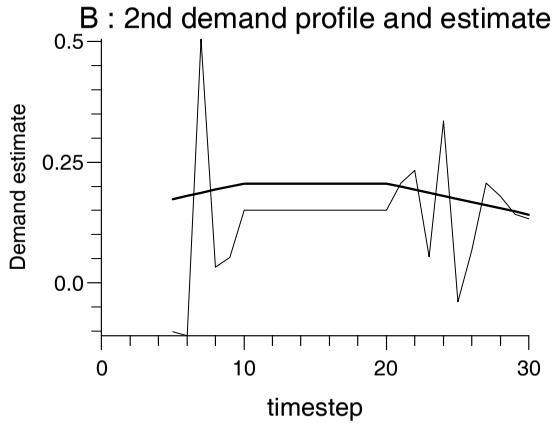

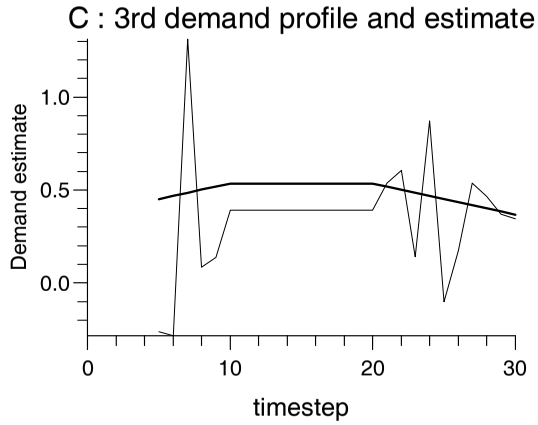

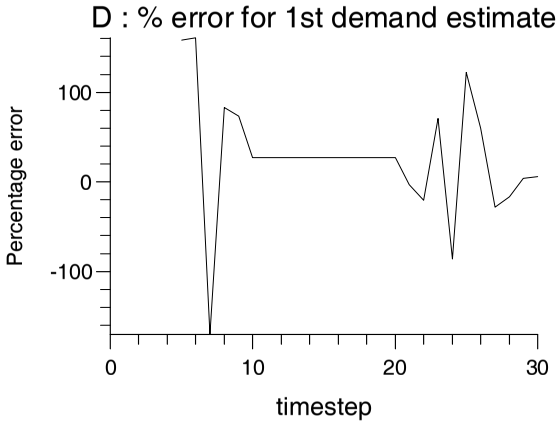

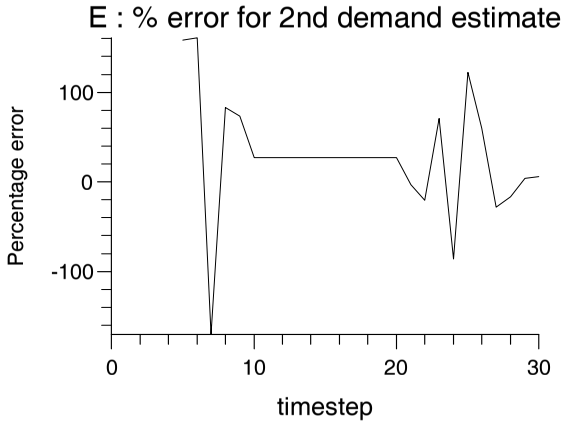

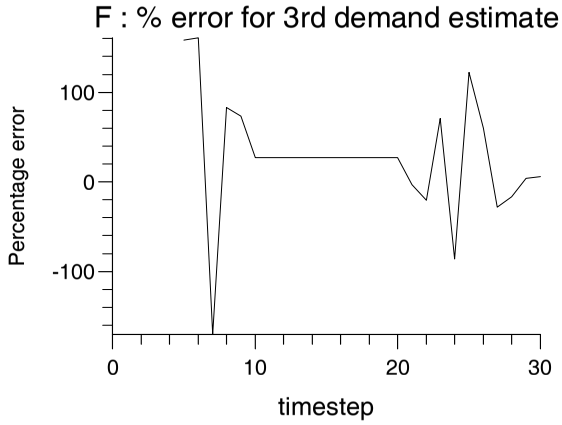

Experiment 10.27

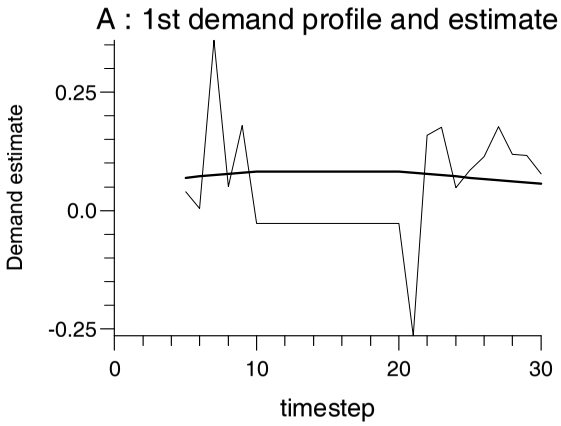

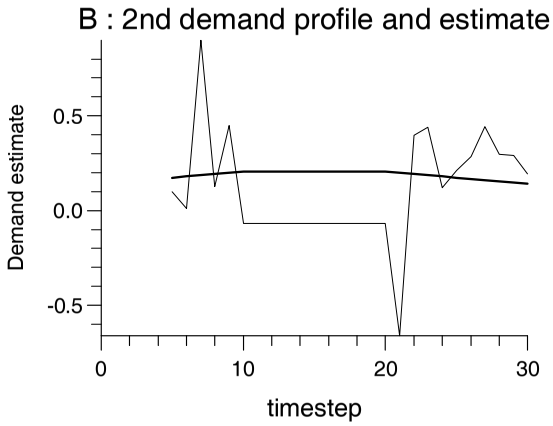

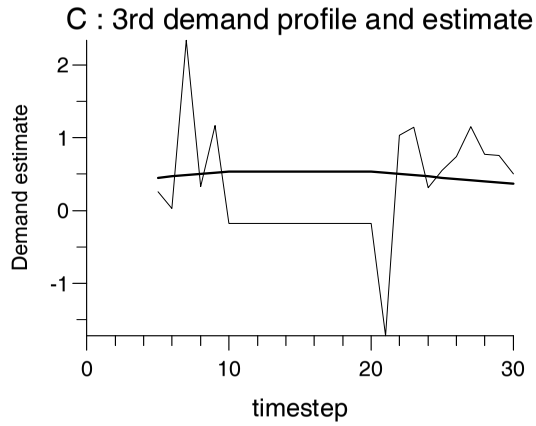

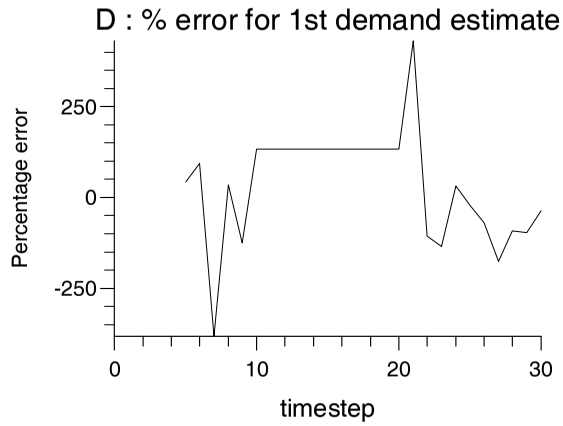

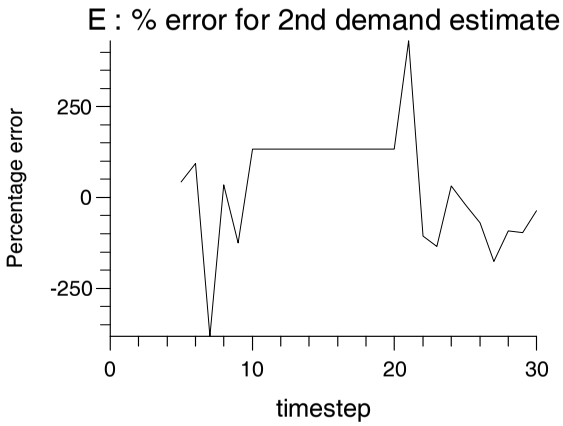

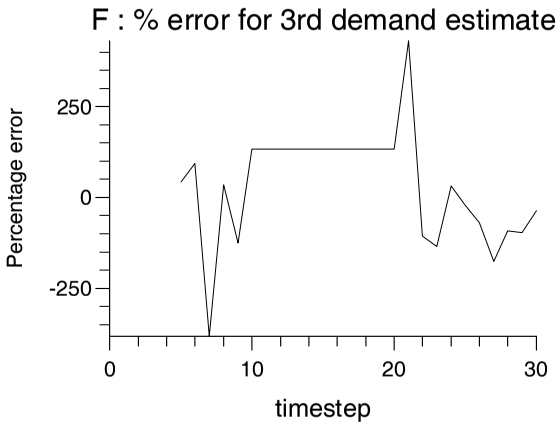

Experiment 10.28

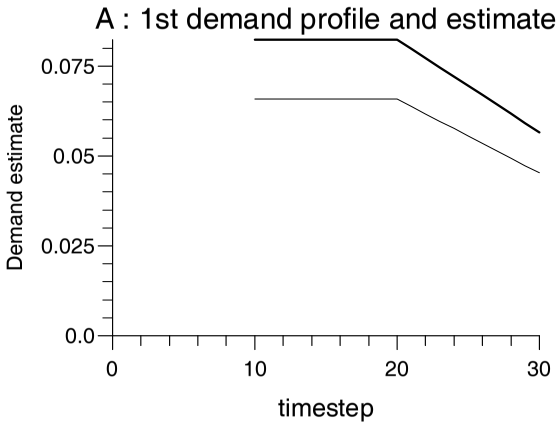

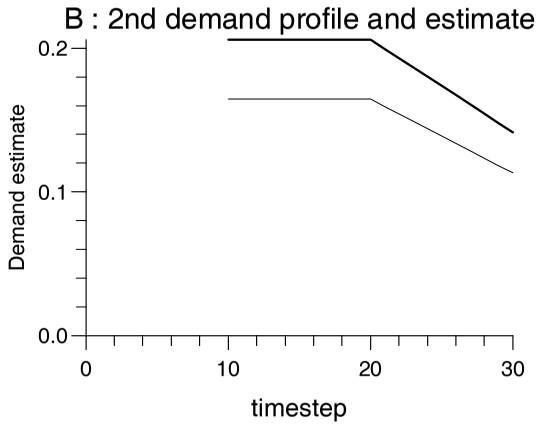

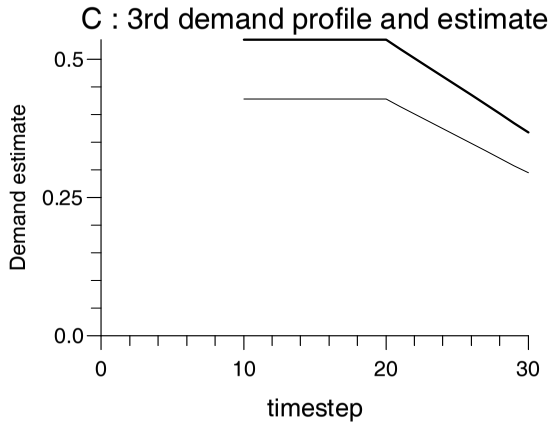

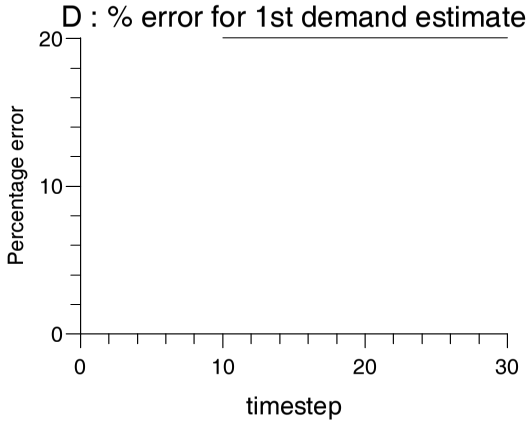

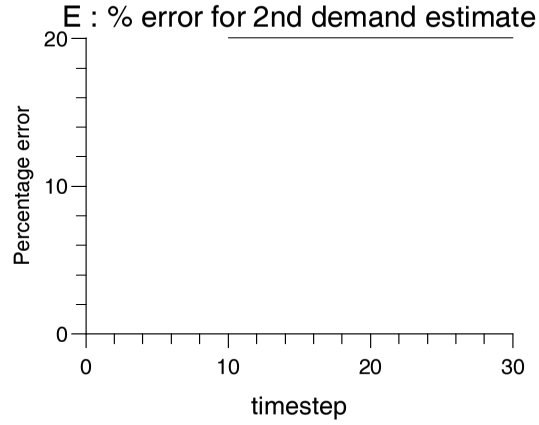

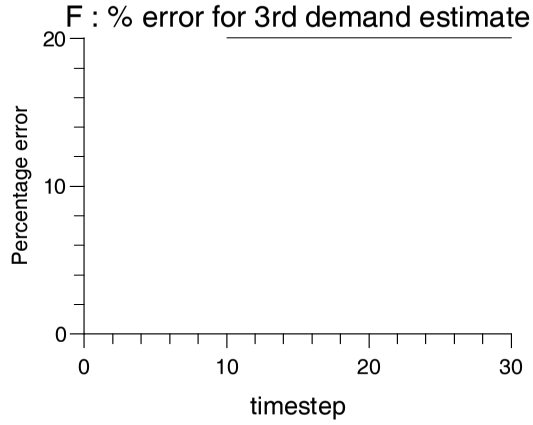

Experiment 10.29

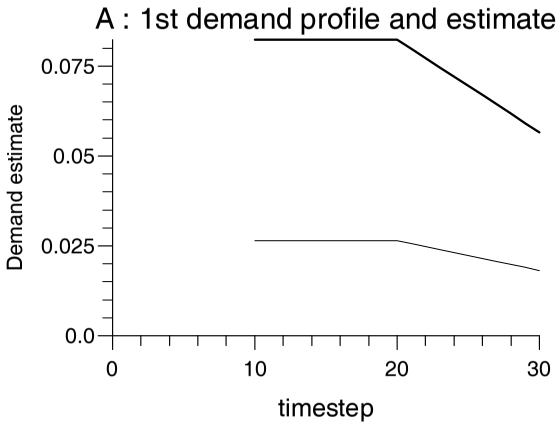

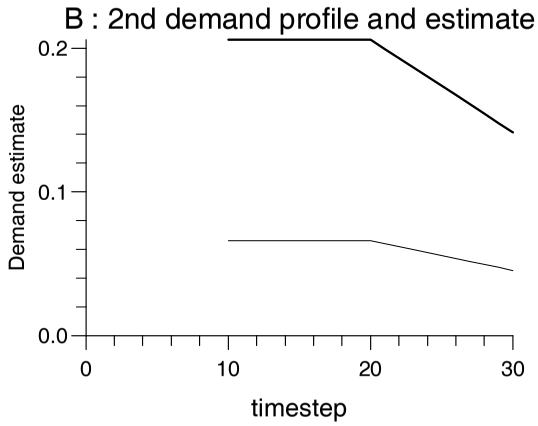

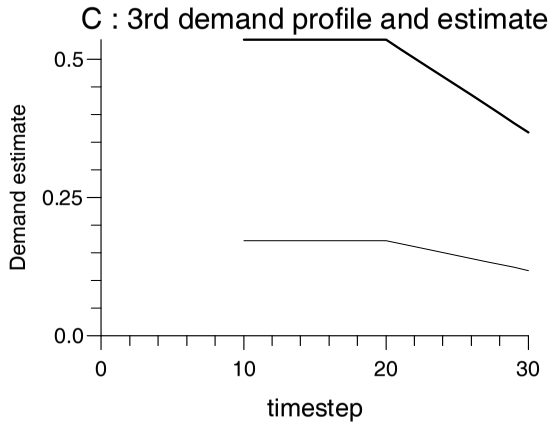

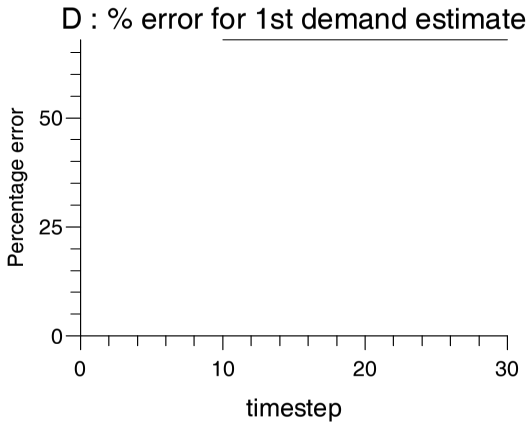

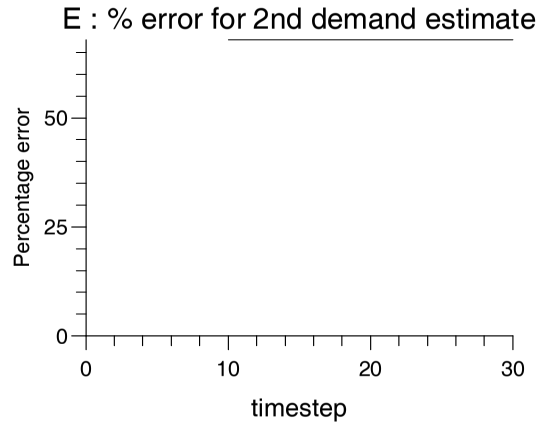

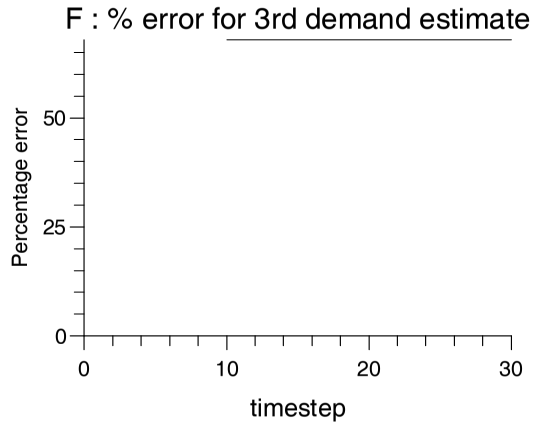

Experiment 10.30

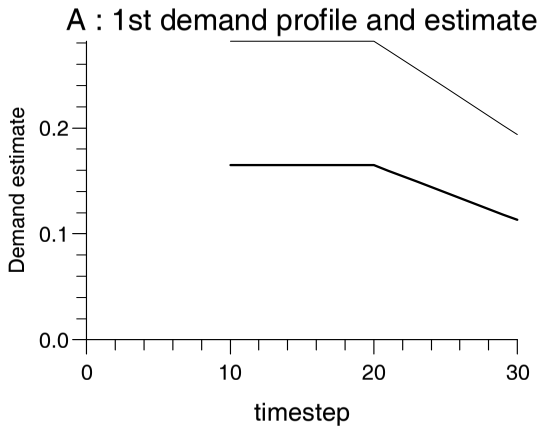

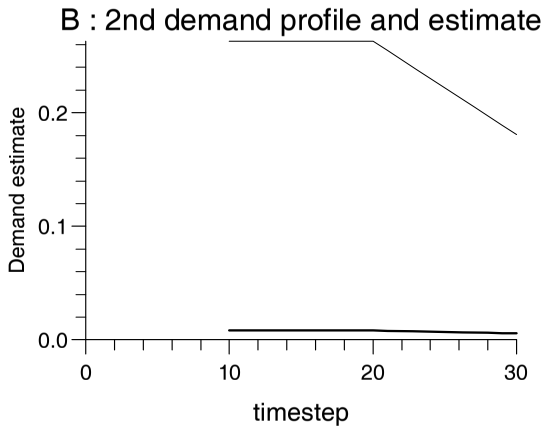

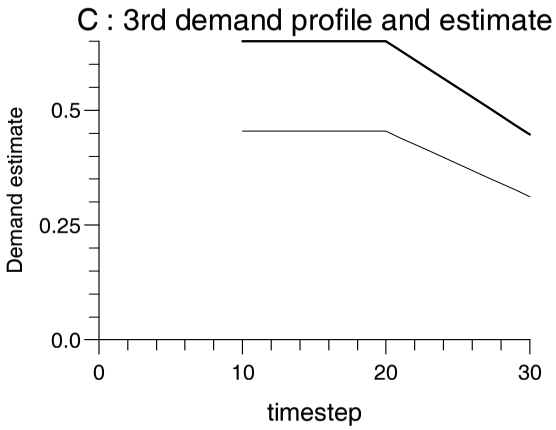

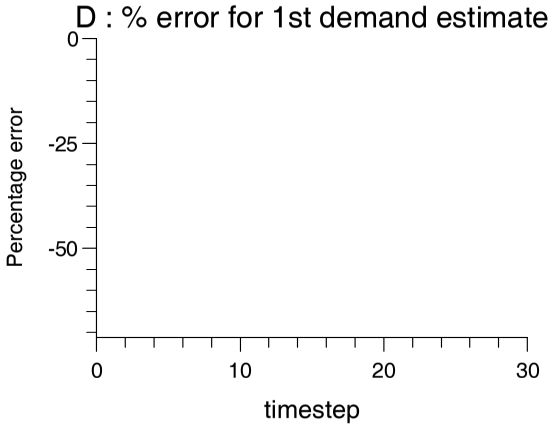

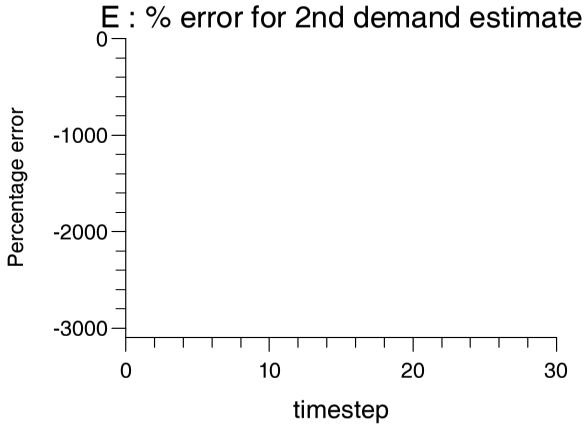

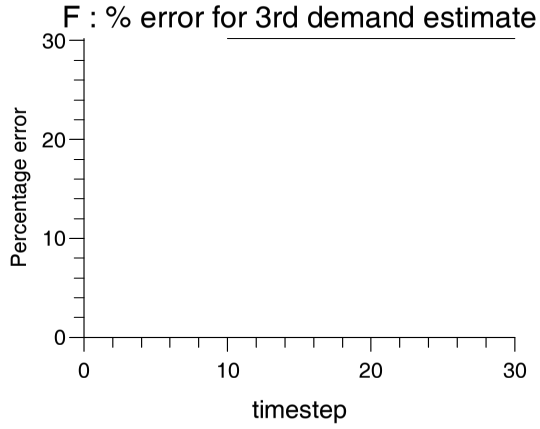

Experiment 10.31

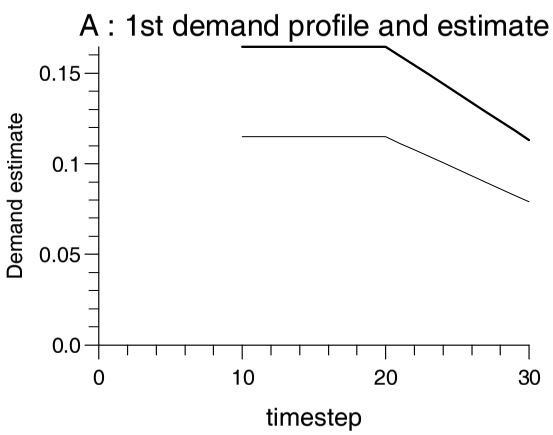

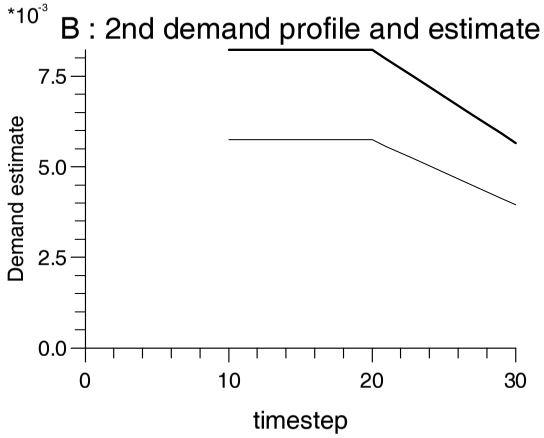

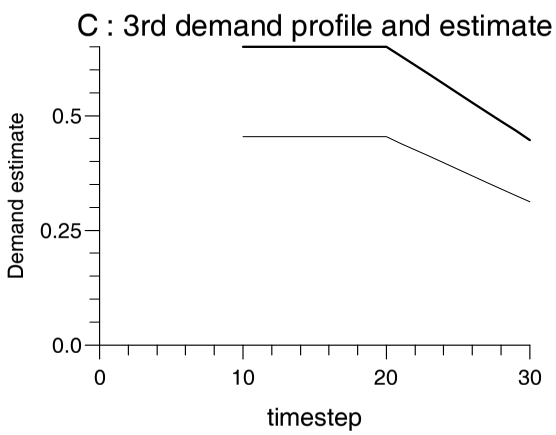

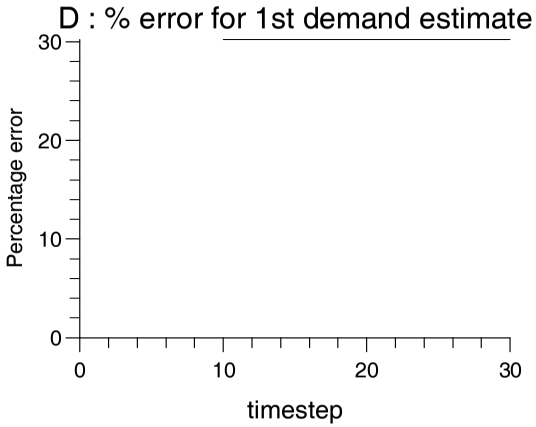

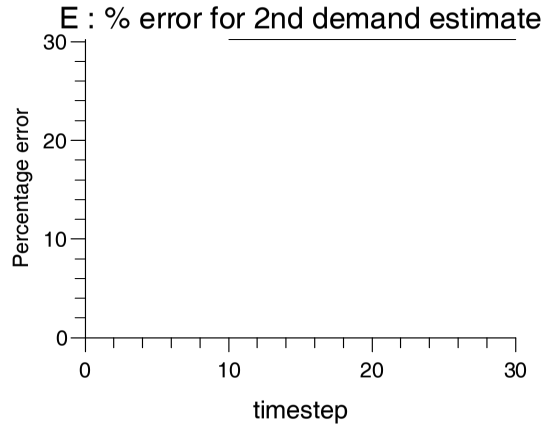

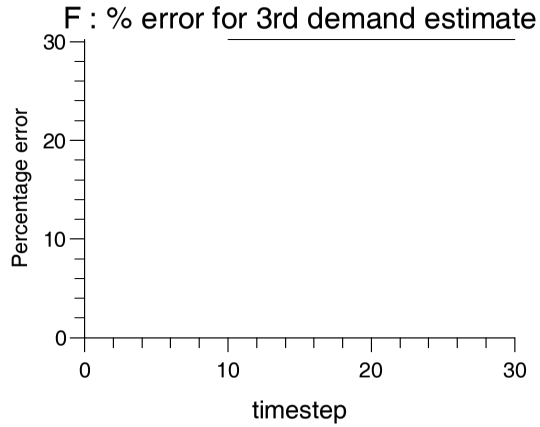

10.5.3 Discussion

The performance of $\mathcal{M}6$ model based dynamic observers showed the same dependency on θ as dynamic observers based upon previous flow estimation models. The dynamic observer based on an $\mathcal{M}6$ model converged perfectly for $\theta = 1$ when the $\mathcal{M}0$ model used to generate the pressure data was constructed on an identical mesh. However, as θ moved close to $1/2$, the observer completely failed to converge. Similarly to dynamic observers based upon previous flow estimation models, the assigned observer eigenvalues became more sensitive as θ moved from 1 to $1/2$, and a theoretical study of whether the Hautus condition is near to failing for $\theta = 1/2$ would be useful. As with $\mathcal{M}4$ systems, $\mathcal{M}6$ systems have time-varying system matrices. As with $\mathcal{M}4$ systems, the theoretical analysis of firstly, the observability of $\mathcal{M}6$ systems, and secondly, the convergence of dynamic observers constructed upon $\mathcal{M}6$ systems, would be worthwhile future research.

When data was taken from an $\mathcal{M}0$ model with a much finer discretisation, the $\mathcal{M}6$ model based dynamic observer did not perform so well. The same super-sensitivity that existed with $\mathcal{M}4$ systems exists for $\mathcal{M}6$ systems. As was suggested for $\mathcal{M}4$ systems, perhaps some further investigation into modelling strategies and different observer designs may help to remedy this. For example, perhaps an observer that switched between the different models, $\mathcal{M}5$ and $\mathcal{M}6$, at certain times of day could be designed to estimate the biases, where the $\mathcal{M}6$ model based observer would run over certain 'favourable' timesteps only. Then these estimates of the biases may be kept while an $\mathcal{M}5$ model based observer is run over periods where an $\mathcal{M}6$ model based observer would fail.

When pressure measurement noise was added, but no smoothing technique applied, it could be seen that the estimates of the first two small demands contained less error than with the previous $\mathcal{M}4$ model based dynamic observer designs. When the $\mathcal{M}4$ flow integration smoothing technique was also applied, the estimates of the flow demands improved further. However, the last two experiments, 10.30 and 10.31, clearly demonstrate the considerable benefit of using $\mathcal{M}6$ models to estimate very small flow demands. Unfortunately, the error due to measurement noise and modelling error is still unacceptably large.

Although we do not yet have a viable technique for estimating flow demands from

pressure telemetry in the presence of *both* measurement bias and noise, some proposals for future research are presented in the next chapter.

Chapter 11

Final Conclusions and Proposals for Future Work

The fundamental problem in estimating flow demands from pressure telemetry is the sensitivity of the flow demands, especially small flow demands, to modelling and measurement error. When the pressure measurements fed into $\mathcal{M}1/\mathcal{M}2$ models and observers constructed upon $\mathcal{M}3/\mathcal{M}4$ models, were corrupted by noise, the flow demand estimates were swamped by the resulting error. The $\mathcal{M}5/\mathcal{M}6$ modelling approach of summing all the flow demand variables into a single total flow variable seemed to reduce greatly the sensitivity. The flow integration smoothing techniques were also particularly effective. However, although smoothed $\mathcal{M}5$ flow demand estimates were acceptably accurate when pressure measurement noise was present, they were unable to cope with measurement bias. Of the two models, $\mathcal{M}5$ and $\mathcal{M}6$, only observers constructed upon $\mathcal{M}6$ models could cope with measurement bias. However, observers constructed upon $\mathcal{M}6$ models were found to be still very sensitive to modelling error and measurement noise. Hence, so far we do not have a practical technique for flow demand estimation from pressure telemetry. We do, however, have some proposals for future research.

A fundamental problem to investigate is why the $\mathcal{M}6$ systems are so sensitive to pressure measurement noise, and if there is a way of remedying this. However, the sensitivity of the flow demand estimates from observers constructed upon $\mathcal{M}6$ models may be partly due to the observer design. It would be interesting, therefore, to investigate other observer designs, e.g. optimal control techniques [1], and in particular Kalman filters

[12], [9], [8], [10]. Some references [17], [40], [35], have suggested little gain from the extra computational expense involved with Kalman filters. However, in these experiments, the Kalman filter was compared with an observer design with a built in filter. The filtering technique used in this comparison observer relied on the availability of both flow demand and pressure measurements at the sites of gas inflow/outflow. Hence, such a filtering technique cannot be used for our purpose, where flow measurement is not available.

Various theoretical questions raised in the thesis should also be explored. Can the solutions to the numerical models be shown to converge to the solutions to the governing differential equations as the compuational mesh is refined? What are the conditions necessary to guarantee the observability of the time-varying models? When do dynamic observers based upon time-varying models converge?

In conclusion, we have investigated a series of models and made some progress in tackling the practical problems of flow demand estimation from pressure telemetry. However, more research is required, perhaps involving Kalman filters, to find a technique that gives acceptably accurate flow estimates from pressure data from a *real* gas network.

Bibliography

[1] Anderson, B.D.O. and Moore, J.B., *Optimal Control - Linear Quadratic Methods*. Prentice Hall, 1990.

[2] Barnett, S. and Cameron, R.G. *Introduction to Modern Control Theory* (2nd Edition). Clarendon Press, Oxford, 1985.

[3] Benkherouf, A. and Allidina, A.Y., Leak Detection and Location in Gas Pipelines, *IEE Proceedings*, vol.135, Pt.D, No.2, March 1988.

[4] Bunse-Gerstner, A., Mehrmann, V. and Nichols, N.K., Regularisation of descriptor systems by derivative and proportional state feedback, *SIAM J. on Matrix Anal. and Applic.*, **13**, 1992, 46-67.

[5] Burden, R.L. and Faires, J.D., *Numerical Analysis*, PWS-Kent, 1989.

[6] Campbell, S.L. and Terrell, W.J., Observability of linear time-varying descriptor systems, *Siam J. Matrix Anal. Appl.*, Vol.12, No.3, pp.484-496. July 1991

[7] Campbell, S.L., Nichols, N.K. and Terrell, W.J., Duality, observability, and controllability for linear time-varying descriptor systems, *Circuits Systems Signal Process*, Vol.10, No.4, 1991.

[8] Caines, P.E., *Linear Stochastic Systems*, John Wiley, 1988.

[9] Catlin, D.E., *Estimation, Control, and the Discrete Kalman Filter*, Springer-Verlag, 1989.

[10] Chen, Han-Fu, *Recursive Estimation and Control for Stochastic Systems*, John Wiley, 1985.

[11] Clarke, G.M. and Cooke, D., *A Basic Course in Statistics*, Edward Arnold, 1983.

[12] Davis, M.H.A. and Vinter, R.B., *Stochastic Modelling and Control*, Chapman and Hall, 1985.

[13] Fletcher, L. R., Kautsky, J. and Nichols, N.K. Eigenstructure assignment in descriptor systems, *IEEE Trans Auto Cnt.*, **AC-31**, 1986, 1138-1141.

[14] Fraleigh, J.B. and Beauregard, R.A. *Linear Algebra.* Addison Wesley, 1987.

[15] *Applied Optimal Estimation*, edited by Arthur Gelb. M.I.T. Press, 1989.

[16] Gladwell, I. and Wait, R., *A Survey of Numerical Methods for Partial Differential Equations*, Oxford University Press, 1979.

[17] Goldfinch, M.C., *A Study of Observer Methods for Gas Network State Estimation*, British Gas technical report LRS T 678. (1984)

[18] Goldwater, M.H., *Matrix Analysis of the Behaviour of General Gas Networks*, British Gas technical report LRS T112. (1972)

[19] Goldwater, M.H. and Fincham, A.E., Modelling of Gas Supply Systems, *Modelling of Dynamical Systems Volume 2.* Edited by H. Nicholson. Peter Peregrinus, 1981.

[20] Golub, G.H., and Van Loan, C.F., *Matrix Computations*, Johns Hopkins University Press, 1983.

[21] Goodwin, N.H., *A Simple Iterative Method for the Steady State and Transient Simulation of Gas Networks*, British Gas technical report LRS T511. (1982)

[22] Horn, R.A. and Johnson, C.R., *Matrix Analysis*, Cambridge University Press, 1985.

[23] Johnson, L.W. and Riess, R.D., *Numerical Analysis*, Addison-Wesley, 1982.

[24] Kautsky, J., Nichols, N.K. and Van Dooran P, Robust pole assignment in linear state feedback, *Int. J. of Control*, **41**, 1985, 1129-1155.

[25] Kautsky, J., Nichols, N.K. and Chu, E.K.W., Robust pole assignment in singular control systems, *Lin. Alg. and Applic.*, **121**, 1989, 9-37.

[26] Kuo, B.C., *Digital Control Systems*, Holt, Rinehart and Winston, 1981.

[27] Lipschutz, S., *Linear Algebra*, McGraw-Hill, 1981.

[28] Mitchell, A.R. and Griffiths, D.F., *The Finite Difference Method in Partial Differential Equations*, John Wiley and Sons, 1987.

[29] O'Reilly, J., *Observers for Linear Systems*. Academic Press, 1983.

[30] Osiadacz, A.J., *Simulation and Analysis of Gas Networks*, E. and F.N. Spon, 1987.

[31] Paige, C.C. Properties of numerical algorithms related to computing controllability. *IEEE Trans. Aut. Control*, 1981, **AC-26**, 130-138.

[32] Parkinson, J.S. and Wynne, R.J., *Mathematical Modelling and the Application of State Estimation Techniques to Gas Distribution Systems*, Simon Engineering Laboratories, University of Manchester, report No. 04/84. (1984)

[33] Patton, R., Frank, P. and Clark, R., *Fault Diagnosis in Dynamic Systems*, Prentice Hall, 1989.

[34] Pearson, D.W. *Robust Observer Design and Application to Gas Networks*, Coventry Polytechnic, Ph.D. Thesis, 1988.

[35] Piggott, J.L. and Whitley, A.W., *The Use of Kalman Filtering to Estimate Grid Conditions from Telemetry Data - Results from Test Data from No.5 Feeder*, British Gas technical report LRS T 608. (1983)

[36] Richtmyer, R.D. and Morton, K.W., *Difference Methods for Initial Value Problems*, Wiley and Sons, 1967.

[37] Smith G.D. *Numerical Solution of Partial Differential Equations: Finite Difference Methods*. Oxford University Press, 1985.

[38] Spiegel, M.R., *Probability and Statistics*, McGraw-Hill, 1975.

[39] Stewart, G.W. Gerschgorin theory for the generalised eigenvalue problem $Ax = \lambda Bx$. *Math. Comp.*, 1975, **29**, 600-606.

[40] Whitley, A. and John, R.I., *The Use of Kalman Filtering to Estimate Grid Conditions from Telemetry Data - Results of Tests on Simulated Data*, British Gas technical report LRS T 538. (1982)

[41] Wiberg, D.M., *State Space and Linear Systems*, McGraw-Hill, 1971.

[42] Yip, E.L. and Sincovec, R.F. Solvability, controllability and observability of continuous descriptor systems. *IEEE Trans. Aut. Control*, 1981, **AC-26**, 702-707.